Feasibility study

Investigating the Technical- and Economic Feasibility and Sustainability Aspects of Fiber-reinforced Plastic Jetties

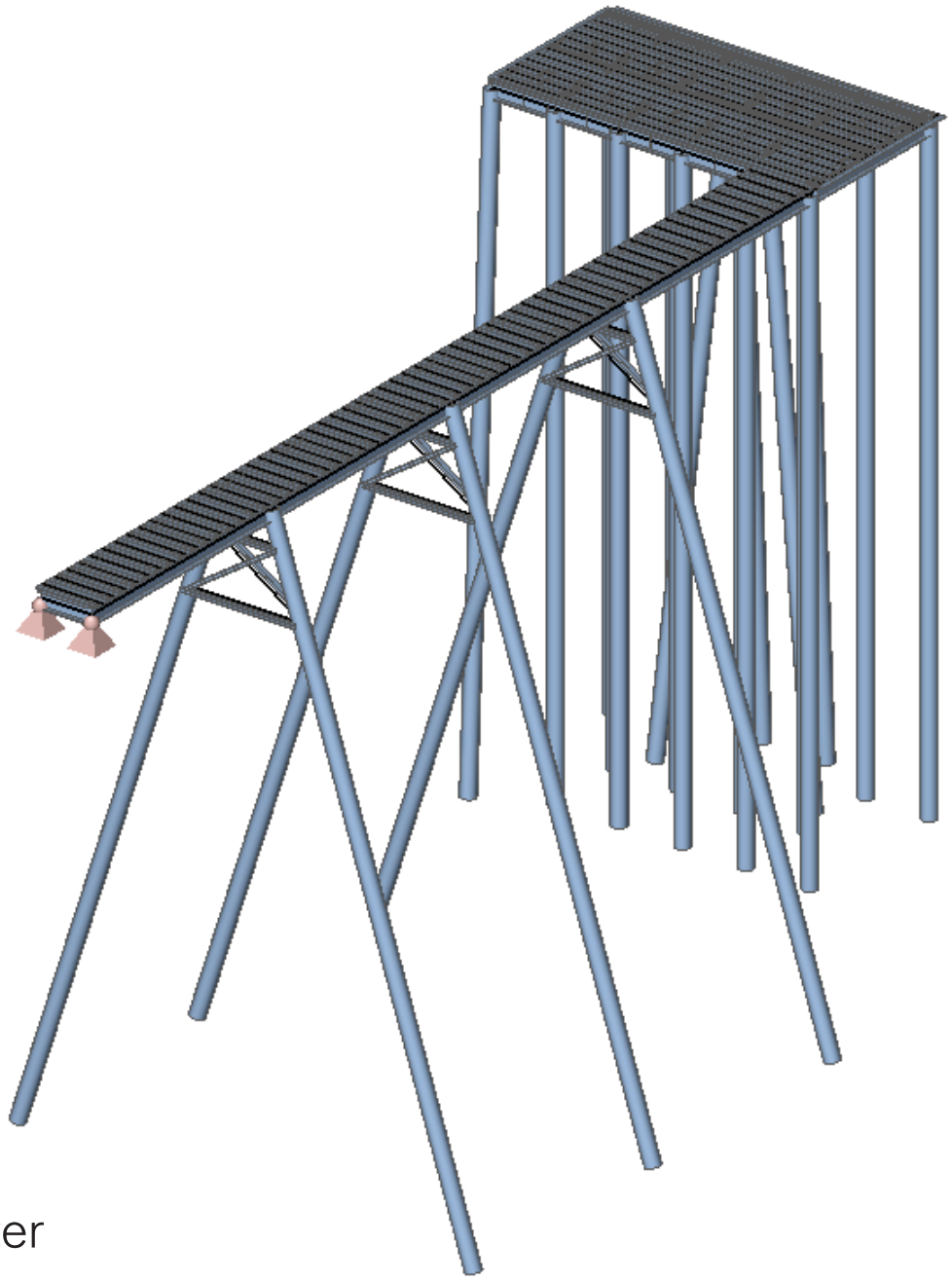

R.Winter

TU Delft

Gemeente Rotterdam

DELFT UNIVERSITY OF TECHNOLOGY

Feasibility study: Fiber-reinforced plastic jetties

Investigating the technical- and economic feasibility and sustainable aspects of FRP jetties

By

Roel Winter

Student number: 4114604

Thesis committee:

Prof. dr. ir. S. J. Jonkman,	TU Delft, chair
Dr. ir. J. G. de Gijt,	TU Delft
Dr. H. M. Jonkers,	TU Delft
Dr. ir. C. Kassapoglou,	TU Delft
Ir. H. E. Pacejka,	Gemeente Rotterdam, daily supervisor

September 22, 2017

Preface

This thesis is the final part of the curriculum from the master track Civil Engineering at Delft University of Technology. The thesis is a test where the candidate applies all of his acquired knowledge in the bachelor and master and proves that that he/she possesses the qualities as desired by Delft University of Technology before receiving the title Master of Science. In this thesis, the feasibility of an fiber-reinforced plastic (FRP) jetty is researched. The motivation behind this topic was the excellent structural and durability properties FRP possess. Nonetheless, no specific research regarding FRP jetties existed so far: this thesis aims to provide such research.

Readers who are interested in the technical design of a FRP jetty are advised to read Part I. Environmental aspects are treated in Part II, where an life cycle assessment (LCA) for the designed FRP jetty is elaborated. Economic prestige of the design is treated in Part III.

I would like to thank Gemeente Rotterdam for granting me the possibility to write my thesis at their office and to provide expertise regarding various topics and operational support. Also, I would like to thank the team off Allnamics: especially Peter Middendorp and Nicolás Moscoso for sharing their knowledge and support for the pile driving analysis.

Furthermore I would like to thank the members of my graduation committee for their input and support during the course of my master thesis. Bas Jonkman, for presiding the committee and broadening my view other than the technical design. Jarit de Gijt, for bringing me in contact with the Gemeente Rotterdam and always coming up with new ideas. Henk Jonkers, for sharing his expertise on sustainable design. Christos Kassapoglou, for sharing his expertise on composite engineering. And Hans Pacjeka, who as a daily supervisor had a lot of valuable input by providing feedback on my ideas.

Last but not least, I would like to thank my mother and sister: they have been of great support during the days in which I wrote my thesis. You always believe in me regardless the path I choose to take. The rest of my family, who I regard as an important aspect of my life. And my friends, which made my study time very worthwhile and a very special time of my life. You all are very dear to me.

Roel Winter
Rotterdam, 2017

Summary

Fiber-reinforced plastic (FRP) is an upcoming material in the construction industry due to characteristic material properties such as its high resistance to corrosion and high strength to density ratio. Also, it is often claimed that structures from FRP have lower life-cycle costs and eco burden compared to constructions made from steel, concrete, or wood; this can be attributed to the low amount of required maintenance and longer life span of FRP. Therefore, FRP seems a very suitable material in the harsh environments where hydraulic structures reside compared to conventional materials.

No actual commercial jetties, besides small pedestrian jetties, are yet constructed from FRP: knowledge regarding the potential financial savings or the environmental impact of such jetties are not well known. Also, specific consequences of constructing a jetty from FRP are unknown, as well the ability of FRP jetties to maintain their structural capabilities over their entire life-time. Therefore, this thesis investigates the feasibility of FRP jetties and judges whether FRP jetties are better alternatives than jetties constructed from traditional materials. In the scope of this thesis, the research is narrowed down to comparing FRP with reinforce concrete (RC).

The main design challenge of FRP in civil engineering related structures is coping with the relatively low stiffness of FRP, as this presumably determines the dimensions of the structural elements and restrictions of the structure as a whole. Governing structural safety criteria in steel and concrete are more often strength related. The research rests on a case study of an RC jetty, which provides boundary conditions and a program of requirements. An FRP jetty is designed which complies with the structural criteria. These criteria were both extracted from the case study and provided by the CUR96, a Dutch design guideline for FRP in civil engineering practice. Most structural elements are designed from scratch: laminates are designed for the flanges and webs in a composite calculator named eLamX2. The finite element method (FEM) software program SCIA Engineer is used for the structural analysis. One dimensional structural elements were first validated before utilizing them in the FEM model. The pile properties and dimensions are based on contemporary literature and commercially available products. The driveability of the FRP piles is researched by means of Wave Equation Analysis of Piles (WEAP), for which the program AllwavePDP is utilized. Furthermore, sustainability aspects of both jetties are researched by means of a Life Cycle Assessment (LCA). The LCA determines how much equivalent greenhouse gases are expelled over the life-time of the jetties for a set of impact categories. These results are normalized by calculating the respective shadow costs for each impact category; this makes the total environmental impact of the structures comparable. The financial feasibility is the last investigated topic; under various scenarios, life-cycle costs of both jetties are investigated. The scenarios contained different variables such as estimates of FRP raw material costs or assumed share of maintenance costs; end-of-life costs were not included in the analysis.

The structural analysis of the FRP jetty indicated that both Serviceability Limit State (SLS) criteria and Ultimate Limit State criteria (ULS) determine the dimensions of the structural elements and the jetty design in general. The most crucial parts are partially embedded FRP piles, which are prone to buckling. Initially, the FRP piles in the detailed design were to be installed to a depth of 13 meter below ground level, but the results from the WEAP indicated that the piles refused during installation before reaching this level. An analysis indicated that driving shorter piles to a depth of 8 meter is

possible: at this depth, the piles do not refuse and have accumulated sufficient bearing capacity by shaft friction to support the superstructure. The eco burden of the FRP jetty was found significantly higher compared to the RC jetty: in the base case LCA, the relative difference is 365 percent higher for the FRP variant. After a sensitivity analysis, the relative difference is still 59 percent higher when comparing the best-case scenario of the FRP jetty with the worst-case scenario of the RC jetty.
The RC jetty also performed better than the FRP jetty regarding life-cycle costs in various considered scenarios. The relative difference in life-cycle costs for the most favorable scenario of the FRP jetty is still 28 % higher compared to the life-cycle costs of the RC jetty.

Due to the poorer performance of the FRP jetty regarding the life-cycle costs and environmental burden, it is concluded that FRP jetties, for the time being, are not better alternatives than RC jetties. Regarding the type of jetty, the conclusion can be generalized. The jetty is designed for the turnover of liquid bulk; imposed loads are generally lower than loads on Ro-Ro, solid bulk, or container transfer jetties. It therefore seems unlikely that FRP does seem to be a better alternative for those cases. Regarding the material choice, the conclusion cannot be generalized. The FRP jetty was compared to an RC jetty. Jetties made from steel or wood are likely more vulnerable to degradation in harsh conditions. The durability properties of FRP might be more beneficial to the assessment of FRP jetties in these cases.
Certain future developments might affect the conclusion. Innovation in manufacturing techniques and an increase of market demand for FRP could lower the price. Besides, biodegradable FRP materials are being developed which potentially may reduce the environmental burden of FRP.

Keywords: FRP, composite design, hydraulic structures, jetty, pile driving, LCA, life-cycle costs

Contents

Acronyms

C2C	cradle-to-cradle.
C2G	cradle-to-grave.
CPT	cone penetration test.
FRP	fiber-reinforced plastic.
FU	functional unit.
GEF	Geotechnical Exchange File.
ILSS	interlaminar shear strength.
IPCC	Intergovernmental Panel on Climate Change.
LCA	life cycle assessment.
LCI	Life Cycle Inventory.
LCIA	Life Cycle Impact Assessment.
MHW	Mean High Water.
MLW	Mean Low Water.
NPV	net present value.
RC	Reinforced Concrete.
SLS	serviceability limit state.
ULS	ultimate limit state.
WEAP	wave equation analysis of piles.

Glossary

batter angle	Inclination angle of a pile; same as rake angle.
camber	the slightly convex or arched shape of a road or other horizontal surface.
NAP	Normaal Amsterdams Peil, reference level for height measurements in the Netherlands.
sumput	A container with the purpose of collecting polluted water.

Introductory

1 Introduction

1.1. Motivation for the thesis topic: feasibility of FRP jetties

The first constructions in hydraulic engineering date back centuries ago. Big improvements in their functionality has been due to access to new construction materials. For instance, the first sluice doors were constructed of wood. Nowadays, the capacity of the biggest sluice gates in the world are, among others things, due to the availability of steel as a construction material. New construction materials may have benefits which conventional construction materials, at the time, did not posses. The introduction of new materials to engineering fields emphasizes a period of research and learning. In recent years, a construction material which is well known in the world of automotive and aerospace engineering entered the field of civil engineering: fiber-reinforced plastic.

FRP is well known for its lightweight, strength and durable properties. For this reason, several sluiced have been constructed and installed in The Netherlands. Figure 1.1 illustrates the biggest sluice doors placed yet in The Netherlands as of January 2017. The doors are 12.9 m high and 6.2 m wide (FiberCore Europe, n.d.). The main reason to use FRP is to increase the durability and to reduce the expenditures in the user phase due to maintenance and repairs.

Whilst several hydraulic structures have been constructed of FRP in recent times, like the above mentioned sluices, there is not yet a jetty of significant size constructed out of FRP. Small scale jetties, called finger-piers, have been constructed of FRP in marinas for small recreational rafts. However, no jetties of sizes which can handle inland waterway traffic such as tankers and small bulk carriers are yet constructed.

There are several definitions of a jetty. The main function of the jetty is to provide a place where ships can be moored and where the exchange of goods, most often gas, oil, or bulk products. The Oxford dictionary describes a jetty as:

"*A landing stage or small pier at which boats can dock or be moored*" (Oxford Dictionaries, n.d.)

De Gijt, in his lecture notes, states that jetties are:

"*Piled structures whose stability depend on pile bearing and lateral load-carying capacity*" (de Gijt, 2004)

The functionality of the jetty largely determines its structure and layout. Examples of jetties with different functionalites are:

Figure 1.1: FRP sluice door measuring 12.9 m x 6.2 m in the Wilhelmina channel, The Netherlands (FiberCore Europe, n.d.)

- Oil jetties
- Liquid natural gas (LNG) jetties
- Bulk jetties (e.g. coal, metal, grain, rice)
- Cruise jetties
- Multipurpose jetties

Jetties are hydraulic structures which are often comprised from piles and a deck. The piled deck system is a cost effective solution to reach deeper water from the shore in order to facilitate berthing places and transfer points for goods. In general, jetties are constructed from wood or concrete and steel. Figure 1.2 and Figure 1.3 illustrate two different jetties.

Figure 1.2: Small jetty in the port of Rotterdam, The Netherlands (Beens Groep, n.d.)

Figure 1.3: Large LNG jetty in the port of Darwin, Australia (Beens Groep, n.d.)

1.1.1. Problem definition

Hydraulic structures are often placed in harsh environments. Variable load cases, salinity, and alternating weather among them. These environments make them prone to degradation and wearing. Engineers design these structures to be resilient against these forces of nature. The main reason to construct a jetty out of FRP is the potential increase in durability which will reduce its lifetime costs. Due to the different nature of FRP than that of steel and concrete, issues arise when designing an FRP jetty. These issues range from structural instabilities and installation difficulties to unknown long-term material properties in specific circumstances. Therefore, research needs to be conducted in order to find out if, besides testing the potential advantages of the application of FRP, structural and safety demands could comply when constructing a jetty from FRP. Also, effects on the environment need to be researched and potential pitfalls need to be mapped in order to make a general statement about the effectiveness of FRP for jetties.

1.1.2. Purpose of the study and project scope

The purpose of this study is to answer the main research question:

"Are fiber reinforced plastic jetties a better alternative than reinforced concrete jetties?"

In the research question, the conventional jetties are narrowed down to Reinforced Concrete (RC) jetties since the case study is based on reinforced concrete jetty (see Chapter 3).

In order to answer the main question, several sub-research questions have been formulated:

- *"Can the structural integrity of a jetty, fully constructed of FRP, be guaranteed with at least the same safety levels required for RC jetties?"*
- *"What are the implications on environmental impact when using FRP to construct a jetty compared to reinforced concrete, over their full lifetime cycles?"*
- *"How do costs of FRP jetties differ from RC jetties during their full lifetime cycles?"*

The sub-research questions are answered in Part I Part II, and Part III respectively. The main question is answered in Section 8.4.

1.1.3. Research description and methodology

For this thesis, the following procedure was selected. First a literature study will be executed to gain knowledge. In this literature study, the following preliminary items will be expanded: applications of FRP, reference projects, material properties, manufacturing techniques, mechanics, structural design of building parts, joints, durability, sustainability, and life cycle assessment methods.

To get a solid idea of the structural performance, costs, durability- and sustainability properties of the FRP jetty, this jetty should be compared to a conventional jetty. Boundary conditions could be assumed, a program of requirements could be set up, and then the jetty could be designed, but the emphasis of this thesis is not on designing a conventional jetty from concrete and steel. It is about the feasibility of an FRP jetty. Therefore, a case study will be chosen. The case study is elaborated in Chapter 3 and contains a program of requirements, boundary conditions and a jetty design in steel and concrete. By using this information, I will enable to focus on the FRP jetty design.

After the literature study and the exploration of the case study, a preliminary design of the jetty will be made. Several variants will be created and considered. One of the variants will be selected and further elaborated. When the variant is selected, a preliminary SCIA model is build. SCIA Engineer is a numerical structural analysis and design software, used at the Gemeente Rotterdam. Engineers there have experience with SCIA Engineer and may provide support in the design phase regarding modeling and software issues.

With the preliminary model, the rough dimensions of the structural elements can be estimated. Main components of the jetty will be beams, decks and piles. Also, handrails should be accommodated. Prefabricated products may be used in this stage.

With the rough dimensions known, a detailed design of the structural elements will be made. The structural elements which will be designed are presented in Section 4.1.1. A selection of materials for different structural elements is done and composites will be designed. This can be done with the help of composite calculator programs like Kolibri or eLamX^2.

When the structural parts are ready, the connections between these parts will be designed. I suspect this will be the greatest challenge in order to ensure the structural stability of the jetty.
By now, the whole jetty is complete. In SCIA Engineering the structural integrity of the model can be tested according to the CUR96 guidelines, which are guidelines for the design of FRP structures. Also, the FRP jetty will be compared with the case study regarding costs and other metrics which are defined in Section 4.1.2.

1.1.4. Report structure

The introductory of this thesis exists, besides this introduction, of a brief recap of the literature study (Chapter 2) and an elaboration of the case study (Chapter 3).

The main body of the report is structured in three parts, related to the sub research questions. The first part assess the technical feasibility (Part I). Readers interested in the final FRP design are referred to Chapter 5; people particularly interested in the pile driving of the FRP piles are referred toChapter 6. The technical design is followed by an LCA which quantifies the environmental prestige of the jetty (Part II. The main body closes with a consideration of the life-cycle costs of FRP jetties (Part III.

Readers interested in the conclusions are referred to the last part of this thesis: Chapter 9 present the conclusions and answer the main research question. In Chapter 10, the content of the research and a future outlook on FRP applications for jetties is discussed. Based on the conclusions and discussion, research recommendations are suggested in Chapter 11.

2

Literature review

The literature study is executed with the intent to gain knowledge of FRP in general, material properties, applications, recent and future developments, durability properties, and sustainability properties.The literature study is available for download at the TU Delft Repository. This section summarizes the most important concepts from the literature study.

2.1. Fiber-reinforced plastic

As timber, steel and concrete dominated the construction industry for decades, FRP starts to develop itself as a serious competitor due to its, among other, corrosion increased resistance and lightweight properties (Kolstein, 2008).

In essence, FRP is a composite. In his book, Nijssen (Nijssen, 2015) uses the following definition:

'A composite is a material structure that consists of at least two macroscopically identifiable materials that work together to achieve a better result'

In essence, FRP consists of a resin and fibers. There is a wide range of available resins and fibers which each contain different properties. Also, the structure of FRP is highly customizable (e.g. fiber direction, wide variety of resins and fibers). Hence, all properties of a FRP component cannot be formulated. But overall, all FRP's may consist the following advantageous properties related to civil engineering.

Fiber-reinforced plastic posses several advantages and disadvantages by nature. The following lists of advantages and disadvantages follow from the literature study (Winter, 2017):

Advantages

- high strength whilst having a low weight;
- highly suitable for customization in form;
- low maintenance costs;
- cost-effective manufacturing processes;
- suitable for customization of specific properties:
  - strength
  - stiffness
  - thermal resistance
  - electrical resistance
  - abrasion resistance
  - excellent chemical and corrosion resistance

Disadvantages

- poor ductility;
- stiffness is low compared to traditional and/or competitive materials;
- limited recycling properties for thermosets and even thermoplastics;
- temperature resistance is limited till 150 °C;
- high initial costs due to high material costs;
- long term properties in civil engineering applications are not well-known;

2.2. Material properties of construction materials for jetties

The conventional building materials for jetties, concrete and steel, have different physical and mechanical properties than fiber reinforced plastic laminates. Table 2.1 present some of these properties in order to give an indication of the differences between the materials. Material properties are adapted from the CUR96 (de Boer et al., 2016).

Material	class/type	E-modulus GPa	Stength MPa	Density kg/m^3
Concrete	(C30/45)	30	45	2600
Steel	(S255)	200	255	7000
Fiber	E-glass	73.1	2750	2570
Matrix	Polyester	35.5	55	1200
FRP				

Table 2.1: Overview of different construction materials and their properties

2.3. Dutch design guideline: CUR96

Several design guidelines are available, but there are not yet hard requirements for the construction of FRP as is for steel and concrete in the Eurocodes. The most prevailing design manual in the Netherlands, and possibly Europe or even globally, is the CUR96 from SBR CUR (de Boer et al., 2016). This design manual is chosen as a design guideline for the FRP jetty. This is due to its up-to-date information (2016), the material that rests on the philosophy and norms from the Eurocodes, and it is the most common design manual for FRP in The Netherlands.

2.3.1. Laminar Theory

Lamination theory is expanded in the literature study (Winter, 2017). It is useful to repeat the list of assumptions:

- Halpin-Tsai for mixure
- Circular fibers
- Perfect bonding

These assumptions work their way into structural models and properties of FRP laminates. Specifically, the usage of the Halpin-Tsai rules for obtaining laminate properties.

2.4. Laminate design recommendations

Several design recommendation are given based on theory and practical experience

The most frequent cited design recommendation is the recommendation to build a symmetrical (distance to mid-plane, thickness, material, and fiber orientation) laminate with respect to the middle plane of the composite (Mallick, 2007; Nijssen, 2015; Nijhof, 2003). This eliminates the extension-bending coupling. This effect is undesirable because it reduces the effective stiffness of the laminate. Mallick also states that the bending-twist coupling can be removed by designing the laminate in such way so that the stiffness components D_{16} and D_{26} equal to zero by only using 0,90 or 0 and 90 fiber orientation angles. However, the effect of the bending-twist coupling on the elasticity is far smaller than extension-bending coupling.

Nijhof recommends to limit the same orientation angle between laminas. As the mechanical properties and thermal properties change with respect to a defined direction if the angle orientation changes, bigger angles induce bigger differences between the laminas (Nijhof, 2003). Nijssen states that stiffness jumps between laminas should be avoided. This can be done by limiting the mutual fiber angels to for instance a difference of 60°.

Nijssen also recommends to work with balanced laminates. For each lamina with the fiber orientation of $+\theta$, a lamina of $-\theta$ should be placed (Nijssen, 2015). Mallick states that is better to alternate fiber orientation angles instead of stacking orientation angles on each other while balancing the laminate(Mallick, 2007). For instance, $\left[+\theta/-\theta/+\theta/-\theta/\right]_S$ and not $\left[+\theta/+\theta/-\theta/-\theta/\right]_S$. However, Mallick also states that when 0, 90, and $\pm\theta$ directions, then adjacent $+\theta$ and $-\theta$ should be avoided. Nijhof recommends to not stack too many laminas of the same fiber orientation. Because if interlaminar stresses occur, a thicker lamina will result in larger interlaminar stresses because the generated forced are larger while the interlaminar plane remains the same (Nijhof, 2003).

By designing an orthotropic laminate, the behavior of the laminate is more insightfull (Nijhof, 2003). If a laminate is orthotropic, then $A_{16} = A_{26} = 0$. Nijssen notes that this can make the laminate relatively heavy (Nijssen, 2015).

3

An overview of the case study: Moerdijk Kolb Seagul

The FRP jetty will be compared to an existing case study to compare its performance. The case study will serve as a benchmark to assess the structural performance, environmental impact and costs efficiency of the FRP jetty.

The selected jetty is the Kolb Seagull jetty in Moerdijk. The selection of this jetty is based on the criteria presented in section Section 3.1. Then, the location is illustrated in section Section 3.3. In section Section 3.4, the program of requirements used for the case study is presented. This program of requirements will be adopted for the FRP jetty. Section 3.5 presents the loads which are used in the design process for the case study. On 20-10-2016 a site visit to the case study took place. During this site visit, pictures were taken. These are presented in Section 3.6. Then the structural models and calculations are shown in Section 3.8.

3.1. Reference choice criteria for the case study jetty and case selection

Two factors were considered regarding the choice of the casey study: size of the jetty, and the availability of boundary conditions.

Size of the jetty

The thesis aims to design an FRP jetty, more specifically to see how big they can be built in a way that they are still structurally stable, are cost efficient, and have a competitive environmental impact. Therefore, the size should be somewhat bigger than existing FRP jetties in order to push the frontiers of what is possible. Later, a prediction can be made if the largest jetties built today could also be designed and constructed in FRP.

Availability of boundary conditions

The case study should be as complete as possible so that most effort can be put into designing an FRP jetty instead of elaborating the case study where information is lacking. This would include items like a program of requirement, known load cases, available drawings, bill of quantities, and cost estimations.

Different types of goods may be transfered on the jetty which may impose different qualities on the jetty. An example: when transporting highly flammable liquids, fire resistant properties may be desired for the jetty. This may complicate the design. Since this thesis in essence is a feasibility study, the case should be kept as simple as possible. In later stages of the design process, this could be regarded.

3.2. Case study: Kolb Seagull, Moerdijk

Based on these criteria the Gemeente Rotterdam, where the thesis is executed, provided a case study which is located in Moerdijk, The Netherlands. At the time of selection, the jetty in Moerdijk was constructed. Also, this was the most recent designed jetty at the company which possessed the criteria stated above. Therefore, a lot of information was available from both documentation and project engineers.

Other alternatives which were considered were constructed a significant time ago and therefore rejected due to their lack of available up-to-date information.

3.3. Location: Westelijke Insteekhaven, Moerdijk

The case study jetty is located in Moerdijk, The Netherlands, as seen in Figure 3.1 in the red circle. In Moerdijk a small harbor is located to provide raw materials and supplies for the industrial area. In one of the harbor basins, indicated by the red circle, the jetty of Kolb Seagull is located as indicated by Figure 3.2. Figure 3.3 illustrated the rough boundaries were within the jetty is constructed. To the north, a small pier is located which was used to berth dredging equipment in order to supply sand to the neighboring area. The average depth of the basis is about -8.4 mNAP. The Mean High Water (MHW) is +0.73 mNAP and the Mean Low Water (MLW) is +0.36 m NAP.

3.4. Program of requirements

In the program of requirements the technical requirements and the boundary conditions of the jetty are described.

General requirements and information

The design lifetime of the case study jetty is set at 50 years. The height of the terrain is NAP+4.5 m.

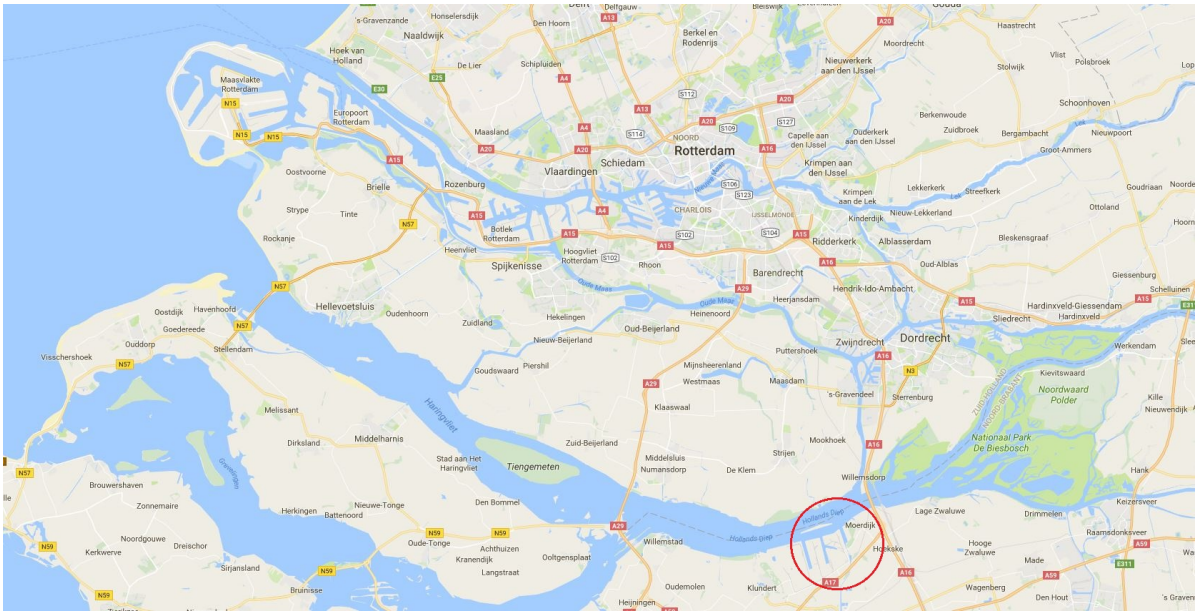

Figure 3.1: Location of Moerdijk, The Netherlands

Figure 3.2: Location of the jetty from Kolb Seagull

The exposure class is XF2: moderate water saturation, with de-icing agent. Table 3.1 provides information regarding characteristic levels of the terrain and water levels.

Figure 3.3: Zoom in at location of the jetty from Kolb Seagull

Reference level	Level with respect to NAP
Terrain	+4.5 m
Abutment	+4.5 m
MHW	+0.73 m
MLW	+0.36 m
Depth harbor	± -8.4 m
Level top access bridge	+5.14 m

Table 3.1: Terrain and water levels with respect to NAP

Design ships

Design ships give dimensions of the expected ships to berth at the jetty. Besides dimensions, also type, weight, water movement, berth velocity, and approach angle are often given in order to account for all the loads on the jetty. However, the jetty itself does not facilitates a berthing place. In front of the jetty, duckdalfs are placed. These duckdalves function as berthing facilities for the harboring ships. It is assumed that wave attack on the jetty is negligible. Hence, no information regarding the design ships is needed.

Safety

The main products which will be unloaded at the jetty are fatty alcohol's. The products are classified as ADR Class 9; UN 3082. ADR Class 9 stands for "miscellaneous dangerous substances and articles" (Rijksinstituut voor Gezondheid en Milieu, n.d.).

Spilling of these alcohols may occur during unloading of the product, when a defect occurs, or when a calamity occurs. Therefore, the potential influence of these alcohols on the jetty structure, if any, should be investigated.

Corrosion
In the program of requirements for the original jetty, no allowances of the amount of corrosion was stated. Instead, the protection which had to be applied was stated. In open water, a coating has to be applied till a depth of 2 m below bottom level. The possibility of sand erosion or removal has to be taken into account. The protection may be combined with cathodic protection.

3.4.1. Design guidelines for the jetty
The loads and the design of the jetty have to comply with the following guidelines:

Item	Norm
Loads	NEN-EN 1990+A1+A1/C2/NL. 'Eurocode 0: Grondslagen voor constructief ontwerp', december 2011 NEN-EN 1991-1-1. 'Eurocde 1: Belastingen op constructies - Deel 1-1: Algemene belastingen'
Concrete	NEN-EN 1992-1-1+C2/NB. 'Eurocde 2: Ontwerp en berekening van betonconstructies', november 2011
Steel	NEN-EN 1993-5 & NB. 'Eurocde 3: Ontwerp en berekening van staalconstructies'
Foundation	NEN-EN 1997-1/NB. 'Eurcode 7: Geotechnisch ontwerp', juni 2012
Emergency exits	ADN 2015: Europese overeenkomst voor het internationale vervoer van gevaarlijke goederen over de binnenwateren

Table 3.2: Required design norms and rules to which the jetty has to comply

The first design will attempt to exclude the usage of concrete and steel, creating a jetty which is only made of FRP. For FRP, the guidelines as described in the CUR96: 'Vezelversterkte kunststoffen in bouwkunde en civieltechnische draagconstructies' are used (de Boer et al., 2016).

3.4.2. Jetty dimensions
Table 3.3 presents the required dimensions of the jetty.

Platform	
Length	10 m
Width	5 m
Level upper deck	NAP +4.5 m
Contract depth	NAP -7.5 m at berth line
Bottom level	± NAP -9.0 m
Access bridge	
Length	30 m (perpendicular on the slope, dependent on connection point)
Width	2 m
Width walkway	1.00 m
Spacing for pipe supports	2.5 m

Table 3.3: Requirement dimensions of the main components of the jetty

3.4.3. Jetty facilities
The jetty has to be equipped with several facilities. Rainwater has to be able to be discarded. Also, polluted water needs to be discarded. This can be done with a sumput and a return pipe to the shore. The program of requirements states that this sumput should be made from stainless steel.

The platform itself should be watertight.

On the access bridge, a pipeline for the product needs to be supported, as well as a return pipe from the sumput and a cable duct for electrical cables and data cables. The design of these elements are not regarded in this MSc thesis. However, their weight has been accounted for in the design of the FRP jetty.
The berth facilities are not regarded in this MSc thesis.

3.5. Loads and load cases

In this section, the assumed loads in the case study are elaborated. An overview of the load cases, eventually used in the detailed design in the FEM model, is presented in Appendix C. Table 3.4 presents the volumetric weight properties used for the strength, stiffness, and stability calculations for the jetty.

Volumetric weight or load	Quantity	Unit
Dry soil	18	kN/m^3
Saturated soil	20	kN/m^3
Water	10	kN/m^3
Reinforced concrete	25	kN/m^3
Masonry	22	kN/m^3
Railing	1.5	kN/m
Pipe including facilities and content	2	kN/m^2
Drainage hole, including polluted water	5	kN/m^2

Table 3.4: Volumetric weight and permanent loads

The main variable loads on the platform are presented in Table 3.5. Different variable loads on the platform and the access bridge are defined as well as wind loads. Loads due to waves have not been taken into account. The jetty is located in sheltered waters so the wave attack is assumed to be negligible. On the deck a marine loading arm is mounted. Table 3.6 presents these loads.

Load	Variable load	Unit
Platform	20	kN/m^2
Access bridge	5	kN/m^2
Wind in longitudinal direction	2	kN/m^1
Wind in perpendicular direction	2	kN/m^1

Table 3.5: Variable loads

Vertical force	80 kN
Horizontal force	35 kN
Moment	250 kNm
Wind velocity	40 m/s

Table 3.6: Loads due to the marine loading arm

The temperatures ranges in the summer are set from 28 C° to 19 C° and in the winter from –28 C° to –19 C°.

3.6. Pictures from the site visit

On 20-10-2016 a site visit to the case study was conducted. At the time, the jetty was under construction. This section provides pictures of the site visit. Figure 3.4 and Figure 3.5 show the left side and the right side of the jetty from the bank respectively. These pictures give a good idea of how the jetty is constructed. The jetty consists of an access bridge and a main deck, supported by concrete piles. On top of these concrete piles for the access bridge, beams are placed in order to support the access bridge itself. Figure 3.6 illustrates this in a closeup.

Figure 3.4: Left view from jetty from the bank

Figure 3.7 shows the abutment of the access bridge. Steel reinforcement of the access bridge is connected to the abutment which stabilizes the jetty.
Figure 3.9 shows a closeup of the support beam. Once the pile is driven, a temporary construction support is made of wooden blocks and steel beams. On top of this temporary support, a prefab concrete support beam is placed. On top of this support beam the deck beam is placed. Figure 3.8 illustrates a top view of two deck beams resting on a support beam. Nine bars of steel reinforcement from the concrete pile are visible in this picture as well. The reinforcement steel of the piles, the support beam and the deck beams will be casted together in a concrete joint.
Figure 3.10 shows the reinforcement steel of the pedestal where the loading arm will be placed. The pedestal will be made of concrete and reinforcement steel and transfers the loads from the loading arm to the deck. Figure 3.11 shows the dewatering hole in the deck. The main goods which will be handled on the jetty are fats. These can contain water and therefore need to be collected. In the dewatering hole a tank will be placed in order to capture the contaminated water.

3.7. Technical drawings of the existing situation and jetty

A variety of drawings is available regarding the harbor and the technical design. Figure 3.12 and Figure 3.13 present cross sections of the harbor and the embankment, respectively.

Figure 3.5: Right view from jetty from bank

Figure 3.6: Pile foundation, support beam and access bridge

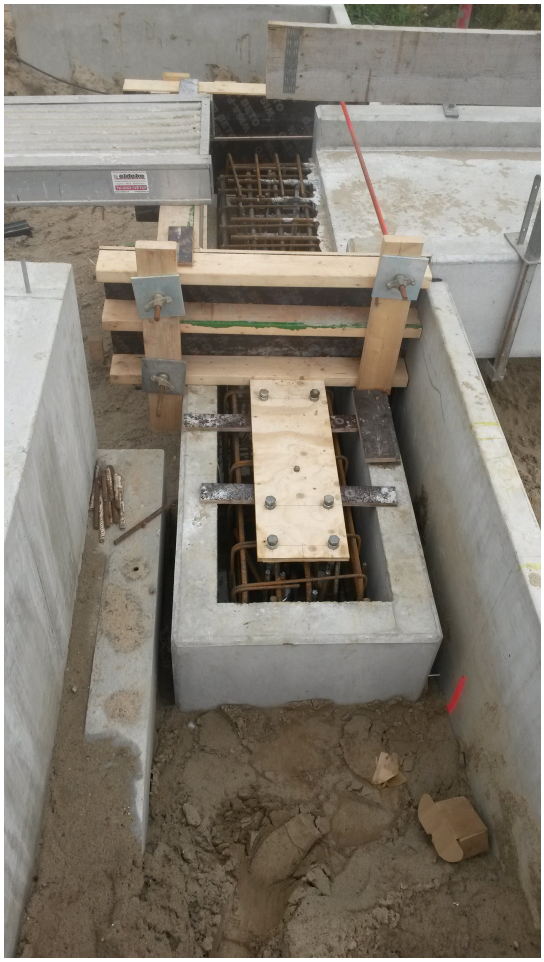

Figure 3.7: Abutment of the access bridge

Figure 3.8: The end of two deck beams resting on the support beam

Figure 3.9: Closeup support beam and temporary construction support

Figure 3.10: The reinforcement steel placed for the platform supporting the crane

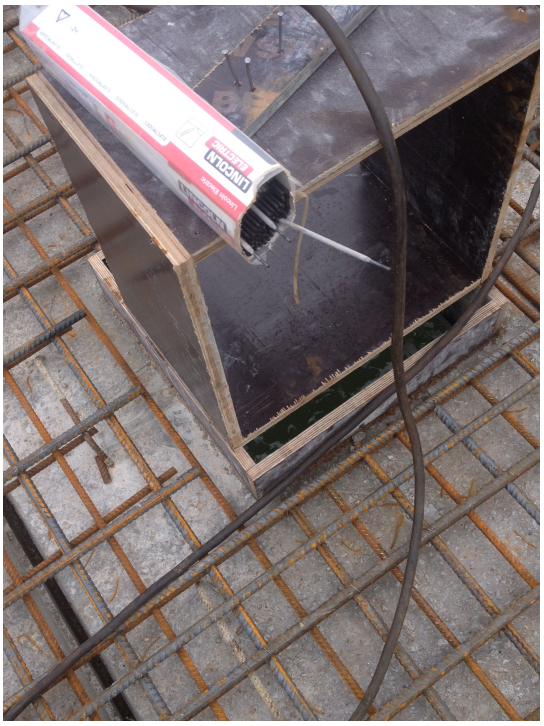

Figure 3.11: A dewatering hole in the deck. A tank will capture residual polluted water here.

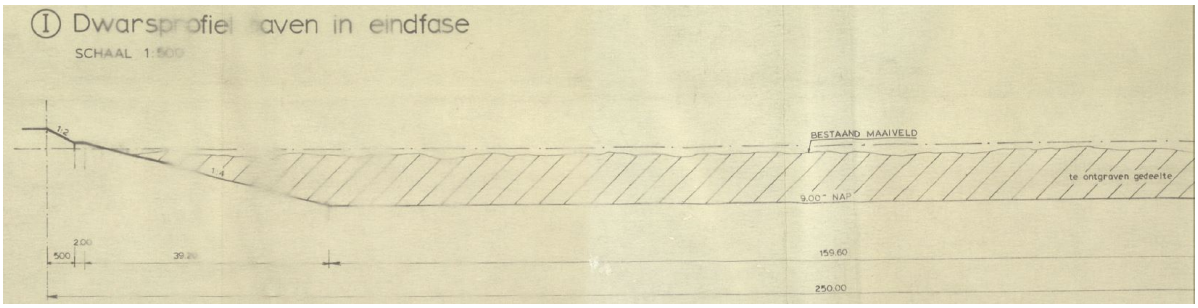

Figure 3.12: Cross section harbor

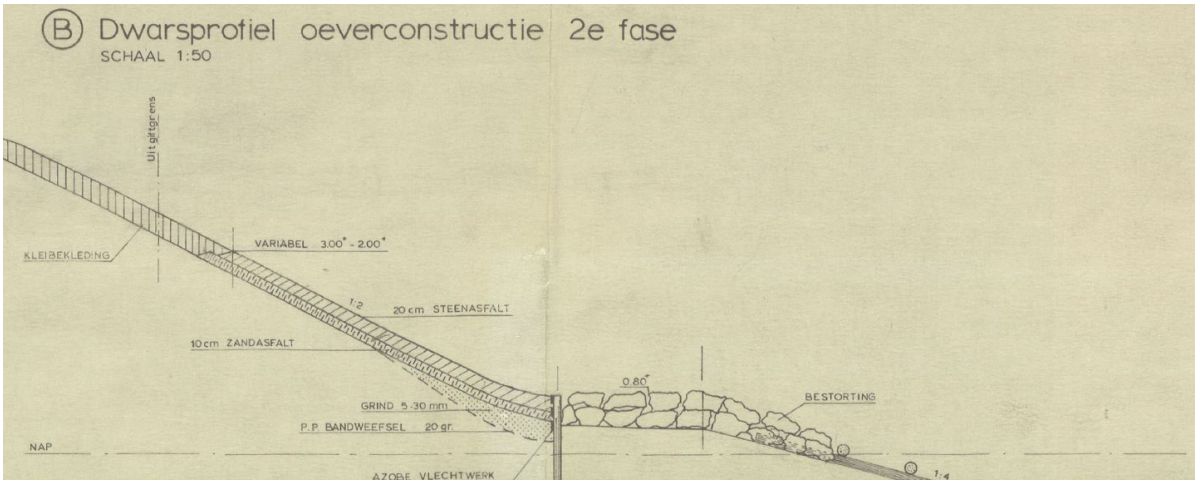

Figure 3.13: Cross section embankment

3.8. Structural design of the case study

3.8.1. Structural description of the model

Three main elements can be distinguished in the jetty: the access bridge, the platform, and the pile foundation. Furthermore, the jetty is mainly constructed out of prefab concrete construction elements. The main elements are beams, edge beams, plates and piles. The prefab elements are equipped with lifting eyes or stirrups in order to provide lifting points. The jetty is assembled with a crane. Also, steel reinforcement protrudes from the concrete. The prefab elements are connected by pouring a concrete floor on these elements. This floor bonds the elements together through the protruding steel reinforcement.

The piles are driven into the ground and trimmed. For the access bridge, beams with openings are placed on top of the piles, where the protruding steel from the piles sticks through. The piles and the beam are then casted together with concrete. Between these pile-beam combinations, prefab deck elements are placed. All the elements up to the platform are then casted together.

The platform gets constructed in a similar way. The piles are driven and trimmed, and on top of these beams with openings are placed. Then, deck slabs are placed between the beams and a continuous deck is poured.

3.8.2. SCIA model

The jetty is modeled as a 3D-plate construction. The calculations are executed with the finite element software Scia Engineer. A mesh size of 275 mm has been used. The calculation makes use of the Mindlin calculation method. Figure 3.14 gives a visual impression of the model.

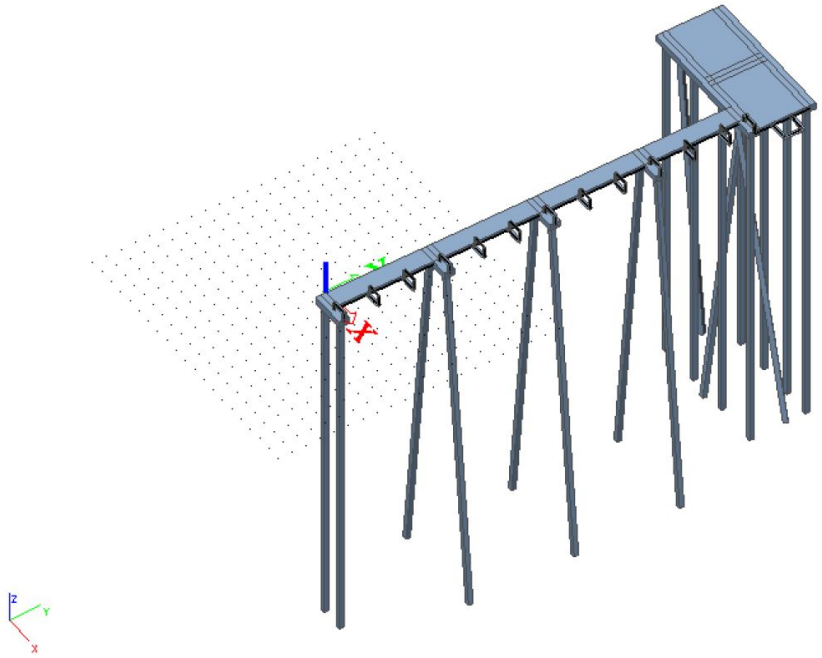

Figure 3.14: Scia model of the jetty

3.8.3. Foundation

For the project, a cone penetration test were executed at several locations. Also, two boring samples have been taken, one at the bank (B1), and one at the planned location of the jetty(B2).

The boring at the bank (B1) shows that the first couple of meters exists of sand, followed by a few meters of clay. Then, a peat layer of 2 m follows. This may give consolidation problems when loaded. Then, thing layers of sand, clay, and loam alternate till a depth of about NAP –24 m. From this depth a sand layer is present container small amounts of loam and peat.
The boring at the planned location of jetty starts at about NAP –8 m (because the boring is located in the harbor basin).
Results of cone penetration tests can be found in Appendix A.1. The boring samples can be found in Appendix A.2. Till a depth of about NAP –20 m mainly loam is found with occasional sand layers of about 2 m thick. From there, the same consistency is found as in boring B1. The layer is mainly sand with small amounts of loam and peat.

For the piles, the stiffnesses of the soil are modeled as springs. For the pile shaft: $k_x = k_y = 1500\,\text{kN/m}^2$ and $3000\,\text{kN/m}^2$. For the pile tip: $k_z = 100\,000\,\text{kN/m}$ and $k_x = k_y = 10\,000\,\text{kN/m}$. The dimension of the prefab piles are 320x320mm. The calculations resulted in the maximum compression forces of 242 kN in the serviceability limit state (SLS) and 309 kN in the ultimate limit state (ULS). The smallest bearing capacity found for the different locations of the piles was 471 kN. Figure 3.15 presents the pile plan for the jetty. Next to the piles, the intrusion angle and rotational angle are given if applicable. In total, 18 piles were installed (excluding the abutment piles).

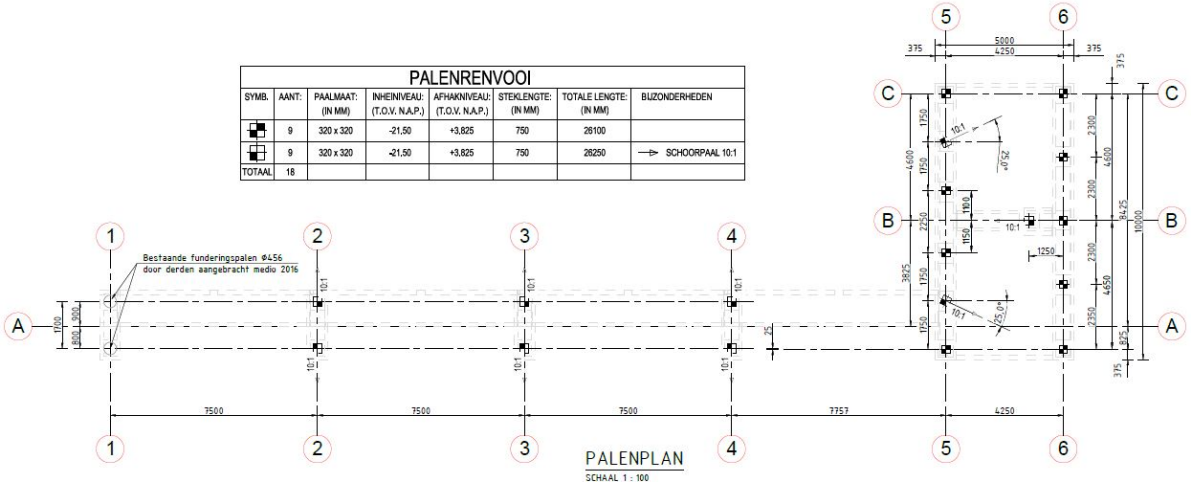

Figure 3.15: Pile plan for the jetty

I

Technical feasibility

"Can the structural integrity of a jetty, fully constructed of FRP, be guaranteed with at least the same safety levels required for RC jetties?"

4

Preliminary design

The preliminary design aims to provide a starting point for the detailed design. This section starts with defining the project boundaries. Then it defines the design objective and sets the physical project boundaries; design metrics are presented after this. These design metrics are needed in order to evaluate the designs. With these project boundaries and design metrics set preliminary design can be made. At the end of this section, these preliminary designs are evaluated in both a qualitative and a quantitative way and a one design is selected for further elaboration.

4.1. System boundaries & design metrics

4.1.1. Design objective and physical project boundaries

The jetty which will be designed will encompass the access bridge, the platform, pile foundation, and the railing. It does not include the onshore bollards, the dolphins, and the abutment. The loading crane and transport pipes are the same as used in the conventional design.

The focus lies on designing the primary components of the jetty. The following items are to be designed for the jetty:

- Platform (also referred to as "deck")
- Access bridge
- (Pile) foundation

Secondary objects which are desirable when delivering a project will not be designed. These include:

- Access stairway (gangway)
- Abutment
- Dolphins
- Onshore bollards
- Safety rails
- Pipe supports

Furthermore, several other items are incorporated with the jetty, hence they fall within the project scope. However, they do not have to be designed.

- Loading arm
- Transport pipes
- Sumput
- Cable trench

The following items are not regarded in the technical design:

- The influence of the products on the structural integrity of the jetty (e.g. alcoholic fats)
- The influence of hygrothermal effects

Figure 4.1 and Figure 4.2 illustrate the components which will be designed in a top view and a side view, respectively.

Figure 4.1: Top view of the boundary conditions

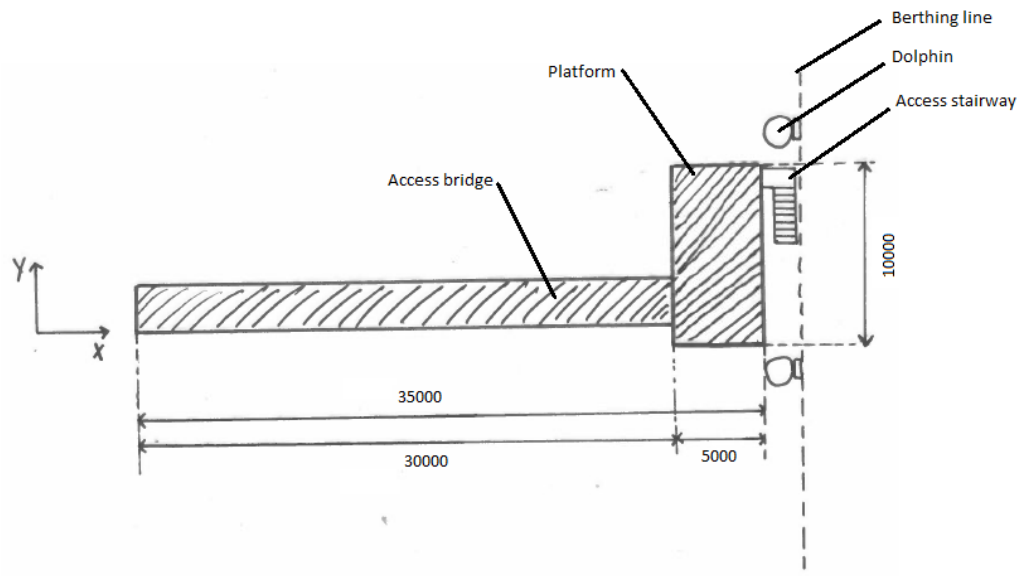

Figure 4.2: Side view of the boundary conditions

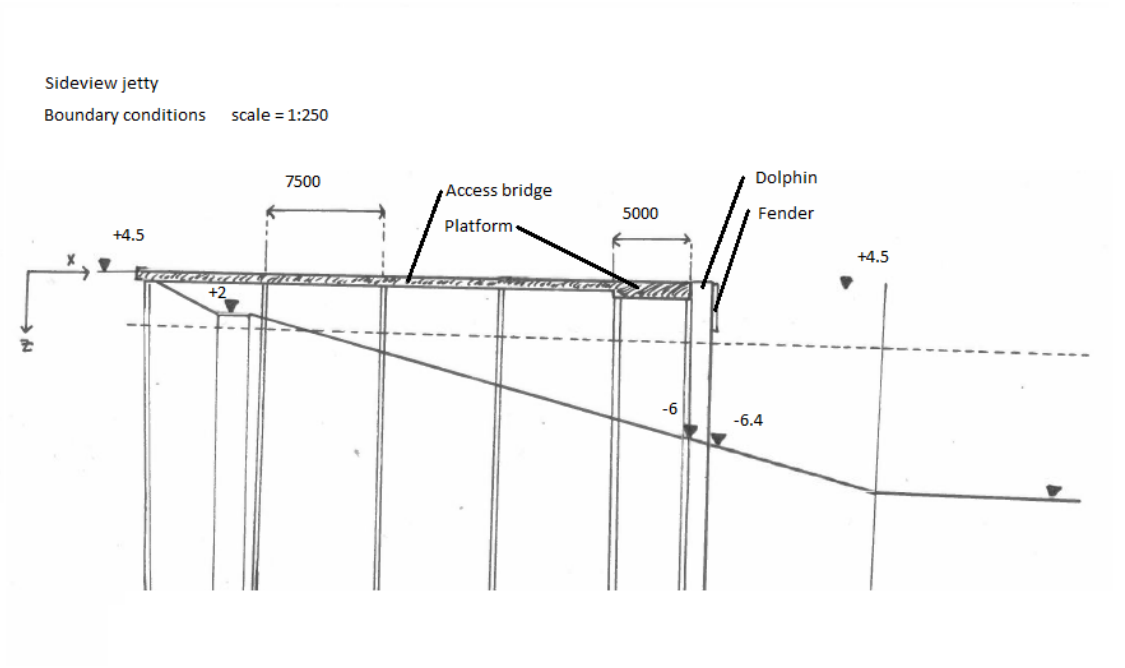

Table 4.1 gives an overview of the components which have to be designed and if they reside within the scope.

Component	Inside design scope	
	Yes	No
Platform	✓	
Access bridge	✓	
Foundation	✓	
Safety rails		✗
Abutment		✗
Loading arm		✗
Transport pipes		✗
Access stairway		✗
Dolphins		✗
Onshore bollards		✗
Bed Protection		✗

Table 4.1: Physical boundaries jetty

4.1.2. Design metrics

Metrics measure the performance of a structure. They indicate how well the structure scores given a certain interest. By formulating design metrics, a direction is given for the design of the preliminary designs. Since the performance of these preliminary designs is measured by the design metrics, each design is created in such way that the total value of the metrics is maximized. The primary design metrics set for this project are:

1. Structural integrity
2. Durability
3. Sustainability
4. Costs
5. Constructibility

Another primary design metric, robustness, may be selected. This relates to the impact resistance of the structure. However, the jetty itself is protected by a dolphin construction. Also, the topic is quite comprehensive. Therefore the design is not checked for robustness. The remaining metrics are defined here:

Structural integrity can be measured with criteria for the ULS and SLS. With these criteria, the structure either suffices or it doesn't. However, over-dimensioning the structure regarding structural requirements might negatively influence the performance regarding other metrics such as costs and sustainability.

Durability relates to how long a structure can comply with its functional requirements. The lifetime of the structure is an important parameter for this. The durability of a structure also influences the maintenance policy and vice versa.

Sustainability in general is a very broad concept and can be measured in various ways. Henk Jonkers provided a workable definition to make a sustainable design (Jonkers. H.M., 2016) (This is not a quantitative formula, moreover a definition for what aspects should be regarded in a sustainable design.):

$$\text{sustainable design} = \frac{\text{functional performance} \times \text{service life}}{\text{environmental impact}}$$

Three aspects appear in this equation: functional performance, service life, and environmental impact.
The functional performance is the quality of the design. Does the design comply with all the criteria? How durable is it? Can it withstand all expected loads?
The service life is the timespan in which the design can perform its intended functions. This is also called the technical life time of the function. The technical life time is different from the economic life time. The economic life time is the time span in which the design needs to perform its intended functions in such way that it is commercially useful.
The environmental impact off the FRP jetty is quantified with with a LCA, see Chapter 7.

Costs relate to how much financial capacity is required to realize the structure and can be expressed in monetary units. In this thesis the monetary unit is euro.

Constructibility is the ease by which constructions can be installed. This metric makes up the technical feasibility together with the structural integrity metric.

These primary metrics depend upon quantifiable units. In this thesis, they are called secondary metrics. An example of a secondary metric is the material quantity: it affects multiple primary metrics. Table 4.3 gives an overview which secondary metrics influence primary metrics. Note that the relation between the primary and secondary metrics can be ambiguous: their relation is relative.

Table 4.2: Influence of secondary metrics on the primary design metrics

Secondary metrics	Design metrics: Structural integrity	Durability	Sustainability	Costs	Constructibility
Material type	×	×	×	×	×
Material quantity	×	×	×	×	×
Material quality	×	×	×	×	×
Distance production location			×	×	
Design life time	×	×	×	×	×
Maintenance policy	×	×	×	×	
Weight					×

Table 4.3: Influence of secondary metrics on the primary design metrics

Secondary metrics	Design metrics: Structural integrity	Durability	Sustainability	Costs	Constructibility
Material Type	×	×	×	×	×
Material quantity	×	×	×	×	×
Material quality	×	×	×	×	×
Distance production location			×	×	
Design life time	×	×	×	×	×
Maintenance policy	×	×	×	×	
Weight					×

4.2. Life Cycle Assessment

An LCA is a tool which can be used to quantify the environmental impact of a product, process or construction (in this text there will be referred to a construction) (H. M. Jonkers, 2016). This methodology identifies the life cycles of a construction. The life cycle which are treated may be freely chosen. However it is important to clearly define them in order to compare a construction to other types of constructions. Then, these life cycles are assessed on their contribution to the total environmental impact of the construction. Insight of the different processes and life cycle stages is achieved and can be used to improve future designs regarding environmental impact.

An LCA consists of four steps according to the ISO 14040 standard (H. M. Jonkers, 2016):

1. Define the goal and scope of the LCA
2. Make an Life Cycle Inventory (LCI). This is a list of input and output materials and processes of the concerned life cycle stages
3. Execute the impact assessment with the help of emission data for different processes and materials. This is also called the Life Cycle Impact Assessment (LCIA)
4. Evaluate the LCA, giving a critical reflection and a discussion on the assessment

In order to include sustainability as a design metric, the goal and scope of the LCA already have to be defined in order to integrate this into the design process. Therefore, Section 4.2.1 provides a scope for the LCA and the goal of the LCA. Chapter 7 further elaborates these steps and the LCA itself.

4.2.1. Goal and scope of the LCA

This section provides a scope and a goal for the LCA.

The goal of this LCA is:

> *"Compare the environmental impact of an fiber reinforced polymer jetty and a conventional jetty constructed of steel and concrete, both having the same technical requirements regarding structural integrity, durability, and lifespan"*

The LCA acts as a tool to quantify the metric of sustainability for the two constructions.

The functional unit is defined as the total jetty, which encompasses the access bridge, the platform, pile foundation, and the railing. It does not include the onshore bollards, the dolphins, and the abutment. Also, the loading crane and transport pipes are excluded from the functional unit. These items are not taken into account because they are the same for the conventional jetty as they are for the FRP jetty.
The functional unit largely coincides with the physical boundaries of the jetties as described in Section 4.1.1.

Figure 4.3 defines the system boundaries and illustrates the general flow patterns and processes when constructing a jetty. These processes will be regarded in the LCA. Four main life phases are identified: the production of the construction materials in a factory, the construction of the jetty itself, the usage phase and the end of life phase. Every phase requires different machinery and equipment in order to complete the processes or tasks. The time span for the usage phase is set equal to the lifetime of the structure, which is 50 years.

For the LCA, the following environmental impact categories will be taken into account:

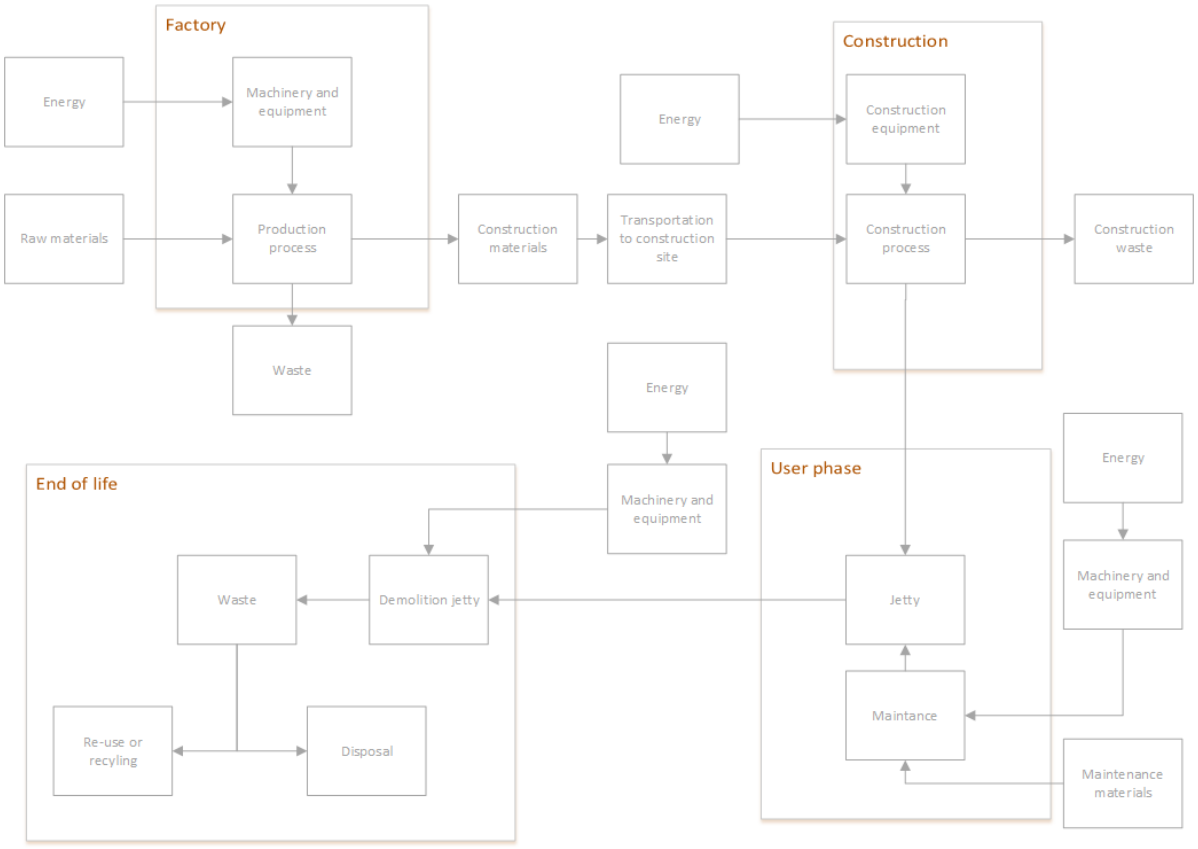

Figure 4.3: The elements which will be include into the LCA

1. Global Warming Potential (GWP)
2. Ozone Depletion Potential (ODP)
3. Abiotic Depletion Potential (ADP)
4. Human Toxicity Potential (HTP)
5. Fresh Water Aquatic Ecotoxicity Potential (FAETP)
6. Marine Aquatic Ecotoxicity Potential (MAETP)
7. Terrestrial Ecotoxicity Potential (TETP)
8. Photochemical Oxidation Potential (POCP)
9. Acidification Potential (AP)
10. Eutrophication Potential (EP)

In recent time, the topic of FRP has been present in several theses at the Hydraulic Engineering department of the Delft University of Technology. In order to compare the LCA on different constructions, the impact categories chosen are the same as used in the theses of Trude Maas (Maas, 2011) and Ramon van der Valk (Van Der Valk, 2017). Trude Maas also included the following additional environmental impact categories: biotic depletion potential, energy depletion potential, and land use.

4.3. Alternatives to the jetty

In essence, a jetty might not necessarily needed. What is needed, is a facility to berth a ship and the possibility to unload the product. Multiple solutions are able to facilitate these functions. Therefore, a small variant study is executed.
The main criteria are:

- Minimize costs
- Leave the dimensions of the harbor intact
- Fast deliver of the structure

The main functions are:

- Facilitation of a mooring place at NAP +4.5 m

The main objective of this thesis is to assess whether FRP jetties are better alternatives than concrete and steel jetties. However, other hydraulic structures may fulfill the same functions as the jetty does. For a complete overview, several alternatives are highlighted in this section. These however, are not further elaborated in the scope of this thesis.

Figure 4.4 illustrates some variants which could fulfill the berthing function and the placing of the loading arm. These include:

- Quay wall
- Extended quay wall
- Floating platform
- Bridge

When constructing the quay wall, a lot of soil needs to be dredged. In case of heavy sedimentation, the harbor needs to be dredged often, resulting in high maintenance costs. The extended quay wall requires a lot of sand. Also, the bathymetry of the harbor changes, which may come with legal challenges. Also, the quay wall and the extended quay wall are strong but require a lot of material. The loads in this project are not severe, therefore a jetty may be the most efficient solution in terms of material usage.
With the jetty being chosen as the variant which will be elaborated, several preliminary designs can be created. The primary and secondary metrics as defined in section Section 4.1.2 serve as guidelines for these preliminary designs.

Figure 4.4: Side view of the alternatives

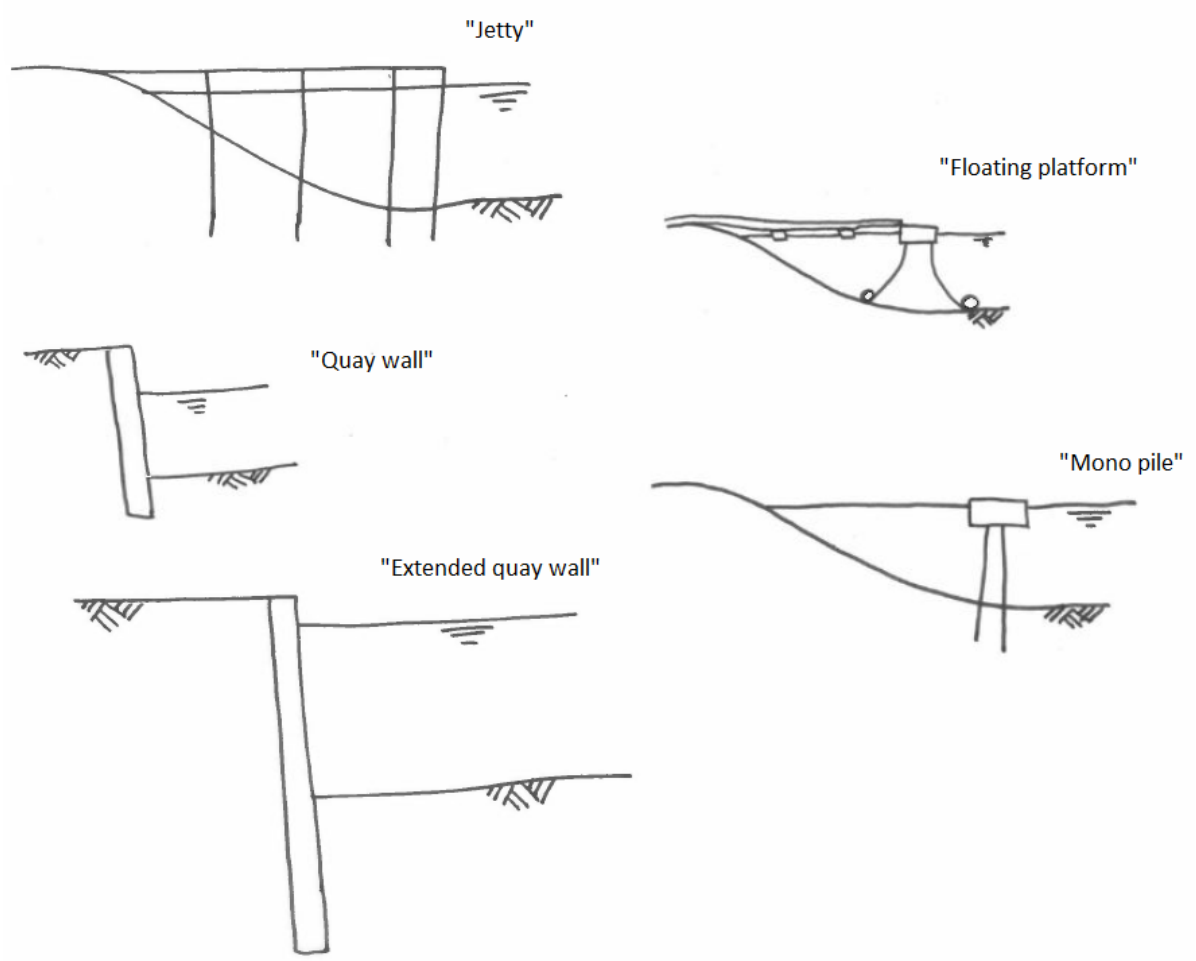

4.4. Preliminary design: Access bridge

The access bridge has to accommodate two functions: transporting workers from and to the platform of the jetty and support the pipe lines and a cable trench from the platform to the bank. In the technical requirements, the total width of the access bridge is set at 2.5 m, reserving 1.3 m for the pedestrian walkway and 1.2 m for the pipes and cable trench. Therefore, a console is made from a beam and support piles to facilitate both functionalities. The support piles also act as the foundation piles.

The variable load on the access bridge is 5 kN/m^2, which is comparable with a cyclist and pedestrian tracks on a road bridge. With this load, four different options are regarded for the deck of the pedestrian walkway: plastic planks, an FRP grating, sandwich panels, and a pultruded cross section. The pultruded cross section is illustrated in Figure 4.7, the alternative sections in Figure 4.6 and Figure 4.5 (supported on a square beam and L-beam respectively).

Figure 4.5: Variations access bridge supported on L-profile

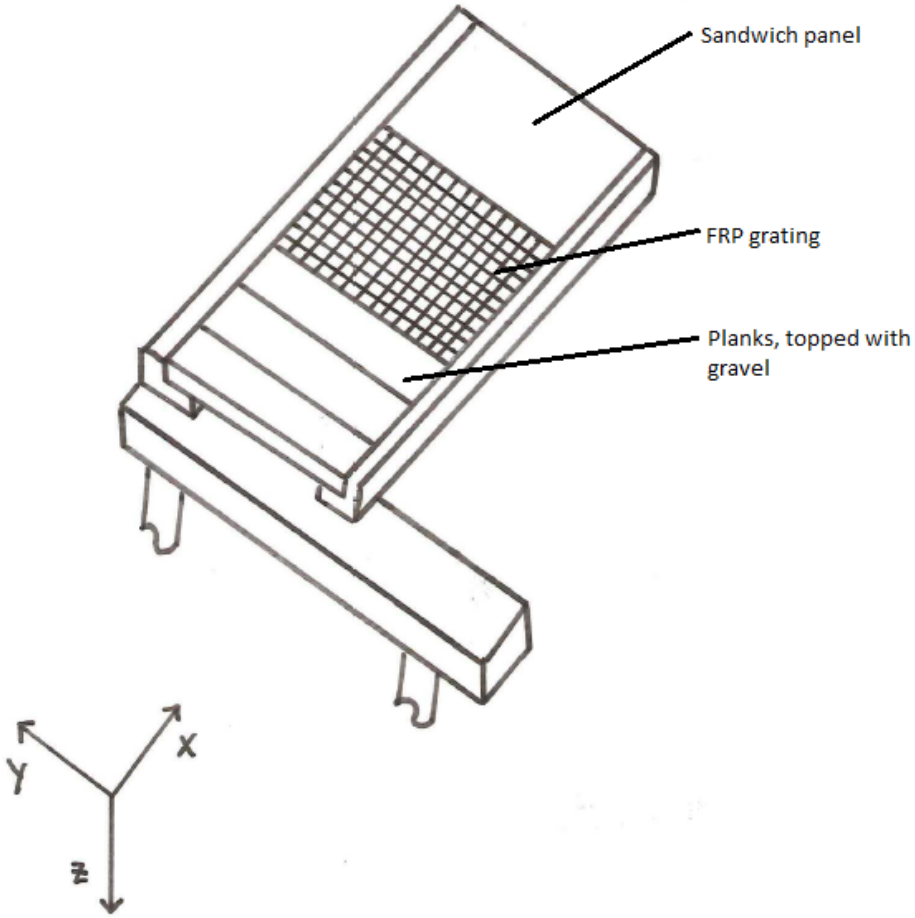

Figure 4.6: Variations access bridge

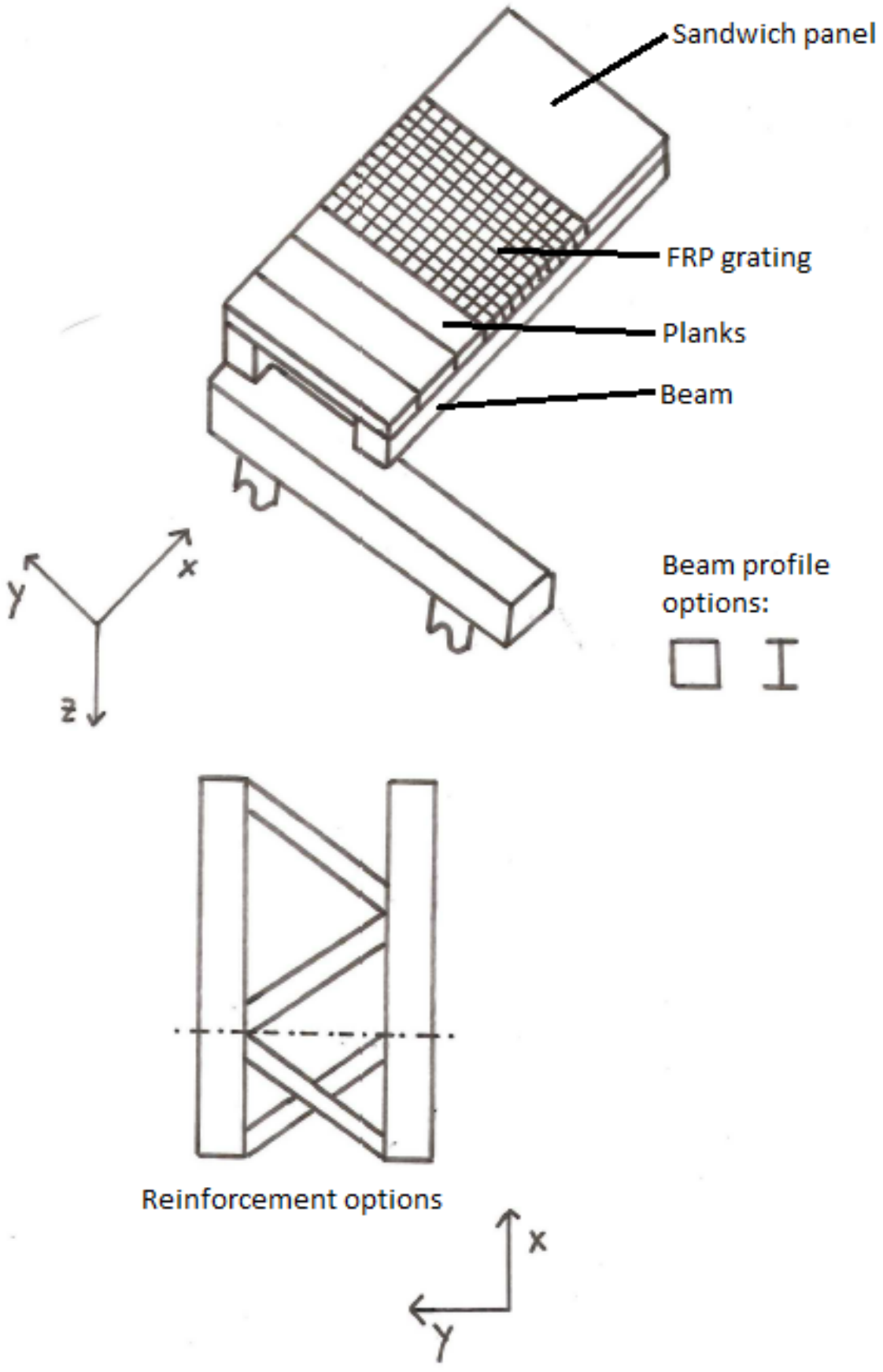

Figure 4.7: Pultruded access bridge variations

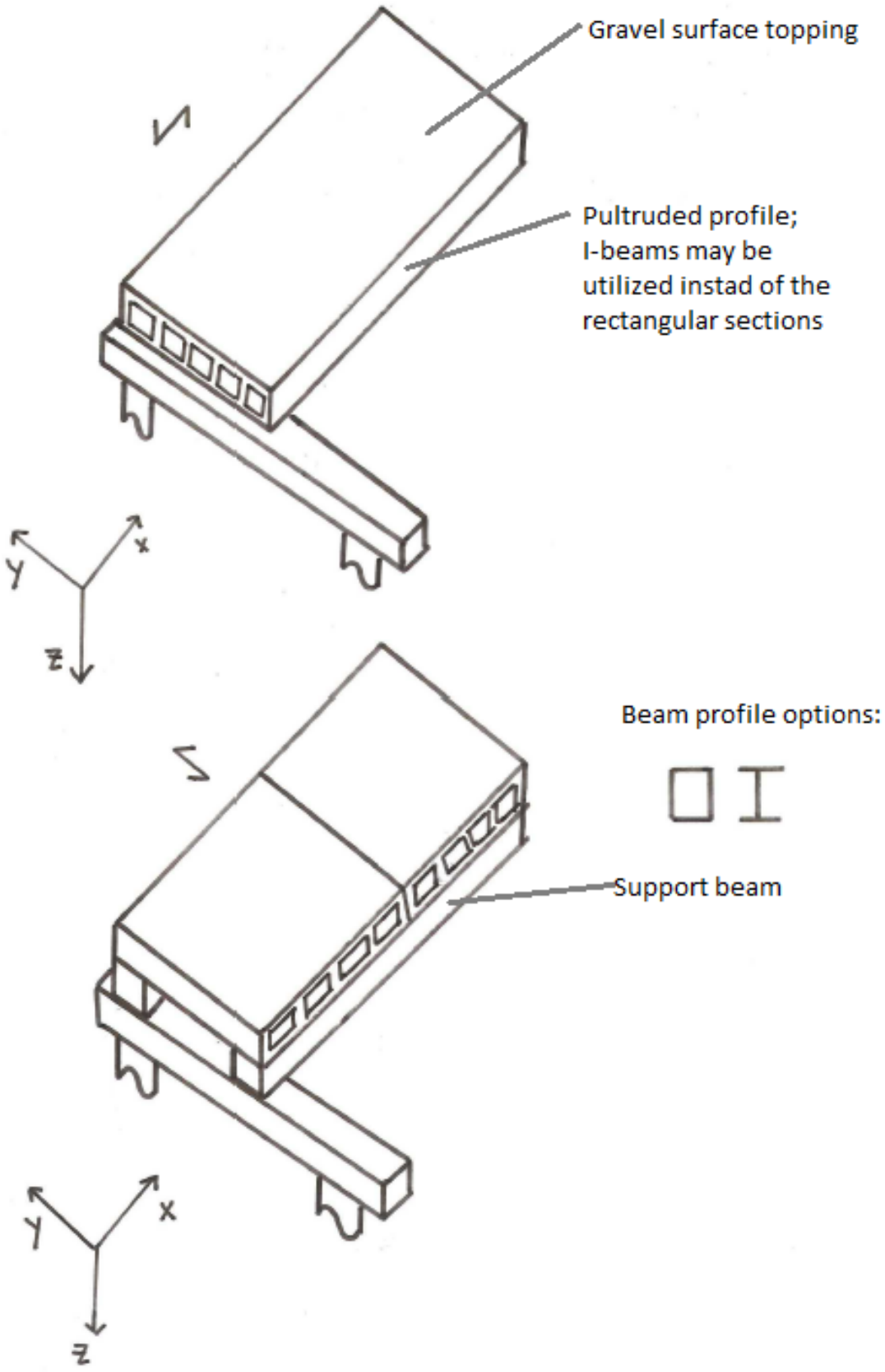

4.5. Preliminary design: Platform

The main functions of the platform are: supporting the loading arm and the transfer product, and the workers. In the technical requirements, the total width of the platform is set at 5 m width and 10 m length.

The variable load on the platform is 20 kN/m^2, which is comparable with the load of heavy traffic on a bridge. The same options are regarded for the deck of the platform as are regarded for the access bridge: plastic planks, an FRP grating, sandwich panels, and a pultruded cross section. Due to the high loads, the plastic planks and the FRP grating seem highly unlikely to be suitable. The pultruded cross section is illustrated in Figure 4.9, the other sections in Figure 4.8.

Figure 4.8: Single pultruded deck for the platform variant

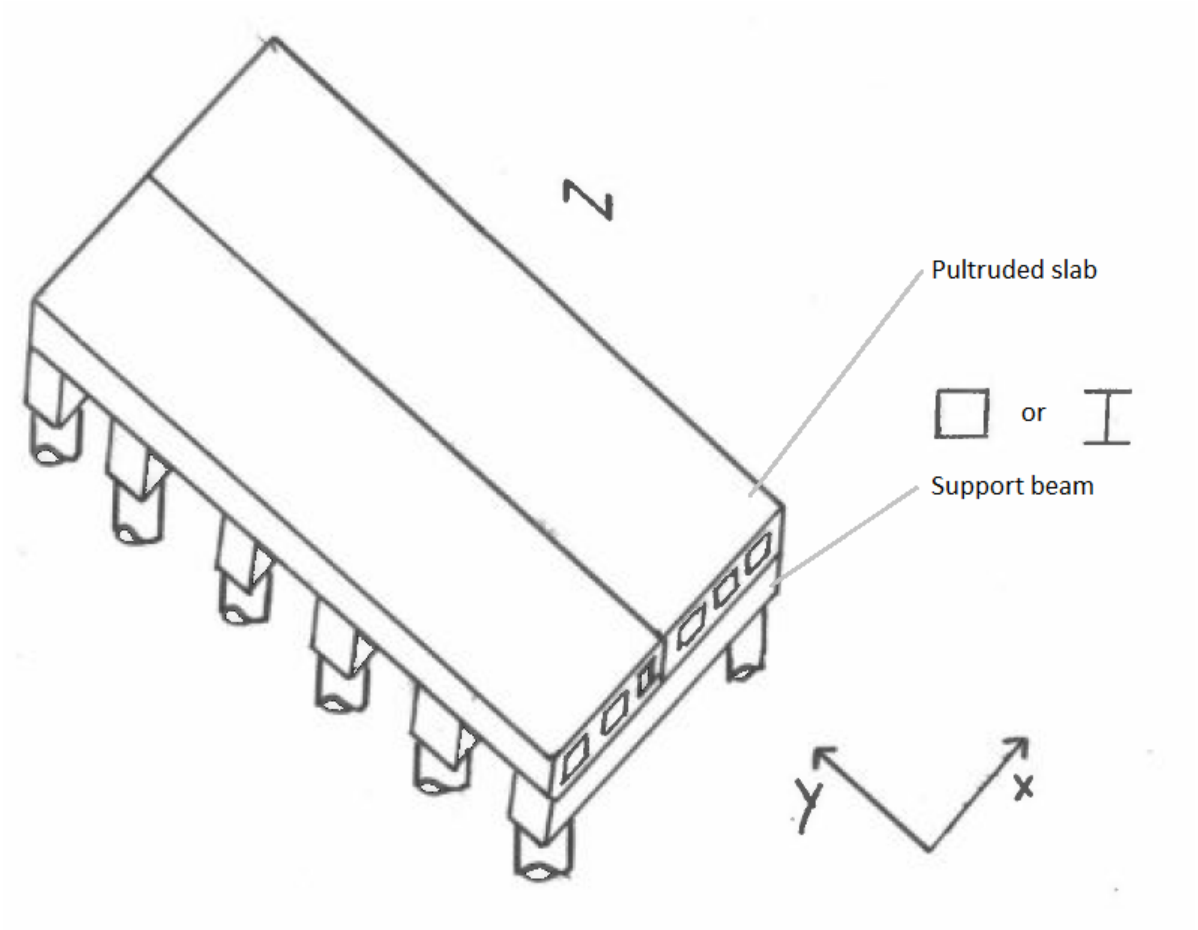

Figure 4.9: Possible variations for the platform

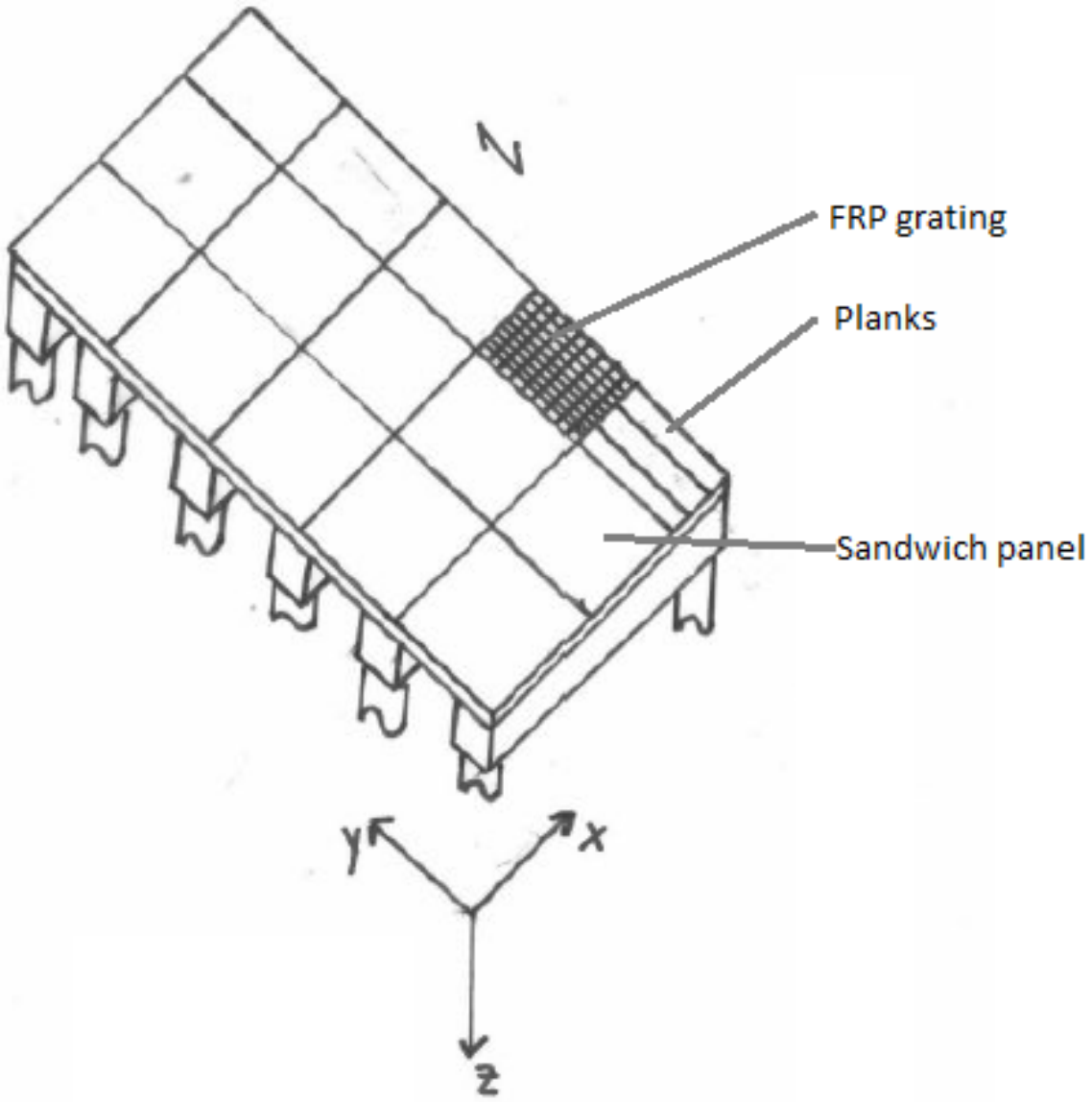

4.6. Prelminary design: Foundation

The foundation consists of a console which is formed by piles and a beam. The console supports the pedestrian walkway and the pipes and cable trench as described in Section 4.4. The overall design of the consoles depends very much on the distance between the consoles. The bigger the distance, the bigger the spans, but the fewer piles are needed. This can be optimized, resulting in a design which requires the least amount of costs or material.

Figure 4.10 illustrates different layouts for the console. In layout E, the piles are situated at the ends of the pedestrian walkway. This may be beneficial since the loads on this section are far bigger than the load of the pipes and the cable trench. If strength, stability, or deflection criteria are not met, the piles may be reinforced by connecting them with members as depicted in F.

For the piles, the most suitable load-bearing FRP pile according to a meta study of Zyka and Mohajerani (Zyka & Mohajerani, 2016) is selected. This pile has a diameter of 475 mm, a wall thickness of 4.6 mm, a bearing capacity of 2162 kN, and an ultimate axial load capacity of 4000 kN.

The definite layout to be further elaborated is design B.

Figure 4.10: Different console layouts

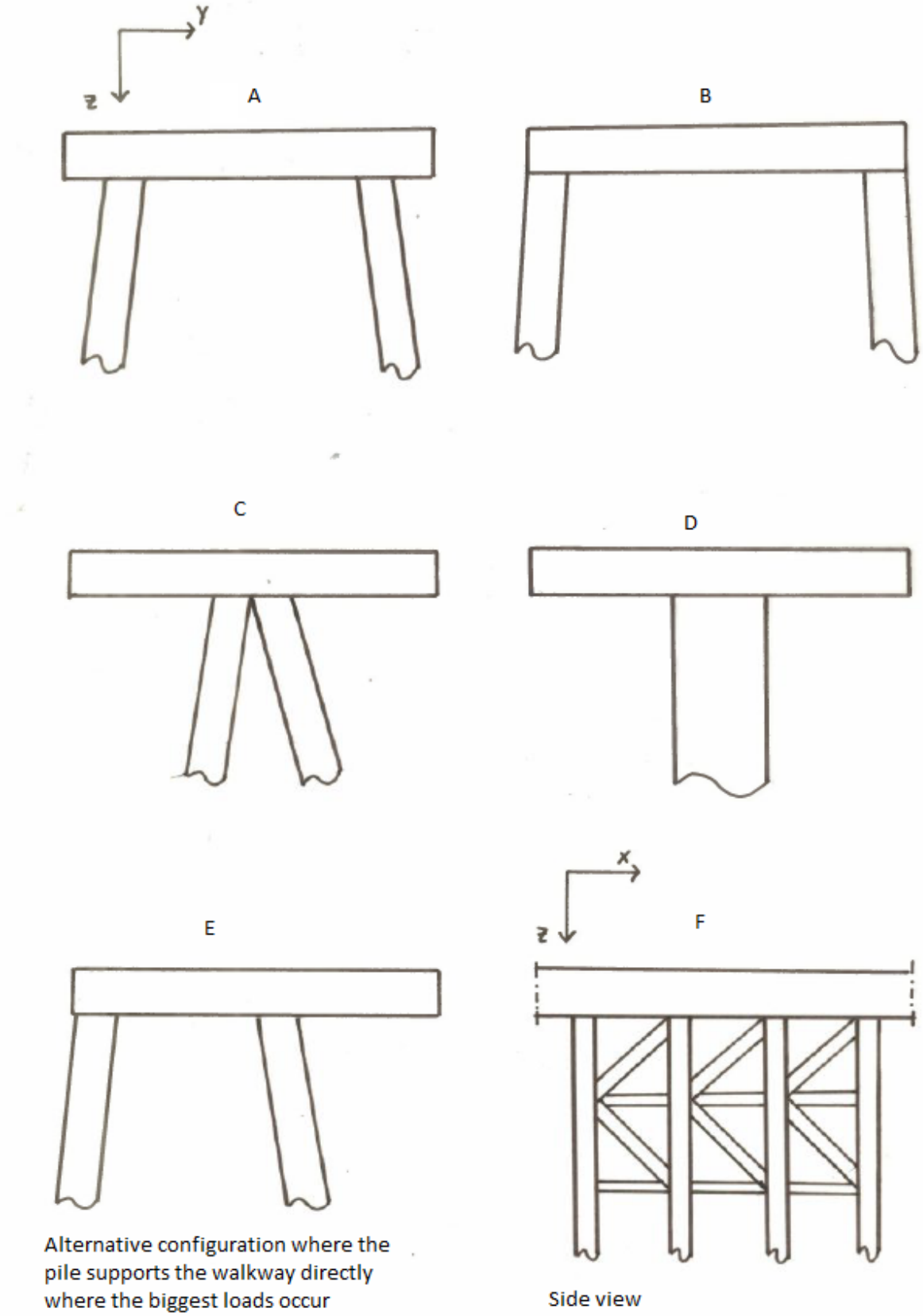

4.7. Material choice

There is a huge variety in material choice for both the resin and the fibers. For the preliminary design, the most common types in the construction industry are regarded. For resins, these are polyester, vinyl, and epoxies. For the fibers, these are glass and carbon fibers.

Thermoplastics and thermoset resins are treated in the literature study. As a starting point, a thermoset resin is selected for its better structural properties. From the three main properties stated above, the epoxy resin has the best structural performance. Therefore, initially the design will be elaborated with an epoxy resin.
However, for the pulltrusion production process, epoxies are less suitable due to their two component nature. Therefore, for structural parts produced with the pulltrusion process, a polyester or vinyl ester is used in the design.

E-glass, R-glass are most often used in the construction industry. Whilst carbon fibers have better structural properties, they are far more expensive. Of these glass fibers, E-glass is the most used due to its good strength to cost ratio. Therefore, a first design will be based on E-glass. In the detailed design when the ULS and SLS criteria have been met, deviations may be researched.

Concluding above paragraphs, the primary material choice for the jetty is a combination of E-glass and an epoxy resin due to their structural properties. In later stages of the design, when a design is elaborated which complies with the stated structural criteria, other materials can be regarded which benefit other metrics such as environmental impact.

4.8. Load and stress estimation

With a load estimation on the structure, the dimensions of the elements can be estimated. For this load estimation, a variable load of $5\,kN/m^2$ for the access bridge. For the platform, a distributed load of $24\,kN/m^2$ is taken into account. This is the distributed load multiplied by 20 % in order to account for the load of the loading arm on the platform.

4.9. Evaluation preliminary design variants

In this section, the idea behind the usage of the selection criteria for the evaluation of the preliminary design are stated. Since these criteria are not defined in the program of requirements (Section 3.4)

In general, for FRP structures in the construction industry, the SLS criteria are decisive (with respect to the ULS criteria) (de Boer et al., 2016)(Schutte, 2016). Therefore, a first check on SLS criteria will be done in order to find a suitable design. Then, the material quantity required to comply with the check is estimated so that a cost estimate can be made. Then, the economic most viable product will be selected. Other metrics as described in Section 4.1.2 will be further elaborated in later design stages.

Quantitative description

The most common SLS criteria describe limitations of deformations and vibrations.
The CUR96 states a static deflection of 1/250 times the length of the member is commonly used (de Boer et al., 2016).
FRP constructions are sensitive to vibrations (de Boer et al., 2016). The specific stiffness, that is the ratio to the stiffness of a material and its specific mass, is high for FRP. Furthermore, Justin Walop informed that when a deformation criteria of a maximum deflection of L/250 or L/300, the natural

frequency of the structural member most often is higher than 5 Hz (Walop, 2017). Also, if the natural frequency is lower than 1.25 Hz or higher than 4.6 Hz, no harmonic load has to be accounted (de Boer et al., 2016).

The bending of a simply supported beam under a distributed load q is given by (de Boer et al., 2016)

$$w_{tot} = \frac{5}{384}\frac{q * L^4}{\sum_i EI_i} + \eta\frac{1}{8}\frac{q * L^2}{\sum_i G_i A_i} \tag{4.1}$$

Where:

w_{tot}	: total midspan deflection in m
q	: distributed load in N/m
L	: length of the beam in m
EI_i	: bending stiffness of part i in Nm^2
$G_i A_i$	: shear stiffness of part i in N
η	: area correction factor dependant on the shape of the cross section

where the first part of the formula relates to Euler bending and the second part refers to Timoshenko bending. The Timoshenko bending accounts the influence of shear deformation. In general, the shear deformation can be neglected for long spans or if $EI_i >> G_i A_i$ (American Society of Civil Engineers (ACMA), 2010). For an I-beam, η = 1.0 (de Boer et al., 2016). For an evaluation of the preliminary design, shear deformation is neglected to obtain a workable formula. Together with the SLS bending requirement, the equation can be rewritten to:

$$EI_i = \frac{5}{384}\frac{q * L^4}{\delta_{max}} \tag{4.2}$$

Thus, a formula is found for a first indication of the required bending stiffness of the structural units.

The variants can be divided into two categories. First, long longitudinal support beams, topped with one of the three deck systems (planks, grating, sandwich). The three deck systems range in structural capacities and price. Secondly, a longitudinal pultruded section. This section integrates the longitudinal support beams and the deck systems into one structural element. This may lead to cost saving in production and construction.

All variants are supported by hollow FRP piles. This FRP pile seems to be the most viable pile regarding bearing capabilities and costs (Winter, 2017). However, it must be noted that the regarded piles have a length of 10 m and are driven 6 m into the ground. In the case study, the required length of the concrete piles for the jetties are 26 m and need to be installed to a depth of about 20 m. The dead weight of the FRP as a whole is expected to be less than it is for the concrete jetty. Therefore, installation depth of the piles and hence pile length may be shorter. However, regarding the preliminary design, the same required length and installation depth for the FRP piles is chosen as for the reinforced concrete piles in the case study: this will probably provide a safe upper boundary.

For the determination of the cost of the access bridge, the regarded span is an important parameter. This parameter influences many dimensions. For instance, longer span leads to larger loads on the piles, but also reduces the amount of piles required to be installed. In order to get an indication of the influence of the span length on costs, the costs for different span lengths have been estimated. The span for the access bridge in the case study is 7.5 m. The longest lengths found for FRP bridge spans are also 7.5 m (Winter, 2017). Therefore, the regarded spans in this design phase are 5.5 m, 6.5 m and 7.5 m. In a later design phase, an optimum regarding span length will be calculated.

Table 4.4 and Table 4.5 present the estimated costs for the access bridge and the platform, respectively. To make a fast first indication, standard structural members were selected from BIJL profielen (W.B. Bijl Profielen B.V., 2015b, 2015a) and Flexxcon (FlexxCon B.V., 2017). For most of them, prices were also available. When the price was unavailable, estimations were made by scaling the price of comparable units with the ratio of the areas of the available and unavailable price.

The planks are manufactured by a pultrusion process.

	L_{span}		
	5.5 m	6.5 m	7.5 m
Grating, supported by beams	40400	48100	44900
Planks, supported by beams	45500	53200	50000
Longitudinal pultruded section	55300	53200	52200

Table 4.4: Estimated costs in € for the access bridge, including the superstructure and the piles

We can conclude that for the access bridge, the most economic viable option is the grating, supported by beams.

With the experience of the preliminary design of the access bridge, the variants of the platform were narrowed down to two variants, see Figure 4.8 and Figure 4.9. Due to the larger loads on the platform (e.g. the variable load is four times bigger) the dimension of the structural members will be bigger. Therefore, the variable load on the platform in this design stage is increased with 20 % to account for the dead load with γ. This leads to a distributed load of $20 * 1.2 = 24\,\mathrm{kN/m^2}$.

For the first variant (Figure 4.8), a main support member is placed in the direction of the pile rows in order to facilitate a support edge. On these two main support members, beams are placed which will support the deck. If the main support beams would support the deck immediately while resting in the transversal direction of the platform, the amount of piles would probably be too high in order to be cost competitive or to provide a good bearing capacity by the piles.
Several shapes are convenient for the design of the beams, such as I-profiles or rectangular profiles. To determine the shape of the beam profile, the efficiency of material usage is of prime concern to reduce costs and environmental impact. The bending moment capacity and shear force capacity are important for beams because they are the sectional properties which determine the deflection of the beam. Therefore, the second moment of area should be maximized as well as the shear plane. I-profiles have proven to be efficient and are therefore selected as the beam profile.

In the second variant (Figure 4.9), the deck is integrated with the beams which support it. So, an integrated profile will span from the main support beams (which rest on the pile heads). This integrated profile may be pultruded or it can be made with vacuum assisted resin injection techniques.

Gratings are not considered for two reasons. First, span widths are limited in combination with the set deflection criteria (FlexxCon B.V., 2017). Second, polluted water needs to be collected. Due to the open structure of the grating, additional measurements have to be taken if a grating is chosen for the platform.

Figure 4.11: Preliminary design for the platform with two variants

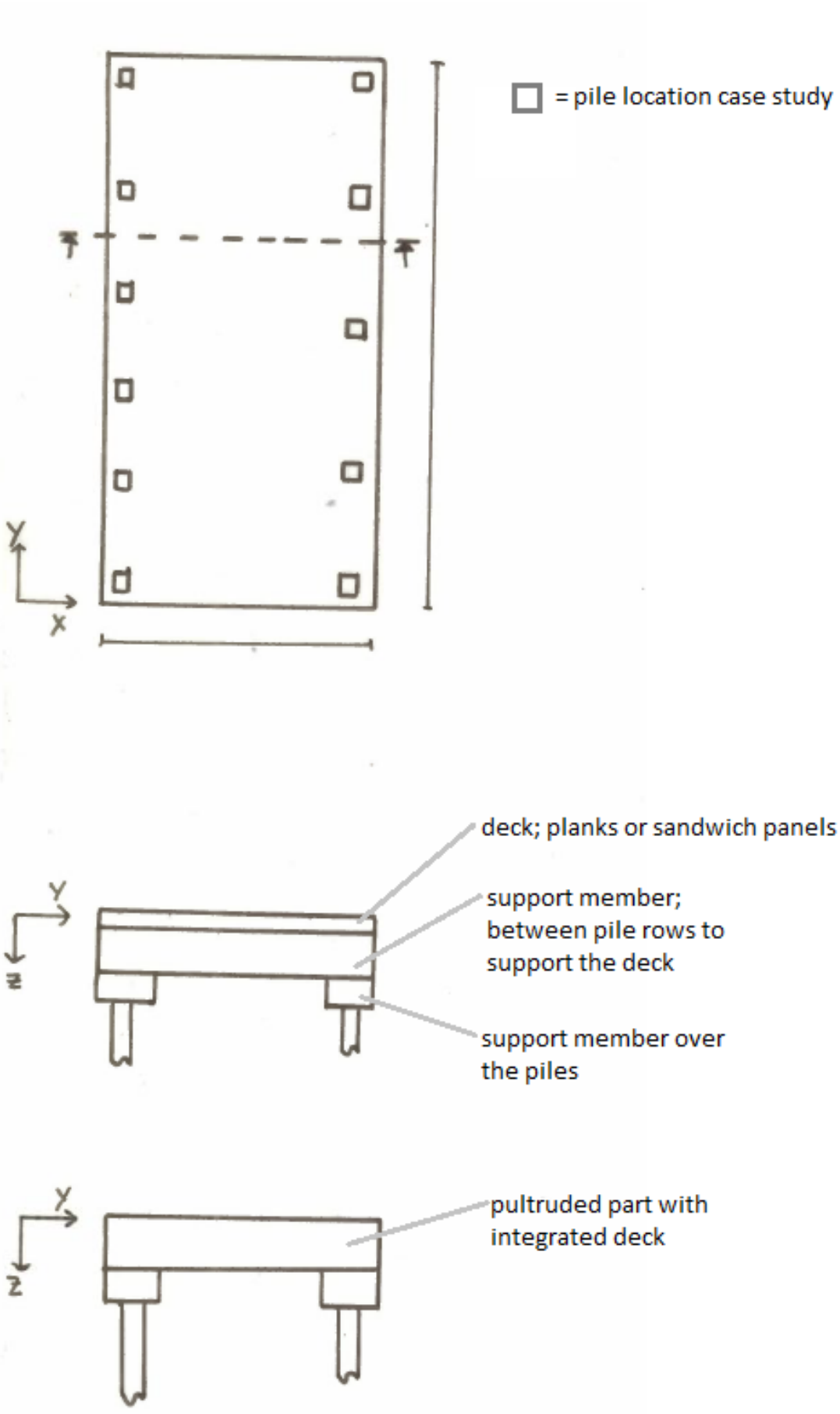

The costs for the two variants are:

Planks, supported by beams	€68.000
Longitudinal pultruded section	€90.000

Table 4.5: Estimated costs in € for the platform

Hence, for the platform the combination of planks supported by longitudinal beams is financially the most lucrative one.

For starters, the piles are located at the same locations as in the case study. Two parameters are used for an indication to the bearing capacity of the piles; the distance between the piles in the longitudinal direction of the platform (l_1) and in the transversal direction (l_2). The load on a bearing pile is approximated with:

$$P = \frac{1}{2} * l_1 * l_2 * Q_{platform} * \gamma = \frac{1}{2} * 5 * 2.3 * 20 * 1.2 = 138\,\text{kN} \tag{4.3}$$

The hollow FRP piles from BAC Technologies allegedly have a bearing capacity of circa 2162 kN and an axial load capacity of 4000 kN (Zyka & Mohajerani, 2016). These piles have a diameter of 475 mm. The bearing capacity is determined for piles with a length of 10 m and 6 m driven into the ground. So for now, it is assumed that this pile layout suffice for FRP piles as well.

Qualitative description

While the preceding quantitative analysis takes into acount primilary structural integrity and costs, more metrics determine the performance of the jetty (see Section 4.1.2). Therefore, an additional qualitative analysis is made.

Access bridge

For the access bridge, the economic most viable option seems to be a combination of two beams and a grating. Besides being the most economic option, the grating also posses other good qualities. The grating requires the least amount of material of the variants. This results in a lighter construction. Gratings are commonly made by a pultrusion process or by a molding process. The selected grating is a high load bearing grating, which is manufactured by a molding process (FlexxCon, n.d.). An isophthalic polyester is used for this grating. This means that it will not be very suitable for recycling purposes (Winter, 2017). However, the system has good durability properties; a very low maintenance and an estimated lifespan of at least 40 years (FlexxCon B.V., 2017). The actual life span may be far longer.

The grating can be attached to the beams by nuts and bolts. This may be done either on the outside of the flange or by drilling a hole in the beam. Also, the whole span can be prefabricated and then transported to the site by road- or water transport. Because the system is lightweight, it will probably be possible to install it with one or two cranes as frequently done by FiberCore for heavy duty bridges (FiberCore Europe, n.d.).

Platform

A structure of planks supported by beams seems economically the most viable option. It must be noted that the installation costs have been estimated very roughly and may be much more expensive.
Both the planks and beams combination as well as the complete pultruded section can be prefabricated in a factory. This gives the same advantage as the access bridge: only transport and installation

is needed. Also, because the structure is light weighted, probably light installation cranes will suffice for the installation of the platform.

The advantage of the complete pultruded profile is that assembling effort will be lower than the assembling effort of the planks and beams. Also, the structure is more closed, which in general leads to lower interlaminar shear stresses which may cause delamination (Nijhof, 2003).

Both concepts are made from pultruded products; a polyester resin and a glass fiber. Hence, the environmental impact is largely determined by the amount of material used and the amount of joints made.

Both concepts perform more or less equal on the regarded metrics, except for costs. The significant lower costs of the planks and beams combination is therefore decisive: this concept will be further elaborated in the detailed design phase.

Foundation
The selected foundation is a hollow FRP pile. This is based on a review of Zyka et al. of different composite piles in which the hollow FRP pile was regarded most suitable (and having the most potential) as a vertical load bearing pile composed of FRP (Zyka & Mohajerani, 2016). The pile design is elaborated in Section 5.8.

4.10. Conclusions and discussion of the preliminary design

4.10.1. Conclusions of the preliminary design

The access bridge will be constructed of two I-beams topped with an FRP grating.
The platform will be constructed of several I-beams spanning in the short direction of the platform. On top of these beams, planks will be placed to create a working platform.
The piles will be further elaborated.

The I-beams will be made of E-glass and a thermoset polyester resin. The glass fibers are selected because of their cost competitiveness and proven presentation in the construction industry. The polyester resin is selected because it lends itself best for the pulltrusion process. The planks will be manufactured the same way as the I-beams and with the same materials.
The grating panels will be made by a molding process and a polyester resin. The grating itself does not consists glass fibers.

5

Detailed design of the FRP jetty

This section presents the technical design of the FRP which encompasses the dimensions of the jetty and its structural elements. The preliminary design provides a rough template for the detailed design, summarized in Section 4.10. The detailed design evolved significantly with respect to the preliminary design: the number, length, and dimension of the piles, the modeling of the joints, and the load cases amongst others have been improved during the detailed design process.

First, a 3D model is presented in order to give the reader a complete picture of the jetty. Then, the structural elements in the jetty are presented; this is followed by an example calculation of the SLS and ULS checks for the beam at the access bridge. After the main structural elements, the joints in the structure are presented. Appendix D provides a full overview of the designed elements for the jetty.

5.1. Overview of the technical design

This section gives an overview of the technical design. Also, the structural elements are specified. Figure 5.1 and Figure 5.2 illustrate 3D views of the FRP jetty from two different angles. Table 5.1 presents the structural elements designed for the FRP jetty. In general, the postfix 1 indicates the location at the access bridge whilst the postfix 2 indicates the location at the platform. In an earlier design stage, two structural elements named Girder 2 and Pile 1 were designed, but these structural elements are omitted due to design reconsiderations.

Section	Structural element
Access bridge	Beam 1
	Plank 1
	Girder 1
	Pile 2
Platform	Beam 2
	Plank 2
	Pile 2

Table 5.1: Overview of structural elements

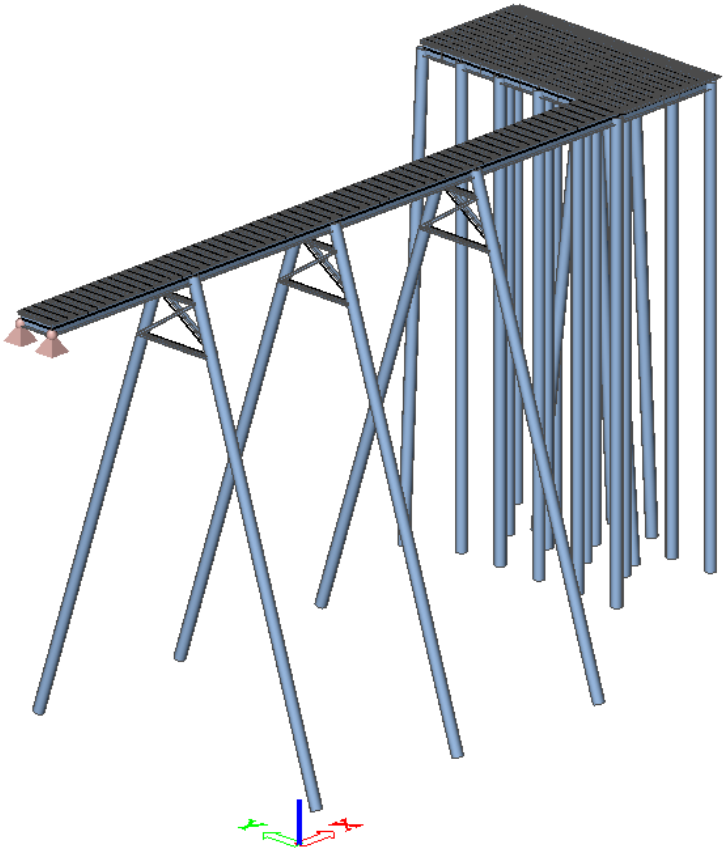

Figure 5.1: 3D overview of the jetty

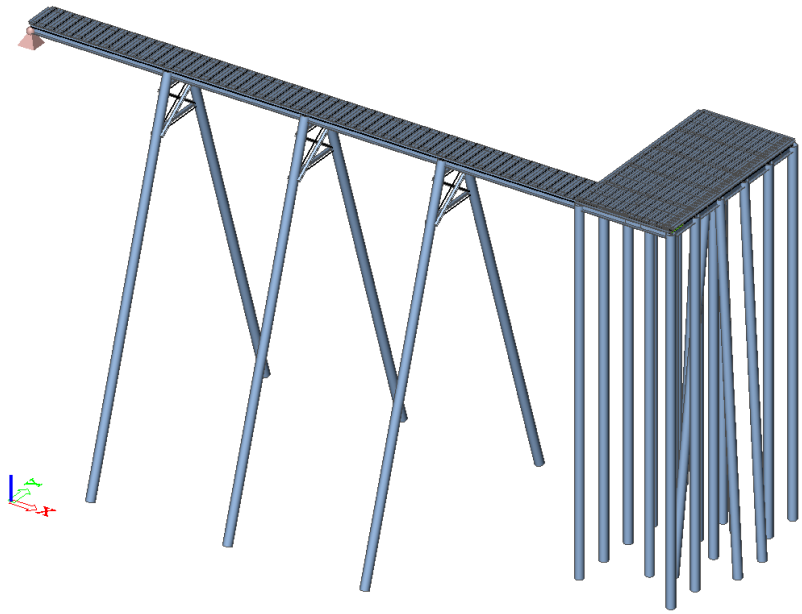

Figure 5.2: 3D overview of the jetty

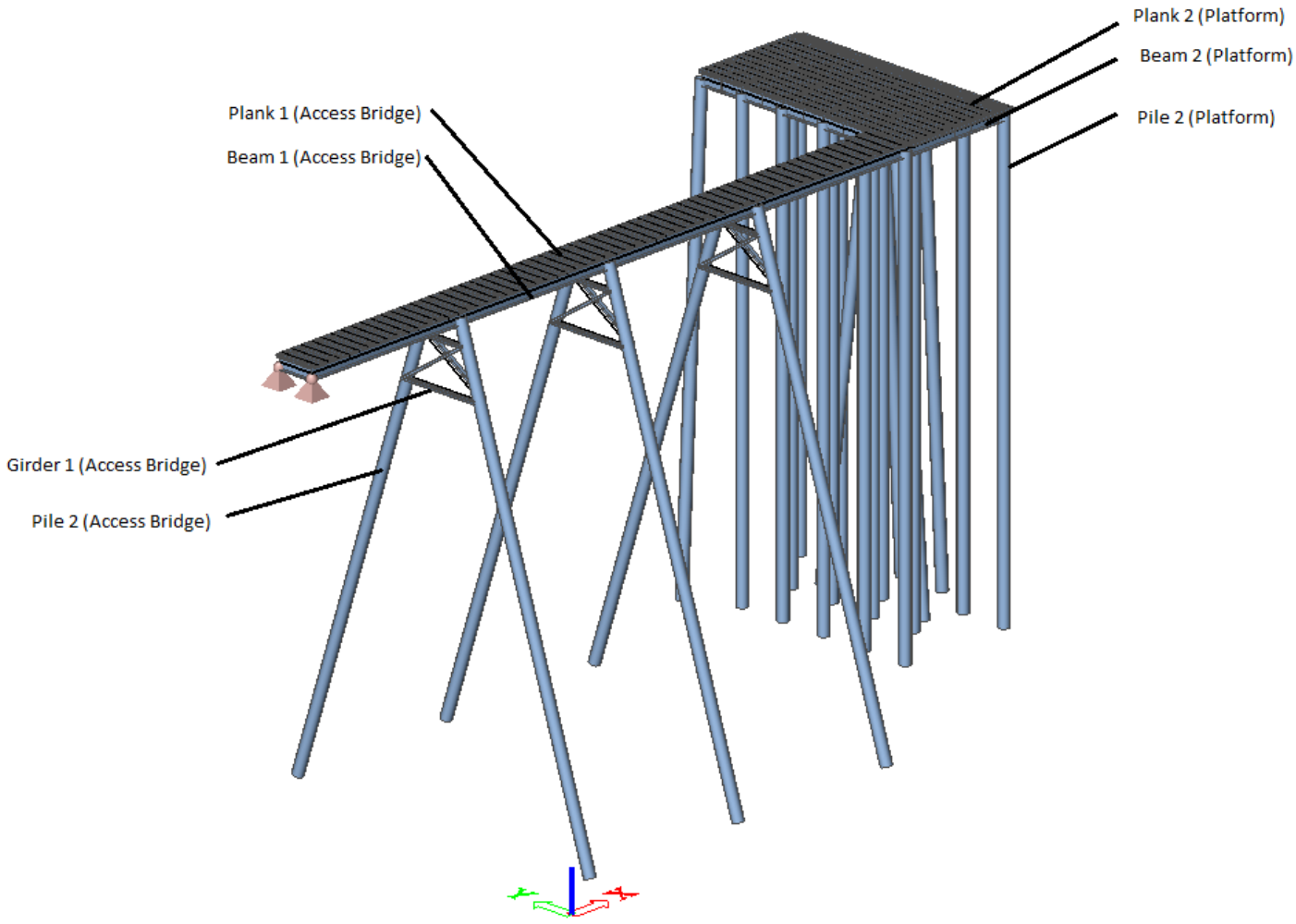

Figure 5.3: 3D overview of the jetty

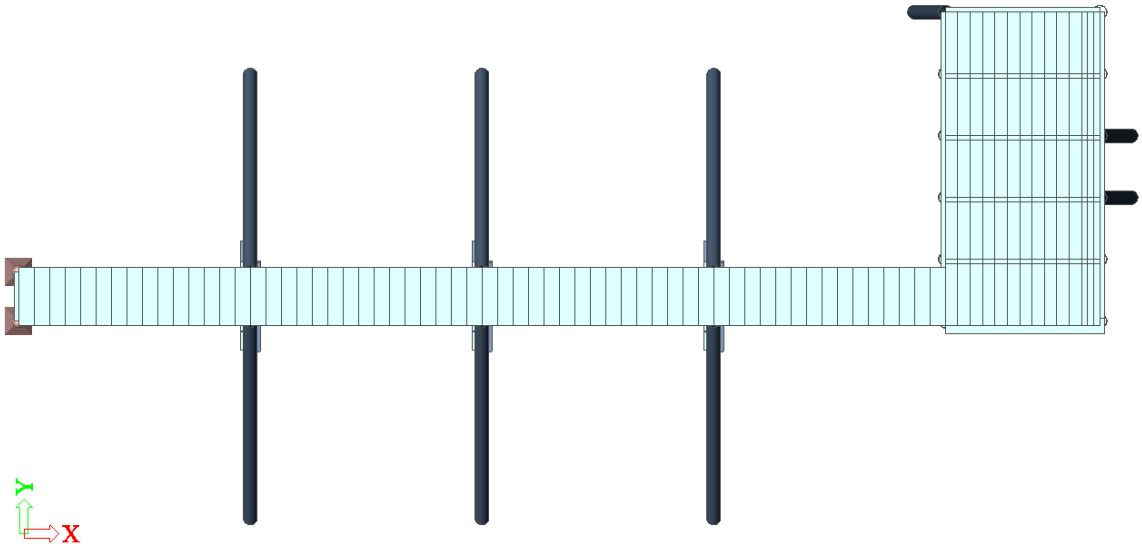

Figure 5.4: 3D top view of the jetty

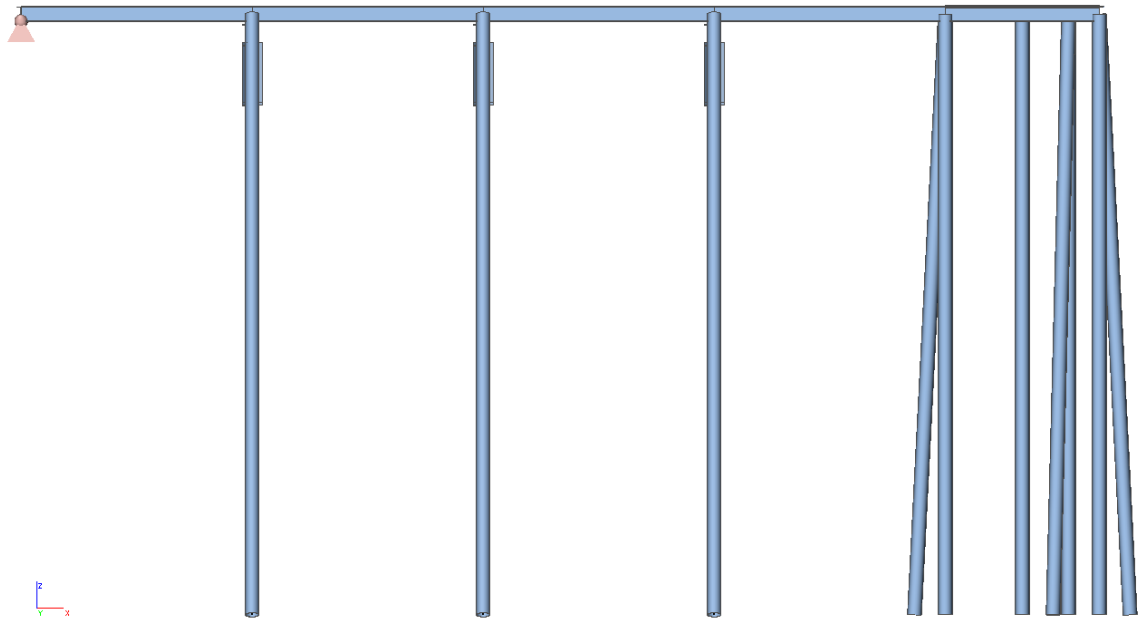

Figure 5.5: 3D side view of the jetty

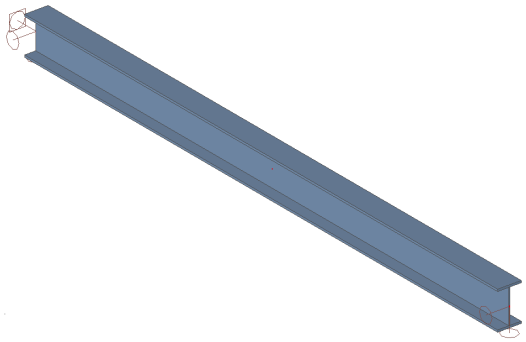

Figure 5.6: 3D image of the beam at the access bridge

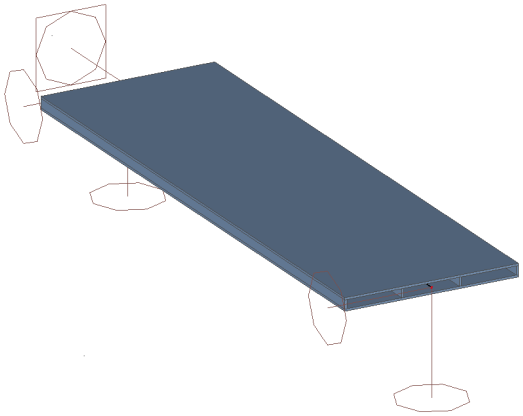

Figure 5.7: 3D image of the plank at the access bridge

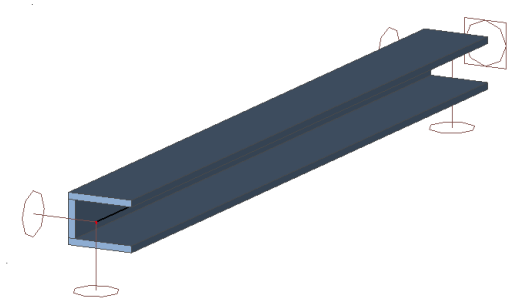

Figure 5.8: 3D image of the girder at the access bridge

Figure 5.9: 3D image of the pile

5.1.1. Functional description of the structural elements

This section provides a functional description of the beams, planks, girders, and piles. Figure 5.3 indicates the location of the structural elements.

The **beams** are an important structural element in the jetty; they carry the planks and transfer the load to the piles. Three beams are designed named beam 1, beam 2, and beam 3. In the preliminary design phase it was determined that I-profiles are the most suitable cross section of the beams.

The main function of the **planks** is to provide a working platform for workers, material, and equipment. The main variable loads are introduced to the beams via the planks.

The **girders** provide two functions; adding stiffness between piles and act as a console. The lateral deviations of the pile head need to be reduced to an acceptable level. One way to facilitate this is by adding reinforcement bars, as is one function of the girders. These can be placed in horizontally or in a cross, or both. Besides the additional stiffness, the flange of the girders acts as a console by providing a bearing platform for the beams.

Piles bear the superstructure and induce the imposed forces to a sand[1] layer which posses enough bearing capacity to carry the whole structure.

[1] Soil consists of clayey sand layers: see cone penetration test results in Appendix A.1

5.2. Notes on the design process

This section presents notes on the design process. Figure 5.10 illustrates the design process. The preliminary design resulted in rough estimations of structural elements. In this section these elements are modeled for exact dimensions and compositions. Then, the elements are processed with FEM package SCIA Engineer to obtain a 3D model. With this model, internal forces and stresses can be generated. This output data is used for the ULS and SLS checks. If the structure does not complies, an iterative loop is started, redesigning the structural elements. If the structure complies, it is argued if a further optimization is necessary. If so, also an iterative loop is started. If not, the definitive structural design is reached.

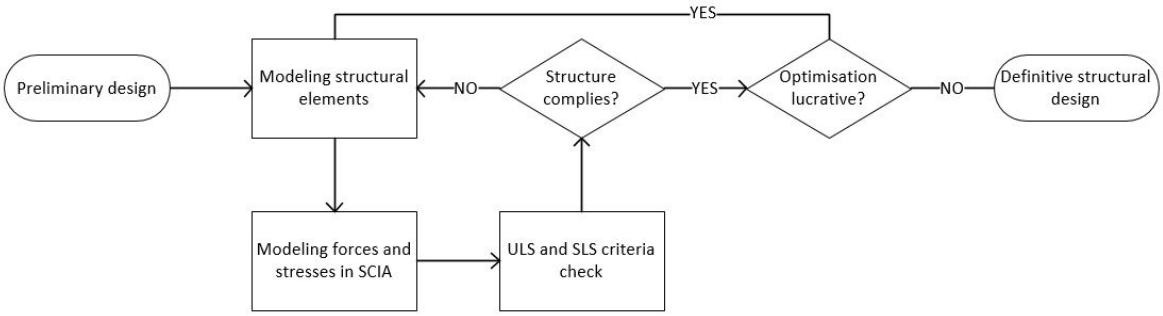

Figure 5.10: Design process of the design phase

First, generalized material properties, extracted from the preliminary design, were used to construct the structural elements. Then, these structural elements were checked according to the ULS and SLS criteria. The governing critierion determined the dimensions of the element, mainly by varying profile height. When a basic design was reached wich complied with all the criteria, the laminates were designed in more detail with $eLamx^2$. This resulted in ABD-matrices for flanges and webs of the structural elements. Then, the checks were executed again and the height was varied to comply with the ULS and SLS criteria.

Both analytical formulas and FEM software were used to calculate internal forces and displacements. The ULS and SLS checks were calculated with analytical formulas. The deflection was also calculated with FEM software SCIA Engineer. This was done to check the analytical results. Also, the analytical results rest on simple assumptions for the static model of the jetty. With the FEM analysis the coherent response of the jetty was analyzed to provide a deeper understanding of the mechanical responses.

5.3. Structural model assumptions

Several model assumptions have to be made in order to properly model the structure. Among them are assumptions for the static model of the structural elements, cross sections and their interactions. Assumptions for the laminate design are presented in the respective section (see Section 5.4).

5.3.1. Model assumptions at micro level for the plies and laminates

Fiber reinforced plastic composite are complex at micro level and assumptions need to be made in order to develop theories. The assumptions which are made are important and perpetuate trough the macro level response since it influences the mechanical properties of the laminate.
The following assumptions at micro level are made:

1. Perfect bond exists between fibers and matrix
   - The bonding is infinitesimally small
   - No-slip condition; the bonding is non-shear deformable
   - The strength of the bonding is as strong as it needs to be
2. The fibers have circular cross sections
3. Maximum strain (1.2% and 1.6% for normal stress and shear stress, respectively)
4. Kirchhoff hypothesis:
   (a) Normals remain straight
   (b) Normals remain unstretched
   (c) Normals always make a straight angle with to the neutral plane

The assumptions 1 to 3 are congruent with the applied theories for the mechanical response of the plies and laminate: the Halpin-Tsai equations to determine the mechanical properties of a ply, and the classical lamination theory for the mechanical response of a laminate. Assumption 4 is used in the structural analysis of plates. This theory also accounts for shear deformation.

5.3.2. Static model of the structural elements

It is important to substantiate the applied static model, since the static model heavily influences the internal force distribution and displacements. Two ways have been regarded to model the planks on the beams and the beams on the piles and girders; both-end hinged or both-end fixed. In the both-end hinged model, the joint is not able to transfer a moment, while the both-end fixed model is able to transfer a moment. Hinged joints can be achieved by using mechanical joints, while fixed joints can be realized with both adhesive joints and/or mechanical joints (Winter, 2017).

Regarding the ease of disassembly, mechanical joints seem easier to disassemble than adhesive joints when bolted because the bolts just have to be removed. Heavy machinery has to be used to remove adhesive joints, which might influence the integrity of the structure. While this might improve the load resistance capacity of a joint, it makes the structural elements less fit for reuse. Hence, from the perspective of disassembly, both end hinged is preferred.

Another argument for the double hinged model is because this model generates higher deflections at mid span. Since, as it turns out, this is often a decisive criterion, the double hinged model represents a safe upper boundary.

Taking the above into account, the beams, planks, and girders are therefore modeled as both-end hinged with the intention to fasten the structure with mechanical joints.

5.3.3. Structural model assumptions at cross section level

Several assumption regarding the mechanics at cross section level need to be made in order to align several theories and effects, namely; classical laminate theory, orthotropic effects, and production effects. In the following section, an I-profile will serve as a reference cross section to explain the structural assumptions.

In an I-beam, the flanges mainly provide the bending resistance capacity and the web mainly provides the shear force resistance capacity as indicated by Figure 5.11. In order to tailor the laminates for the flanges and web to their specific needs, they can be split into three laminates. Figure 5.12 illustrates how the I-beams are modeled as three different laminates: two flanges and a web.

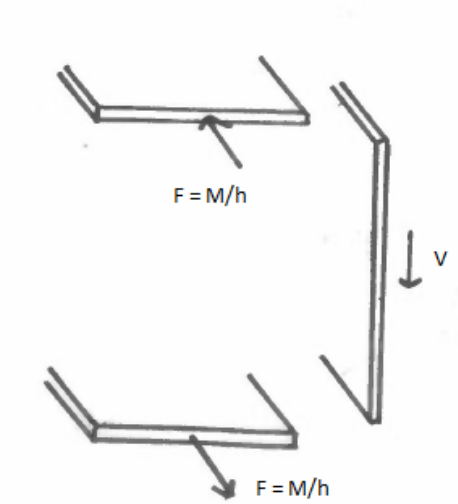

Figure 5.11: Sections which account for bending moment and shear force

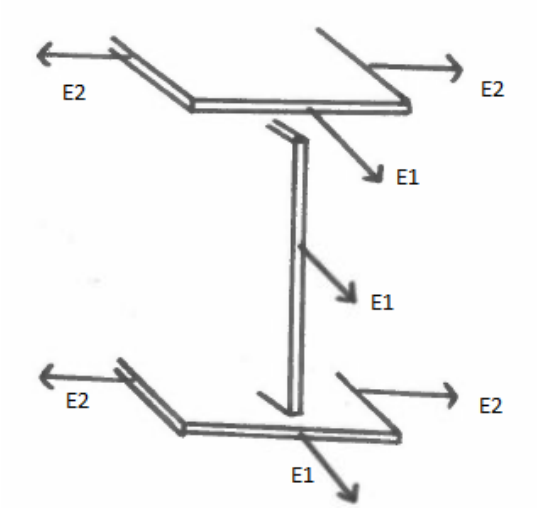

Figure 5.12: Split up of the I-beam into laminates

For each laminate, there are two main stiffnesses; the principal, or longitudinal direction (E_1, or E_x) and the secondary, or transverse direction (E_2, or E_y). From the ABD-matrix, a flexural and a membrane E-modulus can be derived. The beam is loaded with a line-load and not with pure bending. Therefore, the membrane stiffness of the flange laminate is used and not the flexural stiffness. The shear resistance is determined by the shear plane A_v, the part of the cross section which is stiff for bending. According to NEN-EN 1993-1-1:

$$A_v = A - 2bt_f + (t_w + 2r)t_f \tag{5.1}$$

This structural model is simplified and not precisely represents reality. Certain effects need to be taken into account during the design process; assumptions of the classical laminate theory, Poisson effects, and production effects.

The classical laminate theory assumes a plane stress. For I-beams, this is not the case; the load is imposed on the full width of the flange and shear stresses occur between the flanges and the web. This shear flow is illustrated by Figure 5.13 for an I-beam. Therefore, the stresses in the flanges are not in plane stress.

Because of the orthotropic properties (i.e. the difference in longitudinal and transverse stiffness and Poisson effects), the joint between flange and web influences the deformation of the flange and the

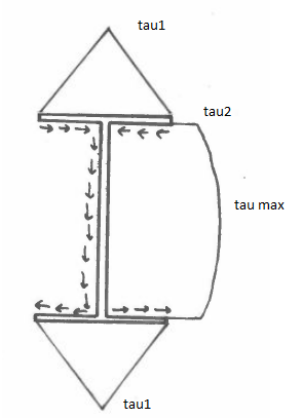

Figure 5.13: Shear stress flow in an I-beam due to an imposed load on the section

web. When an orthotropic plate is stressed in its longitudinal direction, it will deform in its transverse direction due to Poisson effects. With FRP laminates, $E_1 > E_2$, which may induce a large major Poisson ratio ν_{12}, and hence large transverse contraction when high axial longitudinal deformations occur. Presumably, the joint between web and flange inhibits deformation of the plate and the cross section will be stiffer. A side effect of this is that stress concentrations may form near the joint due to the inhibited deformation.

Furthermore, glass mats can be bent into the profile which makes a single mat to be able to be present in both the flange and the web. Presumably, this will strengthen the cross section since shear stresses from the flange may be transfered more gradually to the web. With the three plate model, it is inherently assumed this will only take place at the interface between web and flange.

5.3.4. Structural models in the FEM software SCIA Engineer

A FEM model of the jetty is developed with three main intentions: check the analytical calculation of the occurring stresses, strains, and deflection; investigate the coherence of the total structure; model the deflection of the piles combined with the soil response. This section presents the model development and usage.

With the development of the FEM model, two functions have been taken into account: creating a model which accurately resembles the physical properties of the beam (and hence an accurate structure responses) and reduce complexity of the model. These functions are often opposites: the more complex the physical and mechanical function of a product, the more complex the model needs to be to accurately describe its responses. This thesis aims to provide a feasibility; therefore a model is constructed to provide reasonable estimates which do not differ significantly from the 'reality' case, which includes orthotropic effects in the model.

The FEM model consists of a 1D beam. The cross section is manually created and the stiffnesses calculated from the ABD matrices for the different laminates are adequately assigned to the different sections in the cross section (that is, the longitudinal stiffnesses in the beam direction E_1 for the web and flange). Deformation due to shear stress is accounted in the deflection of the structural elements in the FEM model.

Table 5.2 presents the midspan deflection for the structural elements for a similar line load. The deflections generated by the FEM model coincide quite accurately to the analytical model.

Structural element	Analytical model [mm]	1D model [mm]
Beam 1	14.90	14.90 (+0.0%)
Beam 2	14.90	14.90 (+0.0%)
Plank 1	6.23	6.30 (+1.1%)
Plank 2	7.76	8.10 (+4.3%)
Girder 1	5.81	5.80 (-0.2%)
Girder 2	6.92	6.90 (-0.2%)

Table 5.2: Midspan deflection of the analytical model and the FEM model of the structural elements. Between the brackets the relative difference is indicated with the analytical solution

Differences can be explained due to the different assigned area of the cross sections which can be accounted for shear capacity. For instance, for the I-beam in the analytical solution a shear capacity area was assumed as[2]:

$$A_y = (h - t_f) * t_f \tag{5.2}$$

$$= (400 - 26) * 14 = 5236\,\text{mm2} \tag{5.3}$$

SCIA Engineer utilizes a 2D FEM model to calculate the area which can be accounted for shear capacity resistance. For the beam, an area of 4456 mm2 is calculated. Hence, the resistance against shear deformation is less for the 1D beam compared to the analytical model. For beam 1 and beam 2, this has no significant impact on the midspan deformation. However, this does explained the differences for the planks and girders. When inserting the shear capacity area generated by the 2D FEM model into the analytical solution, the analytical solution generates the same deflection. By means of the above analysis, the 1D model is validated and utilized in the FEM model.

Besides a 1D beam model, two other models were made: a 2D isotropic plate model and a 2D orthotropic plate model. These models yielded unsatisfactory results with respect to the analytical solution and increased complexity of the model. Therefore, these models are not used in modeling the FRP jetty in the FEM model[3].

[2] As convenient for steel profiles (Staalsupport, n.d.)
[3] See also Section 10.1.1 for a discussion on this item

5.4. Laminate design for the structural elements

The design of the laminate is a key factor in the structural response of the structural elements to imposed loads. The laminate can be tailored for specific needs, such as high axial stiffness or high shear stiffness. First, a brief general section regarding laminate design is presented followed by an elaboration of one laminate, namely the flange of beam 1.

Chapter 2 presents a recap of the literature study where also the design recommendations are given for the laminates and Section 5.3.1 states the model assumptions for the laminate design.

The material choices for the fibers and resin are adopted from the preliminary design. For the resin, this is an epoxy; for the fibers, this is E-glass. Material property quantities are derived from CUR96. The fiber content volume is set at 60 %, which is possible for pultrusion processes.

The mechanical properties of the plies and laminates are calculated both analytically and with $eLamX^2$. $eLamX^2$ is a freeware composite calculator, developed at the Technische Universität Dresden (TU Dresden, n.d.). Lamina properties from lamination software should be checked because several assumptions for micro mechanics have to be made when calculating lamina properties. Different assumptions for micro mechanics may lead to different mechanical properties at cross sectional level. This problem was encountered with the eLamX^2 software when calculating the mechanical properties of laminas. At first glance, the lamina properties calculated with the equations from the preceding paragraph do not coincide with the results from eLamX^2 for the stiffness in the transversal direction (E_2) of laminas. eLamX^2 uses $\xi = 0.5$ in the Halpin-Tsai equations. This value rests on the assumption that the width of the fiber is a quarter of the thickness, hence an elliptical fiber section is assumed. The CUR96 assumes circular fiber sections, leading to a fiber width to thickness ratio of 1 which results in $\xi = 2$ (de Boer et al., 2016). Therefore, the transversal stiffness for laminas is entered manually in the program.

5.4.1. Example: Laminate design for beam 1

This section exemplifies the laminate buildup of beam 1 in order to give the reader insight into the laminate design process. The design process of the remaining structural elements is largely similar.

As stated in the preceding section, the mechanical properties were both calculated analytically and with eLamX^2 . Table 5.3 presents the mechanical properties of the material from CUR96 (de Boer et al., 2016). The subscript f refers to the fiber, the subscript m refers to the matrix.

Property	Symbol	Unit	E-glass	Epoxy
Density	ρ	kg/m^3	2570	1250
E-modulus	E	GPa	73.1	3.1
Poisson ratio	ν	–	0.24	0.39
Shear modulus	G	GPa	29.48	1.115

Table 5.3: Fiber and resin properties for the ply, from CUR96 (de Boer et al., 2016)

The fiber volume content (v) is set at 60 %, which leaves 40 % for the matrix. The rule of mixture then yields the density of the composite: $\rho_c = v_f * \rho_f + v_m * \rho_m = 2042\,\text{kg/m}^3$. Then, with the Halpin-Tsai equations the mechanical properties of the plies can be calculated (de Boer et al., 2016)(Mallick, 2007):

$$E_L = v_f * E_f + v_m * Em = 45.1\,\text{GPa} \tag{5.4}$$

$$E_T = E_m * \frac{Ef + 2 * \left(v_f * E_f + v_m * E_m\right)}{v_m * E_f + v_f * E_m + 2 * E_m} = 13.57\,\text{GPa} \tag{5.5}$$

$$v_{LT} = v_f * v_f + v_m * v_m = 0.3 \tag{5.6}$$

$$G_{LT} = G_m * \frac{G_f + v_f * G_f + v_m * G_m}{v_m * G_f + v_f * G_m + G_m} = 3.911\,\text{GPa} \tag{5.7}$$

$$G_{TT} = G_m * \frac{\left(3 - 4v_m\right) * G_f + v_f * G_f + v_m * G_m}{\left(3 - 4v_m\right)\left(v_m * G_f + v_f * G_m\right) + G_m} = 3.545\,\text{GPa} \tag{5.8}$$

where the subscript L and T respectively stand for lateral and transversal. These properties are used as input data for eLamX^2 to construct the laminate.

For the beam, two laminates are designed: a flange laminate and a web laminate. The flanges are designed in such way that their axial stiffness modulus is high, the web is designed to possess a high shear modulus. The flanges concentrate their fiber direction volume along the beam axis (0°) to maximize the membrane stiffness of the laminate in order to improve bending moment resistance capacity. The web has more varied fiber direction volumes to maximize the shear stiffness which in turn will increase the shear force resistance capacity. Figure 5.14 presents the membrane- and shear stiffness of the flanges and web of beam 1, respectively. The thickness of the plies varies: in Appendix D.2 a detailed overview of the ply thickness for each laminate is given. Also, in Appendix F the equations to calculate the engineering constants and orthotropic plate properties are given.

Laminate name			Beam 1 - flange - v1								
Buildup			[0/-45/90/45/0/45/90/-45/0/45/90/-45/0]s								
Laminate dimensions			ABD matrix						Hygrothermal expansion		
angle [°]	Σti [mm]	%t	893476,3	190283,2	0	0	0	0	αT_x	5,25E-06	[-]
0	14	53,85	190283,2	582617	0	0	0	0	αT_y	1,81E-05	[-]
45	4	15,38	0	0	185687,1	0	0	0	αT_xy	-1,23E-21	[-]
-45	4	15,38	0	0	0	55637818	9563941	209830	β_x	5,62E-02	[-]
90	4	15,38	0	0	0	9563941	29826133	209830	β_y	1,96E-01	[-]
	26		0	0	0	209830	209830	9305027	β_xy	-1,20E-17	[-]

(a) Laminate properties of the flange, beam 1

Laminate name			Beam 1 - web - v1								
Buildup			[90/45/0/-45/0/45/90/-45]s								
Laminate dimensions			ABD matrix						Hygrothermal expansion		
angle [°]	Σti [mm]	%t	333759,7	135024,4	0	0	0	0	αT_x	1,37E-05	[-]
0	2	14,29	135024,4	395931,5	0	0	0	0	αT_y	7,84E-06	[-]
45	4	28,57	0	0	132549,5	0	0	0	αT_xy	-1,22E-21	[-]
-45	4	28,57	0	0	0	5302225	1989321	314745,1	β_x	1,48E-01	[-]
90	4	28,57	0	0	0	1989321	7048218	314745,1	β_y	8,44E-02	[-]
	14		0	0	0	314745,1	314745,1	1948899	β_xy	-1,15E-17	[-]

(b) Laminate properties of the web, beam 1

Figure 5.14: Laminate properties of beam 1

With the ABD-matrix of the laminates, the engineering constants can be calculated ($E_1, E_2, \nu_{12}, G_{12}$):

for the flange:	*for the web*:
$E_1 = 31.97\,\text{GPa}$	$E_1 = 20.56\,\text{GPa}$
$E_2 = 20.85\,\text{GPa}$	$E_2 = 24.38\,\text{GPa}$
$\nu_{12} = 0.33$	$\nu_{12} = 0.34$
$G_{12} = 7.14\,\text{GPa}$	$G_{12} = 9.47\,\text{GPa}$

These engineering constant are used as input parameters for the structural elements in the analytical model and the FEM model. With the imposed loads on the structure, the response of the elements can be found. The internal stresses in the individual plies can be checked with eLamX^2 .

With the responses of the structural elements known, the SLS and ULS checks can be executed. This is done in part Section 5.6 and Section 5.7 respectively.

5.5. Reduction of mechanical properties: conversion and material factors

Mechanical properties of the structural elements need to be reduced in order to account for uncertainties in strength and external influence on the long-term quality of the elements: this is done respectively by the material factor γ_M and the conversion factor η_c (de Boer et al., 2016). The CUR96 provides these material- and conversion factors for numerous situations such as different manufacturing processes and the climate in which the element resides. The formulas for the material and conversion factors are (de Boer et al., 2016):

$$\gamma_M = \gamma_{M1} + \gamma_{M2} \tag{5.9}$$

$$\eta_c = \eta_{ct} * \eta_{cv} * \eta_{ck} * \eta_{cf} \tag{5.10}$$

Where:

- γ_{M1} : Partial material factor coupled to geometric deviations and model uncertainties in obtaining the correct material properties
- γ_{M2} : Partial material factor which discounts uncertainties related to the strength characteristics of the material, dependent on the spread of the material properties
- η_{ct} : Conversion factor for temperature influences
- η_{cv} : Conversion factor for moisture influences
- η_{ck} : Conversion factor for creep
- η_{cf} : Conversion factor for fatigue

Table 5.4 presents the material factors for the structural elements. For all elements, a material factor of $\gamma_M = 1.62$ is determined.

Structural element	γ_{M1}	γ_{M2}	γ_M
Beams	1.35	1.2	1.62
Planks	1.35	1.2	1.62
Girders	1.35	1.2	1.62
Piles	1.35	1.2	1.62

Table 5.4: Material factors for the structural elements

Table 5.5 presents the material factors for the structural elements. For all elements, expect the piles, a conversion factor is $\eta_c = 0.71$ is determined; for the piles a conversion factor of $\eta_c = 0.63$ is determined because part of the piles will always be in contact with water.

Structural element	η_{ct}	η_{cv}	η_{ck}	η_{cf}	η_c
Beams	0.9	0.9	0.88	1	0.71
Planks	0.9	0.9	0.88	1	0.71
Girders	0.9	0.9	0.88	1	0.71
Piles	0.9	0.8	0.88	1	0.63

Table 5.5: Conversion factors for the structural elements

5.6. Serviceability Limit State criteria: deflection and vibrations

The Serviceability Limit State encompasses two major criteria: for deflections, and for vibrations. The criteria themselves are derived from CUR96 (de Boer et al., 2016) and Eurocode 7 (NEN, 2011). First, an overview of the SLS criteria is given related to the design of the FRP structure. Then, these criteria are elaborated in the following sections.

Table 5.6 presents an overview of the SLS criteria and Table 5.7 quantifies these criteria for the structural elements. The criteria are limitations in vertical and horizontal direction, and a minimum required natural frequency.

Structural element	Midspan deflection $[\delta_{z,max}]$	Horizontal displacement $[\delta_{hor,max}]$	Minimum frequency [Hz]
Beams	L/250[4]	50	4.6
Planks	L/250	50	4.6
Girder	L/250	50	4.6
Piles	10 % of center line	50[5]	-

Table 5.6: SLS criteria for the structural elements

[4] At midspan
[5] At the pile head

Table 5.7 presents the quantified SLS criteria of the structural elements. For the structural elements

Structural element	Length [mm]	Diameter [mm]	$\delta_{ver,max}$ [mm]	$\delta_{hor,max}$ [mm]	Frequency [Hz]
Beams	7500	-	30	50	4.6
	5000	-	20	50	4.6
	1000	-	4	50	4.6
Planks	1600	-	6.4	50	4.6
	2000	-	8	50	4.6
Girders	1600	-	6.4	50	4.6
	2000	-	4	50	4.6
Piles	-	356	35.6	50	-
	-	456	45.6	50	-

Table 5.7: Quantified SLS criteria for the structural elements

5.6.1. SLS: deformation criteria

Deformation criteria limit the allowable deformation of a structure, which can be a deflection or a rotation. Only the deflection criteria are regarded: they mostly are responsible for the inconveniences when the structure is in service. The criteria are formulated on a local or global level. An example for a local level criterion is the deflection at mid-span for a beam; for a global criterion, one can image the deflection at the corner of a jetty.

Local stability

In the preliminary design phase, a deformation criterion is formulated which states a maximum deflection at mid-span of the beams, planks, and girders of $\frac{L}{250}$. The deformation of a free supported beam due to a line load is given by (de Boer et al., 2016):

$$w_{tot} = \frac{5}{384}\frac{q*L^4}{\sum_i EI_i} + \eta\frac{1}{8}\frac{q*L^2}{\sum_i G_i A_i} \tag{5.11}$$

The global stability

The first draft of the jetty in the FEM model showcased significant lateral deflection of both the access bridge. The global stability criteria were not formulated in the program of requirements. Horizontal deflections criteria of buildings are provided by the Eurocode (Dutch annex: NEN-EN 1990).

Section 5.8.3 further elaborates the global stability of the of the FRP jetty, since this is directly linked to the deflection of the piles.

5.6.2. SLS vibration criterion

Vibration may induces inconveniences in comfort or increase the load on a structural element and therefore has to be accounted for in the design. Due to the lightweight nature of FRP, structural elements made of this material are prone to vibrations (de Boer et al., 2016).

The SLS vibration criterion in the prelinminary design phase states that the natural frequency of the beams, planks, and girders should be equal to or bigger than 4.6 Hz. If the structural elements are designed such that they have a natural frequency higher than 4.6 Hz, no additional load has to be taken into account (de Boer et al., 2016). Passengers induce harmonic loads when walking over a structure and therefore an additional distributed load has to be taken into account. However, this distributed load may be reduced to zero when the natural frequency is lower than 1.25 Hz or higher than 4.6 Hz. Further information regarding the response of passenger bridges due to harmonic passenger loads is elaborated in NEN-EN 1991-2 or EC1991-2 appendix A.

The SLS vibration criterion is a subjective one: designing structural elements such that their frequency is higher than 4.6 Hz may be more costly than adjusting the element for the additional passenger load. But if no vibrations are desired at all, criteria regarding to the natural frequency may be set. The access bridge and the jetty has to be accessible for people: presumably, this will be workers operating the jetty and not a flow of people as is often the case as passenger bridges. This would imply a low harmonic load. However, the potential reuse of the jetty as a (heavy traffic) passenger bridge should be kept in mind and therefore the respective SLS criterion is set.

CUR96 provides a formula to calculated the natural frequency of a beam (de Boer et al., 2016):

$$f_{0i} = \frac{K_n}{2\pi}\sqrt{\frac{\sum E_i I_i g}{qL^4}} \tag{5.12}$$

Where:

K_n : a constant, dependent on the boundary conditions

The value K_n is 9.87 for free supported beams and 22.4 for fixed supported beams[6]. Only the vertical and longitudinal harmonics have been taking into account and not the transversal harmonics since the only transversal load is the wind load, which does not have a harmonic nature.

[6] Dimensions in the analytical solutions are based on free ends, while eventually the beam is supported by fixed ends, see Section 10.1.1

5.6.3. Example: SLS criteria checks for beam 1

An example is elaborated in order to showcase the calculations: this is done for the beam at the access bridge.

Analytical check

For the midspan deflection of the beam, in vertical direction:

$$w_{tot} = \frac{5}{384}\frac{q*L^4}{\sum_i EI_i} + \eta\frac{1}{8}\frac{q*L^2}{\sum_i G_i A_i} = \frac{5}{384}\frac{7219*7.5^4}{19716105} + \frac{1}{8}\frac{7219*7.5^2}{42860476} = 16\,\text{mm} \tag{5.13}$$

The maximum allowed deflection is (see Table 5.7) is 30 mm, hence the structure complies.
For the lowest natural frequency of the beam, we find:

$$f_{0i} = \frac{K_n}{2\pi}\sqrt{\frac{\sum E_i I_i g}{qL^4}} = \frac{9.87}{2\pi}\sqrt{\frac{19716105*9.81}{7128.6*7.5^4}} = 4.6\,\text{Hz} \tag{5.14}$$

So, the value of the lowest natural frequency of the beam with the imposed load is 4.6 Hz and hence complies with the SLS criteria that the lowest natural frequency has to be equal to or larger than 4.6 Hz. Regarding the structural model, this value for the natural frequency can be seen as a lower boundary: both other model situations, end-beam supports both fixed or one free and one fixed, have higher K_n values assigned (22.4 and 15.4 respectively) and hence yield higher natural frequencies. However, higher imposed line loads, as accounted for in the FEM analysis, yields a lower lowest natural frequency. A doubling of the load (i.e. 14 257.20 kN/m) yields a lowest natural frequency of 3.25 Hz. However, by increasing the stiffness of the joint at the beam-end, the support becomes rather fixed than free and the K_n value will increase. With the double load and a K_n value of 14, the lowest natural frequency is 4.61 Hz. Hence, if problems regarding vibrations are expected, this can be solved with stiffening the joints at the beam-ends.

FEM model

The maximum vertical and horizontal displacements of the access bridge beam (beam profile 1) in the FEM model are 26.3 mm and 45.1 mm respectively. On the following pages, 3D displacement illustrations are represnted for the vertical deflection in z direction and the horizontal deflection in x and y direction.

Differences between the analytical and FEM model deflection can be explained due to two reasons: first, the difference in loads acting upon the beam: in the FEM model, also an additional load for the pipe installation is accounted for. Also, in the FEM model, the the supports are modeled as fixed end. This reduces the midspan deflection of the beams and the structural response in general.

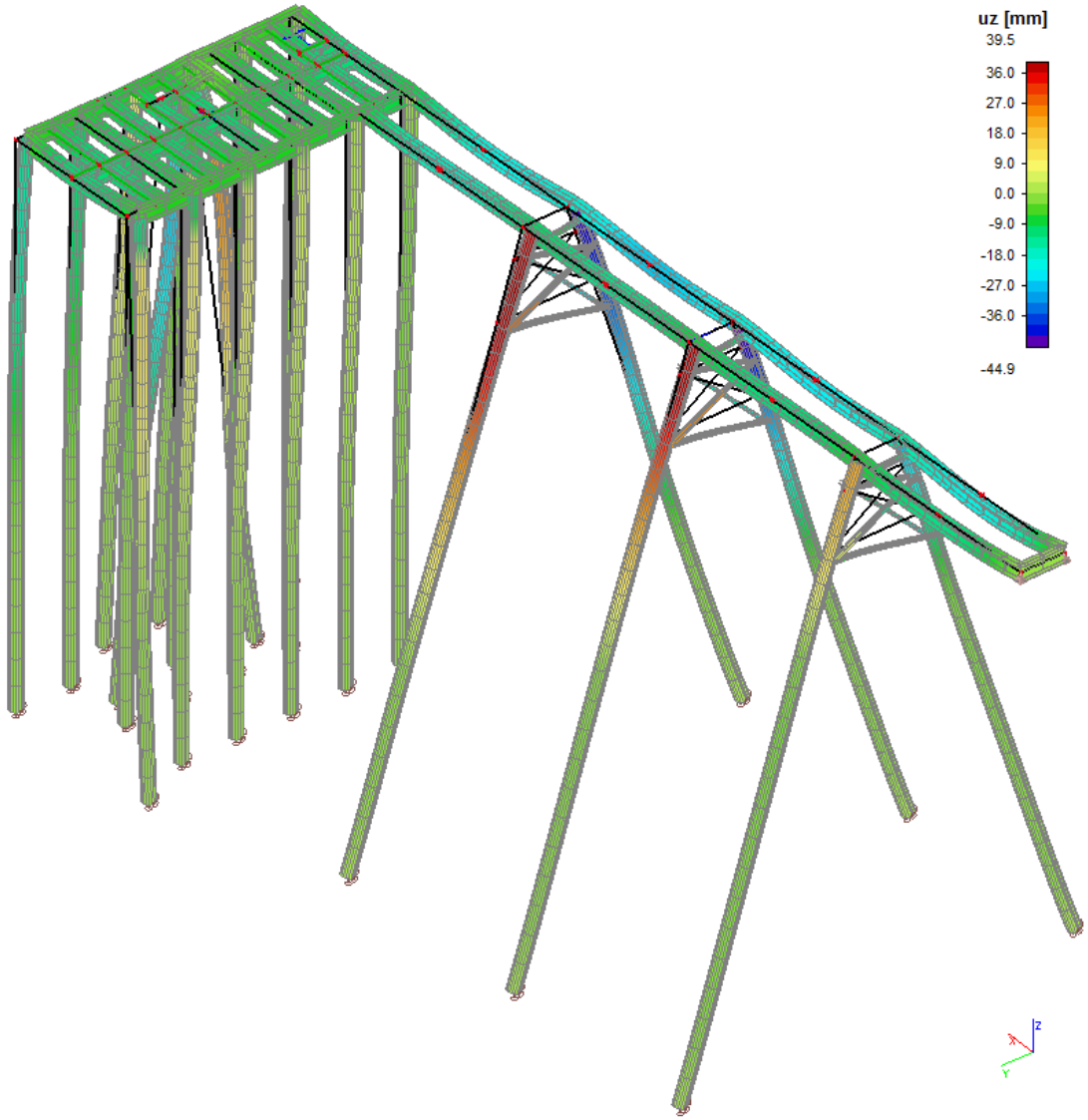

Figure 5.15: 3D render of the vertical displacement due to the SLS load envelope

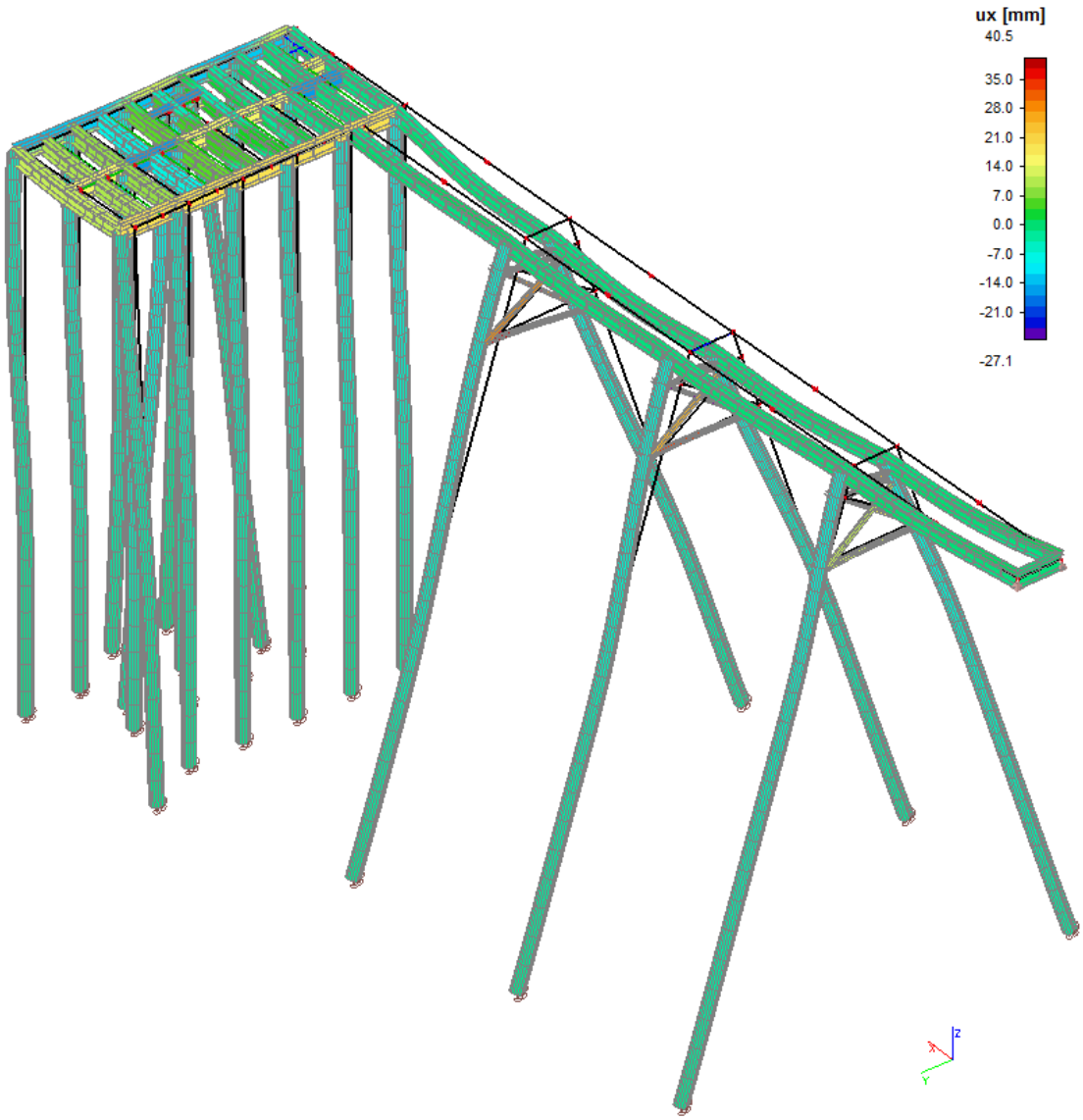

Figure 5.16: 3D render of the horizontal displacement (u_x) due to the SLS load envelope

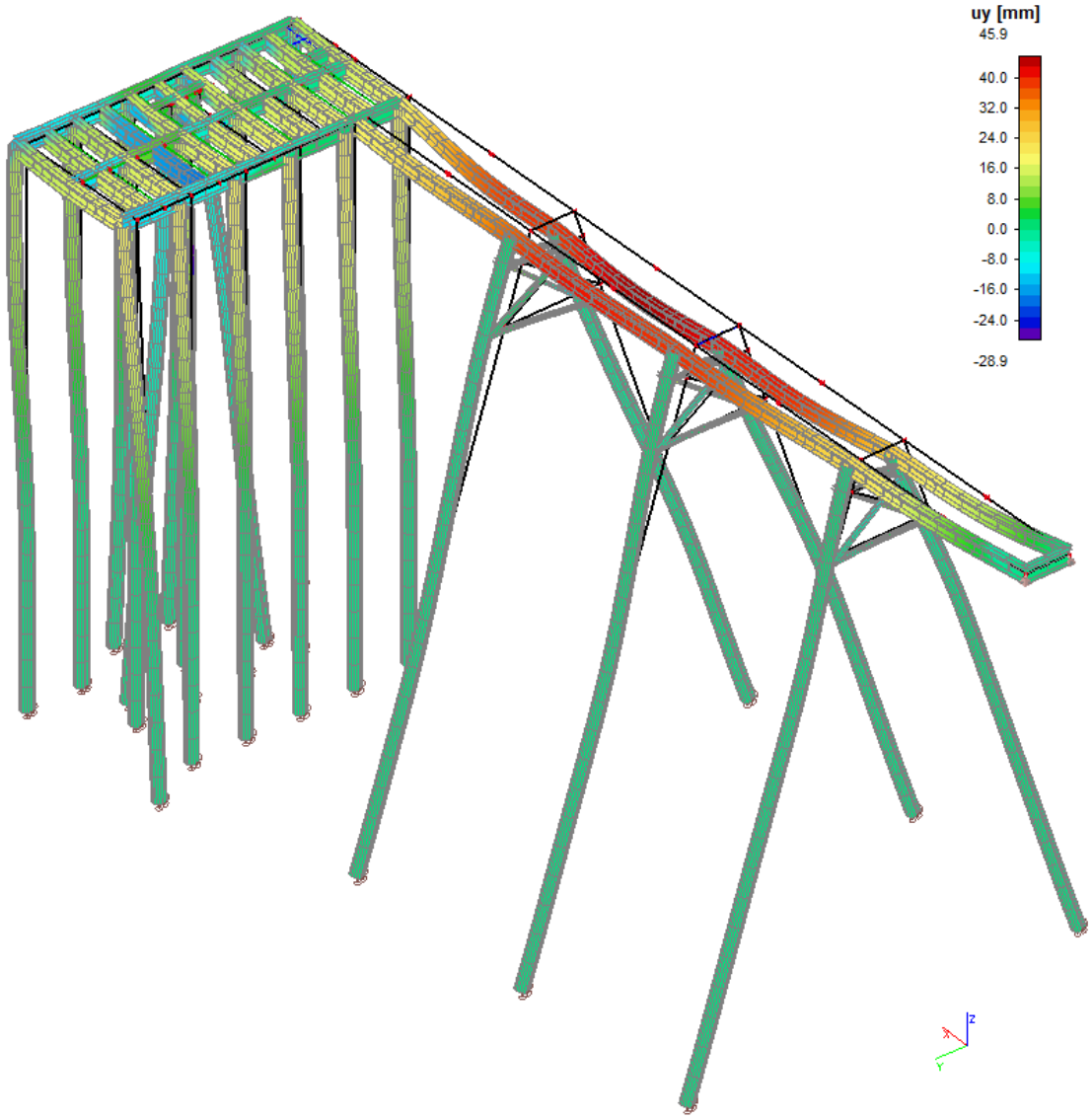

Figure 5.17: 3D render of the vertical displacement (u_y) due to the SLS load envelope

5.6.4. Overview of critical SLS checks

Table 5.8 presents the maximum deflections of the structural elements: all displacements do not exceed the maximum allowed deflection (stated in Table 5.6). The UC is calculated as the actual deflection divided by the allowed deflection.

Structural element	Location	Actual displacement		UC	
		Horizontal	Vertical	Horizontal	Vertical
Beam 1	Access bridge	45.1	26.3	0.9	0.88
Beam 2	Platform	18.9	8.3	0.38	0.42
Beam 2	Loading arm[7]	13.4	10.6	0.27	0.53
Pile 2	Access bridge	40.7	18.6	0.81	0.41
Pile 2	Platform	19	9	0.38	0.20
Pile 2	Loading arm	13.4	8.3	0.29	0.18

Table 5.8: Overview of the maximum displacements and UC's for the SLS envelope

Vibration is not regarded in the model. During the design phase, a switch was made from free end beams to fixed end beams: this increases the natural frequency of the beams (see also Section 10.1.1).

5.7. ULS criteria: strength and stability

For the ULS checks, both a conversion factor and a material factor need to be applied to the mechanical properties of the structural elements and the imposed loads: these are presented in Table 5.5 and Table 5.4 respectively.
In general, the resistance capacity is calculated as:

$$X_d = \frac{\eta_c X_k}{\gamma_M} \tag{5.15}$$

Where:

X_d : design value for a material property
X_k : characteristic value for a material property
η_c : conversion factor
γ_M : material factor

[7] Located at platform, and influenced by the load of the loading arm

5.7.1. ULS strength criteria

The ULS strength criteria relate to the structural resistance capacity and the imposed load on the structure. Two checks on strength are executed: resistance capacity at cross section level and interlaminar shear strength. The ULS strength checks are executed at cross section level.

Resistance capacity at cross section level

Individual resistances for normal force, bending force, shear force and torsion can be superpositioned in the check, resulting in the following formula (de Boer et al., 2016):

$$\frac{N_{Ed}}{N_{Rd}} + \frac{M_{Y,Ed}}{M_{Y,Rd}} + \frac{M_{Z,Ed}}{M_{Z,Rd}} + \frac{V_{Y,Ed}}{V_{Y,Rd}} + \frac{V_{Z,Ed}}{V_{Z,Rd}} + \frac{T_{Ed}}{T_{Rd}} \leq 1,0 \tag{5.16}$$

Since structure responses vary over the length of the structural elements, three points were investigated to find the decisive check: midspan, endspan, and an optimum which lies somewhere between the midspan and the endspan. This optimum is analytically determined and is presented in Appendix F.

Interlaminar shear strength

A composite consists of numerous glued plies together: between those plies shear stresses occur and the strength of this ply cohesion must be checked, otherwise the laminate may fail (Winter, 2017). A check on interlaminar shear strength (ILSS) has to be done:

$$\frac{\tau_{Ed}}{\tau_{Rd}} \leq 1 \tag{5.17}$$

5.7.2. ULS stability criteria

The checks on stability in ULS relate to general- and local buckling. The CUR96 prescribes a method based parallel to the Eurocode: the normal force pressure capacity is reduced with a buckling factor (de Boer et al., 2016). The type of support, that is fixed or free, has a significant impact on the resistance to buckling. Therefore, both the forces in the analytical model and in the FEM model are regarded at the supports of the structural elements.

General buckling

Testing the capacity against general buckling comprises three checks: axially loaded members, lateral torsional buckling, and a combination of both. General buckling effects can be neglected if $\bar{\lambda} \leq 0.2$ or if $\frac{N_{Ed}}{N_{cr}} \leq 0.04$ (de Boer et al., 2016).

Local buckling

The thickness of the laminates are large compared to their length and therefore it is unlikely that failure will occur due to local buckling.

Lateral torsion buckling

Checks on lateral torsion buckling has to be incorporated in the ULS for open cross sections. Lateral torsion buckling effects can be neglected if $\bar{\lambda}_{LT} \leq \bar{\lambda}_{LT,0}$ or if $\frac{M_{Ed}}{M_{cr}} \leq \bar{\lambda}_{LT,0}^{\,2}$ (de Boer et al., 2016).

5.7.3. Example: ULS criteria checks for access bridge beam

This section elaborates an example for the ULS criteria checks for the decisive load on the an access bridge beam: this is the envelope of all regarded ULS load case combinations. See Appendix C for an illustration of the load cases. Table 5.9 presents one of the decisive internal member forces according to the FEM analysis.

Location	N_{Ed}	$V_{y,Ed}$	$V_{z,Ed}$	$M_{y,Ed}$	$M_{z,Ed}$
Mid-span	−22.4 kN	0 kN	0 kN	32.8 kNm	5.2 kNm
Beam end (right)	−22.4 kN	7.8 kN	−46.1 kN	−62.5 kNm	11.4 kNm

Table 5.9: Internal member forces for the decisive beam at the access bridge; member forces from FEM analysis

Figure 5.18 illustrate the normal force in the beam.

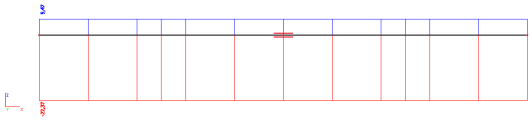

Figure 5.18: Bending moment around y axis

Figure 5.19 and Figure 5.20 illustrate the bending moments in the beam.

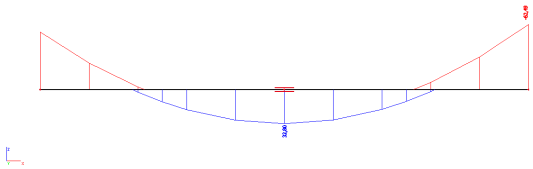

Figure 5.19: Bending moment around y axis

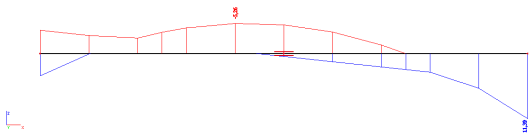

Figure 5.20: Bending moment around z axis

Figure 5.21 and Figure 5.22 illustrate the shear force in the beam.

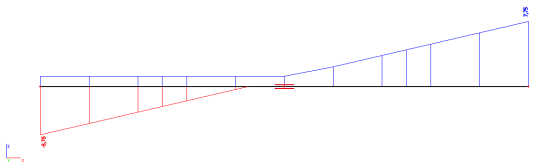

Figure 5.21: Shear force in y direction

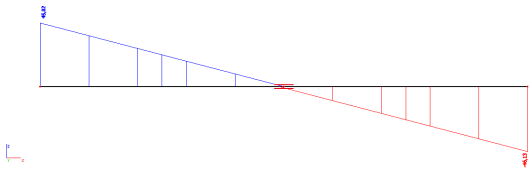

Figure 5.22: Shear force in z direction

Table 5.10 presents the dimensions and material properties for the beam at the access bridge. With the resistance capacity of the beam and the acting forces known, the ULS checks as presented in Section 5.7.1 can be executed.

Beam 1 - access bridge

profile dimensions				laminate - flange			
h	481 [mm]	Ex	31974 [Mpa]	D11	5,0332E-02 [MNm]	d11	893,4763 [MN/m]
b	300 [mm]	Ey	20850 [Mpa]	D22	3,2821E-02 [MNm]	d22	582,617 [MN/m]
tf	26 [mm]	Gxy	7142 [Mpa]	D12	1,0719E-11 [MNm]	d33	185,6871 [MN/m]
tw	14 [mm]			D33	1,0460E-02 [MNm]	d12	190,2832 [MN/m]
A	21607 [mm2]	Vxy	0,33 [-]	D44	3,1333E-04 [MNm]		
		Vyx	0,21 [-]	D55	2,2346E-04 [MNm]		
moment of inertia parameters		laminate - web					
Iy, flange	404300540 [mm4]	Ex	20551 [Mpa]	D11	5,4514E-03 [MNm]	d11	333,7597 [MN/m]
Iy, web	92171475 [mm4]	Ey	24379 [Mpa]	D22	6,4669E-03 [MNm]	d22	395,9315 [MN/m]
Iz, flange	58500000 [mm4]	Gxy	9468 [Mpa]	D12	2,2054E-12 [MNm]	d33	132,5495 [MN/m]
Iz, web	98119 [mm4]			D33	2,1650E-03 [MNm]	d12	135,0244 [MN/m]
Iy	0,0009008 [m4]	Vxy	0,341 [-]	D44	1,0727E-04 [MNm]		
		Vyx	0,405 [-]	D55	1,2150E-04 [MNm]		

crossection properties				SLS crossection properties			
web neglected		web not neglected		web not neglected			
Wy	3361527 [mm3]	Wy	3744704 [mm3]	ΣEI,y	19716104,7 [Nm2]	ΣGA,z	42860476 [N]
Wz	780000 [mm3]	Wz	780654 [mm3]	ΣEI,z	2659500 [Nm2]	ΣGA,y	79161343 [N]
ΣEI,y	2,585E+13 [Nmm2]	ΣEI,y	2,7749E+13 [Nmm2]	Reduced property input for SCIA			
ΣEI,z	3,741E+12 [Nmm2]	ΣEI,z	3,743E+12 [Nmm2]	flange		web	
		Av,z	6371,28106 [mm2]	E,SCIA	22719 [Mpa]	E,SCIA	14602 [Mpa]
		Av,y	15600 [mm2]	G,SCIA	5074 [Mpa]	G,SCIA	6727 [Mpa]
ratio My,Rd/Vz,Rd		ΣGA,z	60322151 [N]	Bending stiffness for lateral torsion			
1,34		ΣGA,y	111412260 [N]	ΣEyIz	2,4418E+12 [Nmm2]		

Stability parameters							
b	150 [mm]	c,my	0,9 [-]	Lateral torsion buckling			
bw	455 [mm]	c,mz	0,9 [-]	C1	1,132 [-]	αf	0,5 [-]
ξ	3 [-]	c,mLT	0,9 [-]	k	1 [-]	λ,LT,f,0	0,5 [-]
q	0,036 [-]	kyy	0,90 [-]	It	3931457,03 [mm4]	Lcr	7500 [mm]
p	0,302 [-]	kyz	0,90 [-]	Iw	6,0579E+12 [mm6]	M,cr	166 [kNm]
f_c,stab,k,f	227 [MPa]	kzy	0,72 [-]	Local flange wrinkling		Local web wrinkling	
f_c,stab,k,w	82 [MPa]	kzz	0,90 [-]	λf,f,LT	2,26 [-]	λf,w,LT	1,36 [-]
ρ,f	0,59 [-]			Φ,f,LT	3,39 [-]	Φ,w,LT	1,58 [-]
ρ,w	0,21 [-]			χ,f,LT	0,17 [-]	χ,w,LT	0,42 [-]
				χ,LT	0,17		

Buckling							
Around strong - axis				Around weak - axis			
L	7,5 [m]	αf	0,50 [-]	L	7,5 [m]	αf	0,75 [-]
K	1 [m]	λf,0	0,50 [-]	K	1 [m]	λf,0	0,50 [-]
		Ncr	4869 [kN]			Ncr	657 [kN]
Local flange wrinkling		Local web wrinkling		Local flange wrinkling		Local web wrinkling	
λf,f	1,00 [-]	λf,w	0,60 [-]	λf,f	2,74 [-]	λf,w	1,64 [-]
Φ,f	1,13 [-]	Φ,w	0,71 [-]	Φ,f	5,08 [-]	Φ,w	2,27 [-]
χ,f	0,61 [-]	χ,w	0,93 [-]	χ,f	0,11 [-]	χ,w	0,26 [-]
Nb,z,f,Rd	1177 [kN]	Nb,z,w,R	647 [kN]	Nb,y,f,Rd	230 [kN]	Nb,y,w,Rd	201 [kN]

Resistance

ηc	0,71 [-]	γM	1,62 [-]				
Flange		Web		Nc,Rd	3275 [kN]	Nb,z,Rd	647 [kN]
fxt,k	384 [MPa]	fxt,k	247 [MPa]	My,Rd	566 [kNm]	Nb,y,Rd	201 [kN]
fxc,k	384 [MPa]	fxc,k	247 [MPa]	Mz,Rd	131 [kNm]	Nb,Rd	201 [kN]
fyt,k	250 [MPa]	fyt,k	293 [MPa]	Vz,Rd	423 [kN]	Mb,Rd	63 [kNm]
fyc,k	250 [MPa]	fyc,k	293 [MPa]	Vy,Rd	782 [kN]		
τxy,k,flang	114 [MPa]	τxy,k,web	151 [MPa]	ILSS	8,77 [MPa]		

Table 5.10: Properties of access bridge beam

Structural capacity of the cross section
The check on the structural capacity[8]:

$$UC = \frac{N_{Ed}}{N_{Rd}} + \frac{M_{Y,Ed}}{M_{Y,Rd}} + \frac{M_{Z,Ed}}{M_{Z,Rd}} + \frac{V_{Y,Ed}}{V_{Y,Rd}} + \frac{V_{Z,Ed}}{V_{Z,Rd}}$$

$$UC_{midspan} = \frac{22.4}{3275} + \frac{32.8}{566} + \frac{5.2}{131} + \frac{0}{782} + \frac{0}{423} = 0.10$$

$$UC_{beamend} = \frac{22.4}{3275} + \frac{62.5}{566} + \frac{11.4}{131} + \frac{7.8}{782} + \frac{46.1}{423} = 0.32$$

Both the unity checks at the midspan and the beam end are $\leq 1,0$, hence the ULS check regarding structural capacity is ok. A higher value for the UC may occur somewhere between the midspan and the beam end, but it is unlikely this will be higher than 1.

Buckling
The UC check on buckling, on both the z and y axis:

$$UC = \frac{N_{Ed}}{N_{Rd,b,z}}$$

$$UC_z = \frac{22.4}{647} = 0.03$$

$$UC_y = \frac{22.4}{201} = 0.11$$

Since both UC's are lower than 1, the beams have sufficient buckling resistance. The local buckling stress in the flanges and the web is accounted for; material imperfections are accounted for by the material parameter γ_m.

[8]The torsion moment acting on the beam is negligible

Interlaminar shear strength

The interlaminar shear stress is based on the model assumptions set in Section 5.3.3: the moment is taken by the flanges and the shear force by the web. In eLamX^2 , laminates can be loaded and the corresponding stress response can be calculated. Table 5.11 presents the input forces on the laminates for the beam at the access bridge.

Location	N_{Ed} [kN]	$M_{y,Ed}$ [kNm]	$V_{z,Ed}$ [kN]	N_{load} [N/mm]	V_{load} [N/mm]
Midspan	22.4	32.8	0	301.9	0
Beam end	22.4	62.5	46.1	507.7	95.8

Table 5.11: Input forces for the interlaminar shear stress calculation for the access bridge beam

Where N_{load} and V_{load} are the force input for the normal force on the flange laminate and the shear force on the web laminate, respectively. The N_{load} is calculated by summing the bending moment divided by the profile height with the normal force on the whole cross section of the beam[9]. This results in the following interlaminar shear stresses:

Cross section part	Regarded location	Interlaminar shear stress [MPa]
flange	midspan	2.13
web	midspan	0
flange	beam end	3.59
web	beam end	3.20

Table 5.12: Interlaminar shear stress for the decisive load the access bridge beam; member forces from FEM analysis

The ILSS resistance capacity for the beam is:

$$ILSS = \frac{ILSS_{polyester} * \eta_c}{\gamma_m} = \frac{20 * 0.71}{1.62} = 8.77$$

Hence, the interlaminar shear stress does not exceed the interlaminar shear stress at the access beam in the flanges and the web.

[9]This is a very conservative boundary: to get the actual normal force per unit length on the laminate, the normal force should be multiplied by the area of the regarded laminate divided by the total area of the cross section

5.7.4. Consideration for beams located underneath the loading arm

While the superimposed loads on beam 1 and beam 2 can be modeled as line loads, beam 3 also bears the load of the loading arm. To incorporate all the imposed loads, a different design approach for beam 3 is needed. Figure 5.23 illustrates a sketch of the situation. The load will induce normal pressure stress along its trajectories from the planks to the pile, which bears the load. The surface area in the direction of the load is much higher at the flanges than it is in the web. Therefore, the greatest change of stress state is expected in the web.

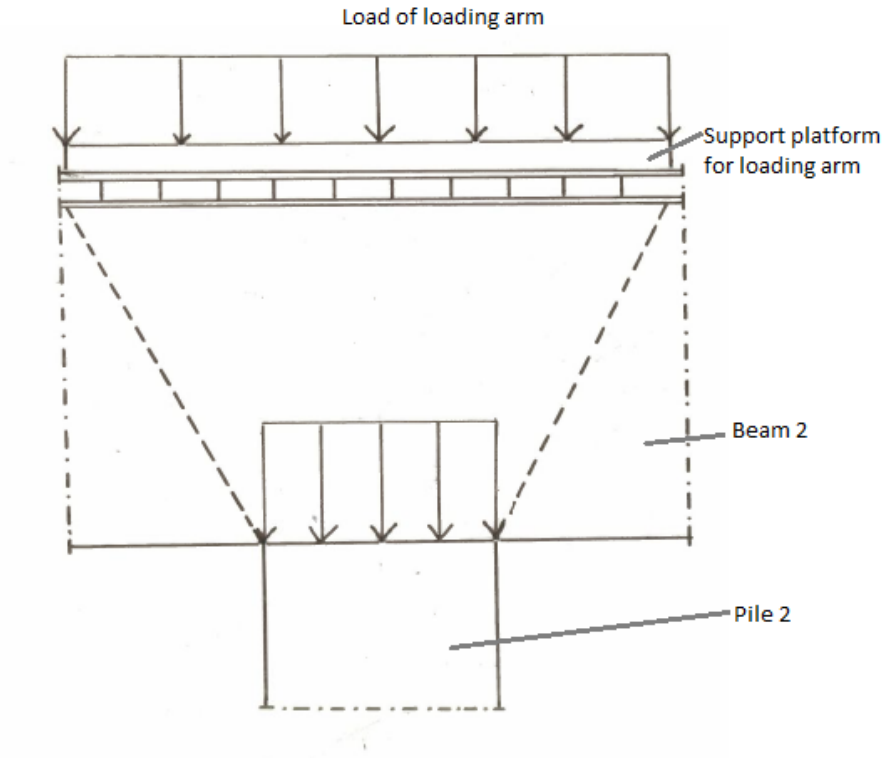

Figure 5.23: Stress trajectories assumption for beam 3

An indication of the required area (or web thickness) is to divide the fundamental load combination of the loading arm by the length over which the beam is supported by the pile times the thickness of the web. The loads from the loading arm are a static load and a bending moment around the x and y axis. The increase in normal stress can be calculated with:

$$\Delta\sigma_z = \frac{F_z}{t_w l_1} + \frac{M_y}{\frac{1}{6} t_w l_1^2}$$

$$\Delta\sigma_z = \frac{F_z}{t_w l_1} + \frac{M_x}{\frac{1}{6} t_w^2 l_1}$$

5.7.5. Overview of critical ULS checks

Table 5.13 presents the maximum UC's for the envelope of all ULS combinations; if UC > 1, the structural elements possess insufficient resistance with respect to the imposed load. Two occasions occur where the UC gets exceeded: for beam 1 at the access bridge and the girder between the access bridge. Both these checks can be discarded with arguments.

Structural element	Location	UC		
		Cross section capacity	Buckling	Lateral torsional buckling
Beam 1	Access bridge	0.3	0.011	1.05
Beam 2	Platform	0.27	0.03	1.00
Beam 2	Loading arm[10]	0.59	0.02	0.50
Girder 1	Between access bridge beams	0.8	0.23	3.54
Girder 1	Wind bracing at access bridge	0.06	0.00	0.29
Pile 2	Access bridge	0.31	0.44	-[11]
Pile 2	Platform	0.41	0.64	-
Pile 2	Loading arm	0.36	0.65	-

Table 5.13: Overview of the maximum UC's for the ULS envelope

First, the check on lateral torsional buckling is based on a situation where only the supports are lateral unsupported; the main body of the beam is not. However, in the FEM model, stiffness to the structure contributed by the planks is not accounted for as they are modeled as a distributed load, equal to their dead weight. Since the planks need to be fastened to the beam, load transfer will take place: especially in the direction of the plank under a parallel wind load to the local beam axis. Hence, the planks provide lateral stiffness. An analogy can be taken with the Vierendeel truss (Schöck Bauteile GmbH, n.d.):

The planks act as the bars perpendicular to the beams and therefore provides stiffness in the direction perpendicular to the beam.

The UC of 3.54 applies to the girder located between the beam ends at the access bridge, directly supporting the access bridge beams as in Figure 5.34. This is the only element, aside from the planks which provide lateral stiffness. If this element is altered, for instance by replacing it by a beam with the same dimensions as the beam at the access bridge, the problem with lateral torsional buckling will most likely not occur.

[10] Located at platform, and influenced by the load of the loading arm
[11] Circular profiles are not prone to lateral torsional bending

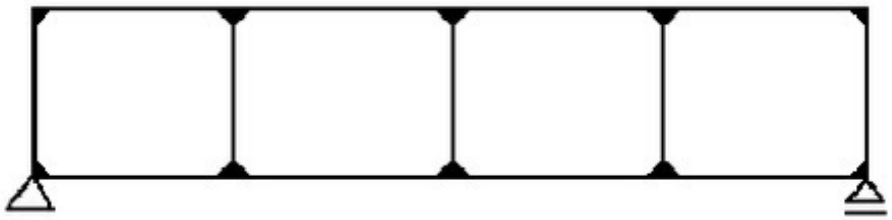

Figure 5.24: Vierendeel truss (Schöck Bauteile GmbH, n.d.)

5.8. Technical design of the piles

The piles are the spill in the design process: they heavily influence the global stability of the FRP jetty and are therefore treated in a separate section. Besides the SLS and ULS criteria, also the feasibility of installation is regarded in Chapter 6.

In the preliminary design phase, the pile dimensions were determined by the deflection criteria. To comply with the deflection criteria, the diameter of the piles was increased. This led to very large pile diameters (about 2 m in width). After a consideration of the results, it was determined to continue with the original pile diameter and properties (see Section 5.8.1).

The choice to continue with the original piles was made because research regarding FRP piles focuses on hollow FRP piles within a certain dimensional range, made available by producers (Winter, 2017). Hence, judgment regarding the technical feasibility will have stronger theoretical arguments (see Section 6.1). Another argument is that the pile embody a significant part of the total material costs of the jetty, so other solutions than scaling up the pile might be financially more attractive. Also, this thesis explores subjects in which the FRP piles are used, expanding the existing body of research regarding the FRP piles.

Figure 5.25 illustrates the definite pile layout for the platform, including the batter angles and direction of the piles.

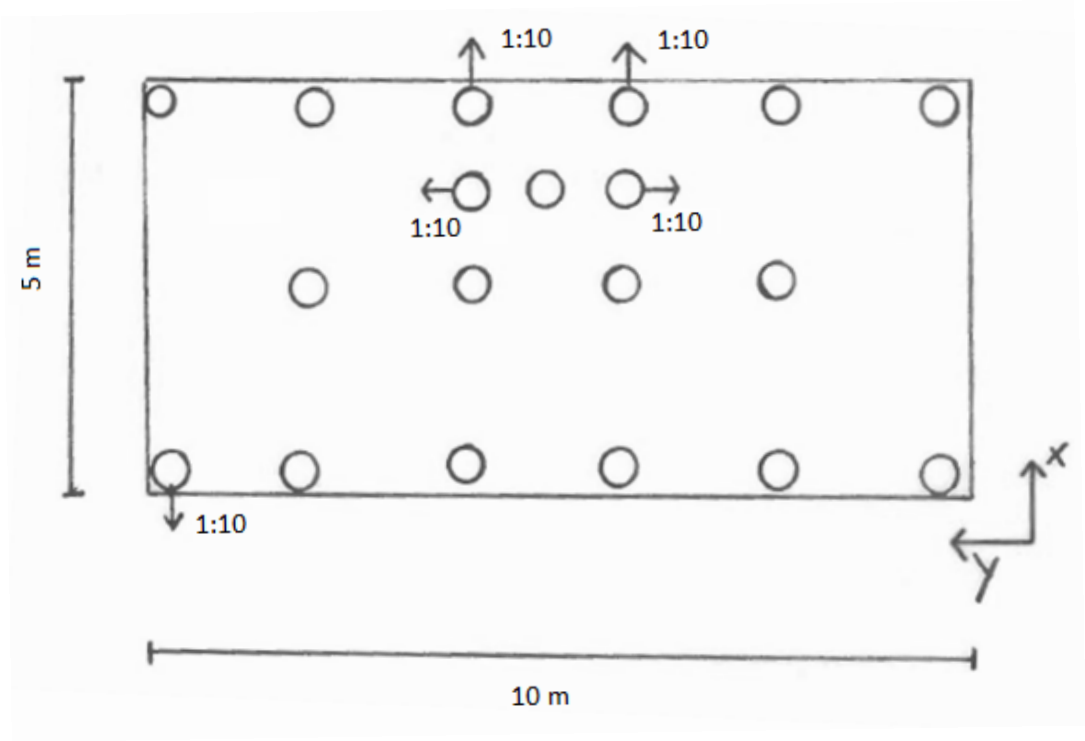

Figure 5.25: Pile plan for the platform of the FRP jetty

5.8.1. Mechanical properties and dimensions of the pile

Pile dimensions and properties are based on the hollow FRP piles researched by Guades et al (Guades, Aravinthan, Islam, & Manalo, 2012) and Zyka and Mohajerani (Zyka & Mohajerani, 2016). Both reviewed the performance and the installation of hollow FRP piles. Table 6.1 presents the physical properties and the dimensions of the selected hollow FRP pile.

Property	Symbol	Value	Unit
Area	A	14 000	mm^2
Density	ρ	1927	kg/m^3
E-modulus	E	23	GPa
Wave speed	c	3455	m/s
Impedance	Z	93 000	kg/s
Wall thickness	t	13/17	mm
Diameter	D	356/456	mm
Length	L	25.5	m

Table 5.14: Physical properties and dimensions of the circular hollow FRP pile

The material factor and the conversion factor for the piles are set at 1.62 and 0.63 respectively.

5.8.2. Modeling of the pile-soil interaction and determination of the geotechnical parameters of the soil

The soil characteristics influence the structural response of the piles due to loading and therefore needs to be modeled adequately. Appendix A.1 and Appendix A.2 present results and locations of the cone penetrations tests and boring samples.

A suitable foundation layer, comprised of sand, is located at –21 m NAP. Cone penetration test 5 is located at the platform, the layer possesses a cone resistance of 20 MPa and a friction coefficient of about 1 %.

The soil-pile interaction is modeled with horizontal and vertical springs. The horizontal stiffness is determined by the method of Ménard, the vertical stiffness is based on technical expertise within the Gemeente Rotterdam.

Modeling of the pile-soil interaction

Several models are available for the modeling of pile-soil interaction: in this thesis, the soil-pile interaction is modeled with horizontal and vertical springs. Analytical models for the lateral response are provided by Blum (Molenaar, Voorendt, Molenaar, & Voorendt, 2016) and Zyka and Mohajerani for the lateral deflection of FRP piles (Zyka & Mohajerani, 2016). Figure 5.26 summaries Blum's idea to model an embedded pile as a bar with a fixed support and an equivalent length. This length is dependent on the embedment depth of the pile and the soil parameters (Molenaar et al., 2016). Figure 5.27 illustrates the effect of additional stability for a console: in to estimate the pile deflection using Blum's model, the console can be modeled as a single pile if the acting horizontal load is halved.

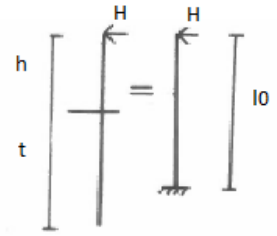

Figure 5.26: Situation for Blum's model

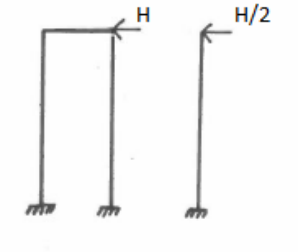

Figure 5.27: Assumptions for the system stiffness

With this model, an analytical estimate of the horizontal pile deflection can be obtain. However, three things should be noticed: first, the model cannot account for girders. These increase the lateral stability and can reduce the console deflection considerably. Second, the model is applicable for a single soil layer: in mosts geological locations where piles are needed, the soil consists of various layers with different properties. Last, the model does not account for shear deformation. An elaborated method to calculate the normalized horizontal pile deflection of FRP piles is presented by Han (Han & Frost, 2000).

More accurate horizontal deflections can be calculated with models which incorporate the modulus of subgrade reaction. In this model, the soil is modeled as an elastic spring as illustrated by Figure 5.28. While analytical solutions to the deflection load problem are elaborate to calculate for this model, FEM software (such as SCIA) is able to quickly calculate deflection and stresses in the pile. Therefore, the spring-model is used to estimate the pile and console deflection due to the imposed loads.

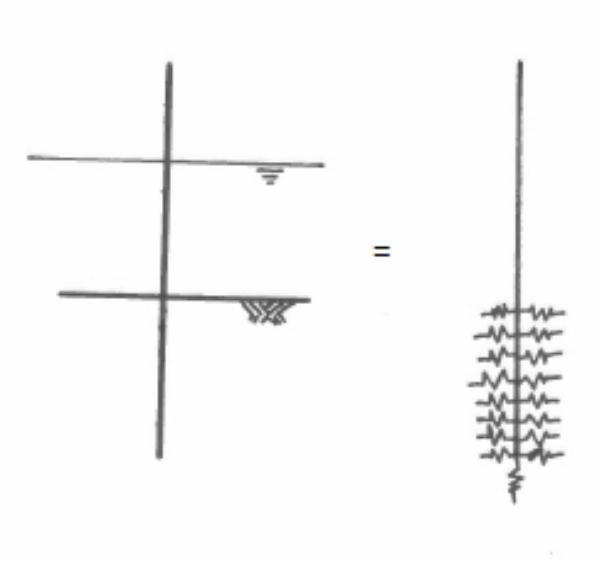

Figure 5.28: Modeling of the soil by using elastic springs

Horizontal modulus of subgrade reaction

The horizontal stiffness of the soil is determined with an empirical formula from Ménard, which is based on in-situ tests using a pressure meter. (Cherqaoui, 2006; Hoefsloot, 2006). The Ménard theory models the horizontal soil reaction as a spring, dependent on the soil type, pile diameter and cone resistance. For further reference, Hoefsloot provides an overview of different models to determine the pile-soil interaction in a report (Hoefsloot, 2006).

The empirical formula from Ménard is:

$$\frac{1}{k_h} = \frac{1}{3E_p}\left[1.3R_0\left(2.65\frac{R}{R_0}\right)^{\alpha} + \alpha R\right] \tag{5.18a}$$

$$R_0 = 0.3\,\text{m} \tag{5.18b}$$

$$R = \frac{D}{2} \tag{5.18c}$$

$$E_p = \beta * q_c \tag{5.18d}$$

Where:

K_h	: horizontal modulus of subgrade reaction in kN/m^3
R_0	: reference radius in m
R	: radius of the pile in m
E_p	: elasticity modulus according to Ménard
q_c	: cone resistance in MPa
α	: rheologic factor according to Ménard
β	: rheologic factor according to Ménard

Note: for non-circular pile cross sections, an equivalent pile radius should be calculated based on an equivalent cross section area.

The in-situ soil has been divided into two areas with different horizontal modulus of subgrade reaction: 15 MN/m^2 and 7 MN/m^2.

Pile grid line	Horizontal modulus of subgrade reaction on relative pile length		
	15 MN/m2	7 MN/m2	SCIA input for 7 MN/m2
1	-	-	-
2	0 to 0.1	0.1 to 0.82	0.1 to 0.8
3	0 to 0.1	0.1 to 0.71	0.1 to 0.7
4	0 to 0.1	0.1 to 0.63	0.1 to 0.6
5	0 to 0.1	0.1 to 0.43	0.1 to 0.4
6	0 to 0.1	0.1 to 0.43	0.1 to 0.4

Table 5.15: Horizontal modulus of subgrade reaction for the piles, indicated at the relative pile distance (pile length = 25 5m)

The first piles at the abutment are consisting concrete piles. These are modeled as fixed end supports.

Vertical modulus of subgrade reaction
For analytical system, the stiffness of the pile and the stiffness of the soil can be incorporated into one single stiffness of the system: this allows the system to be modeled as a single spring, which is useful to calculate structure responses. The vertical stiffness of the system, which in essence is a series, can be calculated with the following formula:

$$\frac{1}{k_{pv}} = \frac{1}{k_{pile}} + \frac{1}{k_{soil}} \tag{5.19a}$$

$$k_{pile} = \frac{EA}{l} \tag{5.19b}$$

where $k_{soil} = 100\,\text{MN/m}$, according to the geotechnical specialist who designed the case study (Dengkeng, 2017).

In the FEM model, only the vertical soil subgrade reaction is used. The stiffness of the pile is inherently accounted in the FEM model and therefore, no single system stiffness is needed but solely the vertical soil subgrade reaction at the pile tip.

Abutment
The abutment is an existing structure, which composes two concrete piles. The concrete piles are fully embedded in soil and have minimum displacement (i.e. < 2 mm in the case study). Therefore, the abutment is modeled as two free end hinges. The translation directions are all fixed (x,y,z); the rotational z-direction is fixed and the y- and z-direction are free.

5.8.3. SLS criteria for the piles

The NEN 9997-1 part 1 prescribes the following the SLS criteria for pile foundations:

- excessive settlement of the pile;
- excessive uprise of the pile;
- excessive horizontal displacements of the pile;
- unacceptable vibrations

The NEN 9997-1 part 1 is based on Eurocode 7-1.

The most important criteria is the horizontal deflection criteria: the Eurocode recommends a maximum horizontal deflection of 50mm (NEN, 2011). This amount of deflection is not surpassed in the FRP jetty. Horizontal deflection criteria are often not specified because conventional jetties from reinforced concrete do not possess such deformations when the design agrees with the ULS criteria. However, FRP can deform a lot before breaking due to its high strength to stiffness ratio. Such deformations also most likely induce instability phenomenons due to geometrical non-linear displacements. Therefore, deformations should be limited or non-linear stability calculations should be included in the structural analysis.

Several variants have been researched to increase the lateral stability for the access bridge[12]:

1. Vary the angle of the piles
2. Add additional girders between the piles (stiffness frames)
3. Add additional piles
4. Combination of more piles and more girders

5.8.4. ULS criteria for the piles

Section 5.7 presents the ULS criteria for the other structural elements; the ULS criteria for the piles have those same checks as well as additional checks. The additional checks relate to the bearing capacity of the pile and the soil.

Bearing capacity

The bearing capacity of the pile, according to Eurocode 7 and its Dutch annex NEN-EN 9997-1:2011, has to be determined with Koppejan. The bearing capacity exists of the tip resistance and pile shaft friction (Molenaar et al., 2016):

$$F_{r;max} = F_{r;max;tip} + F_{r;max;shaft} \tag{5.20a}$$

$$F_{r;max;tip} = A_{tip} * p_{r;max;tip} \tag{5.20b}$$

$$F_{r;max;shaft} = O_{p;avg} \int_0^{\Delta l} p_{r;max;shaft} dz \tag{5.20c}$$

Where:

$F_{r;max}$: maximum bearing force in kN
$F_{r;max;tip}$: maximum tip resistance force in kN
$F_{r;max;shaft}$: maximum shaft friction froce in kN

[12]The images were taken midst of the design process: the pile length is not represented because they were shortened, see also Section 6

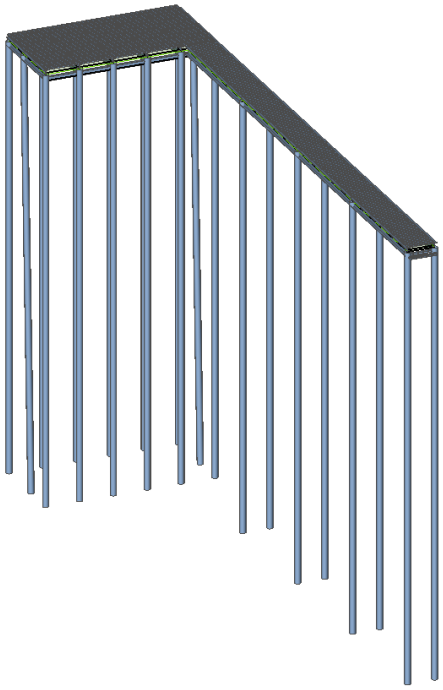

Figure 5.29: First draft of the access bridge and platform

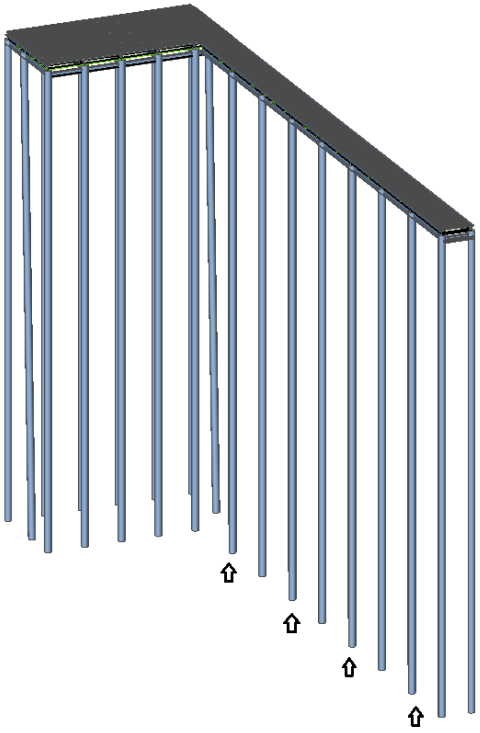

Figure 5.30: Variant of the access bridge with additional piles (indicated with arrows)

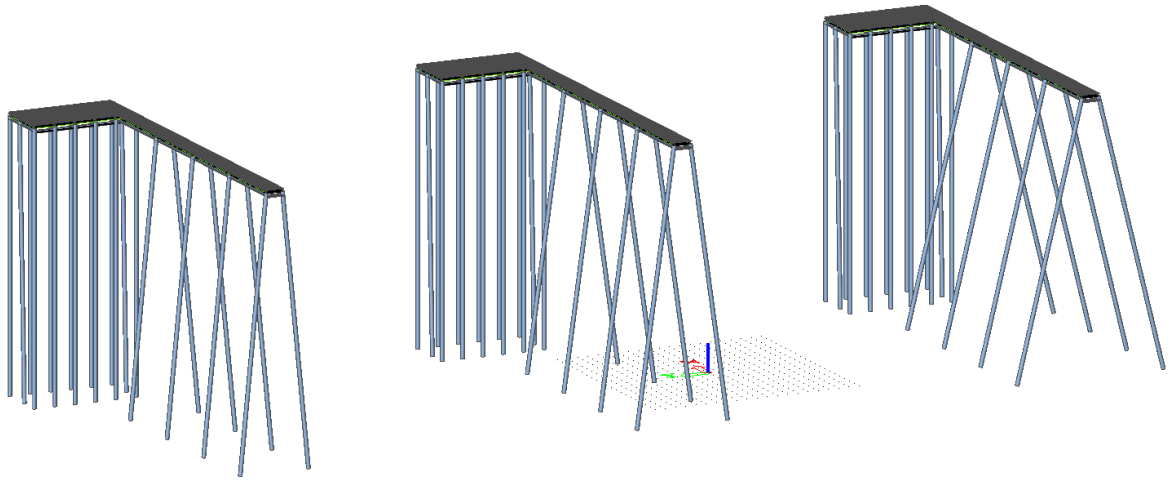

Figure 5.31: Three different variants for the access bridge, each with different rakes for the piles

A_{tip} : cone resistance in MPa
$p_{r;max;tip}$: maximum tip resistance according to the sounding in kN/m^2
$O_{p;avg}$: circumference of the pile shaft in m^2
Δl : length of the pile in m
$p_{r;max;shaft}$: maximum pile shaft friction according to the sounding in kN/m^2

In the Netherlands, the values for the tip bearing capacity and shaft bearing capacity have to be

Figure 5.32: Three different variants for the access bridge, each with different rakes for the piles and additional girders

determined with the method of Koppejan (Molenaar et al., 2016):

$$p_{r;max;tip} = \frac{1}{2}\alpha_p \beta s \left(\frac{q_{c;I;avg} + q_{c;II;avg}}{2} + q_{c;III;avg} \right) \tag{5.21a}$$

$$p_{r;max;shaft} = \alpha_s q_{c;z;a} \tag{5.21b}$$

Where:

α_p	: pile class factor, a reduction for pile installation type
β_s	: reduction factor for piles with a widened foot
$q_{c;I;avg}$	: minimum mean value of the cone resistance in the first influence area
$q_{c;II;avg}$	: minimum mean value of the cone resistance in the second influence area
$q_{c;III;avg}$	: minimum mean value of the cone resistance in the third influence area

5.8.5. Example: ULS check for pile 2 at the platform

The two main unity checks are presented in this section: pile bearing capacity and buckling resistance capacity. Checks regarding the structural capacity of the cross-section were already exemplified in Section 5.7.3.

Pile bearing capacity

The bearing capacity of the pile is determined by using cone penetration test S05 (see Appendix A). Cone penetration S06 possess similar soil characteristics, located in proximity to S06. The pile tip is located at -20.9 m NAP (top of structure = +4.6 NAP, pile length = 25.5 m[13].

For the tip bearing capacity, with $\alpha_p = 1, \beta = 1,$ and $s = 1$:

$$p_{r;max;tip} = \frac{1}{2}\left(\frac{14+10}{2} + 2 \right) = 7\,\text{kN}$$

$$F_{r;max;tip} = 27\,395\,\text{mm} * 7\,\text{MPa} = 192\,\text{kN}$$

[13] A pile drive analysis was done after calculating the bearing capacity, resulting that the piles with a length of 25.5 m were not drivable to the desired depth. The bearing capacity of the these piles are based on outer and inner friction and accumulate to 1000 kN: see Section 6.6.1 for more information

Where:

$q_{c;I;avg}$: 14 MPa
$q_{c;II;avg}$: 10 MPa
$q_{c;III;avg}$: 2 MPa

The calculated value can be regarded as a lower boundary for the pile bearing capacity. When driving hollow piles, plugs are formed due to, among other parameters, the confinement effect of the hollow tube. The soil plug gets loaded and therefore stiffness increases. Therefore it is able to transfer stresses from the tip of the pile to the inner shaft of the pile; new design equations for skin friction factor and end bearing factor were suggested by Gudavalli et al. (Gudavalli, Safaqah, & Seo, 2013). It must be noted that their research is based on very dense sands (which might be the case at the -20 m NAP level in S05) and open-ended steel tubular piles.

For the shaft bearing capacity, negative and positive shaft friction has to be regarded. Negative shaft friction is disadvantageous and occurs when the soil settles faster than the pile. Positive shaft friction is advantageous and occurs when the pile settles faster than the soil.
The negative shaft friction is assumed to be zero. The soil surrounding the piles is not loaded (since all loads are diverted to the deeper soil levels through the pile). The pile settlement occurs due to shortening of the pile due to compressive strengths: $\delta l = \frac{Fl}{EA}$. Since the E-modulus of FRP is relatively low, the assumption that positive shaft friction occurs seems valid.
It is assumed that positive shaft friction occurs from -10 m NAP, which is more or less 2 m below harbor bottom level, with an average value of 2 MPa over the length of the pile where positive shaft friction is assumed (this value is conservative, see S05 in Appendix A. For α_s, a value of 0.0075 is chosen; this refers to a steel profile pile with little ground displacement. The friction of FRP hollow piles were found to have similar characteristics regarding shaft friction compared to steel hollow pipes (Zyka & Mohajerani, 2016). Then, the value for the shaft friction is:

$$p_{r;max;shaft} = 0.0075 * 2 = 0.015\,\text{MPa}$$
$$F_{r;max;shaft} = 1.43 * (21.9 - 10) * 0.015 = 256\,\text{kN}$$

The total bearing capacity of the pile is then:

$$F_r; max = 192 + 256 = 447\,\text{kN}$$

The maximum vertical support reaction in the ULS is 177.71 kN, at the tip pile 3-1. We find for the UC:

$$UC = \frac{N_{Ed}}{F_{r;max}} = \frac{178}{447} = 0.4$$

Hence, the UC regarding pile bearing capacity is OK.

Buckling
Bucking appears to be an important check for the pile design of the FRP jetty: this is due to the long unsupported length of the pile. Also, the relatively low stiffness of the composite makes the piles more prone to buckling. The challenges in determining the buckling load are to include considering shear deformation influences, to estimate the correct boundary assumptions for buckling modes, and determining the buckling length of the piles.

The mechanical and physical properties of the pile have been based on research articles, but no indication for the shear modulus of hollow FRP piles was found. Therefore, a Poisson's ratio of 0.4 is assumed, generating a shear modulus of 8214 MPa.

The influence of shear deformation on the piles is negligible. Han and Frost researched buckling of vertically loaded FRP piles (Han & Frost, 1999) and stated that shear effects should be considered due to the high stiffness/shear modulus ratio. They developed an analytical solution for this problem by incorporating the Timoshenko shear beam theory instead of the Euler-Bernoulli beam theory. The solution is a generalization of the classic solution (i.e. based on Euler-Bernoulli beam theory). The generalized solution possess the shear effect coefficient (λ); when $\lambda \rightarrow \infty$ the classic solution is obtained.

$$\lambda = \sqrt{\frac{G_{xy} k A}{E_x I_y}} = \sqrt{\frac{8214 * 0.585 * 27395}{23000 * 652.3 * 10^6}} = 75.5 \tag{5.22}$$

Where k is the Timoshenko shear coefficient for a hollow circular cross section (Hutchinson, 2001)[14]. Han and Frost found that for $\lambda < 10$ shear deformation significantly has a negative effect on the critical buckling load. Therefore, due to the relatively high value of λ, the influence of shear deformation is omitted and solutions based on the Euler-Bernoulli beam theory are considered in determining the critical buckling load.[15]

The buckling length is determined by formulating an equivalent length and by assuming the bottom boundary conditions as fixed in direction but free to rotate $[\phi \neq 0, \delta = 0]$ and fixed $[\phi = 0, \delta = 0]$ for the top and the bottom of the pile, respectively. Bhattacharya and Madabhushi stated that for these conditions, the effective buckling length is $\frac{1}{\sqrt{2}}$ times the system length (Bhattacharya & Madabhushi, 2008). This system length is determined by a method developed by Davisson and Robinson (Tomlinson & Woodward, 2008). Figure 5.33 illustrates how an installed pile can be modeled as a shorter, fixed pile with an equivalent length L_{eq}.

The stiffness factor is used to determine the equivalent pile length[16].:

$$R = \sqrt[4]{\frac{EI}{kB}} = \sqrt[4]{\frac{13010110}{185 * 10^5 * 0.456}} = 1.114\,\text{m} \tag{5.23}$$

Where k is the horizontal modulus of subgrade reaction according to Ménard. An embedment length of 11 m results from the assumption that mud layer is present in about the first 2 m from the harbor bottom level (which negatively influences the equivalent length). The equivalent length then is:

$$z_f = 1.8 * R = 1.8 * 1.114 = 2.006\,\text{m} \tag{5.24a}$$

$$e = 25.5 - 11 = 14.5\,\text{m} \tag{5.24b}$$

$$L_e = e + z_f = 16.58\,\text{m} \tag{5.24c}$$

The formula holds since $L/R = 9.5 > 4$ (Tomlinson & Woodward, 2008).

[14] The formula used to estimate the Timoshenko shear coefficient is presented in Appendix F

[15] Poisson's ratio of the FRP piles is unknown: ranging the ratio from 0.2 to 0.5 yield a maximum stiffness/shear modulus ratio of 3 (with $\nu = 0.5$ and $G_{xy} = \frac{Ex}{2(1+\nu xy)}$, based on the isotropic relation which in fact is, wrong). In the research, ratio ranging from 15-30 have been found. However, a shear modulus of 144 MPa generates $\lambda = 10$. The axial stiffness to shear modulus ratio then is almost 160, which seems very unrealistic.

[16] Values for the subgrade modulus of the soil were found in Section 5.8.2

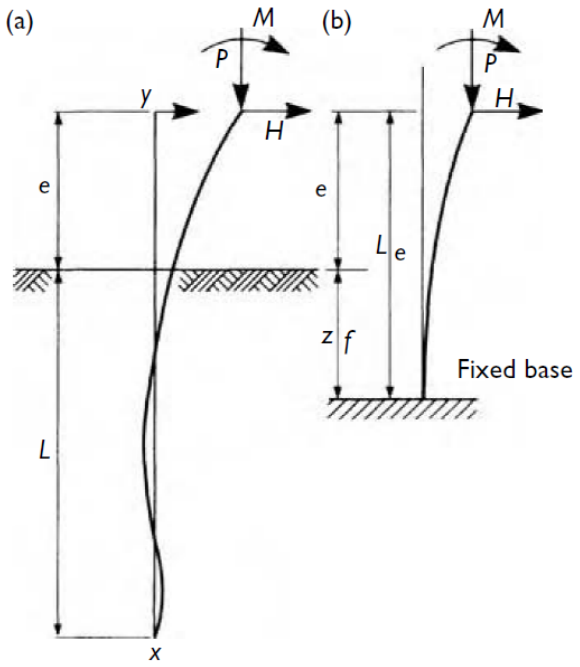

Figure 5.33: Bending of pile at head (a) Partly embedded pile (b) Equivalent fixed base pile (Tomlinson & Woodward, 2008)

The critical buckling load is then:

$$L_k = \frac{1}{\sqrt{2}} * L_{eff} \tag{5.25}$$

$$N_{cr} = \frac{2\pi^2 EI}{L_{eff}} = \frac{2 * \pi * 13 * 10^6}{16.58} = 934\,\text{kN} \tag{5.26}$$

With the critical buckling load, the resistance capacity against buckling can be calculated. In this calculation, local flange buckling has been accounted, but no imperfections have been accounted for (de Boer et al., 2016):

$$\bar{\lambda}_f = \sqrt{\frac{A\rho f_{c,k}}{N_{cr}}} = \sqrt{\frac{23446 * 0.24 * 23446}{934 * 10^3}} = 3.23 \tag{5.27a}$$

$$\Phi = 0.5\left[1 + \alpha_f\left(\bar{\lambda}_f = \bar{\lambda}_{f,0}\right) + \bar{\lambda}_f^2\right] \tag{5.27b}$$

$$\chi = \frac{1}{\Phi + \sqrt{\Phi^2 - \lambda^2}} \tag{5.27c}$$

$$N_{b,Rd} = \chi\frac{\eta_c A\rho f_{c,k}}{\gamma_M} = 0.31 * \frac{0.63 * 23446 * 0.24 * 276}{1.62} = 182\,\text{kN} \tag{5.27d}$$

Values for α_f and ρ (which accounts for local flange buckling) are presented in Appendix D.3.

The UC regarding the buckling:

$$UC = \frac{N_{Ed}}{N_{b,Rd}} = \frac{178}{182} = 0.97 \leq 1 \tag{5.28}$$

Note: the buckling load is calculated with the initially intended length of the pile (25.5 m). After the pile drive analysis it was clear it was impossible to drive these piles to the intended depth. However, it was found that sufficient bearing capacity was found at a more shallow depth, based on the developed inner and outer friction. The resulted new pile has a length of 18.2 m driven to depth of 6 m below ground level. Following the above procedure, the calculated buckling load resistance is:

197 kN pile head is free in translation but fixed to rotate
339 kN pile head is fixed in translation but free to rotate

The maximum occurring normal force in the piles is still 178 kN, and hence the shorter piles also posses sufficient buckling capacity to withstand the maximum normal force regardless of the made assumptions for the boundary conditions.

5.9. Joints of the FRP jetty

This section presents a brief overview of the joints of the FRP jetty. First, some general sketches illustrate different options for the detailing of some joints. Then, one joint is elaborated and tested for structural capacity.

While the in the preliminary design, the joints were modeled as hinges, ultimately in the FEM model they were modeled as fixed in order to reduce midspan deflection. In reality, the joints while be between fixed and hinged; key in modeling the joints is to account for a lot of stiffness in order to make them more fixed-like.

BIJL profielen, a company which produces FRP profiles and bridge decks, utilizes stainless steel bolts and nuts instead of FRP bolts and nuts. The reason for this is of the excessive creep FRP experiences (BIJL Profielen, 2017).

5.9.1. Overview of the joints

The following joints are identified:

- I-profile on pile
- Girder on pile, supporting the I-beam
- Pile head/ring on pile
- Planks on pile
- Wind bracing (girder) on piles

Sketches of access bridge joint

Figure 5.34 illustrated a concept for the joint where the beams of the access bridge are supported by the pile. The girder provides additional support area for the pile.

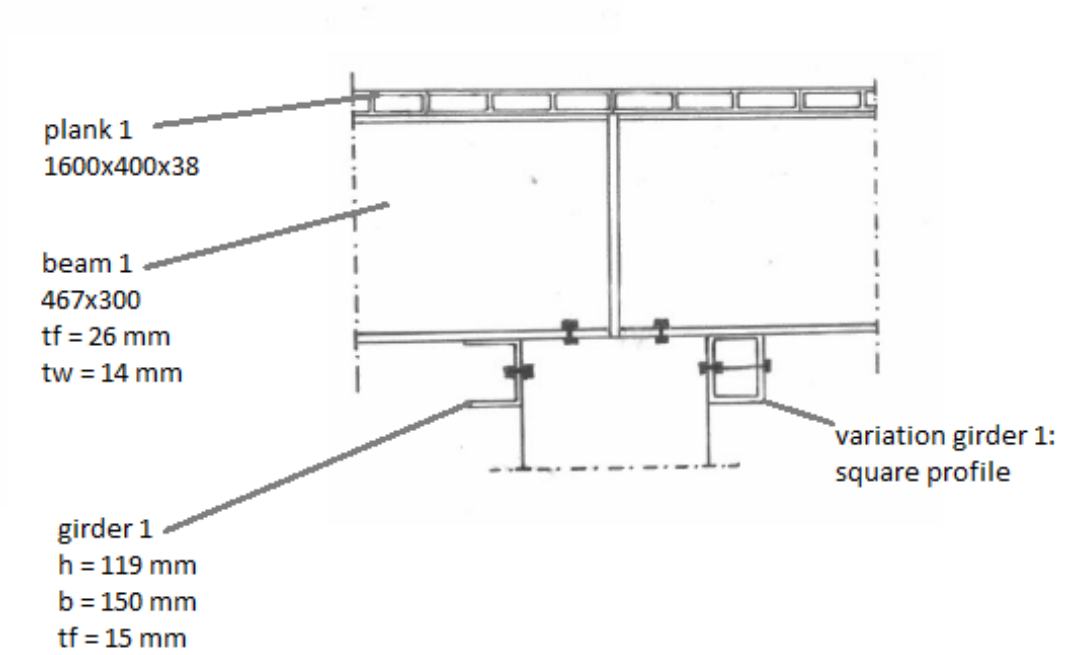

Figure 5.34: Detail for the beam supports

Figure 5.35 illustrates a top view of a possibility to connect the girders. By connecting them and making a square, additional area is created to which the pile can be attached by a pile head.

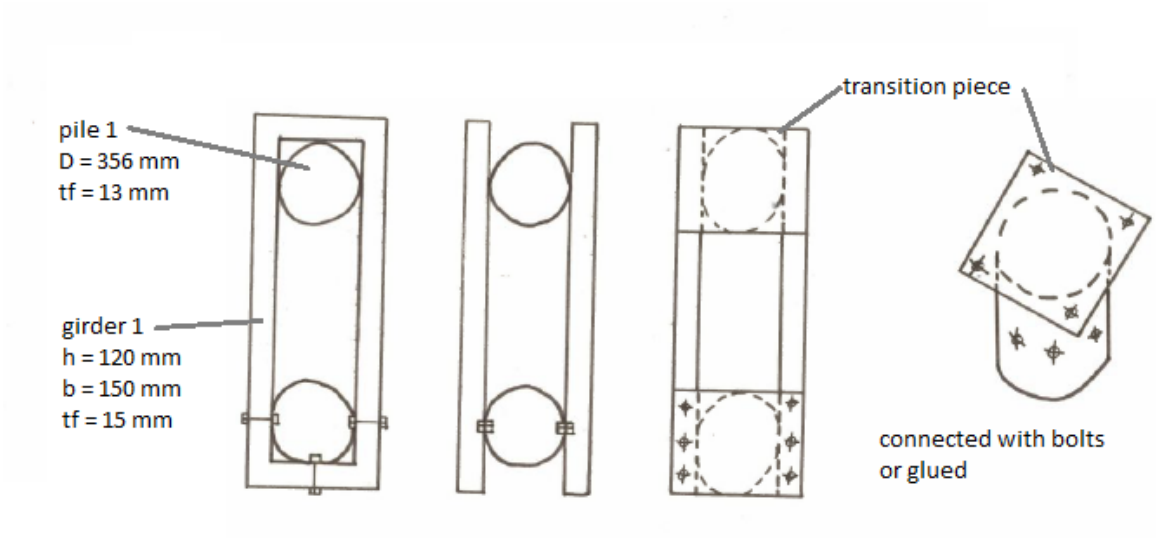

Figure 5.35: Detail for the girder

5.9.2. Renders of the access bridge and platform joints

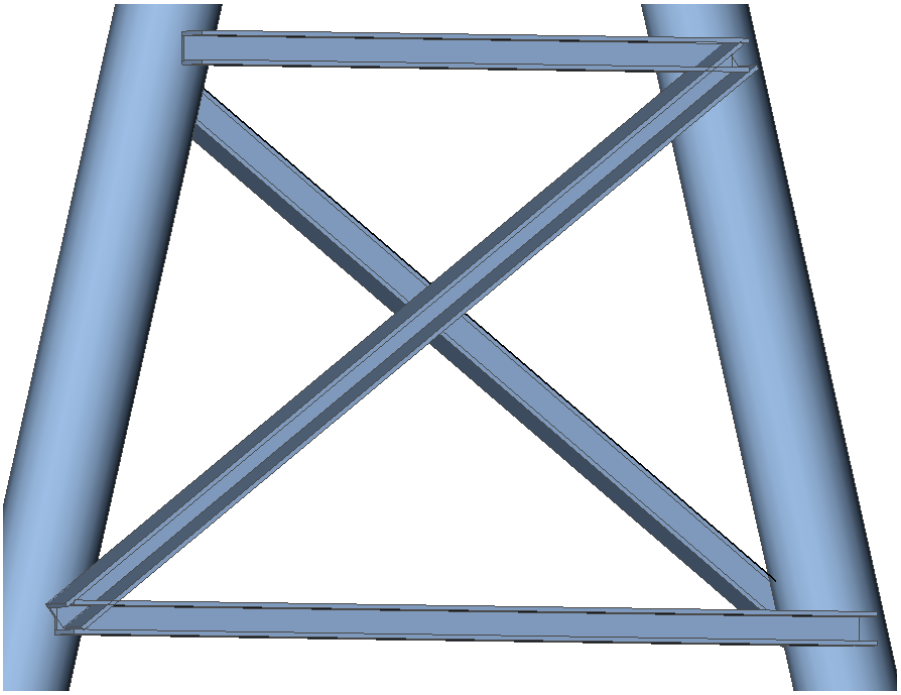

Figure 5.36: Wind bracing underneath the access bridge deck, composed of girders

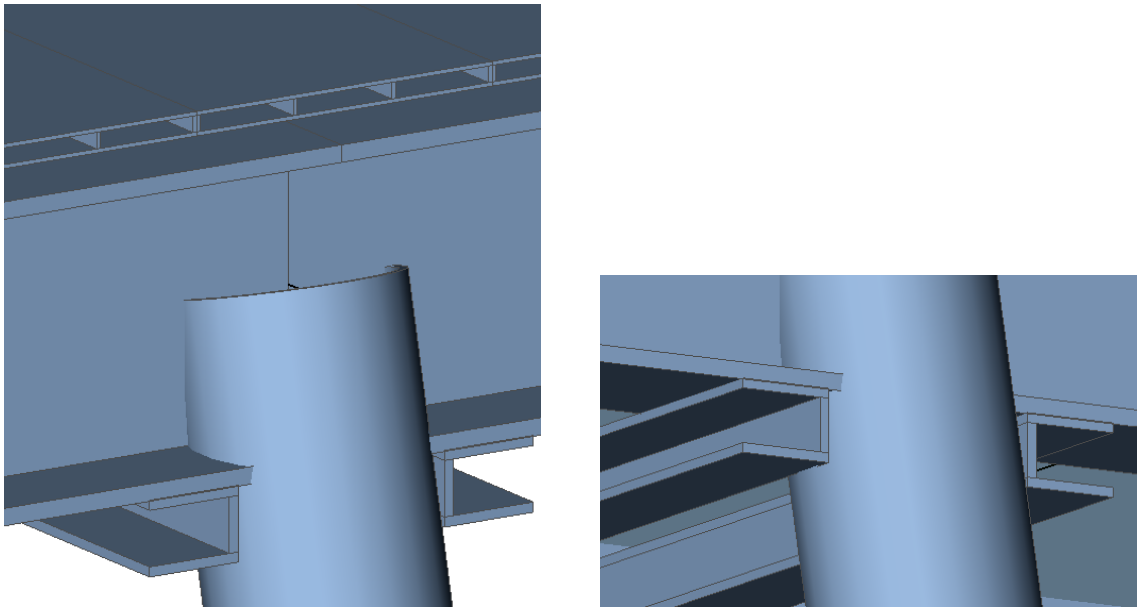

(a) View from above (b) View from below

Figure 5.37: Access bridge joint at the intersection between the pile and access bridge deck

Rendered model of the platform joints
Several location at the platform required attention regarding joint design.

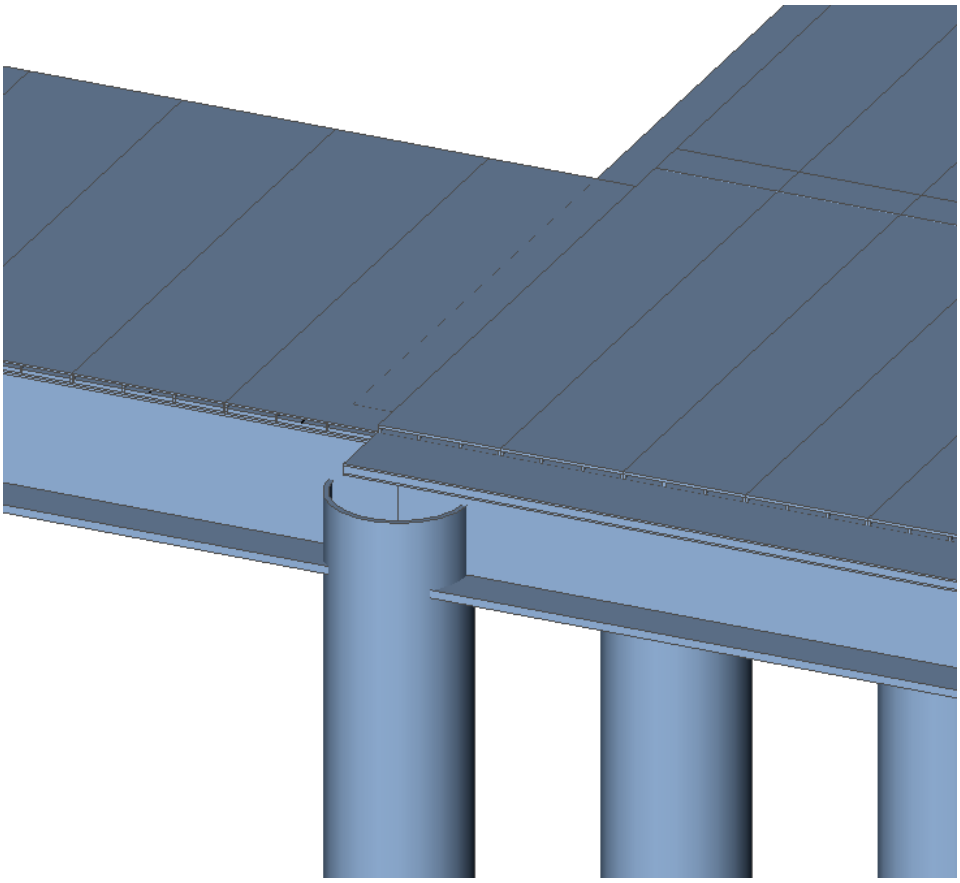

Figure 5.38: Corner adjacent to the access bridge

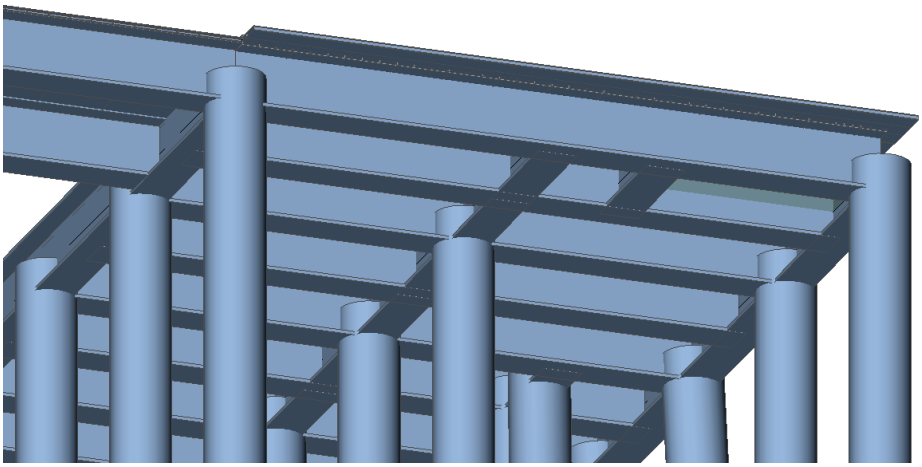

Figure 5.39: View of underside platform

5.9.3. Example: joint at access bridge

One joint is elaborated in this thesis in order to demonstrated the technical feasibility of the joints. The structural criteria provided by the CUR96 are used (de Boer et al., 2016). The joint at the access bridge, connecting the I-beam to the pile head, is elaborated; this is a key joint in the structural design.

First, the resulting forces on the bolts are determined. Then, the capacity of the laminate is checked against the relevant criteria presented in the CUR96 (de Boer et al., 2016). In general, the bolts itself and the laminate have to be checked. However, in the scope of this thesis, the checks are limited to the checks related to the laminate (with the exception of fatigue):

- In-plane loads
  - Bearing failure
  - Net-tensile failure of the laminate
  - Shear failure of the laminate
  - Cleavage
  - Joint buckling
- Out-of-plane loads
  - Puncture
  - Inter-laminar shear
- Fatigue

The joint configuration is chosen as such that only significant in-plane loads occur: after initial configurations it was clear that the resistance of the laminate to out-of-plane loads is lower compared to in-plane loads. Therefore, the out-of-plane loads are effectively canceled. A more detailed description of the types of joints and joint failure mechanisms is presented in the accompanying literature study (Winter, 2017).

Figure 5.40 illustrates the layout of the elaborated joint. Two half-rings with flanges are placed around the pile head, which are fastened with bolts and nuts: the ring then clamps itself onto the pile. The ring and the bolts are produced from stainless steel because of its high stiffness and corrosion resistance. As the joint in the overall structural model is modeled as fixed, this joint should be designed as such. The high stiffness of the steel ring and bolts contribute to the overall stiffness of the joint. Also, using a double row of bolts increased the stiffness of the joint.

There is no physical connection between the bottom of the I-beam and the pile. This is done deliberately because the FRP is presumably not well suited to shear-puncture due to its low lateral stiffness. By 'floating' the beam, no pressure point is created which could penetrate the pile head. Also, only in plane stresses to the joints occur due to normal forces, shear forces, and bending moments in the main bending direction. Hence, the puncture of the FRP due to stresses perpendicular to the plane is limited by avoiding these stresses at all.

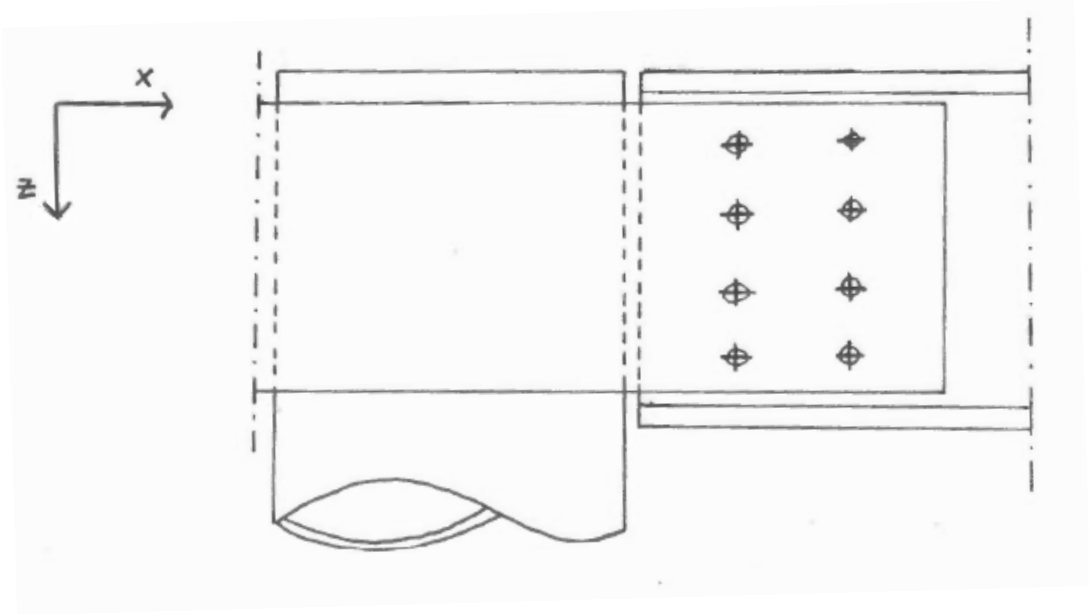

Figure 5.40: Detailed drawing of the elaborated joint at the intersection of the I-beam and the pile head

Several measurement units are used throughout the checks:

d : Diameter of the hole = 26.6 mm
d_b : Diameter of the shaft of the bolt = 25 mm
s : Distance between bolt holes parallel to the direction of the force = 180.33 mm
p : Distance between bolt holes perpendicular to the direction of the force = 180.33 mm
e_1 : Distance to the edge of the laminate and the outer bolt hole parallel to the direction of the force = 50 mm
e_2 : Distance to the edge of the laminate and the outer bolt hole perpendicular to the direction of the force = 37.5 mm
w : Distance surrounding the bolt hole at the edge, $w = 4d_b = 80$ mm
t : Thickness of the flange

Bolt forces
Due to the configuration of the joint, no fixed rotation point exists, but a free rotation point is present. When the dimensions of the bolts and the bolt holes are kept constant, the free rotation point coincides with the center of gravity of the bolts (Stark, 2012). With an equilibrium equation, the bolt forces can be determined. These are then decomposed into two direction: parallel and perpendicular to the load direction. These are the input forces for the structural checks.
The decisive load case for the joint resulted in a normal force of 16.0 kN, a shear force of 53.8 kN, and a bending moment of 65.3 kNm.

The maximum bolt forces due to the bending moment can be found in the following relation (Stark, 2012):

$$R_{Ed,y,max} = \frac{M_{Ed} * z_{max}}{\Sigma\left(y_i^2 + z_i^2\right)} \tag{5.29}$$

$$R_{Ed,z,max} = \frac{M_{Ed} * y_{max}}{\Sigma\left(y_i^2 + z_i^2\right)} \tag{5.30}$$

Where:

$R_{Ed,y,max}$: Resulting maximum force on the decisive bolt in y-direction
$R_{Ed,z,max}$: Resulting maximum force on the decisive bolt in y-direction
y_i : Horizontal distance of bolt i to the rotational center of the bolt group
z_i : Vertical distance of bolt i to the rotational center of the bolt group

$$\sum\left(y_i^2+z_i^2\right)=8*\left(\frac{s}{2}\right)^2=8*\left(\frac{108,33}{2}\right)^2=140\,833\,\text{mm}^2$$
$$R_{Ed,y,max}=\frac{41000*162.5}{140833}=75.3\,\text{kN}$$
$$R_{Ed,z,max}=\frac{41000*54.2}{140833}=25.1\,\text{kN}$$

Then, remaining vertical and horizontal forces can be divided over the amount of bolts (n) added to the bolt by the following formula:

$$F_{Ed,y,max}=R_{Ed,y,max}+\frac{V_{Ed}}{n} \tag{5.31}$$
$$F_{Ed,z,max}=R_{Ed,z,max}+\frac{N_{Ed}}{n} \tag{5.32}$$
$$F_{Ed,max}=\sqrt{\left(R_{Ed,y,max}+\frac{V_{Ed}}{n}\right)^2+\left(R_{Ed,z,max}+\frac{N_{Ed}}{n}\right)^2} \tag{5.33}$$

This results in the following maximum bolt forces:

$$F_{Ed,y,max}=75.3+\frac{16}{8}=77.3\,\text{kN}$$
$$F_{Ed,z,max}=25.1+\frac{53.8}{8}=31.8\,\text{kN}$$
$$F_{Ed,max}=\sqrt{(77.3)^2+(31.8)^2}=83.6\,\text{kN}$$

Figure 5.41 illustrates some basic failure modes for mechanical joints, which involves failure of the laminate: shear failure, net-tensile failure, cleavage and bearing failure. The bolt itself can fail as well: this will not be considered due to the high capacity of the bolts compared to the laminate.

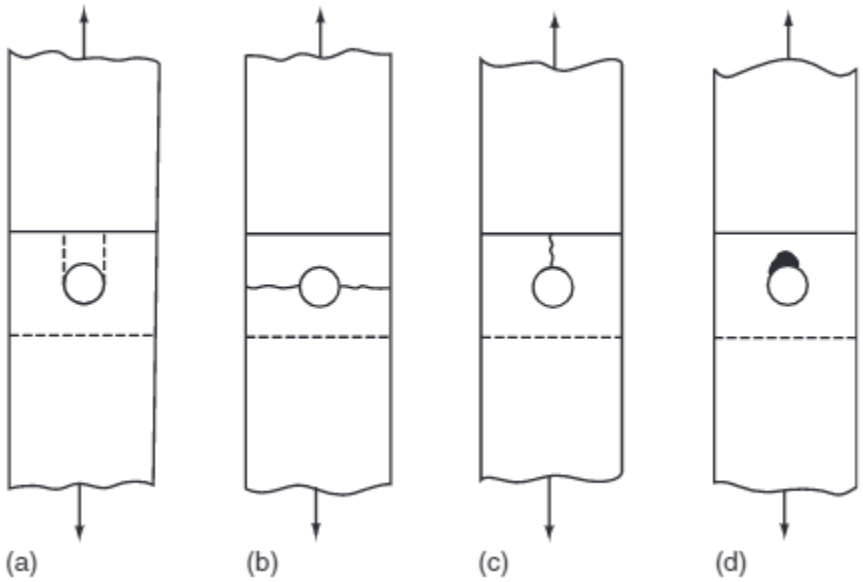

Figure 5.41: Basic failure modes for mechanical joints: (a) shear failure, (b) net-tensile failure, (c) cleavage, (d) bearing failure (Mallick, 2007)

Bearing failure

The resistance capacity for the bearing failure, in the y and z direction, is:

$$F_{b,i,vd,Rd,y} = \frac{f_{c,y,Rd}}{k_m * k_{cc1}} d_b t \tag{5.34}$$

$$F_{b,i,vd,Rd,z} = \frac{f_{c,z,Rd}}{k_m * k_{cc1}} d_b t \tag{5.35}$$

Where:

$F_{b,i,vd,Rd}$: Resistance capacity against bearing failure of the laminate
k_m : Correction factor given as $k_m = k_{m1} + k_{m2}$
k_{cc1} : Stress concentration factor for compression stress at the edge of the hole by the load of the bolt shaft

The value for the correction factor k_{m1} is 1.2 for locked bolts and 2 for bolts prone to rotation, for bearing capacity. Since the joint is a double lab joint, the bolt is restrained from rotating and $k_{m1} = 1.2$. The value for the compression stress concentration factor k_{cc1} is given by $k_{cc1} = \left(\frac{d}{d_b}\right)^2 = \left(\frac{25}{26.6}\right)^2 = 1.13$. The resistance capacity for bearing failure then is:

$$F_{b,i,vd,Rd,y} = \frac{f_{c,y,Rd}}{k_m * k_{cc1}} d_b t = \frac{108}{1.2 * 1.13} * 26.6 * 14 = 27.9\,\text{kN} \tag{5.36}$$

$$F_{b,i,vd,Rd,z} = \frac{f_{c,z,Rd}}{k_m * k_{cc1}} d_b t = \frac{128}{1.2 * 1.13} * 26.6 * 14 = 33.1\,\text{kN} \tag{5.37}$$

Net-tensile failure of the laminate
For a bolted joint consisting of two or more rows of bolts, the stress state next to the bolt hole has to be determined and compared to the tensile strength of the laminate. The stress state next to the bolt gap may be calculated by superpositioning the highest tangential stress at the hole and the highest stress at the hole in tangential direction of the load:

$$\sigma_{tot,v,i,ns,Ed} = \sigma_{v,i,ns,Ed} + \sigma_{bp,i,ns,Ed} \tag{5.38}$$

$$\sigma_{v,i,ns,Ed} = \frac{k_m k_{tc1} F_{v,i,Ed}}{(w-d)\,t} \tag{5.39}$$

$$\sigma_{bp,i,ns,Ed} = \frac{k_{tc2} F_{bp,i,Ed}}{(w-d)\,t} \tag{5.40}$$

with $F_{v,i,Ed} = C_{ri} F_{v,Ed} = 0.6 * F_{Ed,y,max} =$
Where:

C_{ri} : Part of the load carried by the i'th bolt row = 0.6
$F_{v,i,Ed}$: Stress near the hole = $C_{r1} F_{v,y,Ed} = 0.6 * 77.3 = 46.4\,\text{kN}$
$F_{bp,i,Ed}$: By-pass stress near the hole $1 - \sum C_{ri} F_{v,Ed} = 0.4 * 77.3 = 30.9\,\text{kN}$

Then, we find for the total stress near the bolt hole:

$$\sigma_{v,i,ns,Ed} = \frac{1.5 * 2 * 46.4}{(106.4 - 26.6)\,14} = 124.6\,\text{MPa}$$
$$\sigma_{bp,i,ns,Ed} = \frac{1.5 * 30.9}{(106.4 - 26.6)\,14} = 41.5\,\text{MPa}$$
$$\sigma_{tot,v,i,ns,Ed} = 166.1\,\text{MPa}$$

Shear failure of the laminate
The resistance capacity for shear failure is:

$$F_{b,i,so,Rd,y} = \frac{\tau_{xy,Rd}}{k_m} * (2e - d)\,t \tag{5.41}$$

$$F_{b,i,so,Rd,z} = \frac{\tau_{yz,Rd}}{k_m} * (2e - d)\,t \tag{5.42}$$

$$\tag{5.43}$$

Here, the assumption is made that the shear stress capacity in the z-direction is 75 % of the shear stress capacity in the y-direction. The value for $k_m = 1$. We then find:

$$F_{b,i,so,Rd,y} = \frac{66}{1} * (2 * 80 - 26.6) * 14 = 124.1\,\text{kN}$$
$$F_{b,i,so,Rd,z} = \frac{66 * 0.75}{1} * (2 * 80 - 26.6) * 14 = 50\,\text{kN}$$

Cleavage
The resistance capacity for cleavage failure is:

$$F_{b,i,sp,Rd} = \left| \frac{4 f_{t,90,i,Rd} * d * t}{\tan 30\,\mathrm{deg}} \right| \tag{5.44}$$

Here, $f_{t,90,i,Rd}$ is the design tensile strength of the laminate. Substitution of the parameters gives:

$$F_{b,i,sp,Rd} = \left| \frac{4 * 110 * 26.6 * 14}{\tan 30\,\mathrm{deg}} \right| = 283\,\mathrm{kN} \tag{5.45}$$

Joint buckling
Joint buckling occurs with eccentric loaded joints, for instance for a single lap joint. The I-beam is enclosed by a double lap joint and therefore there are no eccentricities. Therefore, the check for joint buckling is omitted.

Capacity checks
Bearing capacity:

$$UC = \left(\frac{FEd,y,max}{F_{b,i,vd,Rd,y}} \right)^2 + \left(\frac{FEd,z,max}{F_{b,i,vd,Rd,z}} \right)^2 = \left(\frac{77.3}{27.9} \right)^2 + \left(\frac{32}{33.1} \right)^2 = 8.63$$

Net tension failure:

$$UC = \frac{\sigma_{tot,v,i,ns,Ed}}{f_{t,i,d}} = \frac{166.1}{108} = 1.54$$

Shear failure:

$$UC = \left(\frac{FEd,y,max}{F_{b,i,so,Rd,y}} \right)^2 + \left(\frac{FEd,z,max}{F_{b,i,so,Rd,z}} \right)^2 = \left(\frac{77.3}{124.1} \right)^2 + \left(\frac{32}{50} \right)^2 = 0.8$$

Cleavage failure:

$$UC = \frac{F_{Ed,y,max}}{F_{b,i,sp,Rd}} = \frac{77.3}{283} = 0.27$$

From the above it is clear that the joint does not comply with the bearing and net-tension criteria. For a similar member in steel, the required thickness would be sufficient since for steel a material parameter of 1 or 1.15 can be used, in contrast with the material parameter for FRP which is 1.62 in this context. The following measures can be taken to satisfy the bearing capacity criterion:

- Increase thickness of the web of the I-beam
- Increase the thickness of the bolts
- Decrease the allowance of the bolt (e.g. by using injection bolts)
- Increase the distance between the bolt rows (which will decrease the force on the bolts due to the larger moment arm)

Increasing the thickness of the web of the laminate to 19.1 mm or increasing the bolt diameter to 36.3 mm. For the latter, the additional requirements with respect to minimum distances to the edges of the plate have to be considered again in order for the formulas to be valid. By utilizing injection bolts, $d \approx d_b$ then the unity check yield 1.42.

The issue may be overcome with a different joint design. Also, the dimensions of the beam may be adjusted: since FRP is highly customizable, a beam with larger profile heights in proximity of the support can be made in order to increase bearing capacity of the joint. Section 10.1.1 suggest an alternative joint type.

5.10. Dead weight of the jetties

Because the light weight properties of FRP are often mentioned as an advantage, the weight of both the designed FRP jetty and the RC[17] jetty from the case study are compared in this section.

The weight of the jetties are calculated by multiplying the volume of the material usage with their respective densities. Table 5.16 presents the bill of quantities for the FRP and the RC jetty. The total FRP is the sum of the weight of the glass an polyester. The FRP hollow piles is represents the weight of the piles only. This different formulation for the weight is used because in the LCA, different approached are used to estimate the environmental impact (seeChapter 7).

	Material	Quantity [kg]	Density $\left[\mathrm{kg/m^3}\right]$
FRP jetty	Glass	24407	2570
	Polyester	8454	1200
	Total FRP	30862	2022
	FRP hollow piles	20556	1927
	Fiber content scaled FRP[18]	31277	1771
RC jetty	C45/55	150109	2450
	C30/37	61275	2450
	Reinforcement steel	19238	7850
	Steel	47	7850
	Stainless steel	44	7850
	Formwork	35[19]	700

Table 5.16: Bill of quantities for the FRP jetty and the RC jetty

The fiber content volume for the FRP hollow piles is estimated by finding the ratio of fiber volume ratio for a combination of glass and polyester which yielded a density of 1927 $\mathrm{kg/m^3}$; this was found for the fiber volume ratio of 53 %.

Figure 5.42 illustrates the weight of the two jetties according to the data in Table 5.16.
The FRP jetty is significantly lighter compared to the RC jetty. The total dead weight of the FRP jetty amounts to 30.862 kg; the total dead weight of the RC jetty amounts to 230.554 kg. The RC jetty is about 7,5 times heavier than the FRP jetty (or a relative change of 650 %).

The difference of dead weight per square meter of the jetty is remarkable. The area of the jetty is $30 * 1.6 + 5 * 10 = 98\,\mathrm{m^2}$. The dead weight of the FRP superstructure is $\frac{10305}{98} = 1.03\,\mathrm{kN/m^2}$; the dead weight of the RC superstructure is $\frac{105595}{98} = 10.57\,\mathrm{kN/m^2}$. This difference is significant: the variable loads on the access bridge and the platform are $5\,\mathrm{kN/m^2}$ and $20\,\mathrm{kN/m^2}$ respectively.

[17] Reinforced concrete
[18] See section Section 7.4.3 for the allocation of material
[19] In $\mathrm{m^2}$

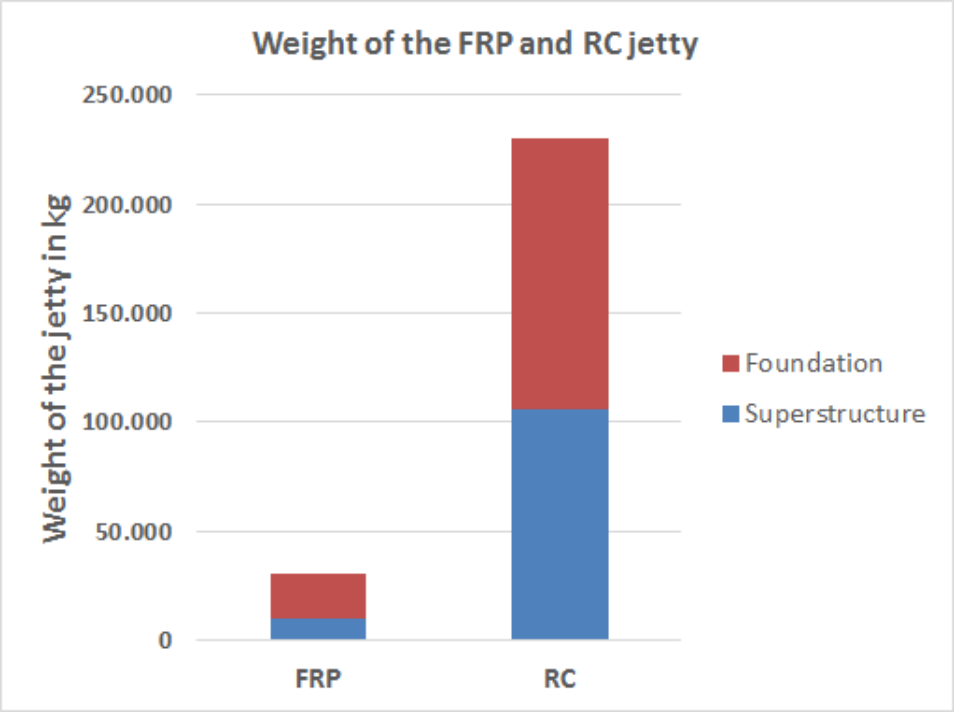

Figure 5.42: Dead weight of FRP and RC jetty in kilogram

5.11. Comparison of limit states of the FRP jetty

With the checks regarding the SLS and ULS completed, the decisive limit state criteria for the structural elements can be determined. Table 5.17 and Table 5.18 repeat the unity checks as presented in Section 5.6.4 and Section 5.7.5 respectively. The lateral buckling resistance for the beams at the access bridge and platform can be disregarded with the Vierendeel analogy and the girder between the beams may be replaced with another profile, like the beam, as explained in Section 5.7.5.

Different SLS and ULS criteria yield the biggest unity checks for the elements. The biggest values for the unity checks of the beams at the access bridge are the SLS criteria. This also holds for the beams at the platform, with exception of the beams located beneath the loading arm: due to great stress introduction of the load arms, the forces in these beams are bigger. Their deformations are limited because they are directly supported by the pile.
The UC regarding SLS are higher for the piles at the access bridge; for the piles at the platform, the ULS unity checks are higher. The deflection of these piles is lower due to the grouping of the piles and the added stiffness of the platform. The most important check for the piles at the platform is the check regarding the buckling capacity.

Structural element	Location	Actual displacement		UC	
		Horizontal	Vertical	Horizontal	Vertical
Beam 1	Access bridge	45.1	26.3	0.9	0.88
Beam 2	Platform	18.9	8.3	0.38	0.42
Beam 2	Loading arm[20]	13.4	10.6	0.27	0.53
Pile 2	Access bridge	40.7	18.6	0.81	0.41
Pile 2	Platform	19	9	0.38	0.20
Pile 2	Loading arm	13.4	8.3	0.29	0.18

Table 5.17: Overview of the maximum displacements and UC's for the SLS envelope

Structural element	Location	UC		
		Cross section capacity	Buckling	Lateral torsional buckling
Beam 1	Access bridge	0.3	0.011	1.05
Beam 2	Platform	0.27	0.03	1.00
Beam 2	Loading arm[21]	0.59	0.02	0.50
Girder 1	Between access bridge beams	0.8	0.23	3.54
Girder 1	Wind bracing at access bridge	0.06	0.00	0.29
Pile 2	Access bridge	0.31	0.44	-[22]
Pile 2	Platform	0.41	0.64	-
Pile 2	Loading arm	0.36	0.65	-

Table 5.18: Overview of the maximum UC's for the ULS envelope

[20] Located at platform, and influenced by the load of the loading arm
[21] Located at platform, and influenced by the load of the loading arm
[22] Circular profiles are not prone to lateral torsional bending

5.12. Conclusions and discussion of the technical design of the FRP jetty

5.12.1. Conclusion: FRP jetties are technically feasible

Regarding the technical design of the FRP jetty, the following conclusions are drawn:

- It seems feasible to construct an FRP jetty based on literature review, dimensions of existing FRP structural elements, and structural analysis of the designed FRP jetty when taking the permanent and variable static loads after installation into account.
- Piles are an important design aspect of the FRP jetty as they have a mayor contribution to the lateral stability; installing hollow FRP piles with a batter angle greatly increases stability which partly compensates the low inherent stiffness of the piles.
- Mechanical joints may prove to be troublesome: when designing beams, special attention should be given, preferably early in the design stage, to resistance capacity of the laminates against in-plane and out-of-plane bolt forces.
- The dimensions of the structural elements is determined by both SLS and ULS criteria, depending on the specific loads and support from neighboring elements.
- The dead weight of the FRP jetty is significantly lower compared to the RC jetty: their total weights are 30.862 kg and 230.554 kg respectively, a relative change of 650 % compared to the FRP jetty.

While the piles are statically able to support the piles, concerns emerged during the literature study regarding installation (Winter, 2017). Chapter 6 elaborates the technical feasibility of the installation of the FRP piles.

The following recommendations regarding the technical design are made:

- FRP has the advantage to be highly customizable and form free. To cope with the insufficient capacity of the FRP material at the joints, an integrated deck can be designed which limits the amount of joints.
- Regarding the load bearing applications of partially embedded piles: research to what degree the structural model assumptions are valid for hollow FRP piles (e.g. translation and rotation restriction of the pile head) and the buckling resistance capacity of piles in pile groups. This is relevant since partially embedded piles are prone to buckling: this was the decisive ultimate limit state criteria for the piles.
- The decisive ULS criterion for piles is the buckling resistance capacity check. Structural model assumptions for the the pile head and pile toe heavily influence the buckling resistance capacity. Also, a full design should be made to get a realistic ratio of the longitudinal stiffness and shear modulus in order to judge if shear deformation can be disregarded in determining the buckling force.
- Research regarding long term structural capacity of piles as suggested by Zyka and Mohajerani (Zyka & Mohajerani, 2016). This research should also investigate crack formation due to dynamic behavior and its influences on partially embedded and submerged piles, as well as creep and its long term influence on the structural capacity of the piles.
-

A discussion regarding the content of this chapter is found in Section 10.1.1.

6

Installation of FRP piles: pile drive analysis

The pile installation is of importance to conclude if an FRP jetty is technically feasible. This section builds on the choice of Section 5.8.1 and discusses the problems encountered with FRP pile installation and presents possible solutions for these problems.

6.1. Pile installation method: driving

From the accompanying literature study, the following findings were made (Winter, 2017):

- Of the different commercially available piles, the hollow FRP pile seems the most feasible when regarding load bearing capacity and cost efficiency
- Theoretical research utilizing WEAP suggested that, with pile and geotechnical conditions approximate to the design situation, hollow FRP can be driven to depth with reasonable bearing capacity.
- Challenges to overcome regarding driving of hollow FRP piles is the low impedance of these piles. Increasing the impedance by adjusting material properties or pile dimensions is not an optimum solution. This solution probably lies in the adjustment of installation techniques. (such as tapered piles. The effectiveness of this method however, is only in granular non-cohesive soils).
- No systematic damage resistance and axial fatigue studies have been conducted for hollow FRP piles
- The research regarding pile installation is focusing mainly on pile driving

Taking these conclusions into account, the following available options seem reasonable to assess the feasibility of the installation of the FRP piles:

- Conduct a pile driving analysis
- Conduct a pile vibration analysis
- Further research the possibility of drilled piles

The remainder of this chapter will focus on the elaboration of a pile drive analysis, based on the following arguments:

1. This type of FRP pile installation is most prominent in contemporary research
2. Pile drive analysis software is able to accurately predict driveability
3. Driving efficiency of different piles can easily be compared by determining the required blow count to reach the desired depth

4. Vibratory analysis are not that predictable as pile driving analysis due to the large amount of parameters which influence the process
5. Pile driving grants higher pile bearing capacity than drilling; this method was used in Section 5.8.1

6.2. Aim of the pile driving analysis

The aim of the pile driving analysis is to research if the pile can be installed to the required depth. This is regarded successful if:

1. The pile can be driven to depth without refusal
2. The structural performance of the pile is not significantly affected

The first item relates to ability of the pile to be driven to the required depth: no refusal may occur during the driving process. Refusal is defined when more than 250 blow counts are required to drive the pile deeper into the soil; this limit is used in common practice to indicate drive refusal (Moscoso, 2017).

The second item relates to the rate to which the structural capacity of the pile reduces due to to driving forces. A distinction is made between short-term and long-term structural performance; the long-term structural performance part is omitted. The reason for this is that is an unknown factor: contemporary research recommends the investigation of the influence of pile driving on the long-term structural capacity of FRP piles (Winter, 2017). The short-term relates structural performance relates to the structural capacity of the pile during and after driving. Indicators of these are:

- The stress due to driving forces does not exceed the failure stress
- The strain due to driving forces does not exceed the failure strain
- The pile does not buckle during driving

The former two, stresses and strains during driving, can be obtained with the pile drive analysis. The latter possess more in-depth research and is not included in the scope of this thesis.

6.3. Methodology

6.3.1. Wave equation analysis

The pile driving analysis, often named wave equation analysis of piles (WEAP) in literature and practice, is a method based on a solution for the wave equation. The pile, soil, and friction are discretized into elements. The hammer blows are modeled as impulses which induce stress waves into the pile, which ultimately drive the pile deeper into the soil. The reader interested in more information regarding wave equation analysis of piles and its developments is refereed to the paper of (Middendorp, 2004).

The pile driving analysis is executed with pile driving analysis software from Allnamics: Allwave Pile Drive Predictior (Allnamics Pile Testing Experts, 2014). The program solves the wave equation with the method of characteristics. Figure 6.1 illustrates the equilibrium equations at a node between two discretized elements (Middendorp, 2004).

The pile is modeled as a 1D element: stress waves only propagate in the direction along the pile axis. It is assumed that the pile only deforms in its longitudinal direction. This is assumption can be made since the length of the piles exceeds the width of the piles. Along with this assumption, no orthotropic effects need to be taken into account: only the stiffness in the direction of the pile is of

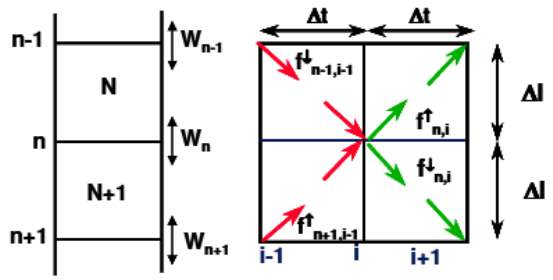

$$f_{n,i}^{\downarrow} = \left(\frac{Z_N - Z_{N+1}}{Z_N + Z_{N+1}}\right) f^{\uparrow} + \left(\frac{Z_{N+1}}{Z_N + Z_{N+1}}\right)\left(2f^{\downarrow} - W_{n,i}\right) \quad (1)$$

$$f_{n,i}^{\uparrow} = \left(-\frac{Z_N - Z_{N+1}}{Z_N + Z_{N+1}}\right) f^{\downarrow} + \left(\frac{Z_N}{Z_N + Z_{N+1}}\right)\left(2f^{\uparrow} + W_{n,i}\right) (2)$$

Figure 6.1: Algorithm of the AllwavePDP program (Middendorp, 2004)

importance.

No reduction on the modulus of elasticity is taken into account during driving. The conversion factor accounts for long-term processes such as creep and relaxation. The material factor accounts for material imperfections. Also, the response of the pile and soil depends on the modulus of elasticity since it influences pile impedance. Therefore, the mean modulus of elasticity is used in the pile driving analysis.

The most important unknown parameter in the assessment of driveability is the impact-fatigue response of hollow FRP piles (Zyka & Mohajerani, 2016).

6.3.2. Main influence factors on driveability of FRP piless

Guades et all. summed the main factors which influenced the driveability of piles (Guades et al., 2012):

- rated energy delivered by the driving hammer
- soil resistance to driving forces
- impedance (dynamic stiffness)
- strength of the pile to resist driving forces

Velez found in his study that hollow FRP piles have similar driving performance with respect to steel pipes (Velez, 2013). He also concluded that for stiffer piles, the soil properties were more relevant to driving performance with respect to the driving performance of less stiff piles: for the later, pile properties were more significant.

Iskander et all. found that the damping had no mayor influence on the driveability of FRP piles (Iskander, Asce, Stachula, & Asce, 2002). Therefore, the damping factor is not changed in the program setup.

6.3.3. Description of main parameters

If the results indicate that a viable set up (i.e. selected hammer and cushions), then other models will be run to investigate the different types of piles in the design. The main variety of parameters in the model are: embedment length of the pile, batter angle of the pile, width of the pile.

Length of the pile

The required depths are relatively deep. Iskander already indicated that for a similar soil profile, this was possible (Iskander, Hanna, & Stachula, 2001). The reinforced concrete piles in the case study have a length of 25.5 m in order to reach to the first solid sand layer. The length of the FRP piles

is based on this length. However, since the dead weight of the FRP structure is lower, it might be possible for the piles to be shorter. Therefore, also a variant of FRP piles with a length of 15.5 m is researched.

Batter angle of the pile
Installing the pile with a batter angle increases its lateral stability, which tends to be of major influence in the technical design. Besides straight piles, three batter angles are investigated: 1:10, 1:7, and 1:4. A batter angle of 1:4 is considered the maximum allowable batter angle for pile driving.

Thickness of the pile
Pile dimensions -> stick to the research. also, improving impedance is costly and not the optimal solution.

The piles presented in contemporary research have a diameter of 356 mm and a thickness of 13 mm (Zyka & Mohajerani, 2016). This pile has a low impedance. However, according to Zyka and Mohajerani improving the impedance to favor driveability properties is not the optimal solution because it is very costly. But, with a pile diameter with the above stated dimensions will not suffice to SLS criteria (see Section 5.8.3). In the design, larger pile dimensions are selected: 456 mm and 17 mm for the diameter and wall thickness, respectively. The wall thickness is linearly scaled with respect to the increased diameter.

Soil profile
The cone penetration test (CPT)'s from Appendix A.1 are available in Geotechnical Exchange File (GEF) format and is used to construct a soil profile in the wave equation program. For the platform and access bridge CPT S05 and S04 are used, respectively.

Hammer
Iskander found in his research, where he used a wave equation analysis program, that single acting hammers consequently performed better than open-ended diesel hammers (Iskander et al., 2001). He provided the following arguments for this results: single acting hammers usually exert shorter dynamic forces than diesel hammers; single acting hammers usually have a heavier ram and shorter stroke with the same rated energy.

6.3.4. Pile properties
Table 6.1 presents the mechanical pile properties of pile 1 and pile 2.

Property	Symbol	Pile 1	Pile 2	Unit
Area	A	14 000	23 446	mm^2
Density	ρ	1927	1927	kg/m^3
E-modulus	E	23	23	GPa
Wave speed	c	3455	3455	m/s
Impedance	Z	0.093	0.156	MNs/m
Wall thickness	t	13	17	mm
Diameter	D	356	456	mm
Length	L	25.5	25.5	m

Table 6.1: Physical properties and dimensions of the circular hollow FRP pile

6.4. Results of the pile drive analysis: initial run

This section presents the most important results of the pile drive analysis. A complete overview of the results is found in Appendix I.

Initially, the parameters in the model set-up were changed continuously to investigate if it was possible to drive the FRP hollow piles to the desired depth. The impedance of the piles were changed by increasing the axial stiffness or the density of the material. Also, the hammer (rather: the impact energy) was changed to find the influence of different types of hammers.

Overview of results

The results of a few models are presented in this section; the remaining can be found in Appendix I. The first models run are indicated with '0.' in their prefix model number. Appendix I presents the models whose results are elaborated in the remainder of this section. All these models are run with CPT S05; the required installation depth is 13.3 m.

Model	Hammer	Pile	d_{max} [m]
0.2	Ihc-30	Pile 1	8.5
0.4	Ihc-30	Pile 2	9
0.10	Vulcan	Pile 2	8.25

Table 6.2: Maximum driving depth d_{max} for different model set-ups

In all the piles refusal during driving was encountered (i.e. more than 250 blows were required to drive the pile to a depth of 0.25 m. The remaining of this section presents those results.

Blow count

Figure 6.2 present the blow count of the FRP hollow pile for model 0.4. At a depth of 8.5 m, a blow count greater than 250 blows is required in order to drive the pile 0.25 m; hence, the pile refuses and cannot be driven to required depth. Due to the low impedance of the pile it is not able to transfer the energy from the blow hammer to the pile tip and to the soil.

Pile tip displacement

Figure 6.3 illustrates the displacement of the pile tip in response of a blow by the hammer (model 0.4). The blow only moves the pile by 0.03 mm.

Verification of the pile bearing capacity

During pile driving, the bearing capacity of the piles can be determined by means as the sum of the shaft friction and the pile resistance[1].
Whilst the piles could not be driven to the initial desired depth, they could be driving to a depth which provided enough bearing capacity. The maximum axial force in the piles determined in Section 5.8 was almost 200 kN. The shaft resistance in model 0.4 already accumulated to circa 1 MN at a depth of 5.5 m.

[1]The bearing capacity of the piles may be determined with WEAP according to NEN 9997-1 (NEN, 2011)

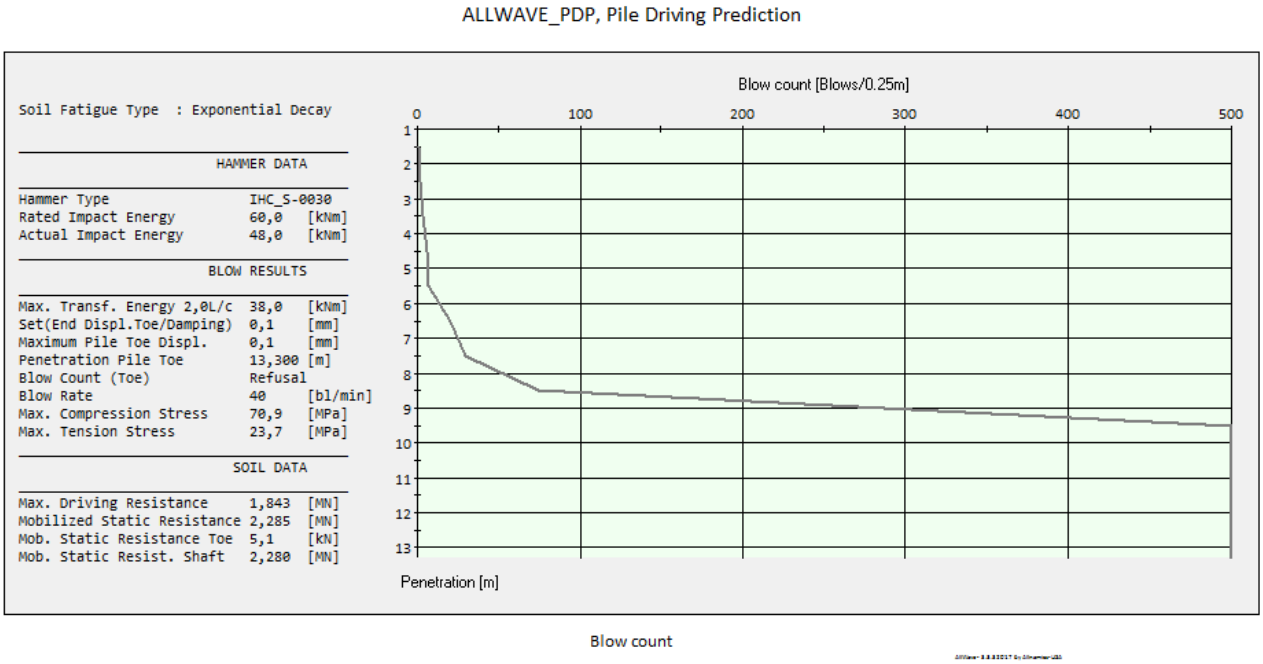

Figure 6.2: Blow count of model 0.4, FRP pile 2

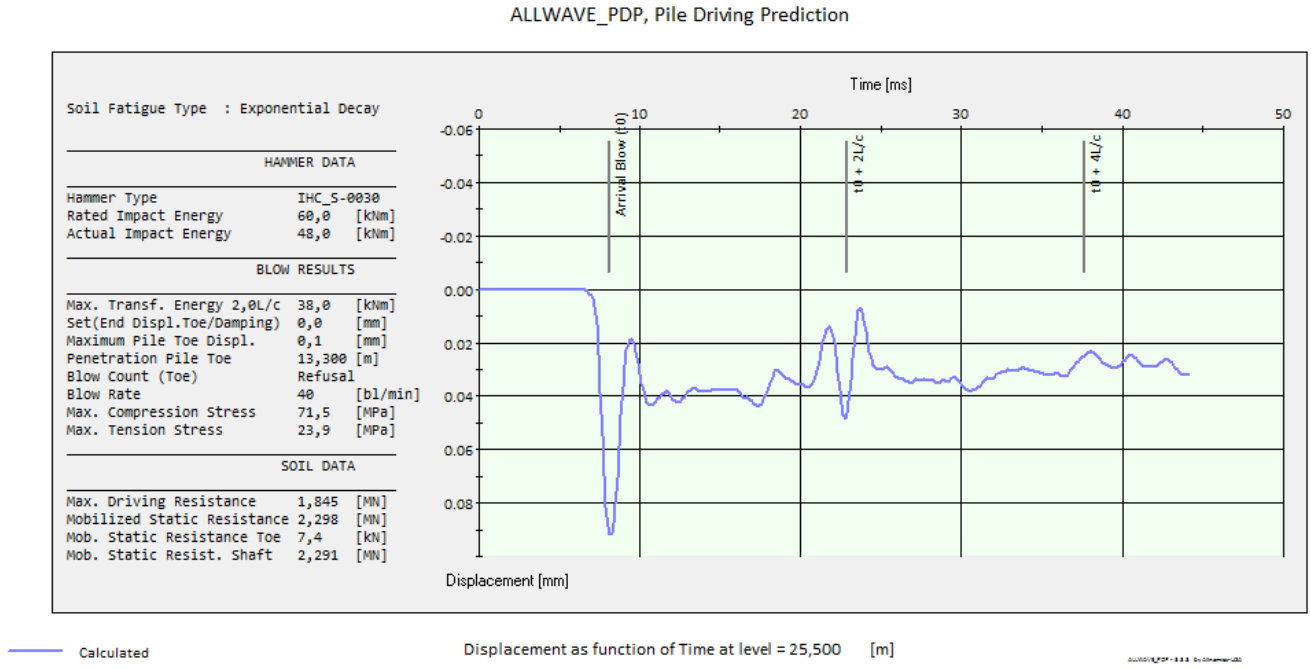

Figure 6.3: Pile tip displacement of model 0.4, FRP pile 2

6.5. Results of the pile drive analysis: 1st iteration

The results from the first set of models indicated that it was not possible to drive the piles to the desired depth without exceeding the blow count criteria. However, a lot of shaft friction was developed relatively quickly. This can be explained due to a reasonable amount of preloading of the soil. It is likely that the harbor was excavated and dredged and that a soil layer of about 10 m was formerly resting on the harbor bottom.

Due to the quick development of friction and, a new model set up in order to investigate the possibility to base the bearing capacity solely on friction.

Overview of results of the 1st iteration

Table 6.3 presents the results of the pile drive analysis for the piles in the technical design: pile 1 with a batter angle of 1:4, and pile 2 with no batter angle and a batter angle of 1:10. All the piles in the models were driven with a light hammer: Ihc-S30, with a rated energy impact of 60 kJ. Model 2.0, 2.1, 2.3, and 2.7 are used in the adopted detailed design with shorter piles. At the access bridge, pile 1 was changed to pile 2 because the reduced installation depth reduced the lateral resistance and hence increased the horizontal deformation.

Model	L	CPT	batter angle	P_c [kN]	d_{max} [m]	Z [MNs/m]	Pile
2.0	6	S05	-	1055	6	0.156	Pile 2
2.1	6	S05	1:10	1056	6	0.156	Pile 2
2.3	6	S05	1:4	1056	6	0.156	Pile 2
2.6	10.5	S04	1:4	641	10.5	0.093	Pile 1
2.7	10.5	S04	1:4	828	10.5	0.156	Pile 2

Table 6.3: Definite model set-up for the designed jetty

Maximum stresses and strains

Table 6.4 presents the maximum driving stresses during driving. The maximum compression stress and tensile stress allowed are -276 MPa and 276 MPa respectively[2]. Also, the maximum allowed strain (1.2 %) does not get exceeded during driving.

Model	Compression wave		Tension wave	
	σ_{max} [MPa]	ϵ_{max} [%]	σ_{max} [MPa]	ϵ_{max} [%]
2.0	62.1	0.27	14.5	0.06
2.1	62.1	0.27	14.5	0.06
2.3	62.1	0.27	14.5	0.06
2.6	69.4	0.3	10.5	0.046
2.7	61.2	0.27	7.1	0.03

Table 6.4: Maximum compression- and tension stress during driving

The results indicate that the batter angle does not influence the maximum compression- and tension stress when the piles are driven to a depth of 6 m below ground level.

[2]Computed as the maximum allow strain times the axial stiffness: 1.2 %*23 GPa = 276 MPa

Blow count
Figure 6.4 present the blow count of the FRP hollow pile for model 2.0. At the required installation depth, 6 m below ground level, the pile is still driveable since the blow count is estimated at 12 blows per 25 cm, which lies well below the earlier defined refusal limit of 250 blows per 25 cm. Due to the low impedance of the pile it is not able to transfer the energy from the blow hammer to the pile tip and to the soil.

Pile tip displacement
Figure I.5 illustrates the displacement of the pile tip in response of a blow by the hammer for model 2.0 at a depth of 6 m below ground level. The blow moves the pile tip by 20 mm. In the figure, the red line estimates the blow count if the CPT values are increased by 20 % and the blue line estimates the blow count if the CPT values are reduced with 20 %.

6.6. Conclusions: bearing capacity based on pile shaft friction

6.6.1. Conclusions of the pile drive analysis

The following conclusions regarding the driveability of the piles can be made:

- The FRP piles which resulted from the detailed design cannot be driven to the initially intended depth of 13.3 m below ground level at the location of the platform.
- At shallower depths,6 m below ground level at the location of the platform, already enough bearing capacity is developed by shaft friction (1000 kN) which is sufficient for the imposed load (180 kN).
- The maximum allowable stresses do not get exceeded during driving when a pile length of 18.2 m is driven to a depth of 6 m below ground level at the location of the platform.

A discussion regarding the content of this chapter is found in Section 10.1.2.

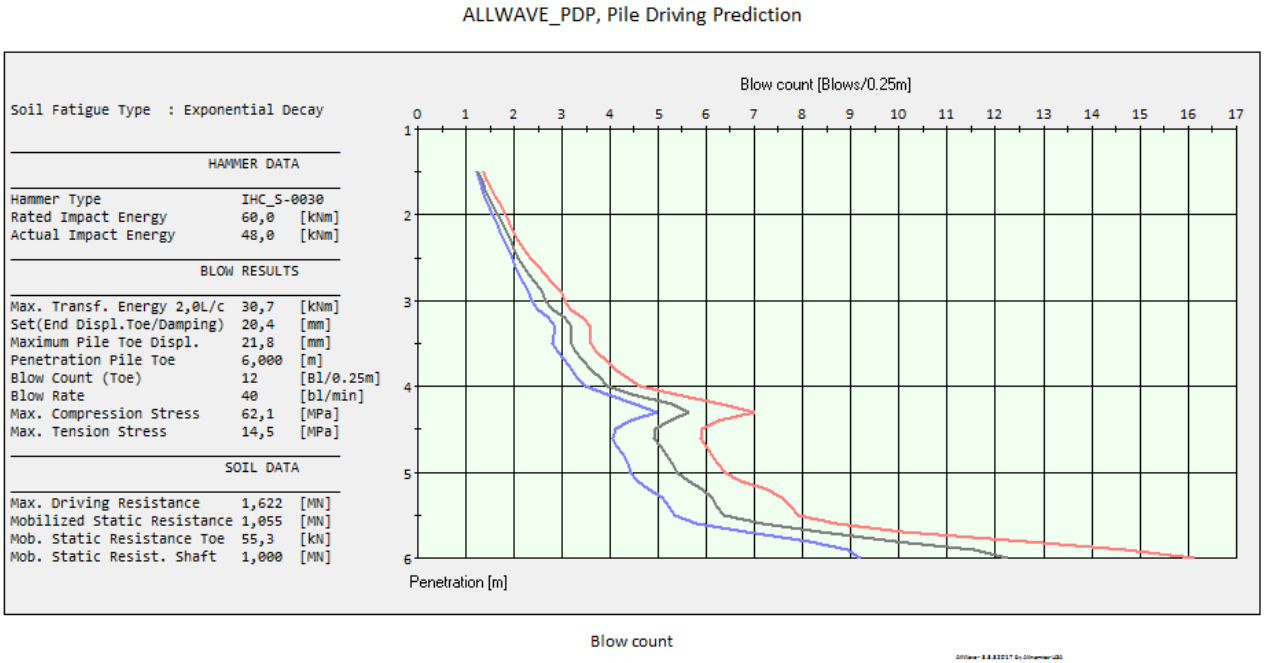

Figure 6.4: Blow count of model 2.0, FRP pile 2

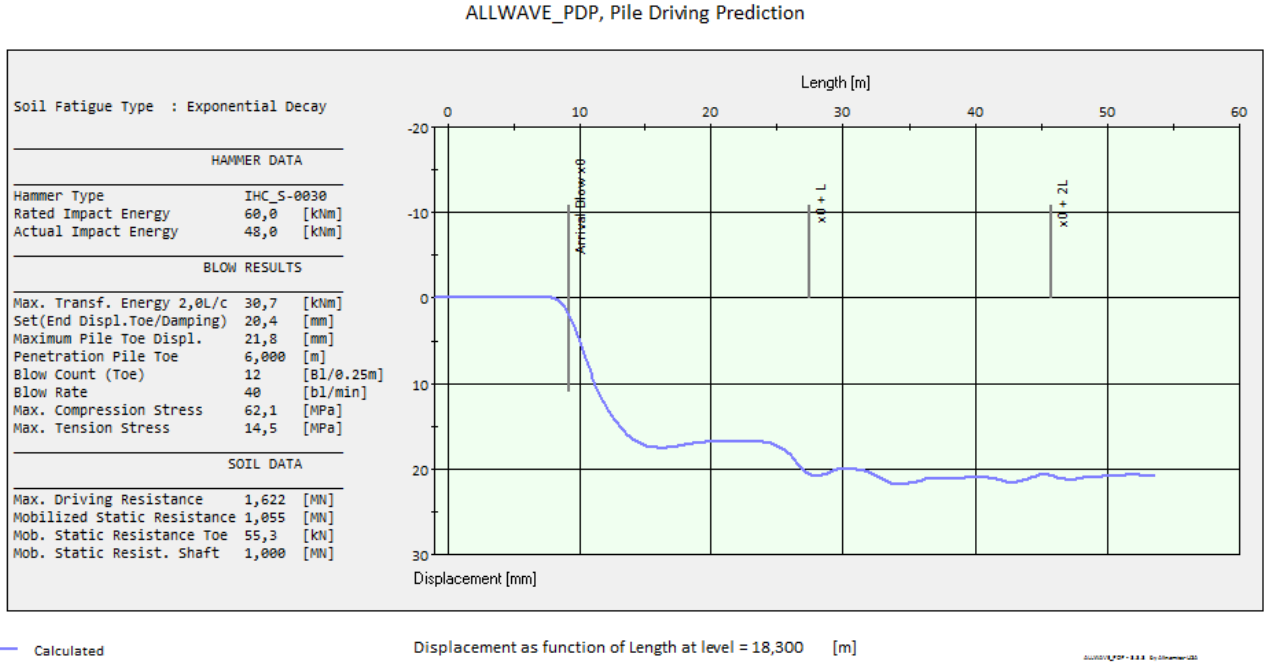

Figure 6.5: Pile tip displacement of model 2.0, FRP pile 2

II

Environmental impact

"What are the implications on environmental impact when using FRP to construct a jetty compared to reinforced concrete, over their full lifetime cycles?"

7

Life Cycle Assessment: comparing the environmental impact of the FRP- and reinforced concrete jetty

In this chapter, the subquestion is aimed to answer:

What are the implications on environmental impact when using FRP to construct a jetty compared to reinforced concrete over their full lifetime cycles?

The goal and scope of the LCA as well as the functional unit were defined in the preliminary design phase, see Section 4.2.1. Over time of the thesis project, the goal and scope have changed. To provide a complete overview of the LCA, treated items are repeated in this section.

7.1. Introduction

7.1.1. The importance of quantifying environmental impact

A well known challenge the world faces is climate change. Since the industrial revolution, emission of greenhouse gases increased tremendously. Contemporary science has large support for the human influence on the climate: in the Fifth Assessment Report of the Intergovernmental Panel on Climate Change (IPCC) it is stated that "Human influence on the climate system is clear, and recent anthropogenic emissions of greenhouse gases are the highest in history. Recent climate changes have had widespread impacts on human and natural systems" (IPCC, 2014). Therefore, designers should acknowledge the environmental impact of their design on the climate system and take the environmental presentation of the design into account when assessing their design variants.

7.1.2. Fast Track LCA

The life cycle assessment is a tool for designers to compare designs on environmental impact and can be divided into two categories: classical LCA and 'Fast Track' LCA (Vogtländer, 2010). The former can be considered more scientifically, while the latter can be considered more practical. The classic LCA investigates very detailed the use of finite resources and the emissions of harmful components, from the start to its grave, to the totality of the product. The 'Fast Track' LCA uses the output generated by the classic LCA to compare two different designs. In this thesis, two different designs are compared. Therefore, a 'Fast Track' LCA will be elaborated.

Two big challenges are met in LCA's (Vogtländer, 2010):

- Allocation of environmental burden
- Definition of the system and the system boundaries

The LCA was first developed to assess design choices within one design related to environmental impact (H. Jonkers, 2017). However, people started to use the LCA tool compare completely different designs which have different performance features, which is like comparing apples and oranges. To be able to compare the environmental performance of two designs, some performance criteria have to be defined. This is defined as the functional unit. Section 7.3.2 elaborates the functional unit for the assessment of the FRP jetty.

The result of the LCA are the eco-costs, or shadow costs[1], of the considered designs. The definition of shadow costs are (H. M. Jonkers, 2016):

"the costs required to bring the environmental impacts of a product or process to an acceptable 'sustainable' level"

These shadow costs are available in many available databases and carry the unit €per unit of equivalent material per impact category. Then, the shadow costs are multiplied by the amount of equivalent material represented by the design. This way, the different impact categories can be expressed as a monetary unit and therefore, summed and compared.

7.1.3. Database: based on Stichting Bouwkwaliteit Nationale Milieudatabase

There are many databases available which quantify impact values for different materials and processes. There are significant differences between these due to the huge variety in options regarding impact allocation and system definition.

The greenhouse effect states that the additional gases expelled into the atmosphere isolates Earth like a blanket and therefore cause a temperature rise. The NEN-ISO 14064-1 states that the most important greenhouse gases are carbon dioxide (CO_2), methane (CH_4), nitrous oxide (N_2O), hydrofluorocarbons $(HFC's)$, perfluorocarbons $(PFC's)$ and sulfur hexafluoride (SF_6). The influence of these gases on the temperature rise is different for each gas. Therefore, the relative influence of different gases are expressed in an equivalent carbondioxide influence. Then, the impact of different gases are easier to compare in designs.

Henk Jonkers from Delft University of Technology provided a database which is based on the database of "Stichting Bouwkwaliteit Nationale Milieudatabase" which is used in this thesis. The database provides values for ten impact categories values and shadow costs for common (construction) materials and equipment; these values are presented in Table 7.2.

[1] Formally called ECI: Environmental cost indicator (H. M. Jonkers, 2016)

7.2. Goal and scope definition of the LCA

Section 4.2.1 presented the goal of the LCA:

"Compare the environmental impact of an fiber reinforced polymer jetty and a conventional jetty constructed of steel and concrete, both having the same technical requirements regarding structural integrity, durability, and lifespan"

This definition is very elaborate. As Section 7.5 discusses, the quantitative results rely heavily on the system boundaries and the assumptions of the LCA. Therefore, in the scope of this thesis, the goal is redefined:

"Provide an estimation of the environmental impact of an fiber reinforced polymer jetty and a reinforced concrete jetty, both having the same technical requirements regarding structural integrity, durability, and lifespan, to give an indication for the better alternative regarding the environmental impact"

7.3. Definition of the system, functional unit and system boundaries

7.3.1. Systems for the FRP jetty and the case study

The system of a product, in this scope, is all input (e.g. energy, materials, building processes) required to create, use, and dispose the product, and the output which goes along with these process (e.g. emissions). Vogtländer describes three different paradigms to describe systems in the context of LCA: 'the chain', 'the cycle', and 'the tree' (Vogtländer, 2010). The former two are commonly referred to as cradle-to-grave (C2G) and cradle-to-cradle (C2C) respectively; the tree gives an overview of the required raw materials needed to manufacture a product.

The cradle-to-gate follows the creation of a product to a semi-finished product; cradle-to-grave follows the creation of a product to its grave; cradle-to-cradle stresses on the potential reuse at end-of-life. Concrete is example for which a cradle-to-gate approach is useful: after it leaves the 'gate' (i.e. the gate of the production plant) it can be processed in many products such as bridges, houses, grouting, etc. The product it is used for heavily influences the outcome of the LCA. The cradle-to-cradle paradigm explores the reuse/recycling/upcycling of the product of the end-of-life. Cradle-to-gate differs from cradle-to-cradle by omitting the end-of-life reuse options.
For the FRP- and RC jetty, the cradle-to-grave and cradle-to-cradle paradigms are considered: end-of-life processes such as incinerations, recycling, and reuse are considered. This is reflected in the score of the LCA: for recycling and reuse, the database does not assign environmental burden; for incineration and land fill, values for the impact categories are available.

Two systems are defined: one for the FRP jetty and one for the (concrete and steel) case study jetty. The total system and its boundaries are indicated in Section 7.3.3. Elliptical boxes are raw materials, end-products, or energy. Square boxes are processes and phases, such as transportation, manufacturing processes, construction, use-phase, and end-of-life processes.

7.3.2. Definition of the declared unit of the FRP jetty

The functional unit is the unit which will be compared in the LCA. Vogtländer defines the functional unit (FU) as:(Vogtländer, 2010):

Functional unit = {system function} per {unit of calculation}{plus optional: main scenario}

A possible definition for the FU then is:

"Facilitating a berth place for a selected design ship where product con be unloaded per unloaded product in tonnes, which complies with the structural design criteria, loads and geo-technical conditions as in Moerdijk, for a life-time of 50 years"

There is a problem when defining the system function. The function of the system is essentially to provide a berthing place were product can be unloaded by ships. The design objective of this thesis is to design an FRP jetty. Therefore, it would be better to restrict the FU to specifications instead of functionality since the design degree of freedom is already narrowed down. This is also called the Declared Unit:

Declared Unit = {specification of product or service} per {unit of calculation}{plus optional: main scenario}

Then, the Declared Unit of the LCA is defined as:

"The amount of construction material required per jetty, with platform dimensions of 10 m *by* 5 m *and an access bridge, both having the level of the upper deck located at* +4.6 m *NAP, which complies with the structural design criteria, loads and geo-technical conditions as in Moerdijk, for a life-time of 50 years"*

The above definition of the Declared Unit is more accurately to quantify as it is less prone to manipulation (companies often manipulate definitions in order to make their product look better (Vogtländer, 2010)). Arguments for including or excluding parts of the system is presented in the next section, Section 7.3.3.

7.3.3. System boundaries

With the specified system and the functional unit set, the system boundaries can be set: this includes all the elements which will be included in the LCA. On the following two pages, the systems of both the FRP jetty and the RC jetty are illustrated. The red line marks the system boundaries; everything inside is considered as the system. In the remaining of this section arguments for setting the system boundaries as is are elaborated. In general, small contributions of elements have been disregarded (Vogtländer recommends cut-off criteria of 2 %).

System for the FRP jetty (everything within the red border is included in the LCA)

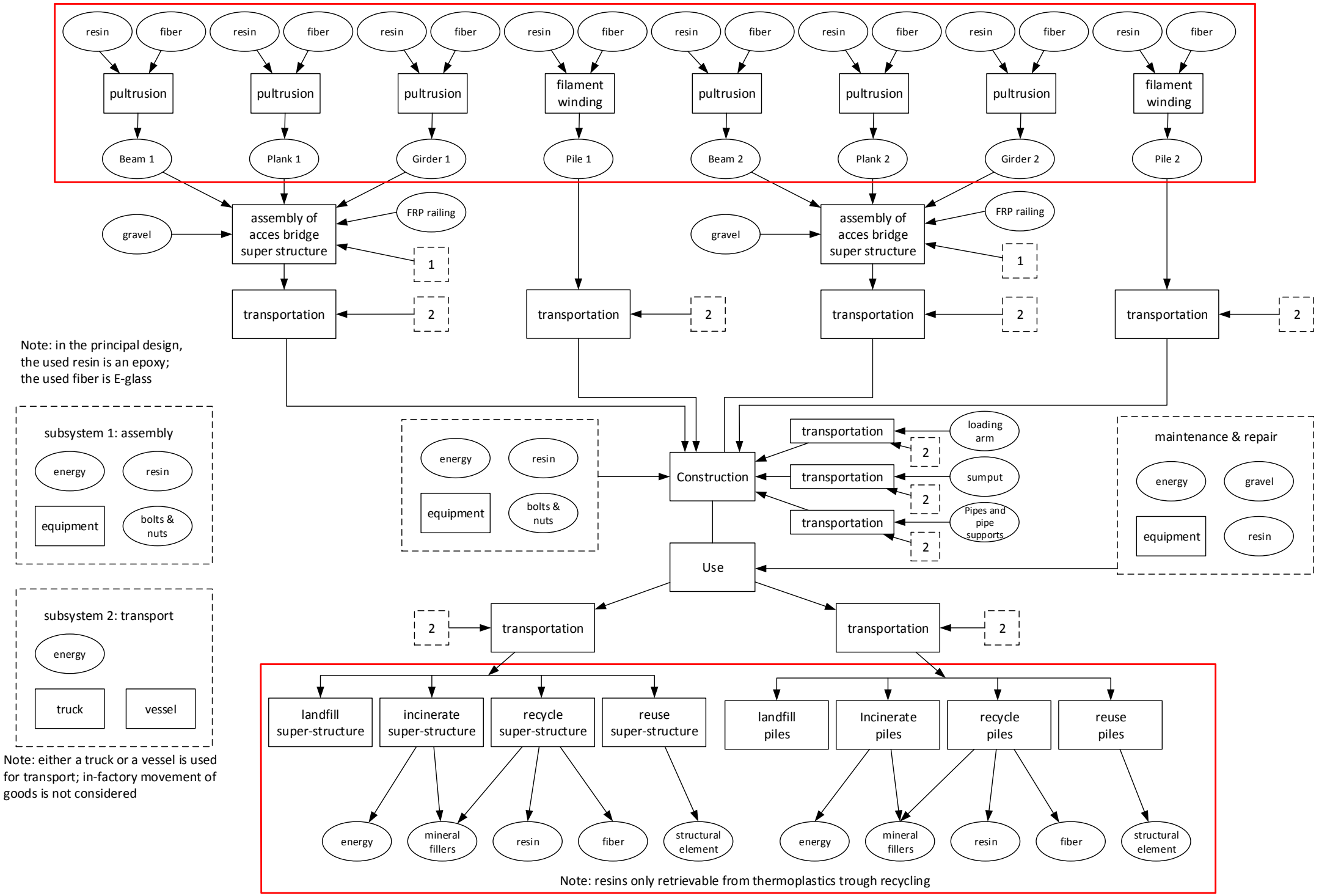

System for the RC jetty (everything within the red border is included in the LCA)

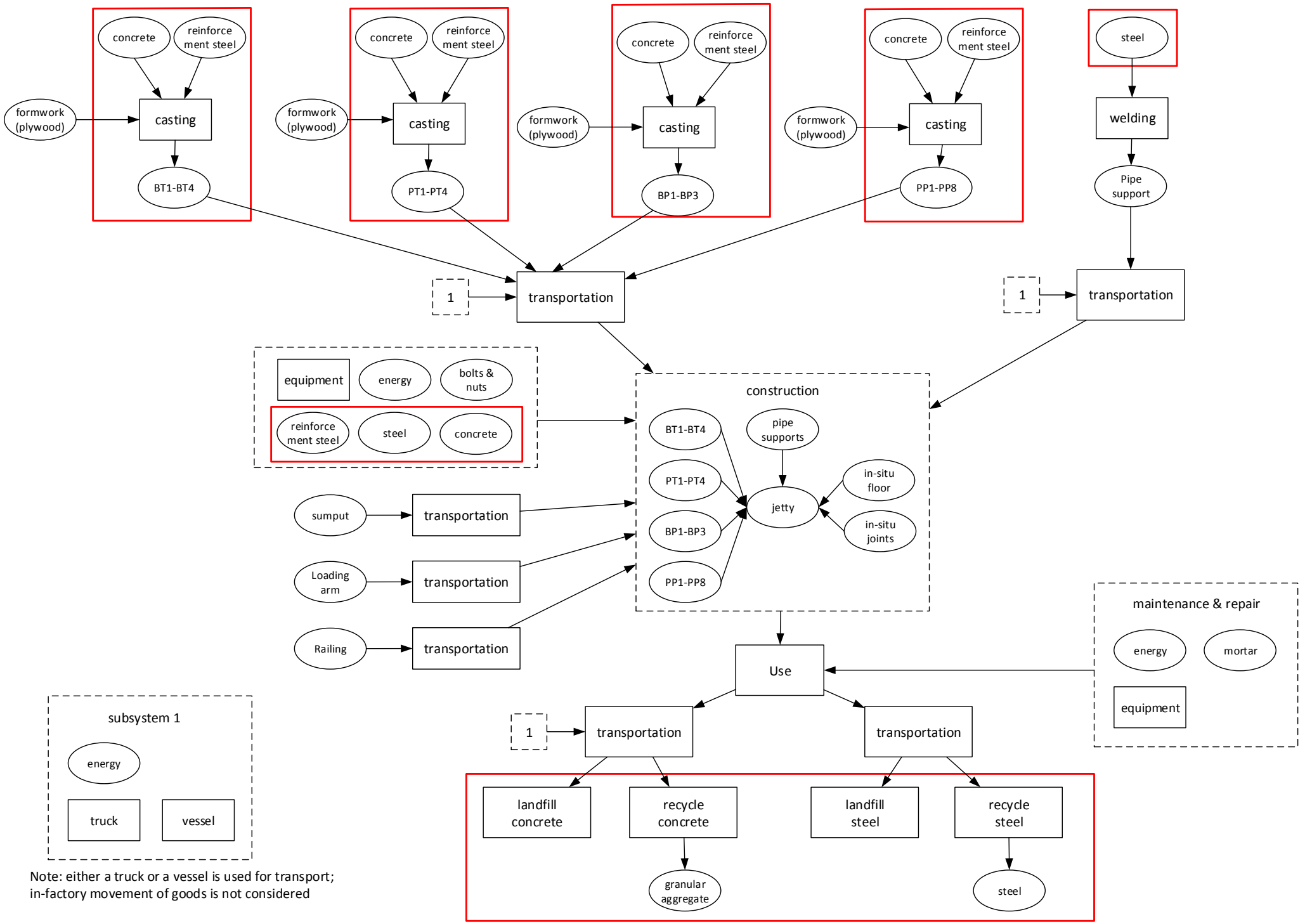

Note: either a truck or a vessel is used for transport;
in-factory movement of goods is not considered

Raw materials
The raw materials for the FRP jetty are resin and fiber. More specifically, a polyester resin and glass fibers are used. Fillers and additives can be applied to FRP elements in order to enhance their properties (Winter, 2017). These materials are not regarded as they are not specified in the design. Also, paints are used in order to indicate the wearing level of top surface of the planks. Gravel has been incorporated in this top layer. Both paint and gravel have not been regarded in this assessment since they are contribution is relatively small to the total impact.

The RC jetty encompasses the following raw materials: concrete, reinforcement steel, steel, plywood (for formwork), and stainless steel. Two different concrete classes are worked in the jetty: C45/55 and C30/37. Steel is used to make the pipe supports. Nuts and bolts are made from stainless steel.

Manufacturing processes of the structural element
The beams, planks, and girders from the FRP jetty are manufactured by the pultrusion process; the piles are produced by filament winding.

The RC jetty is made from prefabricated elements (named BT1-BT2, PT1-PT4, BP1-BP3, and PP1-PP8. Small items such as caps to position the reinforcement steel and nails to make the form work are not regarded.

Construction
The superstructure of the access bridge and the platform of the FRP jetty will be assembled in the factory. The structural elements are fastened with bolts and nuts, glue, or a combination of those dependent on the required stiffness and strength of the joint. The piles are driven into the ground. The top of the piles might require treatment if they are damaged during the driving process. On the pile heads, transition pieces may be welded or fastened on which the beams can be attached. The planks rest on the top of the beams. They can be fastened at their open ends with clips, bolted, or glued. The amount of fastening materials is not determined and therefore these are not regarded within the system boundaries. This holds to for removal of the plastic pile heads if they are damaged. The total superstructure can be assembled in the factory [2], and due to its light weight it might be lifted by a crane and positioned into place in one go, or per section.

The first action for the RC jetty is to drive the piles into the ground. Then, the prefab support beams are placed on the pile heads, which will be cut of in order to expose the reinforcement so this can be connected to the other elements. On the support beams, the prefab plates are then placed. Then the joints are casted together in-situ with concrete after reinforcement has been place to couple the piles, beams, and plates. Then, the top deck is casted in-situ.

The construction has most likely a significant influence on the total environmental impact of the construction (in his thesis, van der Valk designed an FRP quay wall and found that about 15 % of the environmental impact, measured in GWP, was generated in the construction phase (Van Der Valk, 2017)). However, it is decided to not include the construction phase into the impact assessment due to a variety of reasons. First, there are multiple ways of constructing the jetty, which are dependent on factors such as the availability of equipment; the distance this equipment is located form the construction site; using prefab elements or casting in-situ. Furthermore, if a construction method is selected, estimating the amount of equipment needed and how long it is needed is prone to errors. Nuts and bolts have been disregarded in the LCA since their contribution is estimated low and an accurate quantity is hard to state.

[2] As is frequently done for bridges by FiberCore Europe (*FiberCore Europe - Bridges*, 2017)

Whilst general construction costs for the FPR jetty are expected to be lower, driving costs may be higher due to lower capability of the FRP piles to transfer energy from the driving hammer to the soil, hence requiring more blows and more energy to drive the piles to the desired depth. Results from the pile drive analysis are presented in Chapter 6.

Transportation
Transportation is required to get the structural elements, equipment, labor force, and additional supplies to the factory, construction site, and the location where the end-of-life of the structure is processed. This can be incorporated, if data was available, for the LCA. However, the aim is to compare the two designs in general: not to compare the designs for the specific location in Moerdijk [3]. Also, in the LCA of Van Der Valk the share of transportation to the total impact was less than 2 % (Van der Valk conducted an LCA on an FRP quay wall and a steel-combi wall).

However, it is noteworthy to mention the differences between the FRP and the RC jetty. First of all, the FRP jetty is lighter than the RCe jetty, so transportation costs for fuel will probably be lower. Also, the equipment needed to handle (e.g. lift the assembled structures) might be lower, dependent on the construction method.

Jetty
The pipe support and sumput for the jetty were not designed[4]; it can be assumed to be same products as is used in the RC jetty and can therefore be disregarded.

Use-phase
Two main activities are identified during the use-phase of the jetty; operational activities and maintenance.

Both these activities are not regarded in the LCA. The operational activities are regarded the same for both jetties (e.g. power required by the loading arm and pumps) and therefore can be disregarded from the LCA.

For the regarded life-time (i.e. 50 years), the amount of maintenance on both the FRP jetty as the RC jetty seems negligible. Also, the required maintenance is unpredictable and depends very much on the maintenance strategy used. Therefore, the maintenance is disregarded in the LC.

While not including maintenance and life-time in the LCA, they might have a significant impact on the results of the LCA. Therefore, a sensitivity analysis is made (Section 7.5.2) in order to research if they are of significant influence on the result of the LCA.

End-of-life
In the database, three options are available for the end-of-life: landfill, incineration, and recycling/reuse. The former two have impact values assigned to them, the latter has an impact value of zero.

Several options are available at the end-of-life stage for the FRP jetty. The jetty can be landfilled, which is considered the worst option regarding environmental impact. The structure can be incin-

[3] The location of Moerdijk is stated in the Declared Unit because the soil profile influences the dimensions of the structural elements
[4] An estimation of their loads have been incorporated into the load cases

erated: European law regards this as recycling when this happens in an cement oven (de Boer et al., 2016). This is because FRP is a valuable product in the production of cement where the resin acts as fuel and the glass is used in the end-product. Thermoplastic resins are good recyclable, some thermoset resins are recyclable with chemical or thermal processes (de Boer et al., 2016). If the structure is still in good condition it might be reused. However, the material will have degraded due to the creep phenomenon and weather; therefore the loads acting on the structure should be lower than initially designed for.

The RC jetty also has various options; in general, left over materials which will be freed at the end-of-life are concrete and steel. These both can be landfilled, but this is undesirable because the steel is very valuable and the concrete can be applied in other product. The steel is fully recyclable by melting it in a furnace and remolding it. The concrete can be used as aggregate in the construction of roads and pavements after it is crunched to workable sizes.

7.4. Impact assessments of the FRP- and RC jetty

In this section the eco-costs per impact category are presented. Also, the chosen impact values per material are clarified since the database does not always provide details of the product (e.g. fiber volume of FRP material).

7.4.1. Bill of quantities

Table 7.1 presents the bill of quantities for the FRP jetty and the RC jetty. The quantities for the RC jetty are subtracted from the scope statement from the case study; quantities for the FRP jetty were calculated with the designed structural elements Chapter 5.

	Material	Quantity	Unit
FRP jetty	Glass	24407	kg
	Polyester	8454	kg
	FRP	30862	kg
	Fiber content scaled FRP[5]	27925	kg
RC jetty	C45/55	150109	kg
	C30/37	61275	kg
	Reinforcement steel	19238	kg
	Steel	45	kg
	Stainless steel	44	kg
	Formwork	35	m^2

Table 7.1: Bill of quantities for the FRP jetty and the RC jetty

[5]See section Section 7.4.3 for the allocation of material

7.4.2. Eco-costs per impact category

Table 7.2The eco-costs, or shadow costs, are defined in the database for each impact category. The numbers are based on the database of Jonkers (H. Jonkers, 2017).

Impact category	Equivalent unit [kg]	Shadow price [€/kg eq.]
Abiotic depletion	Sb	0.16
Global warming (GWP100)	CO2	0.05
Ozone layer depletion (ODP)	CFC-11	30
Human toxicity	1,4-DB	0.09
Fresh water aquatic ecotoxicity	1,4-DP	0.03
Marine aquatic ecotoxicity	1,4-DP	0.0001
Terrestrial ecotoxicity	1,4-DP	0.06
Photochemical oxidation	C2H4	2
Acidification	SO2	4
Eutrophication	PO4	9

Table 7.2: Shadow prices per kg equivalent unit for the impact categories

7.4.3. Allocation and reference choice from data base

The provided database does not exactly possess all the materials which were used in the design of the FRP and the RC jetty. Hence, methods of allocating these materials have to be developed.

FRP jetty

The database possess both resins (with polyester also available as used in the design) and glass as materials, but also FRP. The material quantities of the resin and the glass can be determined individually, but then the influence of the manufacturing process of to make FRP elements of them is omitted. But with the FRP, two problems arise: neither the fiber content is specified nor the production process.

The fiber content can be estimated since the values of the raw materials (i.d. polyester and glass[6]) are known. By using the rule of mixture (see Section 5.4.1) the fiber volume content is estimated at 41.7 %[7]. Since the equivalent impact values are per kg, also the density of the material has to be changed. With $\rho_{polyester} = 1200\,\text{kg/m}^3$ and $\rho_{glass} = 2570\,\text{kg/m}^3$, the density becomes:

$$\rho_{FRP} = fb\% * \rho_{glass} + (1 - fb\%) * \rho_{polyester} = 0.417 * 2570 + (1 - 0.417) * 1200 = 1771\,\text{kg/m}^3$$

The density of the design laminate is $2022\,\text{kg/m}^3$. Hence, the impact factors of the FRP are reduced by $\frac{1771}{2022} = 0.876$.

The differences between the impact values of glass and polyester separately (i.e. not proccessed into FRP) are signficantly. The two biggest impact categories contributors to the eco-costs are global warming potential and human toxicity, measured in equivalent kg C02 and equivalent kg 1,4-DB. The equivalent kg produced C02 are 18 140 and 37 438 for glass and polyester respectively (106 % increase); the equivalent kg produced 1,4-DB are 6371 and 62 813 for glass and polyester respectively (886 % increase).

[6]This glass is presumably not yet processes to filaments so it can be processed into FRP
[7]Percentage as mass fibers to mass FRP

It is assumed that 75 % of the FRP jetty is recycled by means of fuel and raw material supply to cement ovens, and 25 % of the construction is reused. Either way, the influence of these methods on the impact assessment is zero according the usage of the database.

Reinforced concrete jetty
In the database no indication values for C45/55, but there are for C35/45 and C55/67. Their impact (GWP) per kg rises accordingly to their strength: hence, to achieve a impact values for C45/55 the impact values for C35/45 and C55/67 were averaged out.

It is assumed that 95 % of the steel is recycled and 5 % landfilled; of the concrete, 50 % is landfilled and 50 % is recycled. Steel is a valuable metal and easy to recycle; the recycling rate of 95 % is based on 5 % loss of steel during demolition operations. Wagih, El-Karmoty, Ebid, and Okba found that with an aggregate mixture of 75 % recycled aggregates could achieve the same structural strength as concrete based on all new natural aggregate, for Egyptian standards. Rao, Jha, and Misra researched recycling rates of construction and demolition waste around the world. They found that no specific rates per EU-country were available, but during the late 1990s an average of 28 % of all construction and demolition waste was recycled in the European Union. Furthermore, a report of the European Union stated that achievement of construction and demolition recycling rates higher than 75 % only seemed possible with governmental regulations and restrictions on landfill practices. It is interesting to note that Rao et al. also found that “recycled materials are generally less expensive than natural materials, and recycling in Germany, Holland and Denmark is less costly than disposal”. Taken the above into account and assuming recycling rates increased since the late 1990s, a 50/50 distribution of landfilling and recycling of the concrete seems reasonable.

7.4.4. Results of the impact assessment
Figure 7.1 presents the eco-costs for the FRP jetty and the RC jetty, which are €33080 and €10653 for the FRP and the RC jetty, respectively. The two largest contributers to the eco-costs: global warming potential in equivalent kg C02 and the human toxicity in equivalent kg 1,4-DB.Figure 7.2 presents the global warming potential of both jetties.

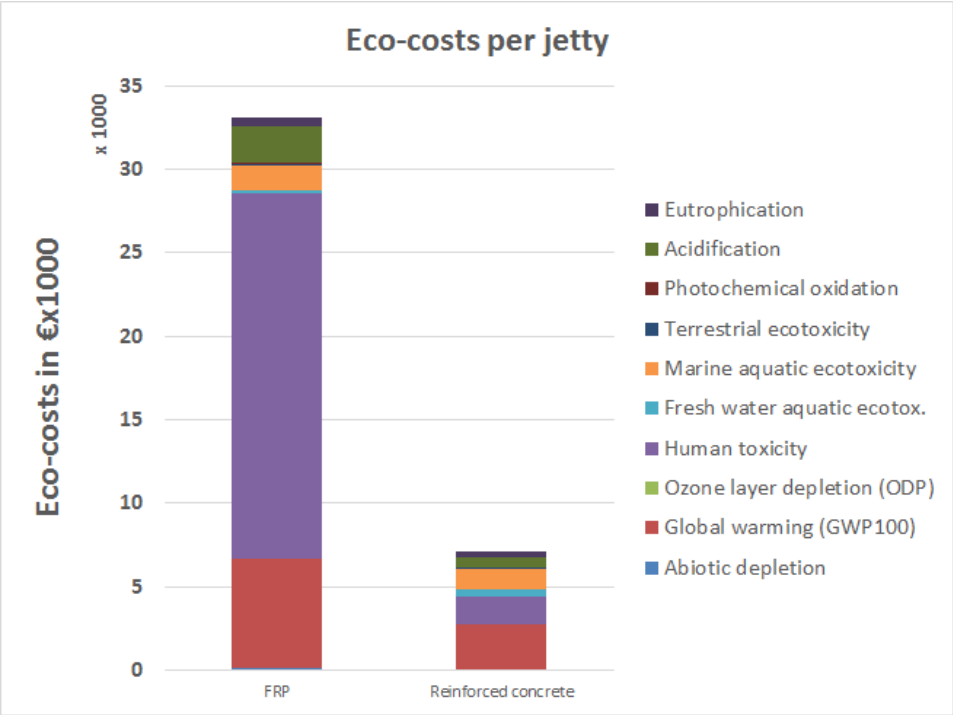

Figure 7.1: Total eco costs for the FRP- and the RC jetty

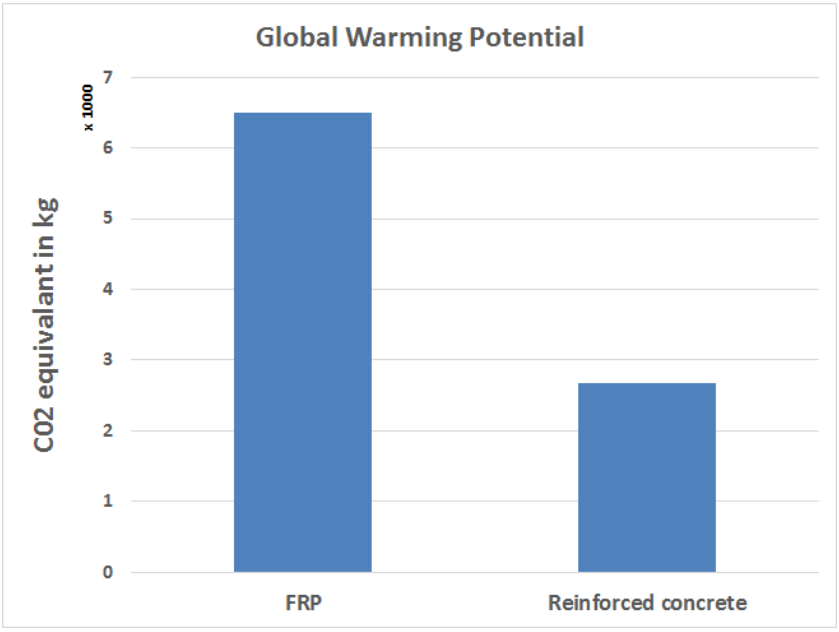

Figure 7.2: Total global warming potential in kg C02 equivalents FRP- and the RC jetty

7.5. Evaluation of the LCA

7.5.1. Evaluation of assumptions

Providing a critical reflection on the system boundaries and assumptions is essential to correctly interpreted the results of the impact assessment. This section evaluates the assumptions made regarding the LCA.

Economic versus technical life span

An often used argument to use FRP as a construction material is due to its durable properties and that over its life time, life cycle costs and environmental impact are lower (Winter, 2017). The RC jetty is designed for 50 years; this life time is presumably chosen for its economic life time. However, the technical design life time will probably be longer. The cement used for the RC jetty is CEM III/B, which has a good resistance in salt water environments (ENCI, 2006).

Various literature claims for a longer life-time of FRP due to better durability properties; however, long-term case studies are not available yet (Winter, 2017). Therefore, attempts to estimate more precise life-time expectancies are omitted.

Allocation of impact values

The conversion of the glass FRP, polyester based material in the database to the designed FRP mixture takes fiber volume content and density into account; however, such estimate is a very rough one. This is because the resins have different mechanical properties, hence influencing the required amount of material needed to comply with the structural criteria.

Besides polyester, the material was also extrapolated to the epoxy- and vinylester FRP's[8]. While for the epoxy a fiber volume content of 37 % was found, recalculating the fiber volume content for the vinylester FRP resulted in a negative fiber volume content (i.e. –65 %). This is because the impact of a FRP vinylester is higher than the impact of vinylester by itself, hence no positive fiber volume content can be found. CUR96 states that the resin is the mayor influencer on the environmental impact (de Boer et al., 2016). Therefore, it is hard to draw strong conclusions if the exact amount of resin in a kg is not known.

Quality of impact values for FRP

The eco-costs in the database for different FRP's is not congruent with CUR96. The eco-costs of one kg of glass FRP made from epoxy, polyester, or vinylester are €1.142, €1.185, and €0.791 respectively. CUR96 states that epoxies have a higher environmental impact than polyesters (de Boer et al., 2016). This questions the quality of the database, or the statement made in the CUR96.

Construction

For a more better estimate of the environmental impact, the construction phase should be regarded. In his thesis, Van der Valk designed an FRP quay wall and found that the majority of the environmental impact was due to the materials, not due to construction and transportation (i.e. about 85 % (Van Der Valk, 2017). Due to the big differences in environmental impact between the FRP jetty and the RC jetty due to materials only (108 % relative increase with respect to the RC jetty), detailed estimates of the environmental impact due to construction activities is not required in order to answer the goal of the LCA.

[8] As denoted in the database provided by H. Jonkers

Raw materials and end-of-life

In the database it is not specified how the raw material is processed, which further decreases the accuracy. For instance, it is very common for steel to be recycled and hence, to process recycled steel into new structures. Also, possibilities of selecting recycled raw materials in the database is limited.

For recycling and reusing, no impact values are assigned. This is a matter of allocation choices: by doing it this way, the recycling should be incorporated in LCA's which use, for example, recycled steel.

Transparency of the manufacturing processes

Manufacturing technique presumably has influence on the production environmental impact of FRP. However, the manufacturing technique nor the fiber volume content are clarified in the database. Therefore, there cannot be made a useful distinguished between manufacturing techniques, nor can two manufacturing techniques be compared regarding environmental impact with the data presented in the database.

Cut-off items

The maintenance is disregarded in the LCA. While this probably is a small amount of the total (perhaps 2 %), a primary reason for using FRP instead of concrete or steel is because of its superior durability properties (Winter, 2017). However, it is highly unlikely that the reduced maintenance effort for FRP jetties will close the gap between the eco-costs of the FRP jetty and the RC jetty since the relative impact increase of the FRP is 211 % compared to the RC jetty.

The precise amount of material required to construct the FRP is not known. This is partly because the material quantity for the construction joints are not regarded due to their small contribution to the total impact value. Also, the construction is not yet optimized: specific pile dimensions may be reduced and different resins may be chosen for different structural elements.

It must be noted that the pipe supports for the FR jetty were accounted while they are not accounted for in the assessment of the FRP jetty. This is because an FRP pipe support was not designed. It would be better to have omitted it for the RC jetty as well, but they have no significant impact on the value of the total environmental impact.

7.5.2. Sensitivity analysis

The design process is an iterative one, improving performance and resource efficiency with every iteration. The designed FRP jetty is not yet fully optimized. A fully optimized design in terms of structural performance also might have a lower environmental impact (e.g. amount of construction material is lower). By means of a sensitivity analysis, the influence of certain parameters can be investigated. Then, a judgment can be made if any gains can be made by improving the design regarding the environmental impact of the FRP jetty.

The chosen cases are based on the preceding chapter. Case 0 acts is the default case which is the original assessment. A description of the sensitivity analysis are described in the remaining of this section; at the end an overview of these cases are presented as well as the results from the sensitivity analysis.

Case 1: Uncertainty in material quantity for the FRP jetty
The jetty is not yet optimized nor fully finished: piles might be dimensioned per specific pile and resins and bolts used in joints are not regarded in the study. Depending on the influence of these aspects, the material load of the jetty may be higher or lower. Therefore, two cases are designed to take this into account: case 1.1 which increases the material quantity of the FRP jetty by 10 % and case 1.2 which decreases the material quantity of the FRP jetty by 10 %.

Case 2: Influence of resin
The impact values of different resins (i.e. polyester, epoxy, and vinylester) vary significantly in the database: one kg of glass FRP made from polyester, epoxy, or vinylester has a GWP of 4.65, 4.42, and 3.44 kg equivalent C02 and a human toxicity of 8.7, 7.4, and 5.7 kg equivalent 1,4-DB , respectively. In case 0, human toxicity accounts for 66 % of the total eco-costs. Therefore, it seems worthwhile to investigate the influence of different resins[9].

Case 3: Enhanced life time of FRP jetty
An assumption is made that the economic- and technical life-time are equal to each other but different for the two jetties: 50 years for the RC jetty and 75 years for the FRP jetty. To take this into account, the eco-costs of the FRP jetty are multiplied with $\frac{50}{75} = \frac{2}{3}$.

Case 4: Incorporation of construction- and transport influences
To give an indication of the influence of construction costs, it is assumed that the material costs make up 95 % and 85 % of the total costs (excluding maintenance & operations) for the FRP- and RC jetty respectively.

Case 5: End-of-life alternatives
In case 0, it is assumed that 75 % of the FRP jetty will be recycled and 25 % reused; for RC jetty, 50 % is landfilled and 50 % is recycled. Case 5 regards different end-of-life scenarios. Case 5.1: 50 % of FRP jetty landfilled, 50 % recycled. Case 5.2: 75 % of RC jetty recycled, 25 % landfilled. Case 5.3: combination of case 5.1 and case 5.2.

Case 6: Extremes resulting from combining cases
The preceding cases all positively or negatively influenced the impact of the jetties. In case 0 it is obvious that the FRP jetty is having a far worse impact compared to the RC jetty. Therefore, case 6 investigates the best-case scenario for the FRP jetty and the worst-case scenario for the RC jetty. For the FRP jetty this means: decreases the material quantity by 10 %, multiplying the end results with $\frac{2}{3}$, replacing the polyester resin with the vinylester resin, and to include transportation and material costs by dividing by 95 %. For the RC jetty, this means to include transportation and material costs by dividing by 85 %.

Table 7.3 presents the cases which have been designed for the sensitivity analysis; Figure 7.3 graphically presents the results of the case impacts.

[9]Impacts have been allocated to density, but not to strength and stiffness as described in Section 7.4.3

Case	FRP jetty	RC jetty	Description
0	-	-	Default case
1.1	+10 %	-	10 % material quantity added to FRP jetty
1.2	-10 %	-	10 % material quantity reduced from FRP jetty
2.1	Vinylester	-	A vinylester is applied instead of a polyester for the FRP jetty
2.2	Epoxy	-	An epoxy is applied instead of a polyester for the FRP jetty
3	factor $\frac{2}{3}$	-	Sum of impact values for FRP jetty gets multiplied by $\frac{2}{3}$
4	Materials 95 % of total	Materials 85 % of total	5 % and 15 % of total assumed for transportation and construction
5.1	+50 % landfilling	-	50 % of FRP waste will be landfilled
5.2	-	+25 % recycling	75 % of concrete will be recycled
5.3	+50 % landfilling	+25 % recycling	75 % of concrete will be recycled; 50 % of FRP will be recycled
6	various	various	FRP jetty best-case scenario; RC jetty worst-case scenario

Table 7.3: Overview of the sensitivity cases for the LCA

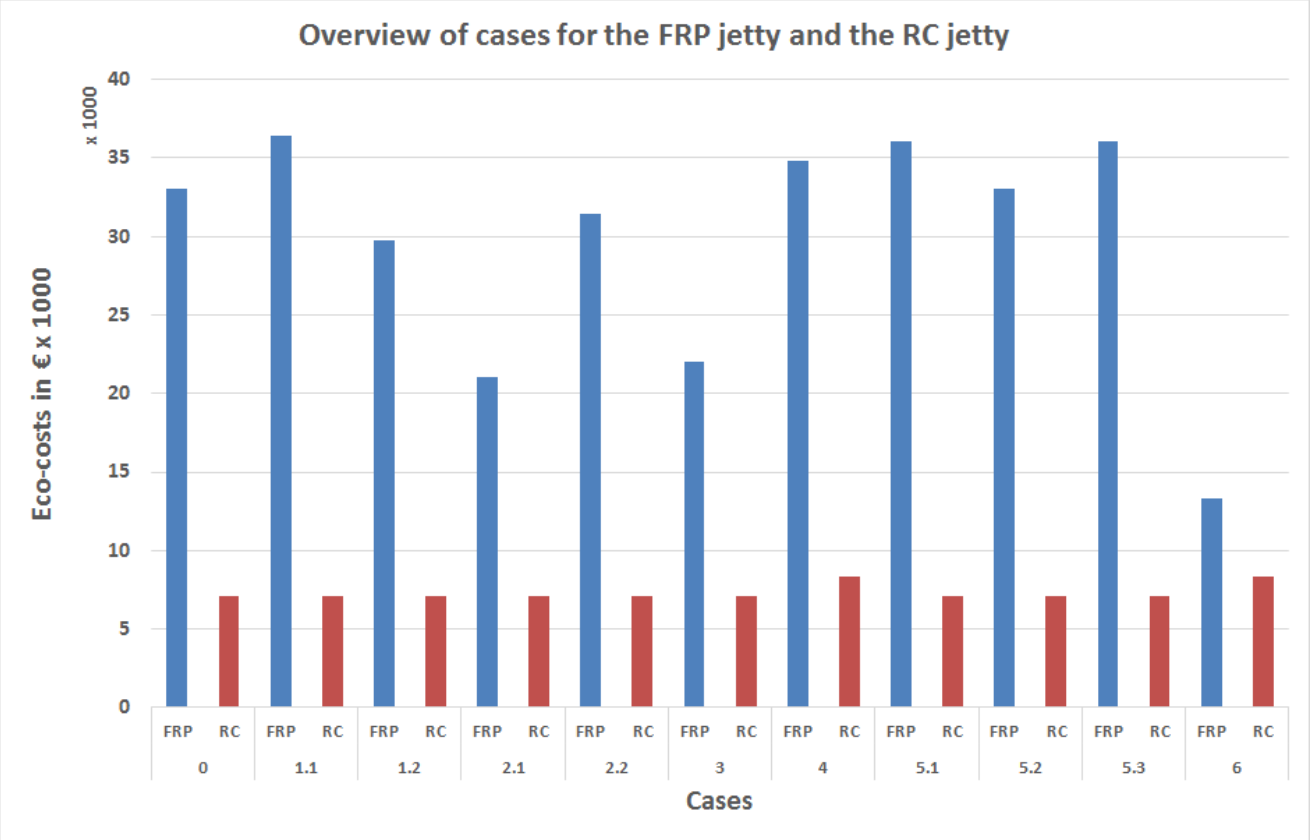

Figure 7.3: Graphical illustration of the sensitivity cases for the LCA

7.5.3. Evaluation of the LCA results

In this section, the goal of the LCA is evaluated:

"Provide an estimation of the environmental impact of an fiber reinforced polymer jetty and a reinforced concrete jetty, both having the same technical requirements regarding structural integrity, durability, and lifespan, to give an indication for the better alternative regarding the environmental impact"

The material eco-costs for the FRP jetty are about 211 % higher compared to the material costs of the RC jetty[10]. Manipulating the material quantities yields no results where the FRP jetty scores better than the RC jetty: the difference between the best-caste scenario for the FRP and the worst-case scenario for the RC jetty differ almost 59 % with respect to the RC jetty. It is assumed to be very unlikely that all advantages of FRP occur whilst all disadvantages for FRP occur. Therefore, based on the defined system boundaries and the used database it can be concluded that the RC jetty has a lower environmental impact compared to the FRP jetty.

The most important contributor to the eco-costs of the FRP jetty is the used resin: for the two biggest impact categories, global warming potential and human toxicity, the relative difference with glass is +150 % and +1050 % respectively; these two categories made up +19.6 % and +66.2 % of the total eco-costs for the FRP jetty respectively[11]. This make the choice of resin evident for the environmental impact; when designing for the lowest possible environmental impact, resins with low environmental impact should be selected early in the design stage.

7.6. Conclusions from the LCA: FRP jetties perform worse than RC jetties

From the evaluation and the sensitivity analysis, the following can be concluded:

- Regarding the declared unit, the FRP jetty performs significantly worse than the RC jetty in the base case (0): shadow costs are almost 365 % higher with respect to the RC jetty for the base case LCA
- After a sensitivity analysis, where plausible differences in value parameters were changed in order to affect the environmental impact of the FRP jetty positively, the FRP jetty still performs significantly worse than the RC jetty: shadow costs are 59 % higher with respect to the RC jetty.
- If the environmental impact of the FRP jetty is to to be lowered, the most significant gains can be made by finding resins with a lower environmental impact (e.g. bio-plastics). The most important contributor to the shadow costs of the FRP jetty is the used resin: for the two biggest impact categories, global warming potential and human toxicity, the relative difference with glass is +150 % and +1050 % respectively; these two categories made up +20 % and +66 % of the total shadow costs for the FRP jetty respectively.

The following recommendations are made regarding the environmental impact:

- The biggest contribution to the environmental impact from the raw materials, according to the database, comes from resins; research regarding the feasibility of incorporating more environmental friendly resins, such as bio-plastics, into FRP jetties could give new insight regarding lowering the environmental impact of jetties
- Many databases which assess impact values for impact categories are available; a free open access database should be available to let scientists and engineers assess their products unbiased

[10] Percentages shown in this section are relative changes computed as $\frac{\text{eco-costs FRP jetty-eco}-\text{costs RC jetty}}{\text{RC jetty}} \text{x} 100\,\%$

[11] For the base case (0) LCA

III

Financial feasibility

"How do costs of FRP jetties differ from RC jetties during their full lifetime cycles?"

8

Financial analysis of the FRP jetty

Assessing the costs of the FRP jetty is important; the market will adopt the FRP jetty only most likely if their life-time costs are lower. This chapter aims to give an indication of the differences in costs between fiber-reinforced jetties and reinforced concrete jetties.

8.1. Financial model set-up

8.1.1. Method of cost calculation

This section elaborates the method used to calculate the costs.

First, the considered costs aspects are elaborated. Then, these are quantified in order to allocate the costs. Concluding, a sensitivity analysis is carried out to investigate variations in the financial model assumptions
To get a complete overview of costs, the costs involved in all phases of the structures lifetime should be regarded. The total costs of the jetty can be divided in a number of cost areas:

- Design costs
- Construction costs
- Material costs
- Maintenance costs
- Operational costs[1]
- Disposal costs
- Eco-costs

The following of these costs are disregarded in this thesis: design costs, operational costs, disposal costs, and eco-costs. Design costs and operational costs are omitted because they are assumed to be the same. Disposal costs are dependent on the end-of-life of the jetty. They depend on the end-of life action of the jetty, which can be reuse, recycling, or landfilling, analogous to the LCA end-of-life[2]. Eco-costs are considered in Chapter 7.

[1] Operational costs for commercial activities on the jetty, e.g. required power for the loading arm
[2] Due to time constraints, the end-of life cost are not regardid in this analysis

8.1.2. Cost allocation

This section quantifies the cost variables: unit price, construction cost ratio, maintenance cost ratio, and interest.

Unit price for material

Material costs for the FRP jetty are determined with two methods: based on bulk FRP, and based per stretching meter for the beams, blanks, and girder. In both cases, the material costs for the piles are based per stretching m. With the bill of quantities and the unit costs (bulk and per stretching meter), a cost estimation for both the material costs of the FRP and the RC jetty can be made.

Table 8.1 presents the unit costs for the FRP jetty and the RC jetty in terms of bulk unit costs (€/kg) and as reference (€/m of structural element)[3].
The bulk costs for FRP are given as a range: for the applied FRP in the jetty (polyester and E-glass), the lowest bulk costs are 4 €/kg and the highest bulk costs are 7 €/kg.
The costs given as a reference, are based on comparable prices in the market: these costs are composed by scaling the costs by the relative area of the reference costs. For example:

$$\text{Cost structural element}\left[€/\text{m}\right] = \frac{A_{\text{structural element}}\left[\text{m}^2\right]}{A_{\text{reference product}}\left[\text{m}^2\right]} * \text{Costs reference product}\left[€/\text{m}\right]$$

With A being the cross sectional area in m^2. The unit price for the hollow FRP piles is given by Zyka and Mohajerani as costs per stretching meter (Zyka & Mohajerani, 2016). The other reference costs are based on a cost brochure of BIJL products (W.B. Bijl Profielen B.V., 2015b)

The unit material costs for the RC jetty are found for in-situ concrete, prefab concrete, reinforcement steel, formwork, and concrete piles. The unit costs are based on unit prices made available by the Gemeente Rotterdam (van der Meer, 2017).

Jetty	Name	Unit price	Unit
FRP jetty	Beam 1	281	€/m
	Beam 2	287	€/m
	Plank 1	84	€/m
	Plank 2	120	€/m
	Girder 1	70	€/m
	Pile 1	111	€/m
	Pile 2	186	€/m
	Polyester, E-glass	4 to 7	€/kg
	Vinylester,E-glass	5 to 8	€/kg
	Epoxy, E-glass	7 to 10	€/kg
RC jetty	In-situ concrete	130	€/m^3
	Prefab concrete	173	€/m^3
	Reinforcement steel	1.2	€/kg
	Formwork	100	€/m^2
	Concrete piles	199	€/m^3

Table 8.1: Unit prices for elements of the FRP jetty and the RC jetty

The sumput, railing, and loading arm are omitted from this life cycle costs analysis because they are

[3]The material costs are based on data presented in the accompanying literature study (Winter, 2017)

assumed to be the same for both the FRP and the RC jetty.

Construction costs
Construction costs are based on the case study. For the case study, material costs and construction costs are available for the items regarded in the scope of this thesis (see Section 4.1.1). The initial costs are defined as the sum of the construction costs and the material costs. In the case study, the material costs amounted for 63 % of the initial costs, hence the construction costs amount for $1 - 63\,\% = 27\,\%$ of the initial costs.

The costs are, however, based on the RC case study; the ratio is arguably different for FRP. The in-field construction time might be lower. BIJL bruggen produces its bridges indoors and transports it to the desired location by truck or boat, where the bridge can be lifted in place with a crane (Bergen, n.d.).
For the base case, the construction costs ratio will be the same as for the RC jetty.

Maintenance costs
Maintenance costs were taken as a percentage of the total realization costs[4]. The costs over the economic lifetime of the jetty (i.e. 50 year) were discounted to the net present value (NPV). De Gijt suggested for RC jetties a percentage of 2 %. One of the highly appreciated properties of FRP is its high durability. Therefore, a very low percentage of 0.5 % is taken as the maintenance cost ratio for the FRP jetty.

Interest rate
Due to maintenance, costs will be made in the future. However, the value of money changes over time. In order to make a comparison of costs made over a time span, these costs have to be discounted to one moment in time to make them comparable. The base case interest rate is set at 3 %. Higher interest rate are advantageous for larger future investments. Since the maintenance costs are the only future costs which needs to be accounted, the RC jetty benefits from higher interest rates since its maintenance cost ratio is lower compared to the maintenance cost ratio of the FRP jetty.

[4]The definition of total realization costs are composed from material- and construction costs in this research

8.2. Overview of the life-cycle costs cases for the FRP- and RC jetty

8.2.1. Bill of quantity and unit costs

Table 8.2 presents the bill of quantities for both the FRP jetty and the RC jetty. Additionally, Table 8.3 presents a bill of quantity for FRP jetty where the the material quantities are expressed in quantity of structural elements. Furthermore, Table 8.1 gives an overview of the unit costs for both jetties.

	Material	Quantity	Unit
FRP jetty	Glass	24407	kg
	Polyester	8454	kg
	FRP	30862	kg
RC jetty	C45/55 (prefab)	150109	kg
	C30/37	61275	kg
	Reinforcement steel	19238	kg
	Steel	47	kg
	Stainless steel	44	kg
	Formwork	35	m^2

Table 8.2: Bill of quantities for the FRP jetty and the RC jetty per bulk material

	Material	Quantity	Unit
FRP jetty	Beam1	61.6	m
	Beam 2	79	m
	Plank 1	90	m
	Plank 2	125	m
	Girder 1	44.34	m
	Pile 2	485	m

Table 8.3: Bill of quantities for the FRP jetty per structural element

8.2.2. Overview of the cases

The assumed financial variables may deviate from the actual scenario. To investigate the influence of these financial variables, various cases are formulated to conduct a sensitivity analysis. An overview of the cases is presented in Table 8.4. Case 0 acts as the base case: the financial variables used in this case seem the most likely to happen. The remaining of this section gives a brief description of the cases.

Case	Unit costs type		Construction cost ratio [%]		Maintenance ratio [%]		Interest [%]
	FRP	RC	FRP	RC	FRP	RC	
0	Reference	Bulk	0.67	0.67	0.5	2	3
1.1	Bulk (high)	Bulk	0.67	0.67	0.5	2	3
1.2	Bulk (low)	Bulk	0.67	0.67	0.5	2	3
2	Reference	Bulk	0.75	0.67	0.5	2	3
3	Reference	Bulk	0.67	0.67	0.1	2	3
4	Reference[5]	Bulk	0.67	0.67	0.5	2	3
5.1	Reference	Bulk	0.67	0.67	0.5	2	5
5.2	Reference	Bulk	0.67	0.67	0.5	2	5
6	Bulk (low)	Bulk	0.75	0.67	0.1	2	3

Table 8.4: Overview of cases for the sensitivity analysis of the life-cycle costs assessment

Where:

Construction costs ratio : Ratio of construction costs with respect to the sum of the realization costs[6]

Maintenance ratio : Annual maintenance costs as percentage of realization costs

Interest : Annual interest factor as a percentage realization costs

[5] Realization costs are multiplied with $\frac{50}{75} = \frac{2}{3}$

[6] With realization costs being the sum of the construction costs and the material costs

It must be noted that in all cases, the material costs of the FRP piles and RC piles are always based on reference products. The remainder of this section elaborates the cases qualitatively. In general, the cases are variations on the base case (case 0).

Case 0: Base case
This cases serves as the base case: the variables here are set to the most likely values.

Case set 1: Unit price
In order to compare to see if the reference price make sense, the price of the FRP jetty is also calculated for the determined bulk price. The higher- and lower boundary of the set bulk price range are calculated.

Case 2: Construction cost ratio
As argued in the preceding section, the construction cost of FRP may be lower. Due to the light weight of the FRP, transportation and installation costs require less energy and less heavy equipment. Therefore, the construction cost ratio is adapted in case 2: the construction cost make up 75 % of the total cost instead of 67 %, effectively bringing down the realization costs.

Case 3: Maintenance costs
Assuming a scenario where no maintenance is cost is required for the FRP jetty: the maintenance cost ratio is reduced to 0.1 %.

Case 4: Durability
In agreement with the LCA, a case is made where the costs are allocated to the potential longer life span of the FRP (see Section 7.5.2). The same life span adjustments can be made: the technical life span of the FRP jetty and the RC jetty are assumed to be 50 year and 75 year respectively. Then, the effect of the potential longer life span is accounted for by multiplying the realization costs with $\frac{50}{75} = \frac{2}{3}$. For the NPV of the maintenance costs, a projection of 75 years is done instead of 50 years.

Case set 5: interest The last case set test the influence on interest. The interest only affects the net present value of the maintenance costs, since this is the only costs not occurring in the construction phase but annually over the life time. Therefore, besides a comparison with the base case (maintenance of FRP and RC 0.5 % and 2 % respectively), a higher interest rate is also compared for 1 % maintenance costs of the FRP jetty. The maintenance costs of the RC jetty are based on the suggestion of de Gijt.

Case 6
In this scenario, all the variables are changed so that the lowest possible costs for the FRP jetty and the highest possible costs for the RC jetty are generated. Besides the used financial variables, the total life-cycle costs are also multiplied by 2/3 as in case 4.

8.3. Results of the life-cycle cost analysis of the FRP jetty and the RC jetty

Figure 8.1 presents the costs of the base case for the FRP jetty and the RC jetty. The projected life-cycle costs for the FRP jetty and RC jetty are €275.870 and €107.986 respectively.

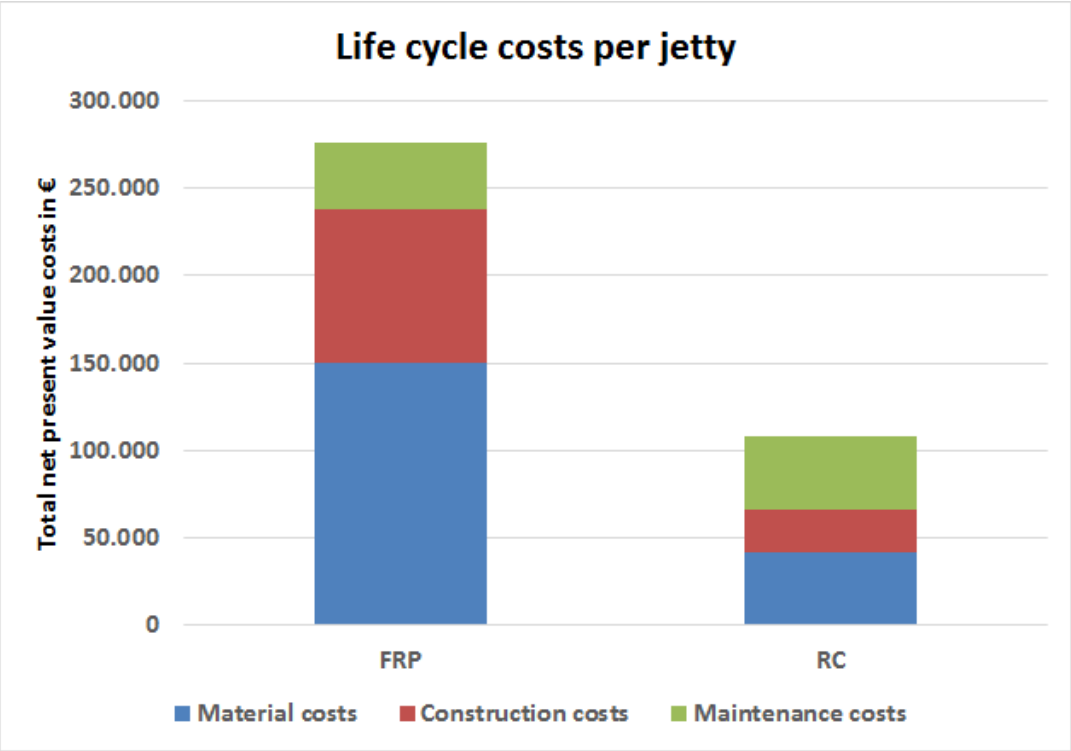

Figure 8.1: Life cycle costs for case 0: the base case

Figure 8.2 illustrates the cost allocation to the structural elements of the FRP jetty for the base case. It is clear that the biggest material costs are made by the FRP hollow piles: they make up 56 % of the total material costs.
The material costs ratio of the piles to the total material cost are indicated in Figure 8.3 for the FRP- and the RC jetty; the foundation segment indicates the material costs of the piles. Whilst for the FRP jetty the piles account for 56 %, the material costs for the piles of the RC jetty only account for 22 %.
Figure 8.4 presents the projects life-cycle costs for the elaborated cases for the FRP- and RC jetty.
Several findings are discovered when analyzing the results:

- In the base case, the projected life-cycle costs of the FRP jetty are €275.870 and the life-cycle costs of the RC jetty are €107.986.
- The RC jetty performs better than the FRP jetty regarding life-cycle costs in all the regarded cases. Life-cycle costs for the most favorable scenario for the FRP jetty still resulted in life-cycle costs 28 % higher than the life-cycle costs of the RC jetty[7].
- If maintenance is omitted for the FRP jetty but included for the RC jetty, the life cycle costs of the RC jetty are still lower
- The part of the costs which is made by the piles differs greatly from the FRP jetty to the RC jetty. Piles make up 62 % of the total material costs of the FRP jetty. In the RC jetty, the piles make up 22 % of the total material costs.
- Higher discount rates are favorable for RC jetties since this lowers the NPV related to the maintenance for the RC jetty.

[7] Relative change computed as $\frac{\text{costs FRP jetty-costs RC jetty}}{\text{costs RC jetty}} * 100\,\%$

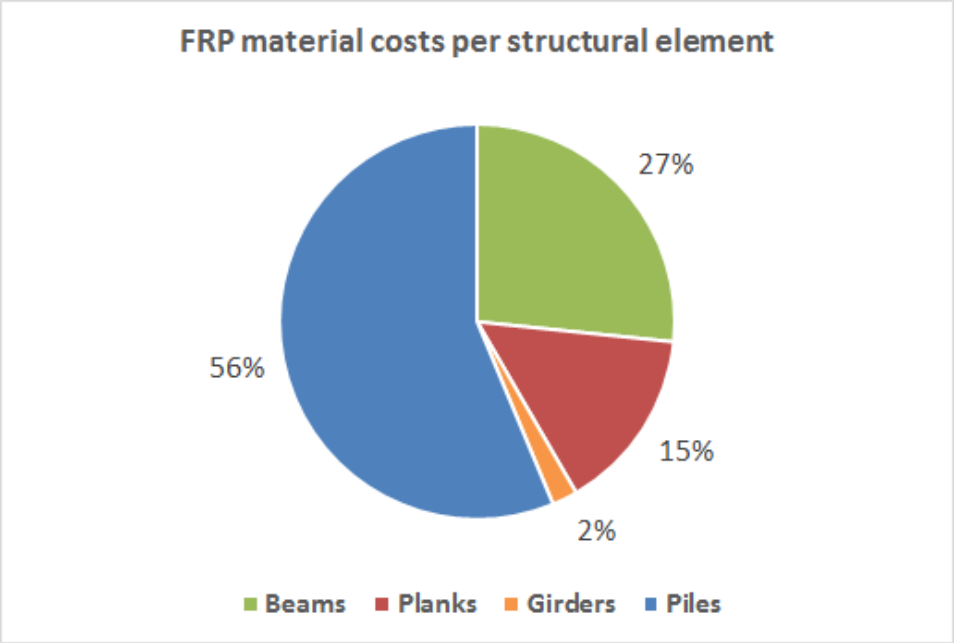

Figure 8.2: Costs allocation to structural element for the FRP jetty, base case

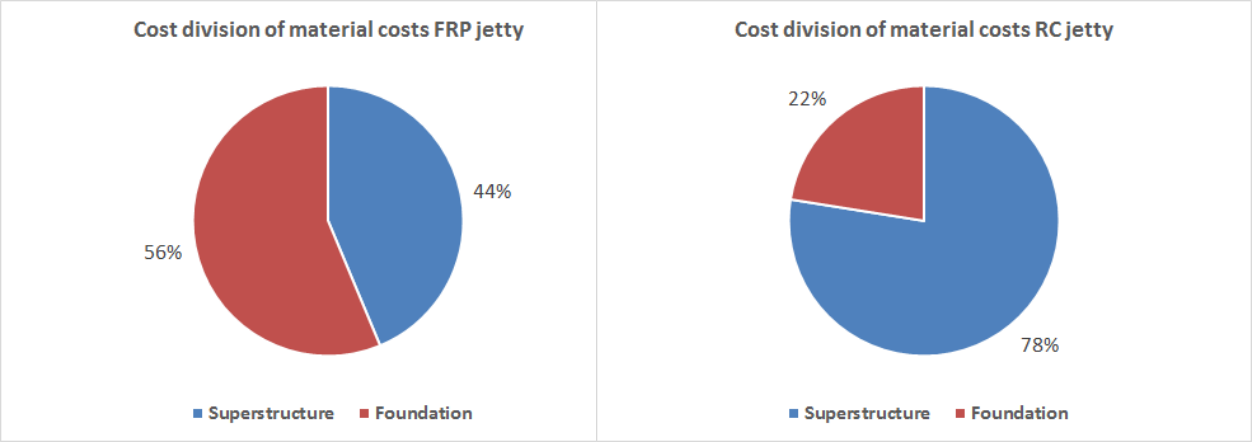

(a) FRP jetty (b) RC jetty

Figure 8.3: Cost allocation of the jetties to superstructure and foundation

8.3.1. Discussion of the life-cycle costs results for the FRP jetty and the RC jetty

In the bulk costs (i.e. per kg) for the FRP components, the labor from the manufacturing process is included. Different manufacturing processes have different costs implications; further specifying this could get a more accurate. The total material costs for cases where the upper bulk limit (i.e. 7 €/kg) is remarkably close to the scaled costs from pultruded reference products: €275.870 and €287.744 respectively. This indicates that the bulk costs are more on the higher end. It should be noted though, that the bulk price is based on a fiber content volume of 65 %; in the beams, planks, and girders, the fiber content volume is 60 %.

Converting the FRP piles to costs per kilogram of material results in:

$$\frac{\text{costs of FRP piles}}{\text{total volume FRP piles} * \text{density FRP}} = \frac{€84.530}{25 * 18.2\,\text{m} * 24\,336\,\text{mm} * 1927\,\text{kg/m}^3} = 4.11\,€/\text{kg}$$

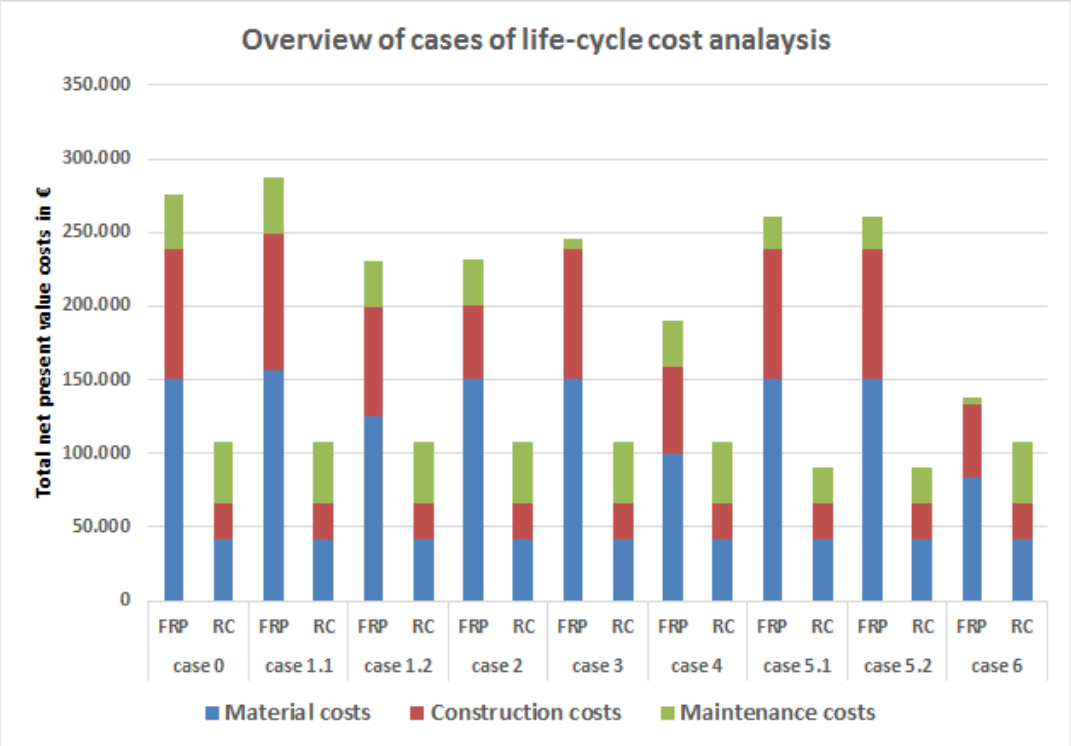

Figure 8.4: Relative difference in life-cycle costs of the FRP jetty with respect to the RC jetty

This price corresponds with the low-bulk price of 4 €/kg.

The end-of-life costs and benefits have not been regarded; however, it is seems unlike that this would make FRP jetties more lucrative given the significant higher costs. If the technical lifetime exceeds the economic lifetime than parts of the structure may be reused and therefore resold [8]. Decommissioning and demolition costs should then be investigated for both jetties.

Other recent thesis topics at the Delft University of Technology regarding FRP hydraulic structures found different results regarding the financial feasibility of the investigated structures. Zorgdrager found that the NPV of the life cycle costs of an FRP lock gate to be slightly better (2.4 % than the life cycle costs of a steel gate, for a life-time of 50 years (Zorgdrager, 2014). Van der Valk found that the costs of FRP quay walls were significantly higher than conventional structures: the designed quay wall was roughly 12,5 times more expensive with respect to a steel combi wall (Van Der Valk, 2017).

[8] End-of-lifetime scenarios were investigated in Chapter 7

8.4. Conclusion: FRP jetties are not lucrative

Regarding the financial feasibility of the FRP, the following is concluded:

- In the base case, the total costs of the FRP jetty amounted to €276.000; the total costs of the RC jetty amounted to €108.000.
- The RC jetty performs better than the FRP jetty regarding life-cycle costs in all the scenarios; total costs for the most favorable scenario for the FRP jetty still resulted in total costs being 28 % higher relative to the total costs of the RC jetty.
- It seems unlikely that, in contrast to statements made regarding the durability and low maintenance of FRP, high initial costs of FRP will be compensated due to lower expenditure during the life-time of the jetty.

Recommendations regarding cost improvement:

- Investigate the potential resell value of the FRP superstructure. Important aspect to investigate are topics related to structural degradation of the jetty after the intended life time (what loads can the structure carry after its service life?); what is the expect life time of the reused structure? In such analysis, also the potential end-of-life benefits (or costs) of the RC jetty should be investigated.

Conclusions, discussion, and recommendations

9

Conclusion: FRP jetties are no better alternative than RC jetties

The main research question of this thesis is:

"Are fiber reinforced plastic jetties a better alternative than a conventional jetty, constructed from concrete and steel?"

The answer on this question can be found by judging the performance of the FRP jetty on its technical feasibility, economic feasibility, and environmental impact; this resulted in the following subquestions:

- Part I: Technical feasibility: *"Can the structural integrity of a jetty, fully constructed of FRP, be guaranteed with at least the same safety levels required for RC jetties?"*
- Part II: Environmental impact: *"What are the implications on environmental impact when using FRP to construct a jetty compared to reinforced concrete, over their full lifetime cycles?"*
- Part III: Financial feasibility: *"How do costs of FRP jetties differ from RC jetties during their full lifetime cycles?"*

The conclusions are divided to the three parts accordingly:

Part 1: Technical feasibility

- It seems feasible to construct an FRP jetty based on literature review, dimensions of existing FRP structural elements, and structural analysis of the designed FRP jetty when taking the permanent and variable static loads after installation into account.
- Piles are an important design aspect of the FRP jetty as they have a mayor contribution to the lateral stability; installing hollow FRP piles with a batter angle greatly increases stability which partly compensates the low inherent stiffness of the piles.
- Mechanical joints may prove to be troublesome: when designing beams, special attention should be given, preferably early in the design stage, to resistance capacity of the laminates against in-plane and out-of-plane bolt forces.
- The dimensions of the structural elements is determined by both SLS and ULS criteria, depending on the specific loads and support from neighboring elements.
- The dead weight of the FRP jetty is significantly lower compared to the RC jetty: their total weights are 30.862 kg and 230.554 kg respectively, a relative change of 650 % compared to the FRP jetty.

- The jetty can be supported by friction piles: the hollow FRP develop sufficient bearing capacity due to inner- and outer skin friction (i.e. 1000 kN)

Part 2: Environmental impact

- Regarding the declared unit, the FRP jetty performs significantly worse than the RC jetty in the base case (0): shadow costs are almost 365 % higher with respect to the RC jetty for the base case LCA
- After a sensitivity analysis, where plausible differences in value parameters were changed in order to affect the environmental impact of the FRP jetty positively, the FRP jetty still performs significantly worse than the RC jetty: shadow costs are 59 % higher with respect to the RC jetty.
- If the environmental impact of the FRP jetty is to to be lowered, the most significant gains can be made by finding resins with a lower environmental impact (e.g. bio-plastics). The most important contributor to the shadow costs of the FRP jetty is the used resin: for the two biggest impact categories, global warming potential and human toxicity, the relative difference with glass is +150 % and +1050 % respectively; these two categories made up +20 % and +66 % of the total shadow costs for the FRP jetty respectively.

Part 3: Financial feasibility

- In the base case, the total costs of the FRP jetty amounted to €276.000; the total costs of the RC jetty amounted to €108.000.
- The RC jetty performs better than the FRP jetty regarding life-cycle costs in all the scenarios; total costs for the most favorable scenario for the FRP jetty still resulted in total costs being 28 % higher relative to the total costs of the RC jetty.
- It seems unlikely that, in contrast to statements made regarding the durability and low maintenance of FRP, high initial costs of FRP will be compensated due to lower expenditure during the life-time of the jetty.

Overall feasibility of the FRP jetty
Taking the above, the following conclusion was made with respect to the main research questions:

"Fiber-reinforced plastic is characterized by its unfavorable stiffness to costs ratio and high environmental impact to material ratio. These, in combination with the relatively low stiffness of FRP, makes the FRP jetty require relatively large material quantities in order to comply with limit state criteria. This makes a jetty designed from fiber-reinforced plastic unattractive from a sustainability and a financial point of view with respect to reinforced concrete. Hence, for the time being, fiber-reinforced jetties are no better alternatives with respect to reinforced concrete jetties."

10 Discussion

The discussion gives provides a critical reflection on the developed content, the practical implications of this research and on my personal design process during the thesis. The first section focuses on the content of the thesis itself; the second section speculates on potential future applications of FRP jetties. The discussion closes with a personal reflection.

10.1. Discussion of developed content

10.1.1. Discussion of detailed design

Technical risks

There are various technical risks when constructing an FRP jetty: most originate due to the lack of experience. This section aims to map technical risks when constructing an FRP jetty.

The low stiffness may induce bigger relative differences in displacement states. In the technical design, variable loading was assumed on all of the platform. However, different structure responses are expected when the jetty is uneven loaded or partially loaded. This varying acting loads causes the jetty to move: especially joints might be vulnerable to fatigue.

Operational activities may also be influenced by the low stiffness of the jetty. The loading arm induces relatively great loads on the jetty. A results of this is the loading arm as a whole may rotate due to differences in displacements of the bearing plate. If operational equipment is sensitive to such displacements or rotations, SLS criteria regarding these displacements and rotations should be included in the program of requirements for operational equipment.

Uncertainty related to long-term FRP hollow pile performance makes it hard to make predictions about the technical feasibility of FRP hollow piles. High durability is expected because in other products, plastics have a very long life time.

Failure of a support pile may invoke more problems for FRP jetties compared to RC jetties. FRP has no plastic capacity: therefore, stress redistribution may prove to be difficult if a pile gets affected by corrosion. Therefore, regular inspection is important to monitor cracks in the FRP piles, as glass may corrode and strength properties decreases when prone to water.

Related to the afore mentioned risk, is the risk of uneven settlement. In the calculations, settlements due to the friction bearing are not accounted into the model. For the long-term, this should be investigated in order to avoid big forces in the structure due to uneven settlement of the jetty.

The influence of moisture and temperature differences on the FRP material is not regarded in this thesis: these may however, especially moisture uptake, have significant influence on the structural performance. One concern is the moisture uptake of FRP piles. Pearson Pilings, a manufacturer of FRP hollow piles, rates the water absorption as < 25 %: Zyka and Mohajerani. found this moisture absorption rate "a questionable figure for structural members in marine environments" (Zyka & Mohajerani, 2016).

Structural model assumptions for the piles
In the structural model for the piles, the assumptions for boundary conditions significantly influence buckling resistance capacity and should therefore be extremely carefully selected. The most important structural model assumptions made fore the FRP piles, in the context of this thesis, are the boundary conditions at the toe and pile head, and the shear modulus: these heavily influence the buckling resistance of the piles.

The boundary conditions for the piles located under the loading arm are questionable. The model rests on the assumptions that the deflection of the pile head are described by $[\phi \neq 0, \delta = 0]$, as is suggested for pile groups (Bhattacharya & Madabhushi, 2008). The buckling resistance capacity is, regarding the model assumption for the pile head:

Model assumptions pile head	Buckling resistance
$[\phi \neq 0, \delta = 0]$	197 kN
$[\phi = 0, \delta \neq 0]$	339 kN

Negligible rotation of the pile heads was found for the piles not located underneath the loading arm (i.e. maximum rotation of 0.9 mrad[1]). However, the maximum horizontal deflections is almost 30 mm. Hence, modeling the boundary condition as $[\phi = 0, \delta \neq 0]$ might be more realistic, resulting in a buckling resistance of 197 kN. This is sufficient to cope with the maximum normal force of 142 kN for the piles at the edge of the platform and 176 kN beneath the loading arm.

The piles beneath the loading arm show a lateral displacement and rotation in the order of in the order of 20 mm and 9 mrad respectively. Although structures always show some degree of displacements and rotations, the question is whether these are significantly small to assume the model assumptions for the pile head to be $[\phi = 0, \delta \neq 0]$. In the context of this thesis, the modeling of the piles does not result in insufficient buckling resistance capacity. However, piles earlier in the design process had a longer length and a buckling resistance capacity of 151 kN and 272 kN: bad modeling of reality could lead to insufficient resistance against buckling of the piles.

Besides the model assumption for the head of the piles, the foot of the pile is modeled as fixed with the formulas of Davisson (Tomlinson & Woodward, 2008). Research is needed to investigate if these formulas are also valid for friction piles.

The shear modulus is assumed for the used FRP hollow pile since this was not known: the lowest boundary value of possible shear moduli is assumed with respect to the range of the Poisson coefficient. This led to a stiffness/shear modulus ratio of about 2.6: in the research of (Han & Frost, 1999), ratios up to 25 are presented. If the shear modulus is many times more lower than assumed, shear effects should be accounted for in the pile buckling analysis: this presumable negatively affects the

[1] Note that, displacements and rotations with respect for the modeling of the buckling resistance capacity is done for the ULS displacements and rotations

buckling load resistance.

After the design iteration were the piles were shortened, the buckling resistance of the piles increased, which might be counterintuitive because the pile is less laterally supported over its length. However, longer piles have lower resistance to buckling capacity and this effect is, apparently, stronger than the influence of the lateral resistance of the soil.

Structural model assumptions for the beams

The structural model assumptions for the beams regarding the support modeling at the end of the beams and the force distribution in the cross section (Section 5.3.3).

While in the early- and mid stages of the design process, the beams were modeled as both end hinged. In the preliminary design phase, the loads were underestimated which resulted in beams with insufficient bending resistance. Consequently, in the final model the deflections exceeded the allowed deflections. This problem was resolved by modeling the beams as both end fixed. Joints should be adjusted to this accordingly.

Initially, the structural model of the cross section worked towards the usage of orthotropic plate elements but the results regarding deflection where significantly different compared to the analytical solution and the 1D model solution. The idea was to develop three models: a 1D cross section model, a 2D isotropic plate model, and a 2D orthotropic plate model. In the first model, a custom profile is made in order to cope with the different stiffnesses of the flanges and the web: SCIA Engineer calculates a equivalent stiffness for the whole profile. See Appendix E for a complete overview of the 1D profiles. This model accurately reproduced the same bending deflection as the analytical model produced. Also, bending moments around both axes ($M_y$andM_z) result in stresses in the longitudinal direction of the beam.
The intention second model, 2D isotropic plates, was to provide a base for the orthotropic 2D model. In the 2D isotropic model, the calculated plate stiffnesses for the web and flanges were and inserted; the web and flange were then continuously connected with a fixed line support. In the third model, the orthotropic properties of the laminates were inserted, which resulted from the laminate analysis in eLamX^2 .
Since the 2D isotropic and orthotropic models gave unsatisfying results, and the 1D model agrees with the analytical model, the 2D models are omitted. Also, calculation time in the FEM software would increase tremendously. A possible reason for the 2D models to fail might be the incorrect modeling of the flange-web intersection, or the way the load is applied on the profile.

Review of structural performance of the beams

After a review of the design of the beams, it was concluded that improvement was required in order to be structurally sound: the ILSS (at the platform), intersection detailing of the flange-web intersection, manufacturing technique, and the joints require more attention. There is one design variable which can be adjusted in order to comply with these: increasing the thickness of the web. The manufacturing technique and joints are more elaborated in the two following sections.

The interlaminar shear stress gives problems in the web, mainly where the load arm is situated. The biggest shear force found is 234.91 kN which leads to an interlaminar shear stress of 15.41 MPa. The ILSS has insufficient capacity to deal with this (i.e. 8.77 MPa). This area should be reinforced by either increasing the thickness of the web or increasing the amount of beams: the latter seems more convenient, since this will also distribute stress more evenly, reducing high peak stress concentrations.

The stress transmission, or load continuity, at the intersection of the web-flange should be more investigated. Due to the limited disposable time of the thesis subject, this detailing was not investigated.

Manufacturing technique of the structural elements
The beams, planks, and girders are to be manufactured by the pultrusion process. This manufacturing technique is chosen because of its excellent ability to produce long elements and low costs. Therefore, it is also frequently applied in the construction industry.

However, the pulltrusion process is limited in the sense that fiber angles can only be placed in the principal direction of the element (i.e. 0°); the transversal stiffness results from mats where fibers can be woven into multiple directions.

For pultruded cross section, fiber content volume of up to 70 % is possible, with roving mat ratio's[2] of 0.6 to 1.24 (Mallick, 2007). For a pultruded item with a fiber content volume of 60 %, similar to the designed laminates, 48 % consisted of rovings and 52 % of mats. For the designed flange laminate of beam the access bridge beam, 53.85 % of fibers lays in the 0° direction and 15.38 % in the 45°,–45° and 90° (see Appendix D.2).

With this information, a quick gauge can be made if the pultrusion process is suitable for manufacturing the parts. Let's assume that two different mats are used: one mat containing 0° and 90° fibers, and one mat containing 45° and –45° fibers. Also, the amount of fiber is evenly distributed (i.e. 50/50) to fiber directions. To have sufficient fibers in the 45° and –45° directions in the laminate, the mat combining these two fiber directions has to account for at least $15.4\,\% * 2 = 30.8\,\%$. The same goes for the 90° direction: the 0°/90° has to account for 30.8 % to have sufficient 90° fibers. This leaves $60\,\% - 2 * 30.8\,\% = 38.4\,\%$ for the 0° fibers. The total amount of 0° fibers is this amount plus the 0° fibers from the 0°/90° mat: $38.4\,\% + 15.4\,\% = 53.8\,\%$. This happens to be the required amount of fibers in the 0 % direction. Hence, it seems feasible to produce the flange laminate with the pultrusion technique.

The above check can also be done for the web of the laminate of beam 1. For the designed web laminate of the access bridge beam, 14.29 % of fibers lays in the 0° direction and 28.57 % in the 45°,–45° and 90° (see Appendix D.2). If the two same mats are utilized (0°/90° and 45°/–45°) one can quickly see that is impossible: if the 45°/–45° mat takes up $28.57\,\% * 2 = 57.14\,\%$ to comply with the required amount of the 45's, already insufficient fiber volume fraction is left (i.e. $100\,\% - 57.14\,\% = 42.86\,\%$) to full fill the required amount for the 90° direction.

Because the inability to manufacture the desired I-profile for the access bridge beam, an alternative manufacturing process should be investigated if the beams are to be designed with the stated dimensions (an alternative is increasing the thickness of the web, which enables more mats in the web). Such manufacturing process could be resin transfer molding. However, due to the relative complicated shape of I-beams for a mold, production costs may be significantly higher. Instead of manufacturing the whole beam with the resin transfer molding technique, another suggestion is to produce the web with the resin transfer molding technique and the flanges with the pultrusion. Then, the beams may be jointed together[3]

[2] With rovings being individual fibers in the 0° direction
[3] Joining flanges to a web to create I-beam cross section is a method utilized by BIJL profielen (W.B. Bijl Profielen B.V., 2015b).

It should be remarked that, in the above approach, the thickness of the mats equals the thickness of the fibers, which is not necessarily the case if they are interwoven. If the fibers are loose, the mat thickness may be of double thickness compared to the thickness of the fibers. By contracting the fibers this width may be reduced if the fibers deform. If this is desirable or possible in mats is another question to consider.

Working with continues mats in the profile would limit the composition of the cross section due to the continuity of the mat from the flange to the web. A way to work around this is to glue flanges to a web.

Finally it is important to realize that when mats are utilized, the mechanical properties of the laminate will differ since the stacking sequence and thickness of the plies is influenced.

Joints

A mechanical joint is elaborated in Section 5.9.3, which proved to have insufficient capacity. The high normal force, shear force, and bending moment generated stresses which the laminate of the access bridge beam could not overcome. A solution may be found where the shear force and bending moment are transfered trough other mechanisms and only the normal force remains to be resisted by the web laminate; another solutions is to increase the thickness of the web to increase the joint bearing- and net-tensile failure capacity.

Figure 10.1a presents a side view and a cross section of an alternative joint. Now, the I-beam is placed in a rectangular section and fastened with a bolt. This rectangular section in its turn is fastened to a pile cap. This way, the shear force and the bending moment can be taken by the hood: this happens due to the hindered rotation of the I-beam profile which is realized by developed reaction forces. The hood must be relatively stiff compared to the FRP material: stainless steel would be a suitable option. Then, the only force to be accounted to the bolt force is the normal force.

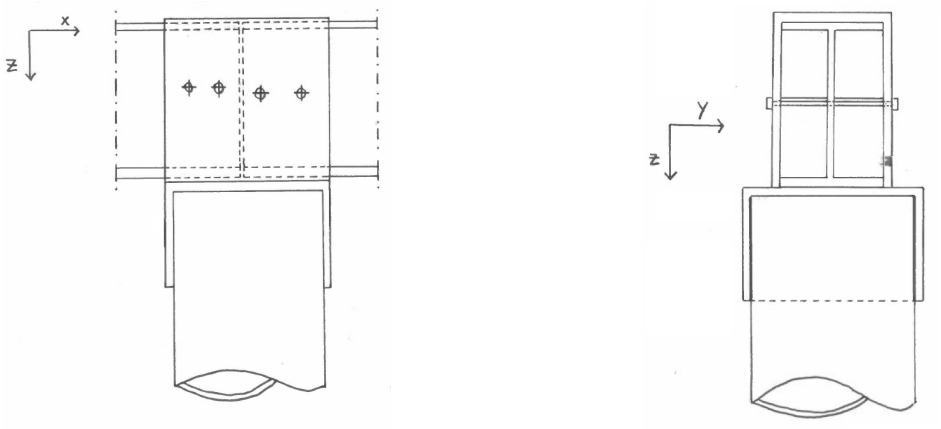

(a) Side view (b) Cross section

Figure 10.1: alternative joint for connecting the access bridge beam to the FRP hollow pile

A first draft for the mechanical joint positioned the bolt trough the flange of the web into the head of the pile. This however, caused the flange laminate to fail due to shear puncture. Therefore, the bolt layout was changed to the forces on the bolt would work perpendicular rather than parallel.

Besides a mechanical joint, also an adhesive joint is considered. However, the area of the support head of the pile proved to be insufficient to provide enough structural capacity. Therefore, a second attempt was made to design a joint with sufficient structural capacity in Section 5.9.3.

Another item to be considered is the structural modeling of the joint. In the FEM analysis, the beam ends are modeled as fixed. However, the bolted joint as elaborated in Section 5.9.3 has a free rotation center (at the center of gravity of the bolts). Hence, modeling the joint as a free supported end might be more realistic.

The usage of sandwich are not investigated: the usage of foams will most likely influence the outcomes of the LCA and life-cycle cost analysis. When considering designing an integrated deck, this option should be investigated.

Determination of the natural frequency of beam elements
The natural frequency is determined by:

$$f_{0i} = \frac{K_n}{2\pi}\sqrt{\frac{\sum E_i I_i g}{qL^4}} \tag{10.1}$$

Where:

K_n : a constant, dependent on the boundary conditions

The value K_n is 9.87 for free supported beams and 22.4 for fixed supported beams.

In a first design iteration, the beam was supported as free ends: this results in lower natural frequencies. However, fixed supported beams generate higher frequencies. Since the SLS criteria was that the natural frequency of the structural elements should be higher than $f_{01} > 4.6\,\text{Hz}$, the fixed beam model is advantageous with respect to the natural frequency. If the load remains the same, modelling the beam ends fixed instead of free results in an increase of natural frequency by a factor $\frac{22.4}{9.87} = 2.26$.

Material reduction opportunities
Three potential areas are identified where material efficiency gains can be made: reconsidering SLS criteria, constructing elements with a camber, and customizing the piles.

Gains in material efficiency might be made by reconsidering the SLS deflection and vibration criteria. After all, these criteria are very common to state where a lot of people reside, such as office buildings and residential housing. However, the jetty researched in this thesis is not continuously in operation: comfort of workers during work might be reconsidered if they are not frequently at the jetty. This of course, does not applies if workers continuously work at the jetty. Or, jetties with a recreative function such as the Scheveningen Pier.

Another option is to manufacture structural elements with a camber: this could limit deformation as the camber can be superpositioned with the deflection due to the loads. Then, for comparable profile dimensions, lower end-deflection can be realized. Pultrusion methods exists where curvature can be manipulated before the resin matrix hardens (Britnell, Tucker, Smith, & Wong, 2003).

Since the piles make up the majority of the costs for the FRP jetty, rethinking piling layout strategy may result in potential material gains. The heaviest loads occur beneath the loading arm and the

piles are designed to resist these loads. However, at other places, they might an excess of structural capacity. The piles might be customized for to gain material efficiency. However, this brings the risk that during installation, the wrong piles might be installed which could lead to failure of the jetty. Also, standardization makes manufacturing processes cheaper. Hence, the potential material gains should be evaluated against the potential installation risks and increase of manufacturing costs.

Program of requirements: sumput and watertightness
A sumput is incorporated in the program of requirements but not designed for the FRP jetty. Also, the platform should be watertight in case the liquid bulk gets spilled. The main function is to collect polluted water; in the RC jetty, this is done by constructing the platform deck under a downward slope towards the sumput. This is possible because the upper deck consists of a monolith concrete plate. However, small gaps exists between the planks of the FRP structure. If no water is allowed to leak from the platform, the top deck should be made watertight. This can be done by gluing the planks together with a resin once they are placed on the beams. This is some implications: the structural model is affected since the planks are now connected, additional resin is needed which further increases the environmental impact of the FRP jetty, and they require more effort to remove or demolish during the end-of-life phase.

Whilst the pipe supports and sumput were not designed, their loads have been incorporated into the load cases working on the FRP jetty. This results is important in the judgment of the structural capacity requirements of the superstructure; however, force introductions and detailing have not been investigated.

Dynamics effects
Dynamic effects could be relevant to the engineering of the piles. Due to the loads of the loading arm, a relative large displacements of the piles occurs. These loads are not always present because the loading arm will not continuously be operational. Therefore, cracks due to fatigue may occur in the pile and the glass fibers may be exposed to water, which can significantly reduce the material strength of the glass fibers.

Remaining work before actual implementation of the FRP jetty
While a design detailed enough to assess the technical feasibility, a more detailed design iteration are required to deliver a design which actually can be constructed. The following tasks are identified:

- Load detailing underneath platform
- Joint detailing
- Select an alternative manufacturing technique[4]
- Remaining ULS and SLS checks of the CUR96[5]

The area located beneath the loading arm is prone to huge loads. This area requires more attention in terms of detailed design. At the load introduction from the loading arm, force trajectories with high peak stresses are formed.

The CUR96 provides a lot of structural checks for the ULS and SLS, but not all checks were executed: focus was on the most important ones to indicate the feasibility of the FRP jetty. It is expected that the influence of these checks is not of significant importance regarding the feasibility research of the jetty. The following CUR96 checks were not executed:

[4]Treated in other section of this discussion
[5]Treated in other section of this discussion

ULS	SLS
Axial tension in the girders	Deformation under exceptional loads
Torsion effects	Damage
Interlaminar tension- and pressure stresses (ILTS)	
Combination of buckling and lateral torsional buckling	
Fatigue	
Quasi-permanent loads and creep failure	
Vandalism	
Fire	

While a check on the cross sectional level for beams is valid according to CUR96 when the design agrees with certain stated requirements, a check on the ILSS check will provide insight to the structural response of the laminates. CUR96 prescribes that laminates which need to be checked for ILSS are membranes and plates with free ends of relative thick flanges (width to thickness ratio < 10), unbalanced thin laminates, strong curvature, and force introductions.

Limit state design criteria for geotechnical design are presented in Eurocode 7 (NEN, 2011). Besides pile bearing capacity, it also suggest criteria for the limitation of vertical pile displacements, displacements of pile groups, and simultaneous failure of pile and soil. For a complete list of ULS and SLS checks the reader is referred to the Eurcode 7 (NEN, 2011).

10.1.2. Discussion of pile installation

Upper and lower boundary strength of the soil

Safety is accounted for by structural- and geotechnical engineers by reducing the strength of the soil by assuming a lower boundary (e.g. the maximum value for the cone resistance to be taken from CPT is 15 MPa). However, for pile drive analysis, the opposite is true: an upper boundary for the strength is assumed. This is because the main thing which needs to be assured is the ability of the pile to be driven with a selected driving set-up, and a higher assumption for the value of the soil strength results in safer predictions.

Difference in calculated bearing capacity

The bearing capacity determined analytically (almost 800 kN at a depth of 13.5 m) differs a lot from the bearing capacity derived with WEAP (about 1000 kN at a depth of 6 m).

Safe boundaries were assumed for the analytical determination for the bearing capacity of pile: the first few meters were not accounted for providing support. However, the CPT indicates a value of that a relatively high value. This is probably due to the load history: the harbor may have been dredged and was loaded with sand before. The difference between the ground level and the bottom level of the harbor is about 8 m.

Only outer shaft friction is accounted for in the analytical calculation, while inner shaft fraction should also be included. The FRP pile is a hollow open-ended pile: shaft friction develops on both the outside and the inside of the pile. The plug effect may reduce inner shaft friction, but a model run determined that it was not significantly reduced when driving to a depth of only 6 m.

Buckling during driving

Buckling during driving is not considered. While Han and Frost found a theoretical solution to incorporate shear deformation in buckling for FRP piles in static cases (Han & Frost, 1999), no such formula was found for driving. Bhattacharya et al. gather the existing recommendations for the prevention of buckling of piles during driving, provided by the Eurocode 7, clause 3.3.1.b from the American Petroleum Institute (2000), and the Japanese Road Association code (JRA 1996) (Bhattacharya & Madabhushi, 2008). However, only the API provides a design formula for the minimum wall thickness of hollow steel core pipes. It is unlike that this design formula is also valid for FRP hollow pipes in general.

10.1.3. Discussion of LCA

In the evaluation section of the LCA (Section 7.5) a critical reflection is given on the life cycle assessment already. Future developments are treated in Section 10.3.2 of this discussion.

10.1.4. Discussion of life-cycle costs

The main aspects influencing the life-cycle costs are the financial variables and the inclusion of cost types. Future developments are treated in Section 10.3.3 of this discussion.

The quantification of the financial variables influences the outcome of the life-cycle costs considerately. The variation of the financial variables in the sensitivity analysis all seem reasonable. However, the worst case scenario for the RC jetty and the best case scenario of the FRP jetty requires all financial variables to occur. The probability of this 'ideal' scenario is questionable, especially when life expectancy is differentiated for the FRP jetty and RC jetty (i.e. 75 years and 50 years respectively), effectively lowering the environmental impact of the FRP jetty with 33 %.

The end-of life phase is not accounted for in the cost assessment: decommissioning costs are omitted as well ass potential resell value. While this would influence the life-cycle costs, this would probably not result in the FRP jetty being more financially lucrative compared to the RC jetty.

Applicability regarding costs to other hydraulic structures

Interesting to note, is that two recent MSc theses focused on the feasibility of FRP quay walls and FRP lock gates. The feasibility study regarding the FRP quay found comparable results regarding costs: FRP was financially not lucrative compared to conventional civil engineering materials (Van Der Valk, 2017). However, in the feasibility study regarding the FRP lock gates the conclusion was drawn that the life-cycle costs of FRP lock gates was better than steel lock gates (Zorgdrager, 2014). This indicates that no general conclusion may be drawn regarding the financial feasibility of FRP hydraulic structures but research regarding specific cases is required.

10.2. Discussion of practical implications

Hybrid structures

Combinations of FRP and RC in a jetty might exploit the advantages of both materials. With respect to each other, the primary advantage of FRP is its light weight; for RC, these are its lower costs and lower environmental impact. Three ideas of hybrid structures are:

- FRP superstructure, RC foundation
- RC superstructure, FRP foundation
- FRP structure, partial FRP foundation, RC foundation beneath loading arm

In the first combination, the FRP superstructure will is from FRP and the foundation of RC. Due to the light weight of the FRP super structure, the structural capacity of the piles may be reduced. This can be done by decreasing the cross section or by shortening the piles, basing bearing capacity on shaft friction. However, the piles are more prone to deterioration effects because they are partly submerged. Arguably, the intention of researching the feasibility of FRP jetties was due to its excellent corrosion resistance and durability properties: therefore, it would make sense to construct the parts of the jetty most prone to deterioration of FRP.

In the second combination, the FRP superstructure is made from RC and the foundation of FRP. The idea behind this combination is that the elements most prone to degradation are made from FRP. This comes with the obvious problem that the weight imposed on the piles is very high. This, in combination with the low buckling resistance of the FRP, requires more piles to be installed. This in turn negatively affects the life-cycle costs and the environmental impact of the jetty.

In the third combination, the whole jetty is made from FRP with exception of the three support piles underneath the loading arm. The three support piles act as a stiff core, which is often used in the construction of high rise office buildings. The main load from the loading arm are transfered by the RC piles. This way, it might be possible for the remaining structural elements to have a lower structural capacity. However, since there is a combination of RC and FRP piles, they experience the advantageous and disadvantageous of both. With this set up, life-cycle costs and environmental impact will most likely still be higher. Also, construction gets more expensive: a light hammer suffices for the FRP piles, but a heavier hammer is required for the concrete piles.

Deducting a quick check it can be seen that, since both the FRP superstructure and piles are more expensive compared to their RC counterpart, no hybrid combination exists which reduce the total costs if the dimensions of the structural elements do not get adjusted.

Another hybrid composition is the usage of carbon fibers in concrete: in Germany, an interdisciplinary consurtion is set up research the application of carbon fiber reinforced concrete (www.bauen-neu-denken.de). Claims made on the site are that "carbon reinforced concrete is sustainable, environmentally friendly, saves material and weighs less". Evidence is collected in this thesis regarding the low weight properties for constructions; sustainability claims proved to be untrue in the scope of this thesis.

Arguments for constructing FRP jetties

This thesis concluded that for the time being, FRP jetties are no better alternatives than RC jetties. Three main areas of the FRP jetty were investigated in order to assess if it is a better alternative than RC jetties: technical feasibility, environmental impact, and financial feasibility. But, there might be other reason to still construct FRP.

FRP possess many interesting physical properties, and maintenance seems the property with the biggest advantage for jetties. This thesis concludes that FRP for jetties does not performs better than RC regarding life-cycle costs and environmental impact. This implies that the effect of lower maintenance in itself cannot turn the tides when placed in context with the overall performance. The advantage of physical properties such as thermal resistance, electrical resistance, and magnetic insulation properties is questionable for jetties: such application would be more significant in for instance, power plaint construction or research laboratories. Chemical resistance may be of significance when transporting hazardous materials on the jetty: but it is hardly imaginable that it will close the gap between the life-cycle costs of the FRP jetty and RC jetty. Such resistance may be realized as well by coating an RC jetty with a plastic layer.

In the literature study it was found that, for a bridge deck with similar required structural capacities, the weight of FRP variants can be up to 10 % to 20 % of its RC counterpart. The results of this thesis agree with this statement: the distributed dead weight of the FRP superstructure is about 10 % compared to the RC superstructure.

A reason to apply FRP in structures in other industries, such as the automotive and aerospace industry, are low weight properties of the material: or rather, the high strength to weight ratio. The light weight of the structure is not an advantage in itself and should be placed in context: hydraulic structures often allot their stability to their dead weight. Arguments that lightweight structures reduce construction costs might be true, but again: it has to be placed in context. The influence of lower construction costs is investigated in the sensitivity analysis and it does not make the FRP structure more financially lucrative. A same calculation could be made for transportation costs since these were not considered.

Two potential advantageous of the low weight are identified: earthquake resistance and calamity response. The impact of earthquakes is modeled by accelerating the ground on which the structure rests: with the second law of Newton $(F = ma)$ it is quickly assessed that lower forces will occur in lighter structures compared to heavier structures. Also, FRP has the ability to deform a lot and dissipate energy this way. The above suggestions are speculations and should be research before making claims regarding the low weight of FRP jetties.

Due to the light weight, the construction speed of FRP jetties is most likely faster: if a jetty gets replaced faster after an event where it is destroyed (due to ship impact, natural violence etc.), missed operational turnover due to unavailability may be limited. Hedging this risk is probably quit costly. Besides total jetty destruction is rare. Therefore, the light weight advantage with respect to calamity response is probably low, if an advantage at all.

10.3. Future outlook

This research concluded that, at the time, FRP jetties are no better alternatives than RC jetties. The question then thesis: Do FRP jetties have the potential to be better alternatives in the future?

10.3.1. An outlook on the technical potential

Thesis scope and scalability of the jetty

If the FRP jetty is to be scaled, several items have to be taken into account, which are predominantly:

- Increase of loads
- Increase of load cases
- Increase of functionality
- Increase of depth

First, additional load cases have to be incorporated: (offshore) wave attack, currents, mooring loads, berthing loads, frost loads. In areas where the jetty is prone to hurricane and earthquakes, proper loads might have to be taken into account and the seismic response of the jetty should be investigated. The scope of this research limited itself to the jetty: dolphins are not regarded. However, FRP proves to be potential competitive material for dolphins compared to conventional ones (Watté & De Herder, 2015).

Different functions of jetties will come with different challenges for FRP jetties, and this is closely linked to the load cases. For instance, a container storage will induce high stresses near the corners of the containers: making a design which is resistant to high static impacts will be challenging. Conveyor belts are often present at jetties where bulk cargo is loaded, which induce vibrations. Therefore, the jetty must be able to cope with fatigue loads, induced by these vibrations. If hazardous bulk is loaded, a consideration has to be made to incorporate fillers to make the FRP material resistant to aggressive environments.

Also, for large scale jetties the non-embedded length of the pile might be longer, as in general the depth of the sea increases sea inwards. This makes the piles, which already poses a low resistance against buckling, vulnerable for failure. Also, the lateral deformation will be large. In this research, these are the two most important design aspects of FRP piles which support an upper deck and are only partly embedded into the soil.

10.3.2. An outlook on sustainability aspsects

Bio-composites

The gap to be closed regarding the sustainable prestige is big; the environmental impact of the FRP jetty needs to be reduced by a factor 4.5 in order to have the same value as the RC jetty. Promising potential for reduction of the environmental burden are bio-based composites.

Three recent MSc theses from the Delft University focused on the sustainable aspects of FRP by considering bio-based materials. Verlinde found that facades made from bio-composites performed two times better compared to glass FRP (Verlinde, 2017); van der Linde found, regarding the production phase, pedestrian bridges made from bio-based FRP material performed four times better compared to glass FRP. Gkaidatzis designed a pedestrian bridge, with a span of 15 m, from basalt fibers and bio-based polyesters: it was even considered better regarding sustainability, costs, and construction feasibility (Gkaidatzis, 2014).

Both the fibers and the resin have potential to decrease the eco-costs in bio-composites. The biggest impact factor in the design of the FRP jetty was human toxicity: Gkaidatzis found that the equivalent impact of basalt fiber was about 4 % of the glass fiber (Gkaidatzis, 2014). The high impact of glass is mainly due to high temperatures needed during the manufacturing process. Due to the low impact of basalt fibers, significant gains in lowering the environmental burden for the jetty can be achieved. Verlinde suggests the sustainable impact may be further reduced by developing the resins and the coatings, since these still contain hazardous materials (Verlinde, 2017); this is in agreement with van der Linde, which states development
The implementation of bio-composites faces a few challenges. Verlinde states that the main challenge is the influence of weathering on bio-based composites (Verlinde, 2017). She also performed rapid age tests on bio-based specimens: in general observed trend in warmth-cold cycles and freeze-thaw cycles was an increase of tensile strength whilst the stiffness decreased (Verlinde, 2017). The low durability was also stated by Gkaidatzis as the main disadvantage of bio-based composites: prime reasons were "the moisture absorption, temperature and fiber-resin low compatibility". Based on these conclusions, research regarding the influence of moisture absorption on the mechanical properties of bio-based composites seems crucial if such material is to be used for jetties, since the piles of the jetty are partially submerged.

Gkaidatzis also linked the life expectancy and environmental impact, durability and sustainability: "Reducing extensively the end of life of a structure such as a bridge by using a non-durable but sustainable material proves to be less efficient in terms of sustainability than using a conventional durable material" (Gkaidatzis, 2014). Therefore, mechanical performance should also be considered in the selection of bio-based raw materials.

Verlinde[6] concludes that bio-composites may solve material scarcity issues; but, since they are not yet fully compostable or recyclable, the quality will always be lower when used as raw material in new products (Verlinde, 2017). Effectively, the bio-composite is down cycled, which does not fit in the circular economy paradigm which aims at raw materials and production techniques to reuse, recycling, or upcycling products at the end-of-life phase. However, Verlinde also states that the recycling of bio-based composites is an underdeveloped area since it is a new technology: a lot of innovation in this area may happen.

Concluding, a research of Pickering et al. is cited which review the recent developments in natural fiber composites and their mechanical performance: "Overall, growth of NFC (natural fiber composite) uptake continues at a rapid rate and there would appear to be a very positive future ahead for their application"(Pickering, Efendy, & Le, 2016).

10.3.3. An outlook on life-cycle costs

In their research where applied life cycle costing and its drivers were reviewed, Ilg et al. formulated the importance of costs on the practical implementation of innovative design very well: "To be competitive, innovative products need to achieve a similar level of life cycle costs to those of conventional products"(Ilg, Hoehne, & Guenther, 2016). An outlook on price development may indicate if FRP will be a competitive material for jetties in the future.

In the scope of this thesis, equal life life-cycle costs for the FRP jetty to those of the RC jetty are obtained by setting the bulk unit price of FRP to 1.9 €/kg. The range of the bulk unit price was set from 4 €kg to 7 €kg: this implies that the material costs of FRP have to decrease 73 and 52 % to the upper and lower boundary respectively to become competitive.

[6]MSc thesis focused extensively on circular implementation of bio-based composites facades

The costs of FRP products may decrease if market demand increases. The demand for fiber reinforced plastic in the construction industry might grow: the glass FRP bridge market in the USA is expected to experience an a compound annual growth rate of 6.4 % between 2016 and 2021 (Markets and Markets, n.d.).

Another aspect to regard is the price development. Nystrom et al. investigated the financial viability of FRP bridges: the cost estimation of a "Future FRP Bridge" was made based on reference cases and expected price developments. This price development was based on a learning curve. However, assumptions were made that no significant cost improvements will be made because "current materials have already experienced the major learning curve gains"[7]. The conclusion was drawn that the Future FRP Bridge will not be financially feasible: for this to happen, radical changes will have to occur regarding the development of new materials and production techniques (Nystrom, Watkins, Nanni, Asce, & Murray, 2003).

The regarded price development specifies to glass FRP. However, gains regarding carbon FRP may be interesting for structural applications as well. Making statements regarding cost development of carbon FRP, in the scope of this thesis, will be highly hypothetical and therefore this item is not elaborated.

10.4. Personal reflection

Design process

I do not regard the design process of the thesis efficient. One big factor which played was the alteration of adding a load case followed by adjusting the structural element. A better approach would be to include all load cases in the beginning and only then start designing the structural elements.

The second moment of area (I_y) was the main parameter which was altered in order to comply with limit state criteria. This is done by increase the height of the profile: the flange thickness was not varied. The same bending stiffness may be acquired with lower material but thicker flanges. A problem which is most likely to be encountered are the increasing inter-laminar shear stresses; this presumably limits the thickness of the laminate.

Personal opinion on the thesis

While there are quite some items which can be further specified or optimized, I think the research done provides sufficient evidence to answer the main question presented in this thesis. Regarding this aspect, I am satisfied.

Improving the report should focus on the agreeableness of the technical results and presenting a more coherent technical design chapter. The technical model evolved a lot during the thesis and different results were written down at various times.

[7] Article was published in 2003, based on the pultrusion technique

11

Research recommendations

Based on the conclusions and the discussion, the following research recommendations are made:

- Research the stability of FRP pile groups. The most important items to be regarded should include the impact on pile group failure of individual pile failure, tolerances for translation and rotation criteria for the support assumptions at the pile head and pile toe, and long-term creep influences. Shear deformation of the FRP piles should be taken into account: the paper of Hand and Frost is a great starting point (Han & Frost, 1999).
- Investigate the earthquake resistance of FRP jetties (e.g. by means of a push-over analysis).
- Design an integrated deck which omits the need for joints. This should be possible with the many available manufacturing techniques of FRP.
- Hybrid jetties constructed of FRP and RC do not seem to produce combinations which provide better alternative than RC jetties. However, hybrid combinations of bio-composites and RC might be a better alternative. Contemporary research sketches a bright picture regarding the developments of bio-composites. A contemporary review is provided by Pickering (Pickering et al., 2016).
- Investigate the long-term structural capacity due to creep and moisture absorption for load bearing hollow FRP piles. The influence of these items on partially embedded, submerged piles should be part of the research.

Furthermore, it is recommended to create a guideline where experiences of FRP construction and design are bundled. Specifically, how to deal with the lack of hard SLS criteria and how to achieve an efficient design process. The latter because the common hydraulic engineer is well equipped with knowledge regarding steel and concrete, but is rather unfamiliar with FRP engineering which possess different challenges.

References

References

Allnamics Pile Testing Experts. (2014). *AllWave-PDP - Wave Equation Program brochure.* Retrieved from http://www.allnamics.eu/wp-content/uploads/AllWave-PDP-Brochure-2014-11-26-EN.pdf

American Society of Civil Engineers (ACMA). (2010). *Pre-Standard for Load & Resistance Factor Design (LRFD) of Pultruded Fiber Reinforced Polymer (FRP) Structures (Final)* (Tech. Rep.). Retrieved from http://dev1.kreysler.com/information/specifications/specs-resources/LRFD%20PreStandard%20-%20Revised%20FINAL%20-%20Nov%209%202010.pdf

Beens Groep. (n.d.). *Working at low tides and high tides in the port of Rotterdam.* Retrieved from http://www.beensgroep.nl/werken-bij-eb-en-vloed-in-de-haven-van-rotterdam/

Bergen, M. v. (n.d.). *Bijl Bruggen promotional video.* Retrieved from https://vimeo.com/128535635

Bhattacharya, S., & Madabhushi, S. P. G. (2008). A critical review of methods for pile design in seismically liquefiable soils. *Bulletin of Earthquake Engineering*(6), 407–446. doi: 10.1007/s10518-008-9068-3

BIJL Profielen. (2017). *Personal communication with a representatieve from BIJL Profielen.* Retrieved from https://www.bijlprofielen.nl/nl?gclid=CMbr07WYmNYCFbEW0wod4lgGNA

Britnell, D. J., Tucker, N., Smith, G. F., & Wong, S. S. F. (2003). Bent pultrusion - A method for the manufacture of pultrudate with controlled variation in curvature. *Journal of Materials Processing Technology*, *138*(1-3), 311–315. doi: 10.1016/S0924-0136(03)00091-8

Cherqaoui, I. (2006). *MSc thesis: Door grond horizontaal belaste palen* (Tech. Rep.). Delft: Delft University of Technology. Retrieved from https://www.google.nl/url?sa=t&rct=j&q=&esrc=s&source=web&cd=1&ved=0ahUKEwjdyO_fyJLVAhUPJ1AKHVoBAJoQFggnMAA&url=https%3A%2F%2Frepository.tudelft.nl%2Fislandora%2Fobject%2Fuuid%3A91707307-f014-458e-88ce-2eecac1ab452%2Fdatastream%2FOBJ%2Fdownload&usg=AFQjCN

de Boer, A., Drogt, B., Klamer, E., Nijssen, R., Peeters, J., van Uden, H., … Rodrigues Ramirez, J. (2016). *CUR-Aanbeveling 96: Vezelversterkte kunststoffen in bouwkundige en civieltechnische draagconstructies* (Tech. Rep.). Delft: SBRCURnet. Retrieved from http://cur-aanbevelingen.nl/CUR-Aanbeveling-096

de Gijt, J. (2004). *Structures in Hydraulic Engineering - Lecture notes on Port Infrastructure - CT5313.* Delft.

Dengkeng, T. (2017). *Personal communication.* Gemeente Rotterdam.

ENCI. (2006). *Hoogovencement CEM III B.* Retrieved from https://www.google.nl/url?sa=t&rct=j&q=&esrc=s&source=web&cd=2&ved=0ahUKEwisof2t58TVAhVQaVAKHXpxBWsQFggtMAE&url=http%3A%2F%2Fwww.enci.nl%2Fnl%2Fsystem%2Ffiles_force%2Fassets%2Fdocument%2Fgrijs_hoogovencement_cem_iii_b.pdf%3Fdownload%3D1&usg=AFQjCNF8x6p4_0www.enci.nl

FiberCore Europe. (n.d.). *FRP sluice doors in the Wilhelminakanaal, Tilburg, The Netherlands.* Retrieved from http://www.fibercore-europe.com/index.php?option=com_k2&view=item&id=576:sluisdeuren-wilhelminakanaal-groot&Itemid=183&lang=nl

FiberCore Europe - Bridges. (2017). Retrieved from http://www.fibercore-europe.com/index.php?option=com_content&view=article&id=410&Itemid=414&lang=en

FlexxCon. (n.d.). *Product sheet R-53612-MGI5.* Retrieved from http://www.flexxcon.com/pdf/en/FLEXXCON-EN-DATASHEET-R-53612-MGI5.pdf

FlexxCon B.V. (2017). *FRP Gratings.* Retrieved from https://www.kunststofroosters.nl/kunststofroosters

Gkaidatzis, R. (2014). *MSc Thesis: Bio-based FRP structures:A pedestrian bridge in Schiphol Logistics Park* (Tech. Rep.). Delft: Delft University of Technology. Retrieved from http://repository.tudelft.nl/islandora/object/uuid%3A81cfde58-90dc-4bd0-9506-01ec1d85839b?collection=education

Guades, E., Aravinthan, T., Islam, M., & Manalo, A. (2012). *A review on the driving performance of FRP composite piles.* doi: 10.1016/j.compstruct.2012.02.004

Gudavalli, S., Safaqah, O., & Seo, H. (2013). Effect of Soil Plugging on Axial Capacity of Open-Ended Pipe Piles in Sands. In *18th international conference on soil mechanics and geotechnical engineering* (pp. 1487–1490). Paris.

Han, J., & Frost, J. (1999). Buckling of Vertically Loaded Fiber-Reinforced Polymer Piles. *Journal of Reinforced Plastics and Composites, 18*(4), 290–318.

Han, J., & Frost, J. D. (2000). Load-deflection response of transversely isotropic piles under lateral loads. *International Journal for Numerical and Analytical Methods in Geomechanics.* doi: 10.1002/(SICI)1096-9853(20000425)24:5<509::AID-NAG79>3.0.CO;2-9

Hoefsloot, F. (2006). *Door grond horziontaal belaste palen, bestaande ontwerpmodellen* (Tech. Rep.). Fugro. Retrieved from https://www.google.nl/url?sa=t&rct=j&q=&esrc=s&source=web&cd=1&ved=0ahUKEwjY_5eoy5LVAhWLbVAKHZCJBMwQFggpMAA&url=https%3A%2F%2Frepository.tudelft.nl%2Fislandora%2Fobject%2Fuuid%3Ac70b7a9f-4b4a-4c92-9d05-8ec4fe54b41b%2Fdatastream%2FOBJ%2Fdownload&usg=AFQjCN

Hutchinson, J. R. (2001). Shear Coefficients for Timoshenko Beam Theory. *Journal of Applied Mechanics, 68*, 87–92. doi: 10.1115/1.1349417

Ilg, P., Hoehne, C., & Guenther, E. (2016). High-performance materials in infrastructure: A review of applied life cycle costing and its drivers - The case of fiber-reinforced composites. *Journal of Cleaner Production.* doi: 10.1016/j.jclepro.2015.07.051

IPCC. (2014). *Climate Change 2014: Synthesis Report. Contribution of Working Groups I, II and III to the Fifth Assessment Report of the Intergovernmental Panel on Climate Change.* (R. Pachauri & L. Meyer, Eds.). Geneva: IPCC. Retrieved from http://www.ipcc.ch/pdf/assessment-report/ar5/syr/SYR_AR5_FINAL_full_wcover.pdf

Iskander, M. G., Asce, M., Stachula, A., & Asce, A. M. (2002). Wave Equation Analyses of Fiber-Reinforced Polymer Composite Piling. *Journal of Composites for Construction, 6*(2), 88–96. Retrieved from http://dx.doi.org/10.1061/(ASCE)1090-0268(2002)6:2(88) doi: 10.1061/(ASCE)1090-0268(2002)6:2(88)

Iskander, M. G., Hanna, S., & Stachula, A. (2001). Driveability of FRP Composite Piling. *Journal of Geotechnical and Geoenvironmental Engineering, 127*(2), 169–176. Retrieved from http://dx.doi.org/10.1061/(ASCE)1090-0241(2001)127:2(169) doi: 10.1061/(ASCE)1090-0241(2001)127:2(169)

Jonkers, H. (2017). *Personal communication.*

Jonkers, H. M. (2016). *Sustainability Reader - Part of course CTB1320 Construction Materials and Sustainability, Delft University of Technology.*

Jonkers. H.M. (2016). *Personal communication.*

Kolstein, M. H. (2008). *Fibre Reinforced Polymer (FRP) Structures.* Delft.

Maas, G. (2011). *MSc Thesis: Comparison of quay wall designs in concrete, steel, wood and composites with regard to the CO2-emission and the LIfe Cycle Analysis* (Tech. Rep.). Delft: Delft Univer-

sity of Technology. Retrieved from http://repository.tudelft.nl/islandora/object/uuid%3A11a2ea26-54ad-44e5-8186-d63d80d9014c?collection=education

Mallick, P. (2007). *Fiber-Reinforced Composites: Materials, Manufacturing, and Design* (3th ed.). Boca Raton: CRC Press.

Markets and Markets. (n.d.). *FRP Bridge Market worth 75.5 Million USD by 2021*. Retrieved from http://www.marketsandmarkets.com/PressReleases/frp-bridge.asp

Middendorp, P. (2004). Thirty years of experience with the wave equation solution based on the method of characteristics. *7th International Conference on the Application of Stress Wave Theory to Piles*.

Molenaar, I. W. F., Voorendt, M. Z., Molenaar, W., & Voorendt, M. (2016). Manual Hydraulic Structures PREFACE TO THE 2016 EDITION.

Moscoso, N. (2017). *Personal communication*. Retrieved from http://www.allnamics.eu/

NEN. (2011). *NEN 9997-1: Geotechnisch ontwerp van constructies - Deel 1: Algemene regels* (Tech. Rep.). NEN. Retrieved from https://www.nen.nl/NEN-Shop/Norm/NEN-999712016-nl.htm

Nettles, A. T. (1994). *Basic Mechanics of Laminated Composite Plates* (Tech. Rep.). George C. Marshall Space FLight Center. Retrieved from https://ntrs.nasa.gov/archive/nasa/casi.ntrs.nasa.gov/19950009349.pdf

Nijhof, A. (2003). *Vezelversterkte kunststoffen: Mechanica en ontwerp* (1st ed.). Delft: Delft University Press.

Nijssen, R. (2015). *Composites Materials - an introduction* (1st ed.). VKCN.

Nystrom, H. E., Watkins, S. E., Nanni, A., Asce, M., & Murray, S. (2003). Financial Viability of Fiber-Reinforced Polymer (FRP) Bridges. *Journal of Management in Engineering*, *19*(1). Retrieved from https://www.researchgate.net/publication/238230569_Financial_Viability_of_Fiber-Reinforced_Polymer_FRP_Bridges doi: 10.1061/ÍŠASCEÍŠ0742-597XÍŠ2003ÍŠ19:1ÍŠ2ÍŠ

Oxford Dictionaries. (n.d.). *Definition of jetty*. Retrieved from https://en.oxforddictionaries.com/definition/jetty

Pickering, K. L., Efendy, M. G. A., & Le, T. M. (2016). A review of recent developments in natural fibre composites and their mechanical performance. Retrieved from http://www.sciencedirect.com/science/article/pii/S1359835X15003115 doi: 10.1016/j.compositesa.2015.08.038

Rao, A., Jha, K. N., & Misra, S. (2007). Use of aggregates from recycled construction and demolition waste in concrete. *Resources, Conservation and Recycling*. doi: 10.1016/j.resconrec.2006.05.010

Rijksinstituut voor Gezondheid en Milieu. (n.d.). *Risks of dangerous goods*. Retrieved from http://www.rivm.nl/rvs/Gevaarsindeling/ADR

Schöck Bauteile GmbH. (n.d.). *Media Relations - Schöck Bauteile GmbH*. Retrieved from http://www.schoeck.com/cache/schoeckmedia_Vierendeel_truss%5B12440%5D_schoeckmedia_image_thumbnailscheme_1280x1900.jpg

Schutte, W. (2016). *Personal communication*.

SCIA nv. (2016). *SCIA Engineer - Theory; Physical and shape orthotropy of plates* (Tech. Rep.). Retrieved from http://help.scia.net/download/16.0/en/OtrhotropTB_enu.pdf

Staalsupport. (n.d.). *Wat is de reden van het verschil in afschuifoppervlak bij I-profielen tussen de TGB en de Eurocode?* Retrieved from http://www.staalsupport.nl/zoeken-detail.asp?pag=367

Stark, J. (2012). *Verbinden: Kenmerken van verbindingen in staalconstructies en het berekenen van mechanische verbindingsmiddelen en lassen volgens Eurocode 3*. Zoetermeer: Bouwen met Staal.

Tomlinson, M., & Woodward, J. (2008). *Pile Design and Construction Practice, Fifth edition* (5th ed.). Taylor & Francis.

TU Dresden. (n.d.). *ELamX^2*. Retrieved from https://tu-dresden.de/ing/maschinenwesen/ilr/lft/elamx2/elamx

van der Meer, A. (2017). *Voorlopig Tarievenbestand_Constructies-2017-1-170710_Roel Winter*. Rotterdam: Gemeente Rotterdam.

Van Der Valk, R. (2017). *MSc Thesis: A fibre reinforced polymer quay wall: Feasibility study* (Tech. Rep.). Delft: Delft University of Technology. Retrieved from http://repository.tudelft.nl/islandora/object/uuid%3A4fdc7065-570c-443e-8954-4f655ba29d2a?collection=education

Velez, J. D. G. (2013). *Experimental study of Hollow Fibre Reinforced Polymer Piles in soft clay* (Tech. Rep.). Ottawa-Carleton Institute of Civil and Environmental Engineering. Retrieved from https://curve.carleton.ca/system/files/etd/757d8b04-87ab-43b3-8397-ed6e2bd38756/etd_pdf/cc9b0d8ad28b3bca34650d1b52084a19/giraldovelez-experimentalstudyofhollowfibrereinforcedpolymer.pdf

Verlinde, M. F. (2017). *Research on a high performance and circular application of biobased composite on a facade - A circular biobased composite facade* (Tech. Rep.). Delft University of Technology. Retrieved from https://repository.tudelft.nl/islandora/object/uuid%3A8a43e668-3d7d-4be4-8eff-30636ad90883?collection=education

Vogtländer, J. (2010). *A practical guide to LCA for students designers and business managers : cradle-to-grave and cradle-to-cradle* (1st ed.). Delft: VSSD.

Wagih, A. M., El-Karmoty, H. Z., Ebid, M., & Okba, S. H. (2013). Recycled construction and demolition concrete waste as aggregate for structural concrete. *HBRC Journal, 9*, 193–200. Retrieved from http://www.sciencedirect.com/science/article/pii/S1687404813000588?via%3Dihub doi: 10.1016/j.hbrcj.2013.08.007

Walop, J. (2017). *Personal communication.*

Watté, K. A. A., & De Herder, R. D. (2015). *The feasibility of standardization of a monopile mooring facility for FSRU's* (Doctoral dissertation, Delft University of Technology). Retrieved from http://repository.tudelft.nl/islandora/object/uuid%3Afd0eecf0-c0c6-497d-90a3-4e5ef80e56f0?collection=education

W.B. Bijl Profielen B.V. (2015a). *BIJL Composiet Planken, brochure.* Retrieved from www.bijlprofielen.nl

W.B. Bijl Profielen B.V. (2015b). *BIJL Price list 2016 Composite floors / Bridge elements.* Retrieved from www.bijlprofielen.nl

Winter, R. (2017). *Literature Study: Feasibility of Fibre-Reinforced Polymer Jetties* (Tech. Rep.). Delft: Delft University of Technology.

Zorgdrager, A. (2014). *Feasibility study on the application of fiber-reinforced polymers in large lock gates* (Doctoral dissertation, Delft University of Technology). Retrieved from http://repository.tudelft.nl/islandora/object/uuid%3Aa9cac1c3-8915-46a6-8080-ceee5c2d2482?collection=education

Zyka, K., & Mohajerani, A. (2016). Composite piles: A review. doi: 10.1016/j.conbuildmat.2016.01.013

A

Geotechnical survey: Cone penetration test and boring samples

A.1. Cone penetration tests at the site location

Cone penetration tests and boring samples are made available by the municipality of Rotterdam, the Netherlands.

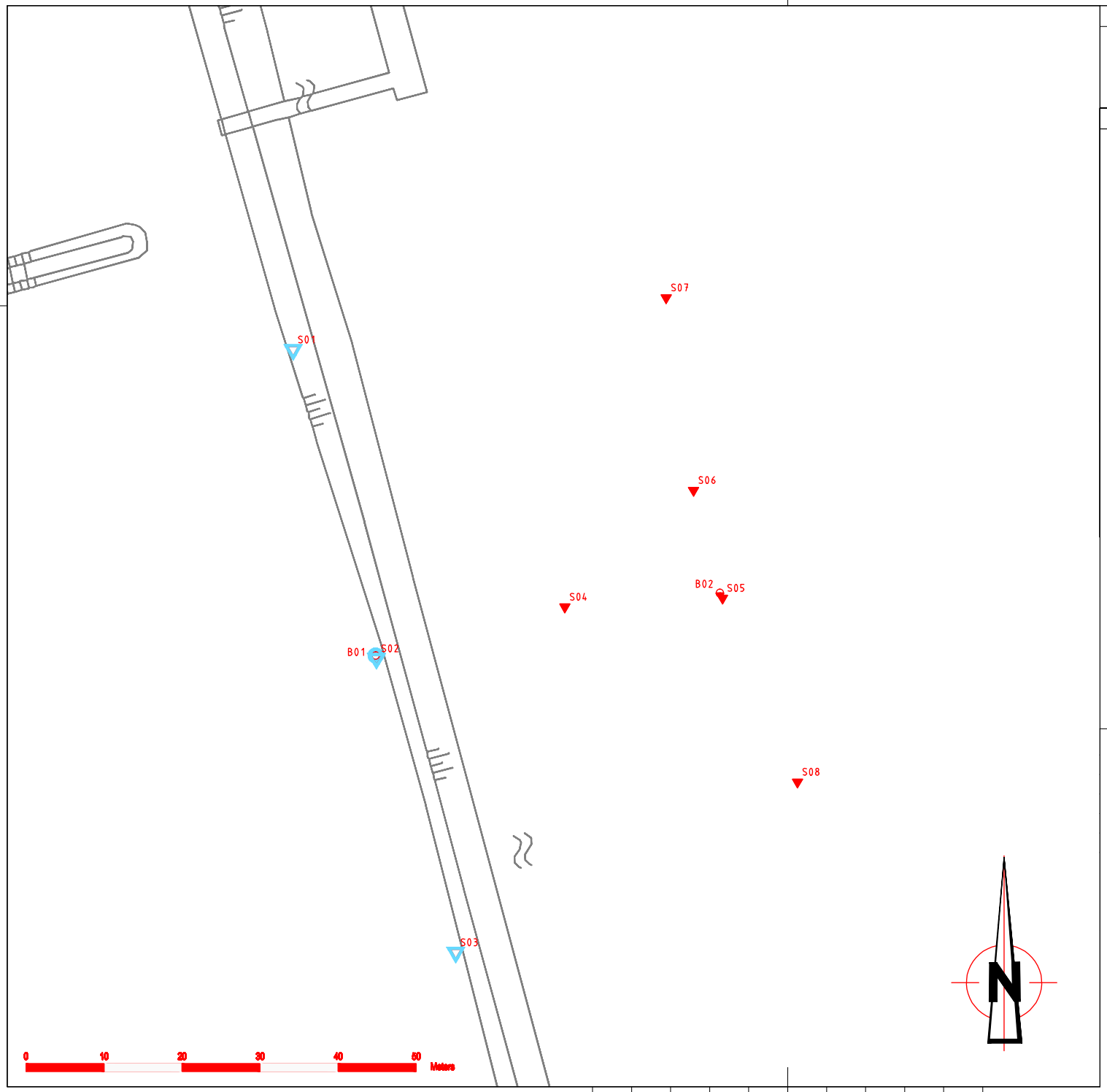

OPMERKINGEN

VERKLARING

- GEPLANDE BORING
- UITGEVOERDE BORING
- GEPLANDE SONDERING
- UITGEVOERDE SONDERING

Gemeente Rotterdam
Ingenieursbureau
Afdeling Geotechniek

Marconistraat 1a
NL-3029AE, Rotterdam
Tel. 010 489 9700

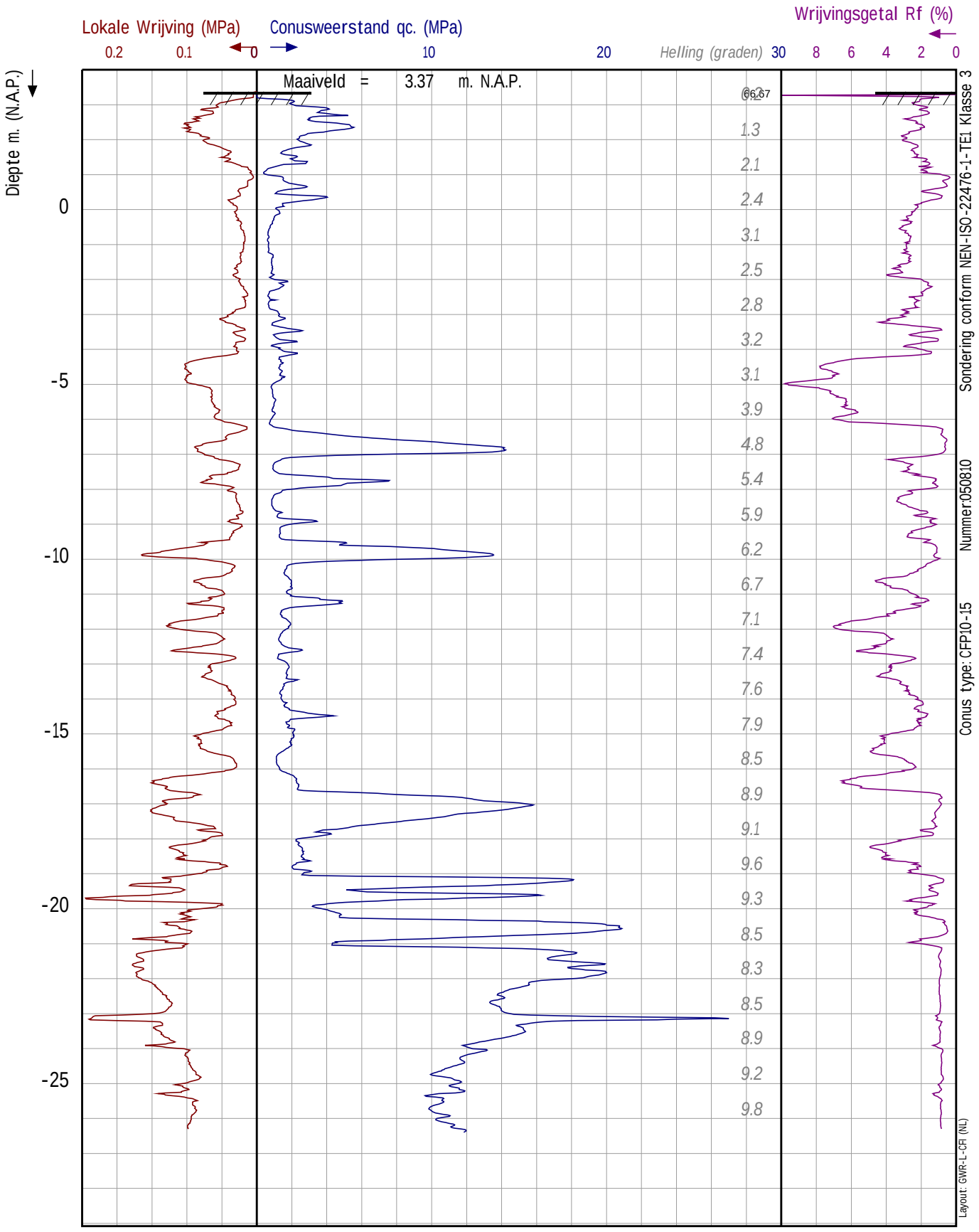

SONDERING:

S01

Gemeente Rotterdam
Ingenieursbureau
Afdeling Geotechniek

Marconistraat 1a
NL-3029AE, Rotterdam
Tel. 010 489 9700

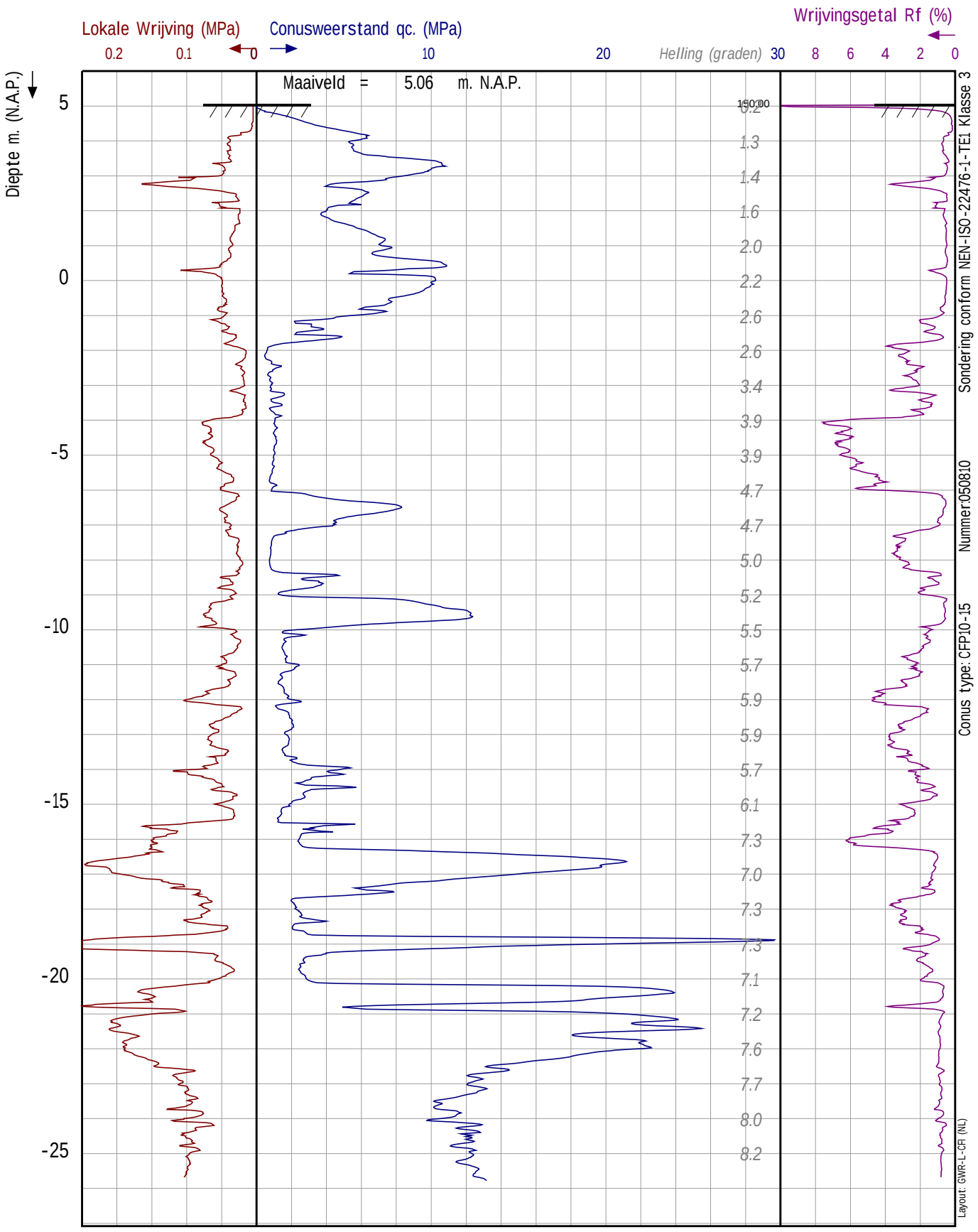

SONDERING:

S02

Pagina 1/1

Gemeente Rotterdam
Ingenieursbureau
Afdeling Geotechniek

Marconistraat 1a
NL-3029AE, Rotterdam
Tel. 010 489 9700

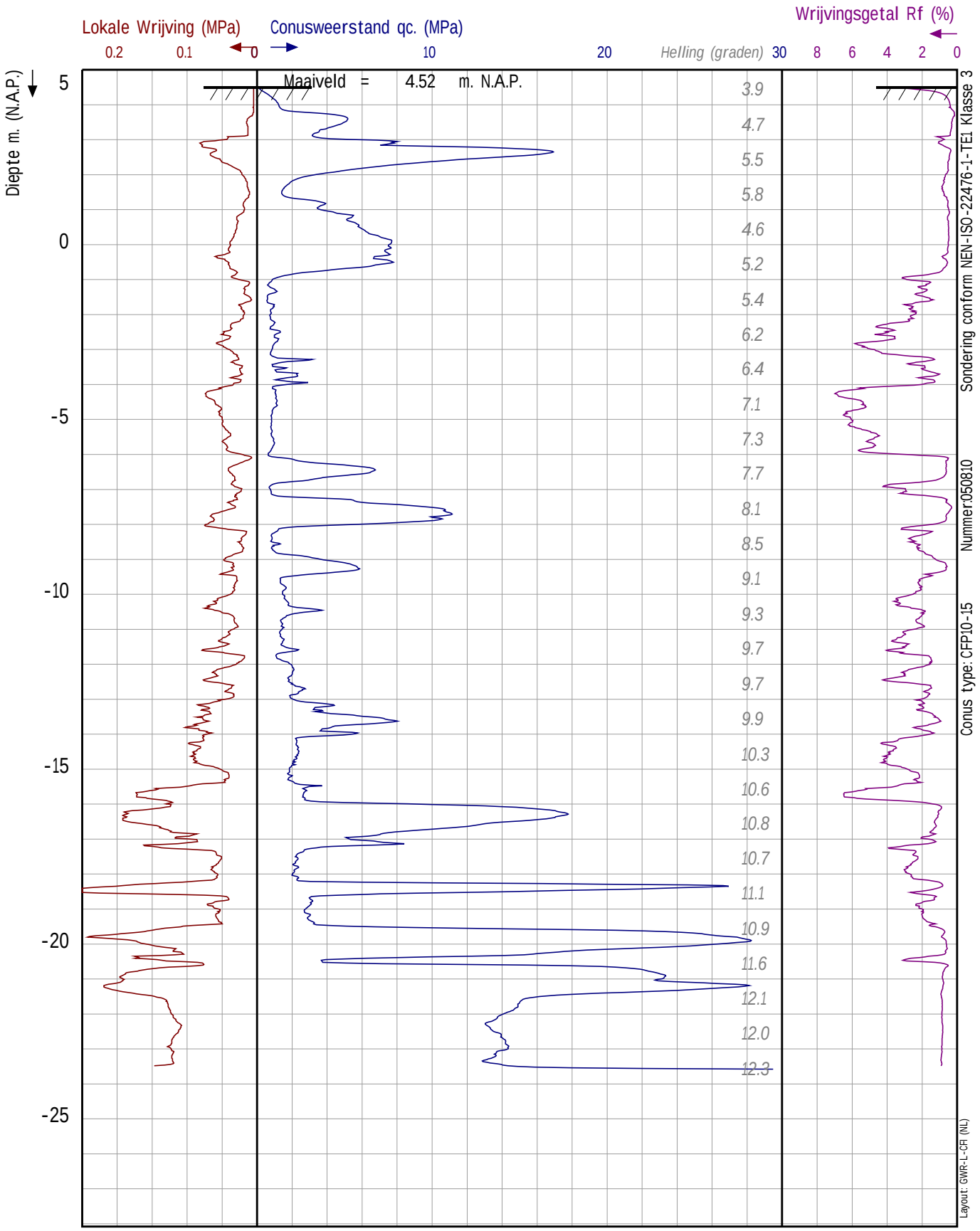

SONDERING:

S03

Pagina 1/1

Gemeente Rotterdam
Ingenieursbureau
Afdeling Geotechniek

Marconistraat 1a
NL-3029AE, Rotterdam
Tel. 010 489 9700

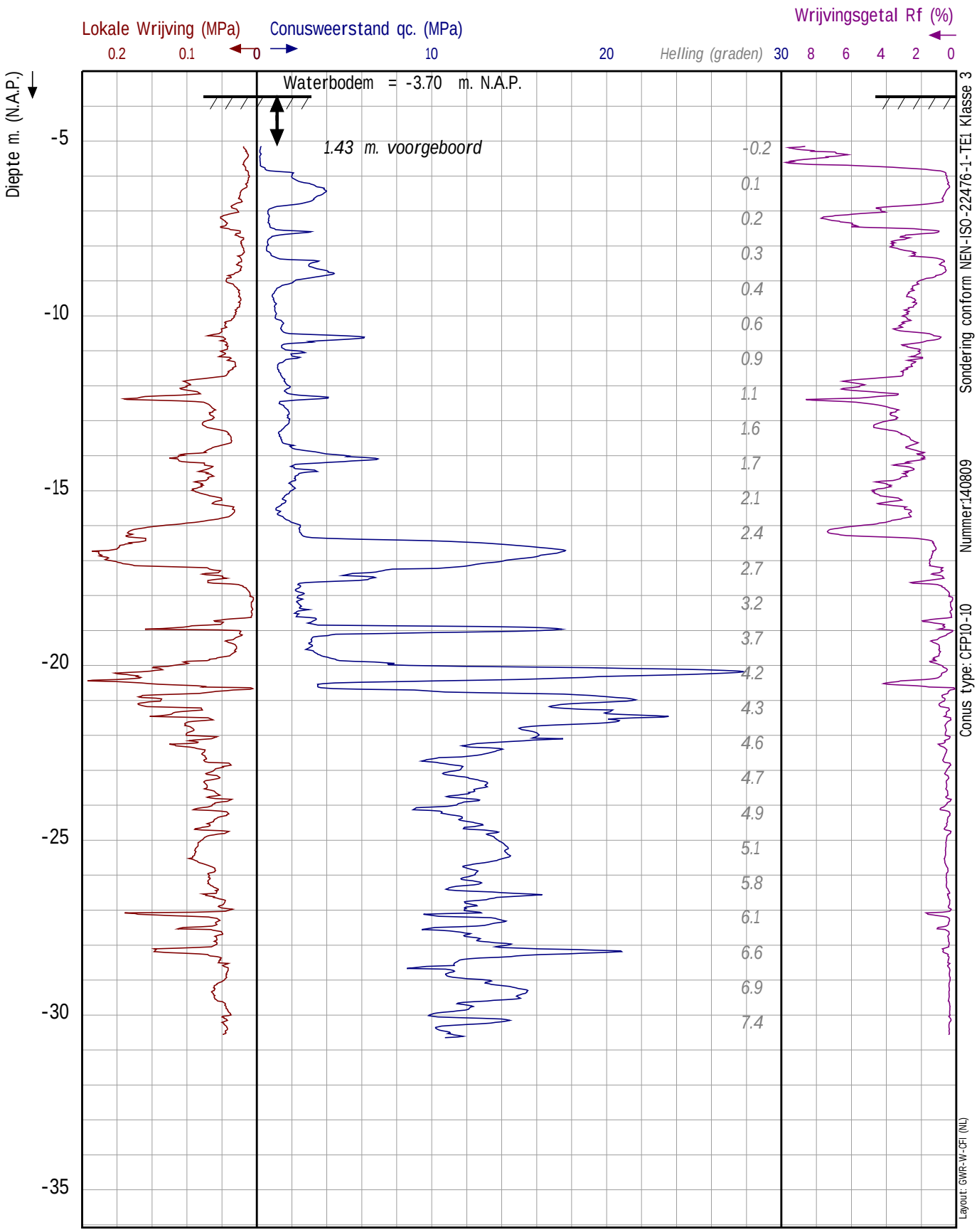

SONDERING:

S04

Gemeente Rotterdam
Ingenieursbureau
Afdeling Geotechniek

Marconistraat 1a
NL-3029AE, Rotterdam
Tel. 010 489 9700

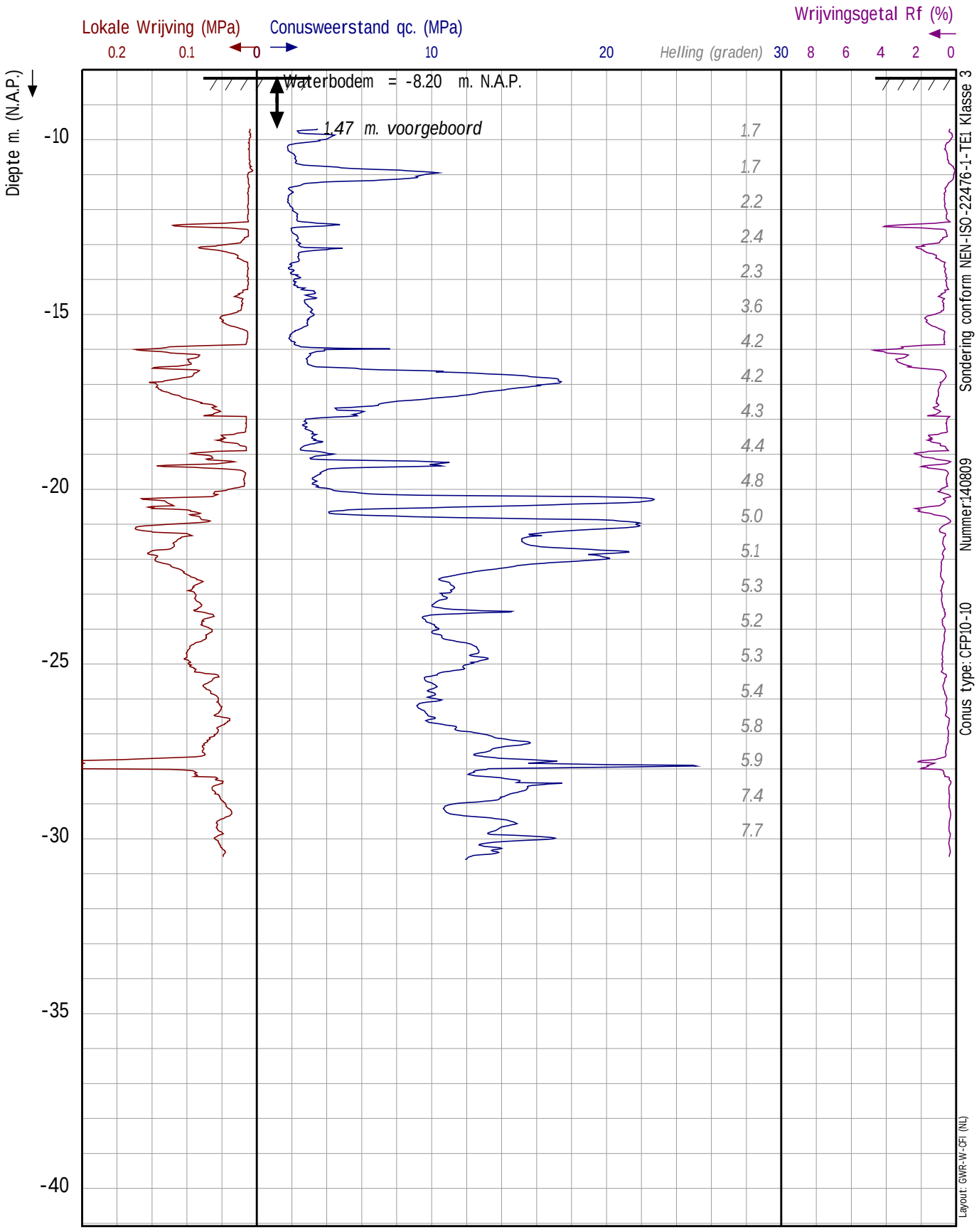

SONDERING:

S05

Gemeente Rotterdam
Ingenieursbureau
Afdeling Geotechniek

Marconistraat 1a
NL-3029AE, Rotterdam
Tel. 010 489 9700

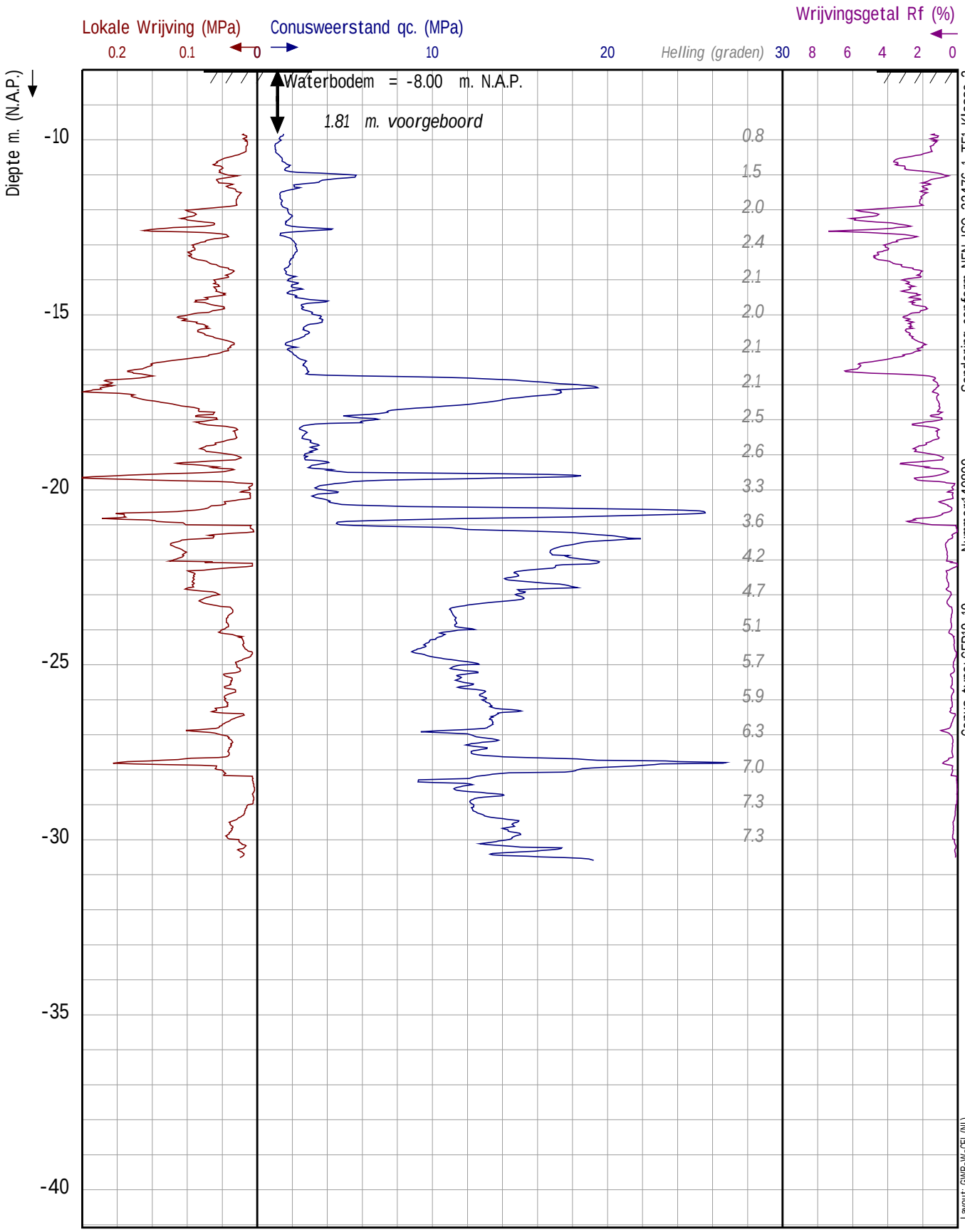

SONDERING:

S06

Gemeente Rotterdam
Ingenieursbureau
Afdeling Geotechniek

Marconistraat 1a
NL-3029AE, Rotterdam
Tel. 010 489 9700

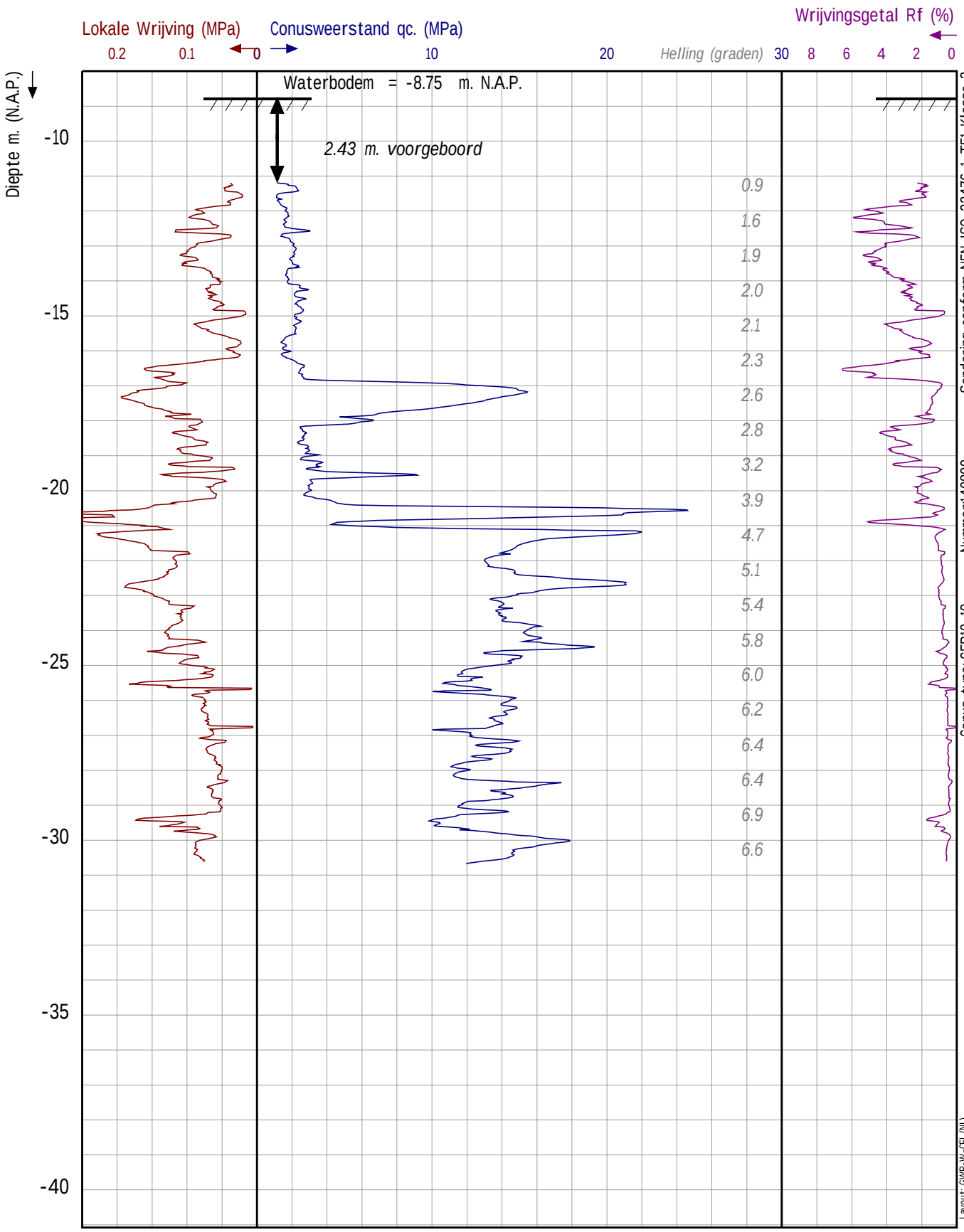

SONDERING:

S07

Gemeente Rotterdam
Ingenieursbureau
Afdeling Geotechniek

Marconistraat 1a
NL-3029AE, Rotterdam
Tel. 010 489 9700

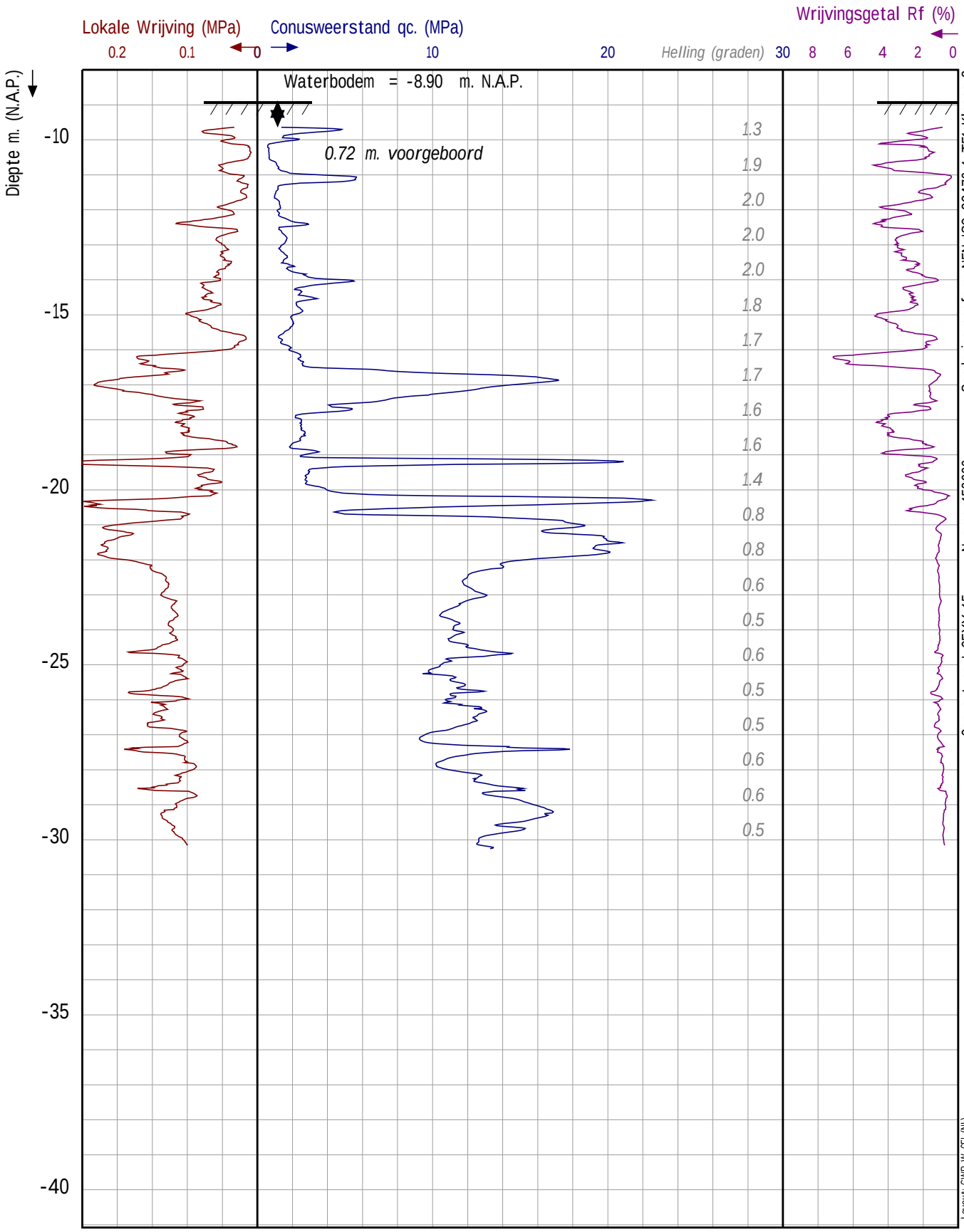

SONDERING:

S08

A.2. Geotechnical survey: Boring samples at the site location

Boring examples of the case study are found, but names of contributors need to be blurred before publication.

Projectnaam: **Kolb Moerdijk**

Gemeente Rotterdam

Veld- en laboratoriummetingen Gww
Afdeling laboratorium

Boring: B01 - 1

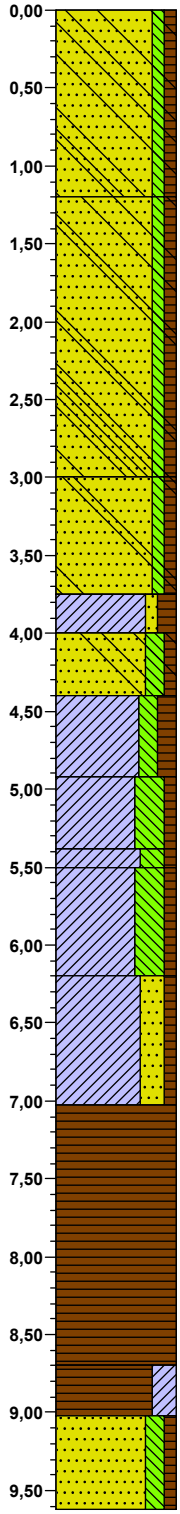

		mk	Yw [kN/m3]	Yd [kN/m3]	w [%]	n [%]	e	Sr [%]	cu [kPa]
3,15									
	Zand, matig fijn, zwak siltig, zwak humeus, laagjes klei								
1,95									
	Zand, matig grof, zwak siltig, zwak humeus, sporen klei								
0,15									
	Zand, matig fijn, zwak siltig, zwak humeus, sporen klei								
-0,60									
	Klei, zwak zandig, matig humeus	1	16	10,4	53,8	60,8	1,55	92,2	
-0,85									
	Zand, zeer fijn, matig siltig, zwak humeus, sporen klei, sporen veen								
-1,25									
	Klei, matig siltig, matig humeus	1	16,5	11	50	58,5	1,41	94	
		1	15,8	9,7	62,9	63,4	1,73	96,2	
-1,77									
	Klei, uiterst siltig, zwak humeus	1	18,4	14,4	27,8	45,7	0,84	87,6	
-2,23									
-2,35	**Klei, sterk siltig, zwak humeus**	1	17,4	13	33,8	50,9	1,04	86,4	
	Klei, uiterst siltig, zwak humeus	1	18,1	13,9	30,2	47,5	0,91	88,3	
-3,05									
	Klei, sterk zandig, zwak humeus, gelaagd	1	18	13,5	33,3	49,1	0,96	91,7	
		1	17,6	12,8	37,5	51,7	1,07	92,8	
-3,88									
	Veen	1	10,2	2	410				
		1	10,4	2,2	372,7				
		1	10,1	2,2	359,1				
-5,55									
	Veen, sterk kleïig	1	11,7	4,4	165,9				
-5,87									
	Zand, zeer fijn, matig siltig, zwak humeus								
-6,47									

Getekend volgens: NEN 5104

Schaal: 1: 50

Projectnaam: **Kolb Moerdijk**

Gemeente Rotterdam

Veld- en laboratoriummetingen Gww
Afdeling laboratorium

Boring: B01 - 2

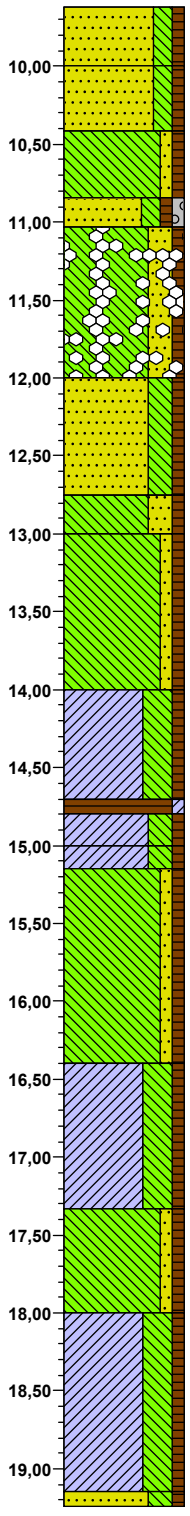

		mk	Yw [kN/m3]	Yd [kN/m3]	w [%]	n [%]	e	Sr [%]	cu [kPa]
-6,47	**Zand, zeer fijn, matig siltig, zwak humeus**								
-6,85	**Zand, zeer fijn, matig siltig, zwak humeus, sporen leem**								
-7,27	**Leem, zwak zandig, zwak humeus**	1	20	16,1	24,2	39,2	0,65	99,4	
-7,69									
-7,88	**Zand, zeer fijn, matig siltig, zwak humeus, zwak grindig**								
	Leem, sterk zandig, zwak humeus, laagjes zand	1	19,7	16,4	20,1	38,1	0,62	86,6	
		1	20,6	17,3	19,1	34,7	0,53	95,1	
-8,85	**Zand, uiterst fijn, sterk siltig, zwak humeus**								
-9,60	**Leem, sterk zandig, zwak humeus**	1	20,1	16,4	22,6	38,1	0,62	97,1	
-9,85	**Leem, zwak zandig, zwak humeus**	1	20,6	17,3	19,1	34,7	0,53	95,1	
		1	20,2	16,5	22,4	37,7	0,61	98	
-10,85	**Klei, uiterst siltig, zwak humeus**	1	19,5	15,7	24,2	40,8	0,69	93,2	
		1	19,1	14,8	29,1	44,2	0,79	97,4	
-11,55									
-11,65	**Veen, zwak kleïig**	1	17,5	12,6	38,9	52,5	1,1	93,4	
-11,85	**Klei, sterk siltig, zwak humeus**	1	18	13,6	32,4	48,7	0,95	90,4	
-12,00	**Klei, sterk siltig, zwak humeus, laagjes veen**	1	20,5	17,1	19,9	35,5	0,55	95,9	
	Leem, zwak zandig, zwak humeus	1	20,3	16,8	20,8	36,6	0,58	95,6	
-13,25	**Klei, uiterst siltig, zwak humeus**	1	19,3	15,3	26,1	42,3	0,73	94,6	
		1	19,2	15,1	27,2	43	0,75	95,3	
-14,18	**Leem, zwak zandig, zwak humeus**	1	20,8	17,5	18,9	34	0,51	97,2	
-14,85	**Klei, uiterst siltig, zwak humeus**	1	19,7	15,7	25,5	40,8	0,69	98,1	
		1	19,7	15,9	23,9	40	0,67	95	
-16,00									
-16,09	**Zand, uiterst fijn, sterk siltig, zwak humeus**								

Getekend volgens: NEN 5104

Schaal: 1: 50

Projectnaam: **Kolb Moerdijk**

Gemeente Rotterdam

Veld- en laboratoriummetingen Gww
Afdeling laboratorium

Boring: B01 - 3

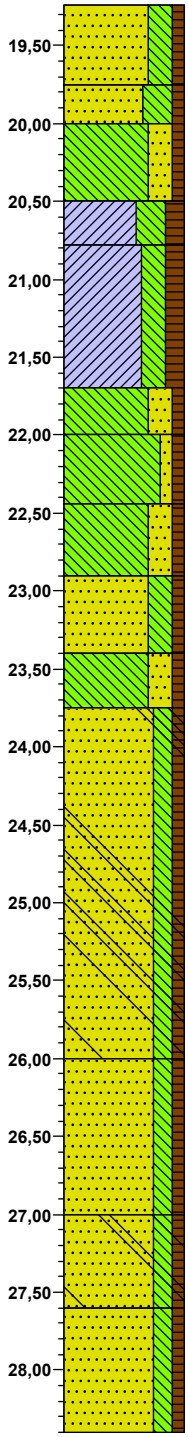

		mk	Yw [kN/m3]	Yd [kN/m3]	w [%]	n [%]	e	Sr [%]	cu [kPa]
-16,09									
	Zand, uiterst fijn, sterk siltig, zwak humeus								
-16,60									
	Zand, uiterst fijn, uiterst siltig, zwak humeus								
-16,85									
	Leem, sterk zandig, zwak humeus	1	19,2	15,3	25,5	42,3	0,73	92,3	
-17,35									
	Klei, uiterst siltig, matig humeus	1	18,1	13,6	33,1	48,7	0,95	92,4	
-17,63									
	Klei, sterk siltig, matig humeus	1	18,5	14,2	30,3	46,4	0,87	92,6	
-18,55									
	Leem, sterk zandig, zwak humeus	1	21,8	19,1	14,1	27,9	0,39	96,7	
-18,85									
	Leem, zwak zandig, zwak humeus	1	20,4	17	20	35,8	0,56	94,8	
-19,29									
	Leem, sterk zandig, zwak humeus	1	19,8	16,6	19,3	37,4	0,6	85,7	
-19,75									
	Zand, uiterst fijn, sterk siltig, zwak humeus								
-20,25									
	Leem, sterk zandig, zwak humeus	1	20,6	17,5	17,7	34	0,51	91,3	
-20,60									
	Zand, zeer fijn, matig siltig, zwak humeus, sporen klei								
-22,85									
	Zand, zeer fijn, matig siltig, zwak humeus								
-23,85									
	Zand, zeer fijn, matig siltig, zwak humeus, laagjes klei								
-24,45									
	Zand, zeer fijn, matig siltig, zwak humeus								
-25,25									

Getekend volgens: NEN 5104

Schaal: 1: 50

Projectnaam: **Kolb Moerdijk**

Gemeente Rotterdam

Veld- en laboratoriummetingen Gww
Afdeling laboratorium

Boring: **B02 - 1**

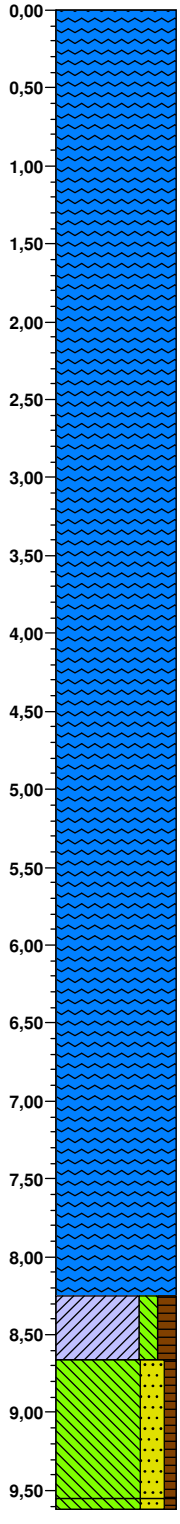

		mk	Yw [kN/m3]	Yd [kN/m3]	w [%]	n [%]	e	Sr [%]	cu [kPa]
0,00	Water								
-8,25	Klei, matig siltig, matig humeus, slib	1	13,7	6,8	101,5				
-8,66	Leem, sterk zandig, zwak humeus	1	20,3	16,7	21,6	37	0,59	97,3	
-9,62	Leem, sterk zandig, zwak humeus	1	20,8	17,8	16,9	32,8	0,49	91,4	

Getekend volgens: NEN 5104

Schaal: 1: 50

Boring: B02 - 2

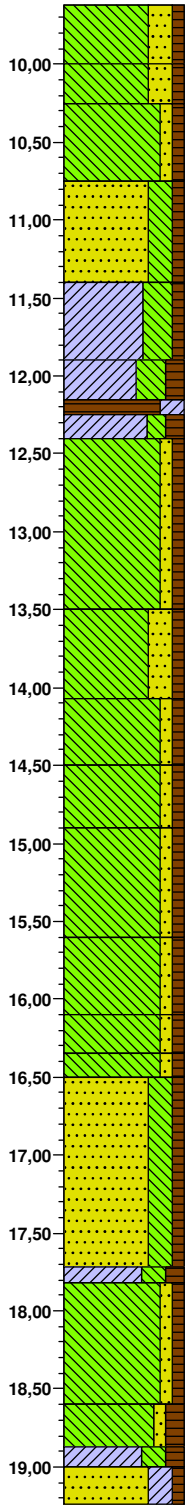

		mk	Yw [kN/m3]	Yd [kN/m3]	w [%]	n [%]	e	Sr [%]	cu [kPa]
-9,62									
	Leem, sterk zandig, zwak humeus	1	20,8	17,8	16,9	32,8	0,49	91,4	
-10,00									
	Leem, sterk zandig, zwak humeus	1	20,6	17,5	17,7	34	0,51	91,3	
-10,25									
	Leem, zwak zandig, zwak humeus	1	20,6	17,1	20,5	35,5	0,55	98,7	
-10,75									
	Zand, uiterst fijn, sterk siltig, zwak humeus								
-11,40									
	Klei, uiterst siltig, zwak humeus	1	19,3	15	28,7	43,4	0,77	99,1	
-11,90									
	Klei, uiterst siltig, matig humeus	1	18,5	13,8	34,1	47,9	0,92	98,1	
-12,15									
-12,25	Veen, sterk kleïig	1	11,9	5.8	105,2				
-12,40	Klei, matig siltig, matig humeus	1	16	10,6	50,9	60	1,5	90	
	Leem, zwak zandig, zwak humeus	1	20,4	16,8	21,4	36,6	0,58	98,4	
-13,50									
	Leem, sterk zandig, zwak humeus	1	19,6	15,5	26,5	41,5	0,71	98,8	
-14,07									
	Leem, zwak zandig, zwak humeus	1	20,8	17,4	19,5	34,3	0,52	99	
-14,50									
	Leem, zwak zandig, zwak humeus	1	21	17,7	18,6	33,2	0,5	99,4	
-14,90									
	Leem, zwak zandig, zwak humeus	1	21,2	18,1	17,1	31,7	0,46	97,8	
-15,60									
	Leem, zwak zandig, zwak humeus	1	19,7	15,6	26,3	41,1	0,7	99,7	
-16,10									
	Leem, zwak zandig, zwak humeus	1	20,1	16,3	23,3	38,5	0,63	98,7	
-16,35									
-16,50	Leem, zwak zandig, zwak humeus	1	20	16,2	23,5	38,9	0,64	97,8	
	Zand, uiterst fijn, sterk siltig, zwak humeus								
-17,72									
-17,82	Klei, sterk siltig, matig humeus	1	16,2	10,9	48,6	58,9	1,43	90	
	Leem, zwak zandig, zwak humeus	1	20	16,1	24,2	39,2	0,65	99,4	
-18,60									
	Leem, zwak zandig, matig humeus	1	18,8	14,5	29,7	45,3	0,83	95	
-18,87									
-19,00	Klei, sterk siltig, matig humeus	1	18,1	13,6	33,1	48,7	0,95	92,4	
-19,24	Zand, uiterst fijn, kleïig, zwak humeus								

Projectnaam: **Kolb Moerdijk**

Gemeente Rotterdam

Veld- en laboratoriummetingen Gww
Afdeling laboratorium

Boring: B02 - 3

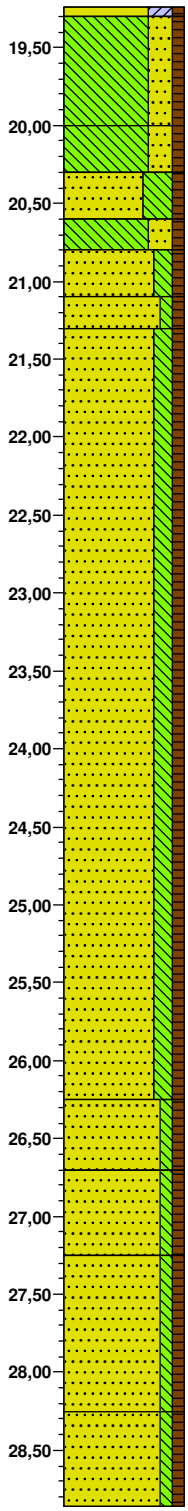

		mk	Yw [kN/m3]	Yd [kN/m3]	w [%]	n [%]	e	Sr [%]	cu [kPa]
-19,30	**Zand, uiterst fijn, kleïg, zwak humeus**	1	21,1	18,1	16,6	31,7	0,46	94,6	
	Leem, sterk zandig, zwak humeus								
-20,00									
	Leem, sterk zandig, zwak humeus	1	21,5	18,6	15,6	29,8	0,42	97,3	
-20,30									
	Zand, uiterst fijn, uiterst siltig, zwak humeus								
-20,60									
-20,80	**Leem, sterk zandig, zwak humeus**	1	21	17,7	18,6	33,2	0,5	99,4	
	Zand, uiterst fijn, matig siltig, zwak humeus								
-21,10									
-21,30	**Zand, matig fijn, zwak siltig, zwak humeus**								
	Zand, zeer fijn, matig siltig, zwak humeus								
-26,25									
	Zand, matig fijn, zwak siltig, zwak humeus								
-26,70									
	Zand, matig grof, zwak siltig, zwak humeus								
-27,25									
	Zand, matig grof, zwak siltig, zwak humeus, sporen leem								
-28,25									
	Zand, matig grof, zwak siltig, zwak humeus								
-28,86									

Getekend volgens: NEN 5104

Schaal: 1: 50

Projectnaam: **Kolb Moerdijk**

Gemeente Rotterdam

Veld- en laboratoriummetingen Gww
Afdeling laboratorium

Boring: B02 - 4

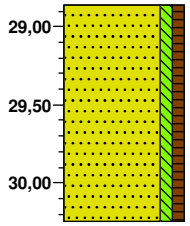

-28,86

Zand, matig grof, zwak siltig, zwak humeus

-30,25

mk	Yw [kN/m3]	Yd [kN/m3]	w [%]	n [%]	e	Sr [%]	cu [kPa]

Getekend volgens: NEN 5104

Schaal: 1: 50

B

Loads cases

This appendix gives an overview of the load cases. The following load cases are applied to the jetty:

- Variable load
- Wind, longitudinal
- Wind, transversal 1
- Wind, transversal 2
- Loading arm
- Planks
- Pipes
- Railing
- Sumput

In the structural calculations, the planks are modeled as a distributed surface load. Hence, the additional stiffness provided by the planks is not accounted for in the model.

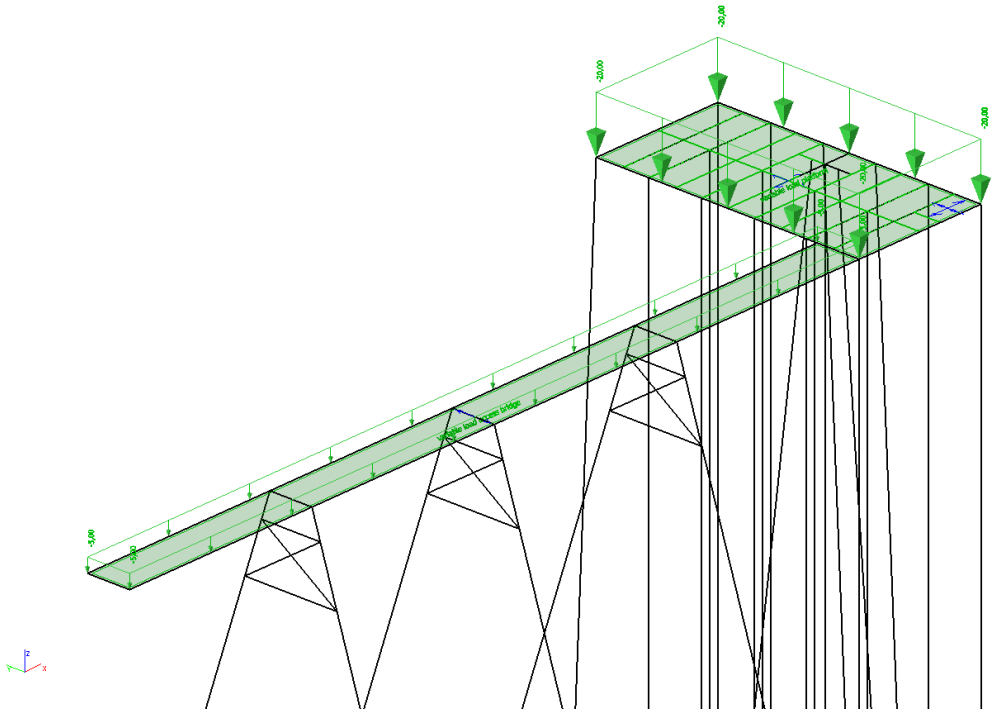

Figure B.1: Load case: variable load

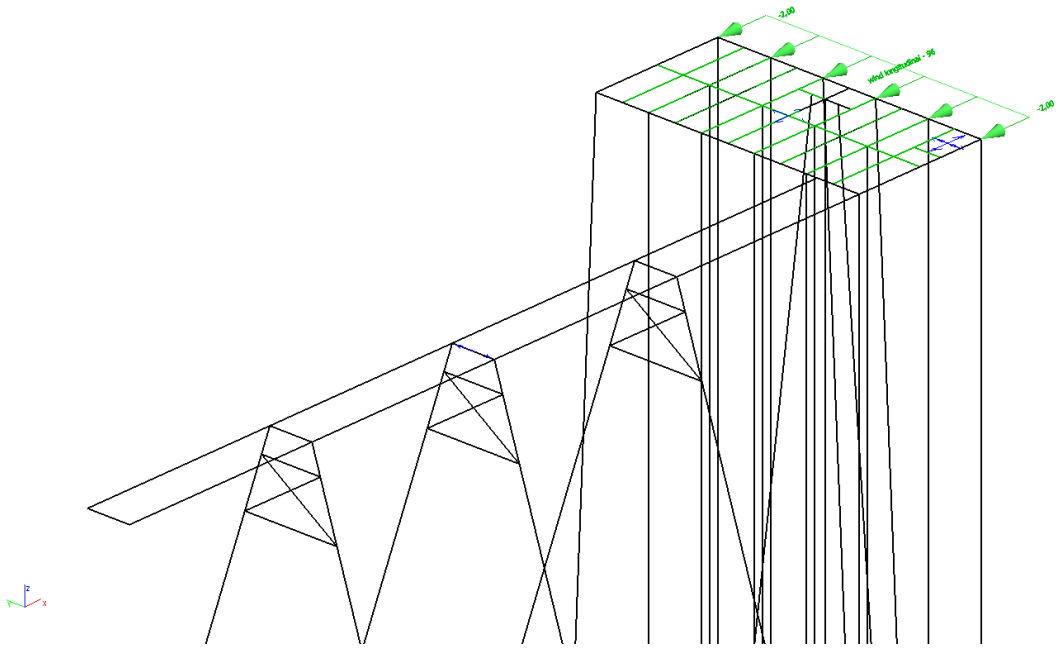

Figure B.2: Load case: wind longitudinal

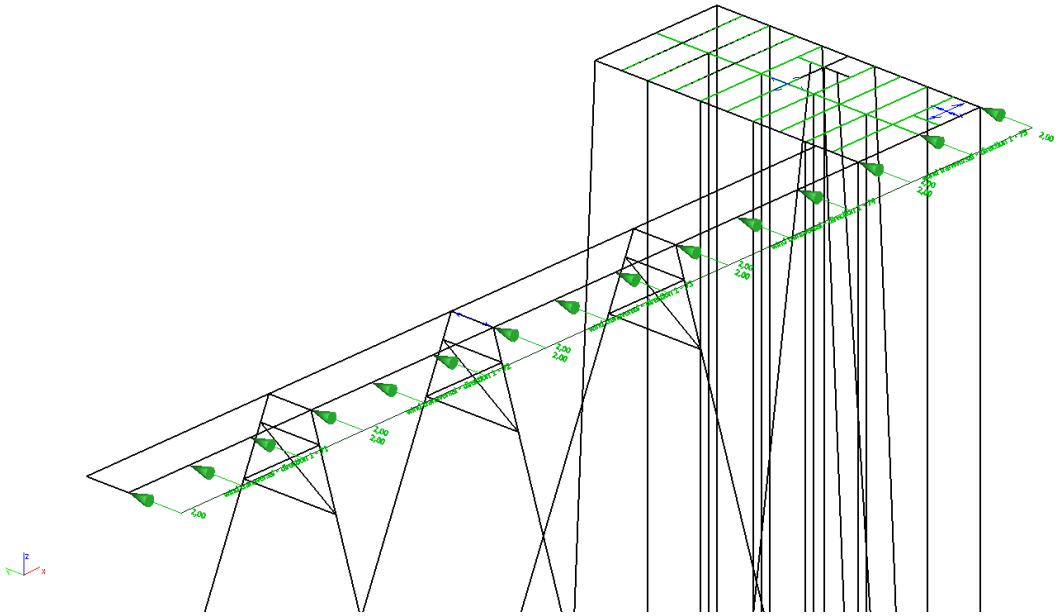

Figure B.3: Load case: wind transversal, position 1

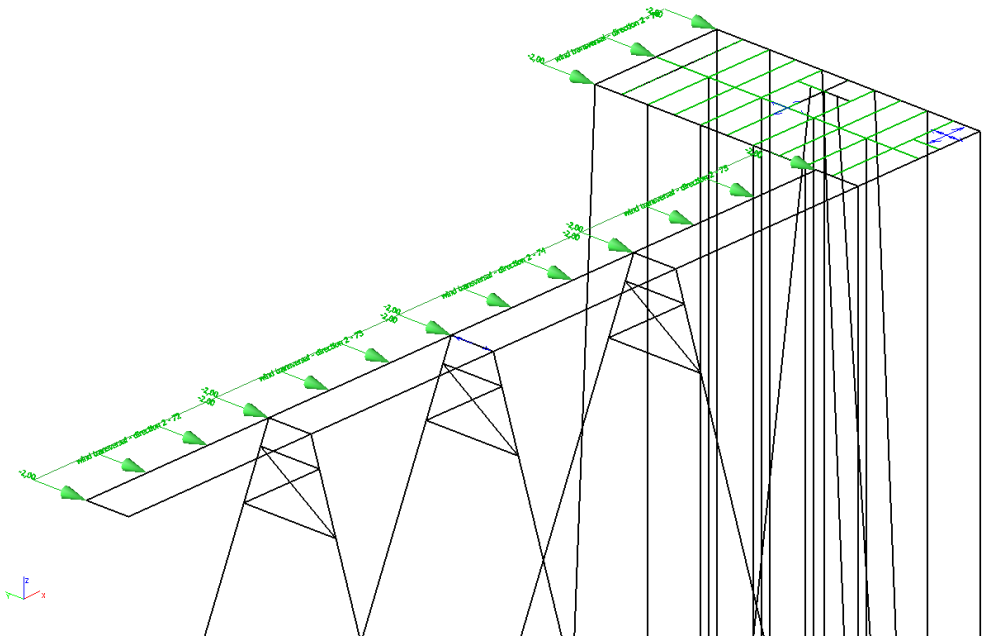

Figure B.4: Load case: wind transversal, position 2

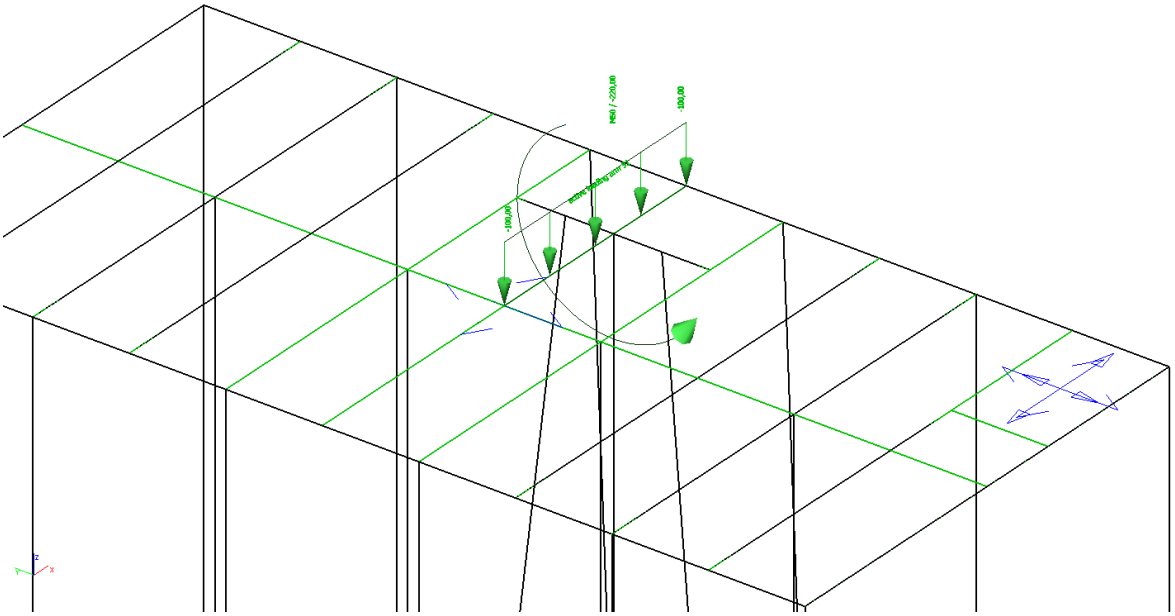

Figure B.5: Load case: loading arm

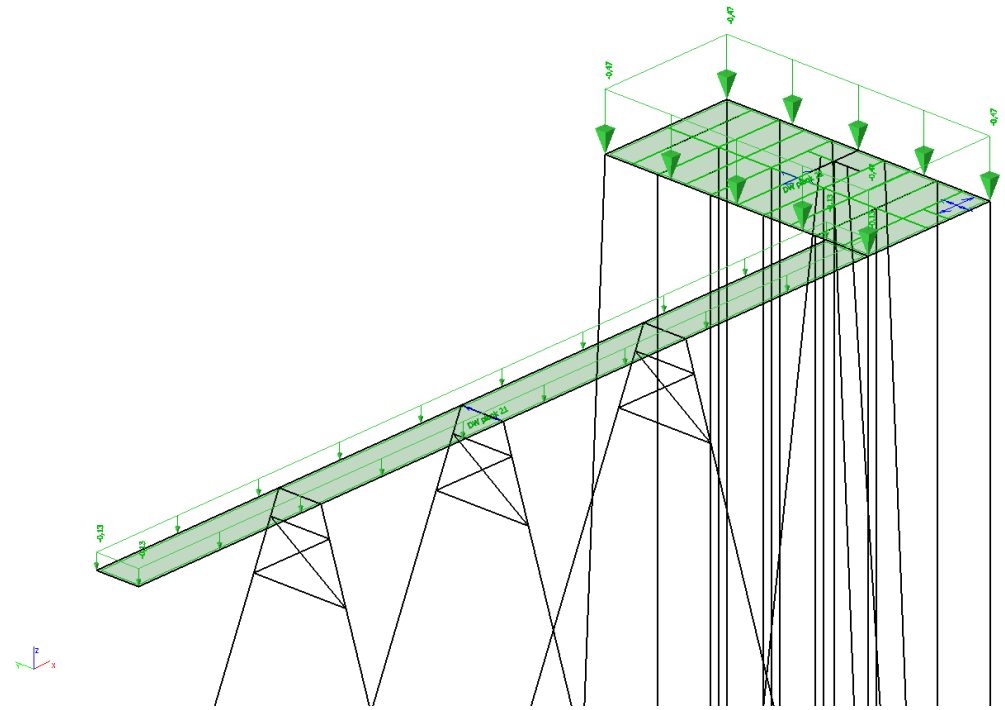

Figure B.6: Load case: planks

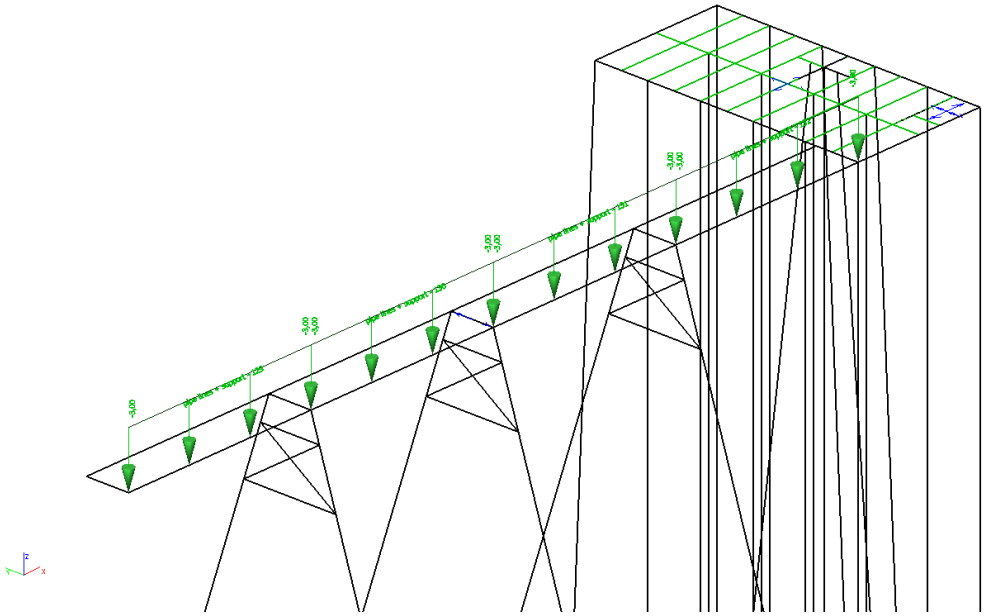

Figure B.7: Load case: planks

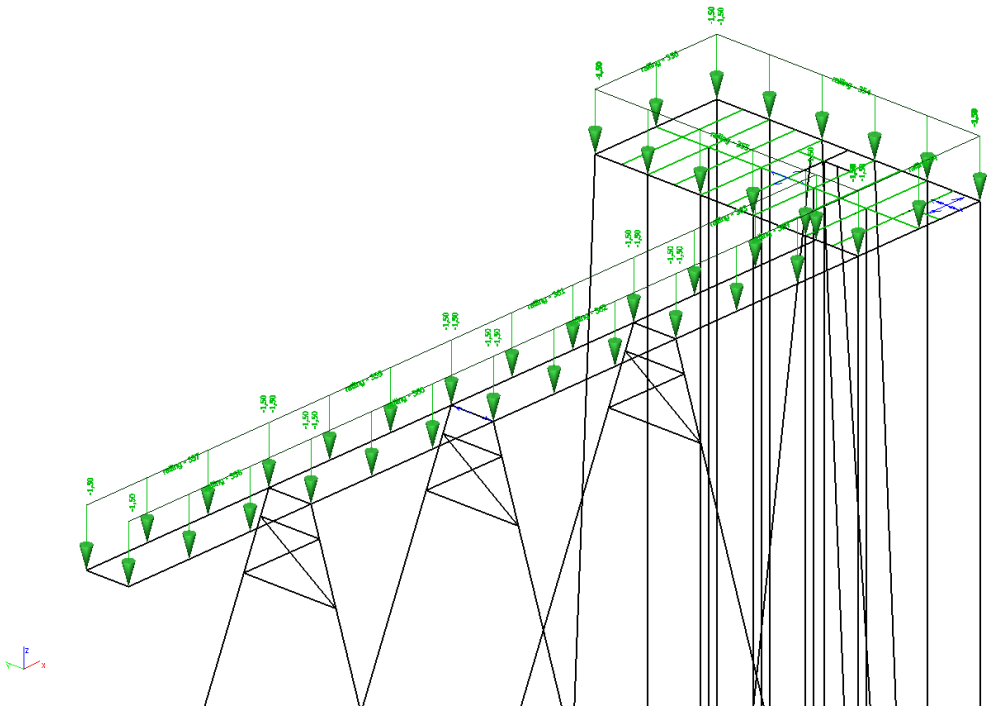

Figure B.8: Load case: railing

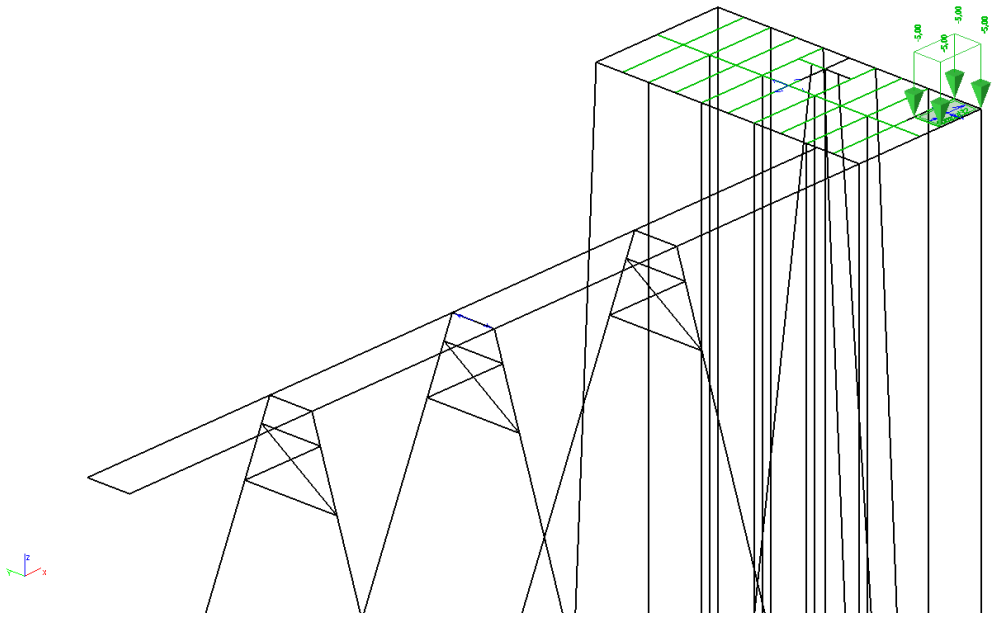

Figure B.9: Load case: sumput

C

Internal member forces and stresses

C.0.1. Mx (torsion)

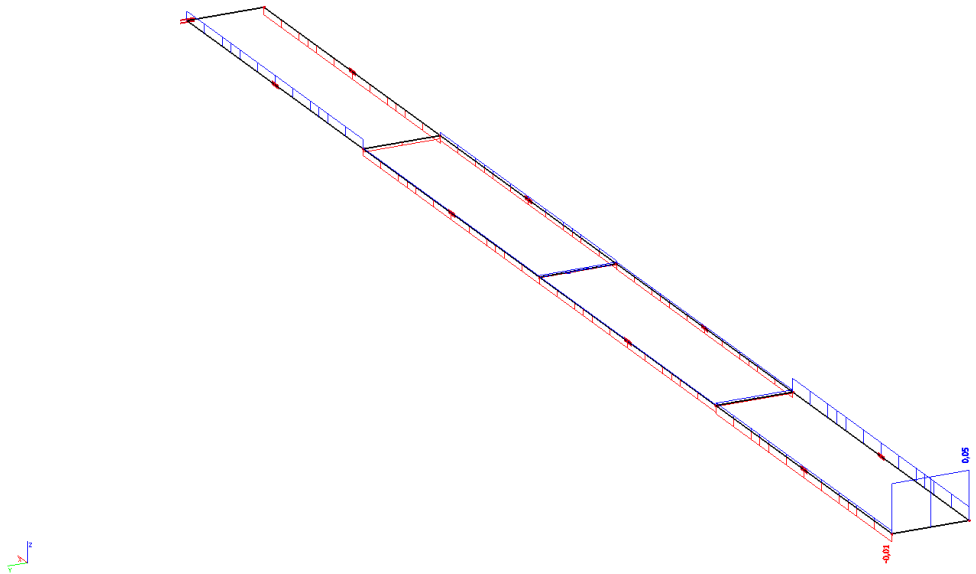

Figure C.1: Mx at access bridge, superstructure

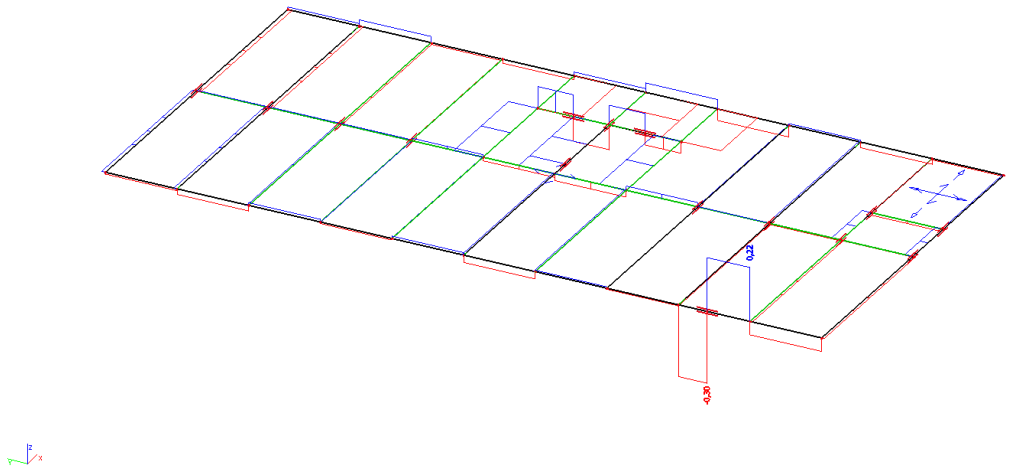

Figure C.2: Mx at platform, superstructure

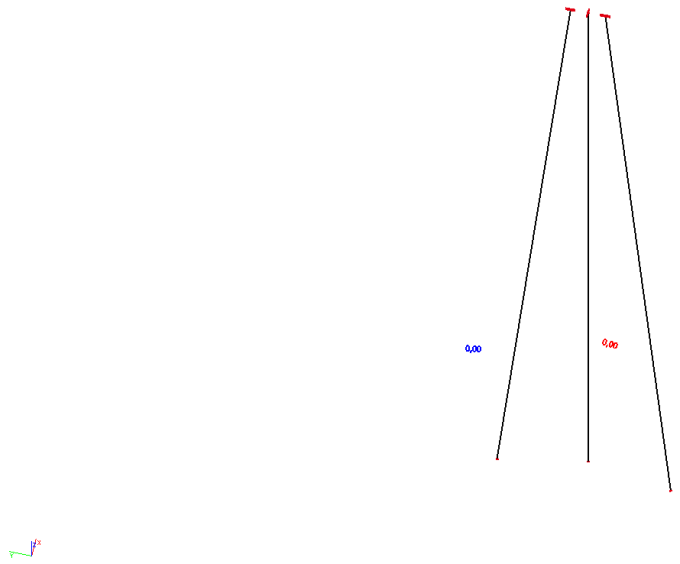

Figure C.3: Mx, piles at platform, piles under load arm

C.0.2. My

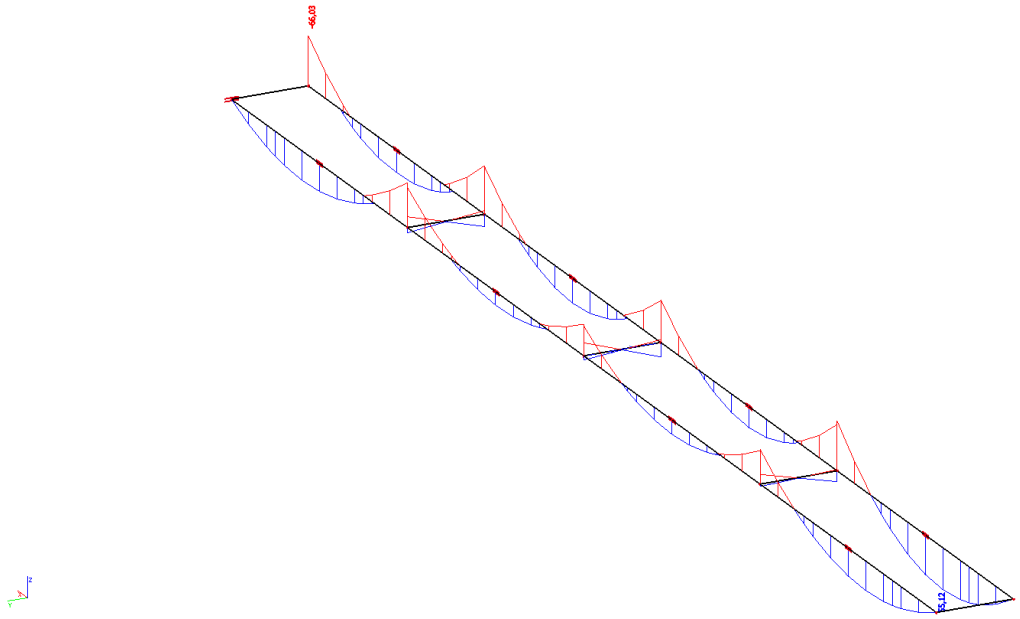

Figure C.4: My at access bridge, superstructure

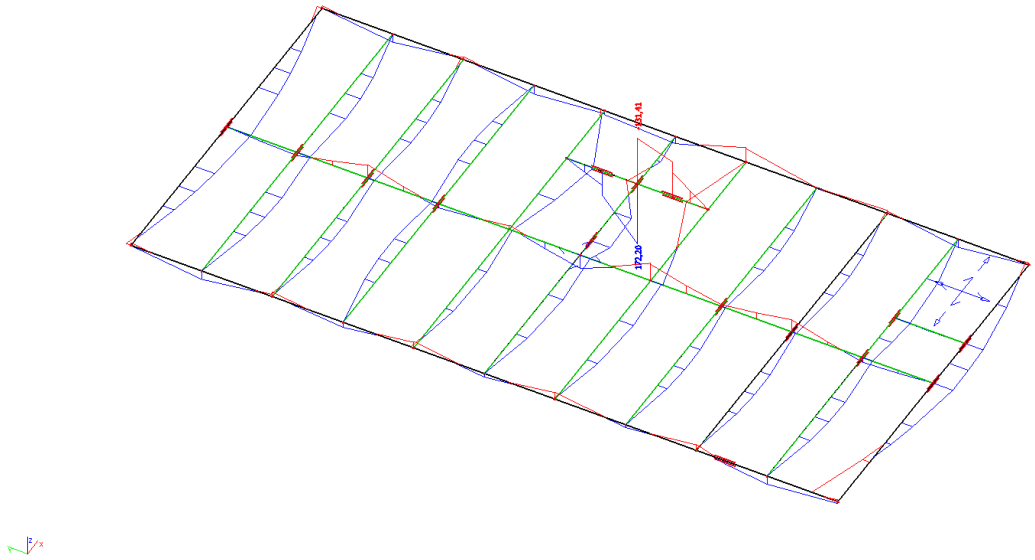

Figure C.5: My at platform, superstructure

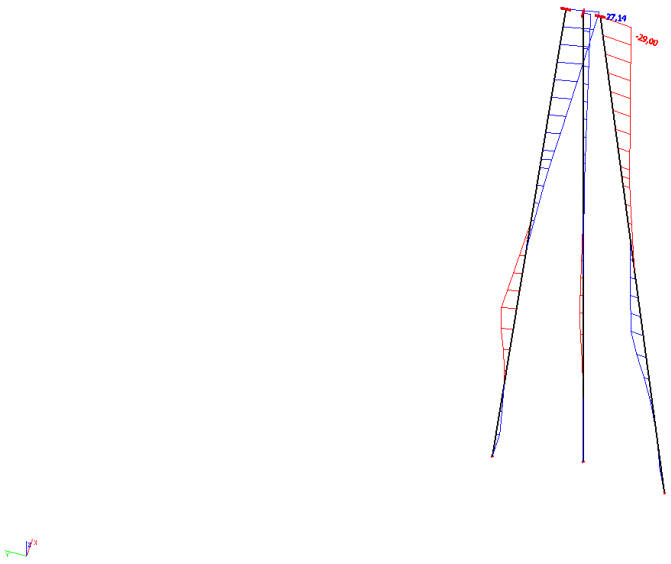

Figure C.6: My, piles at platform, piles under load arm

C.0.3. Mz

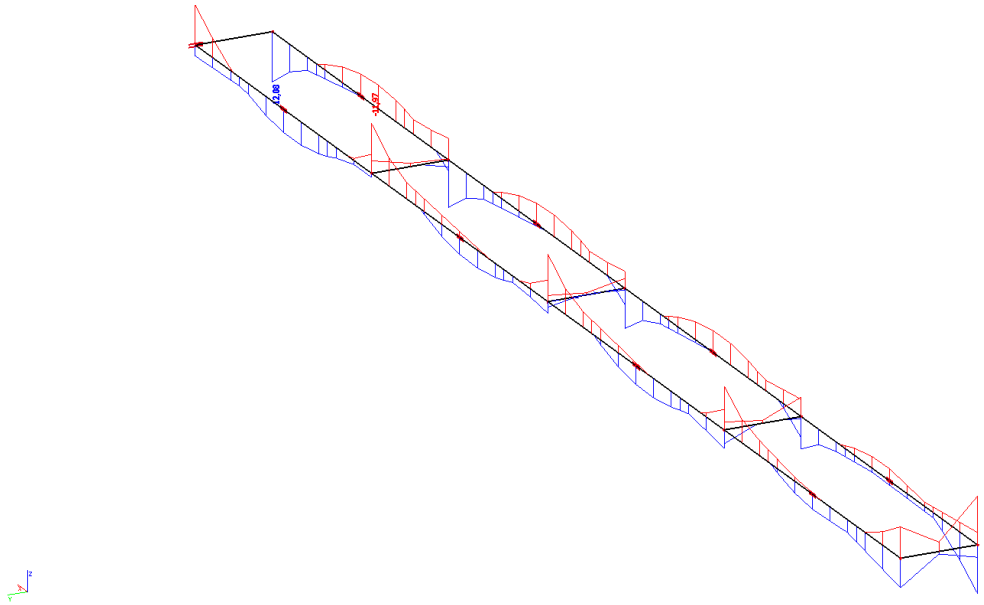

Figure C.7: Mz at access bridge, superstructure

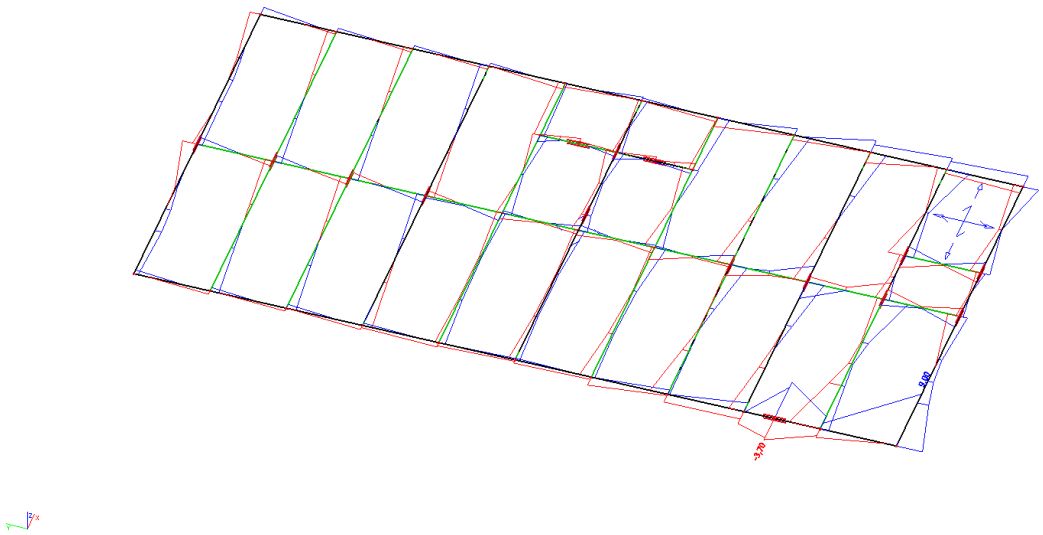

Figure C.8: Mz at platform, superstructure

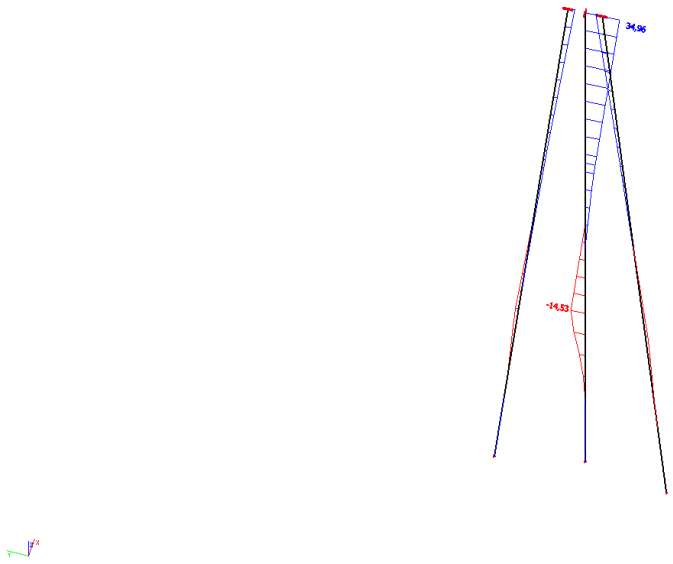

Figure C.9: Mz, piles at platform, piles under load arm

C.0.4. N

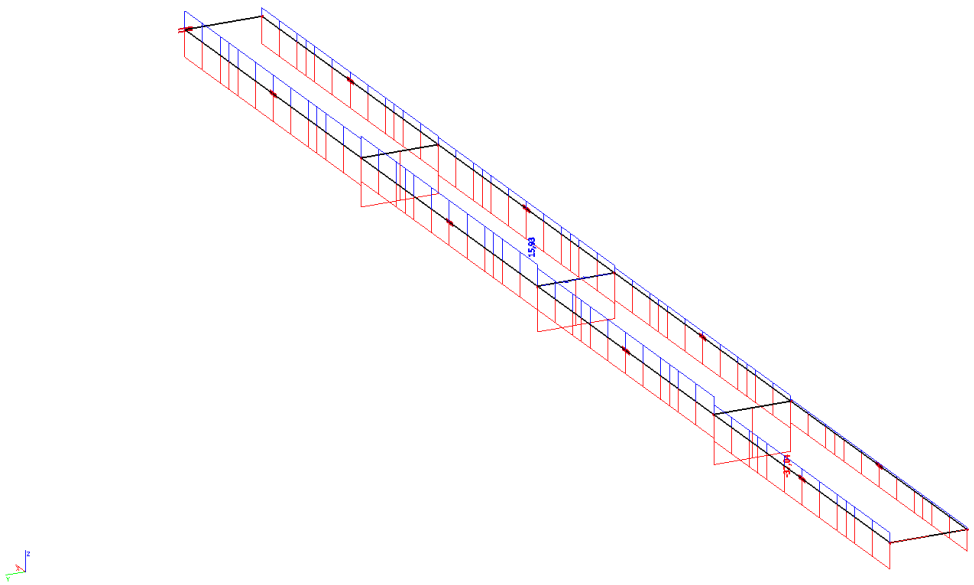

Figure C.10: N at access bridge, superstructure

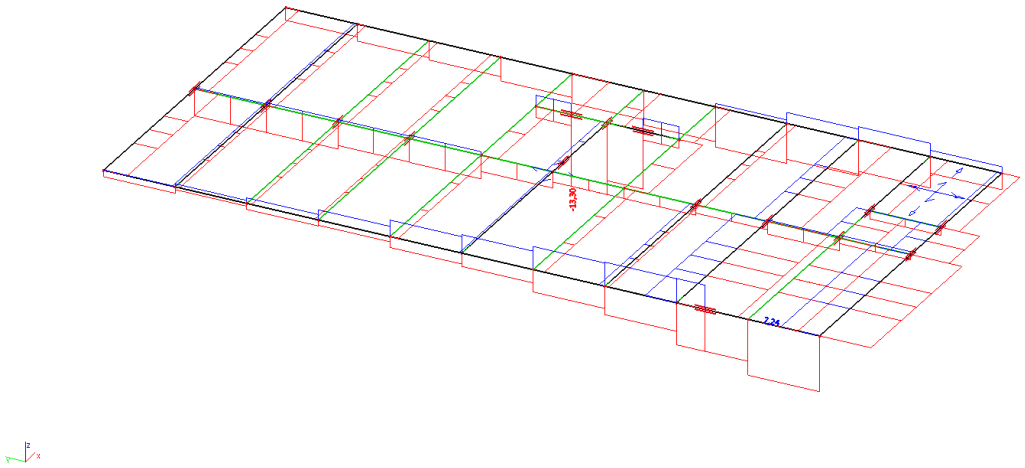

Figure C.11: N at platform, superstructure

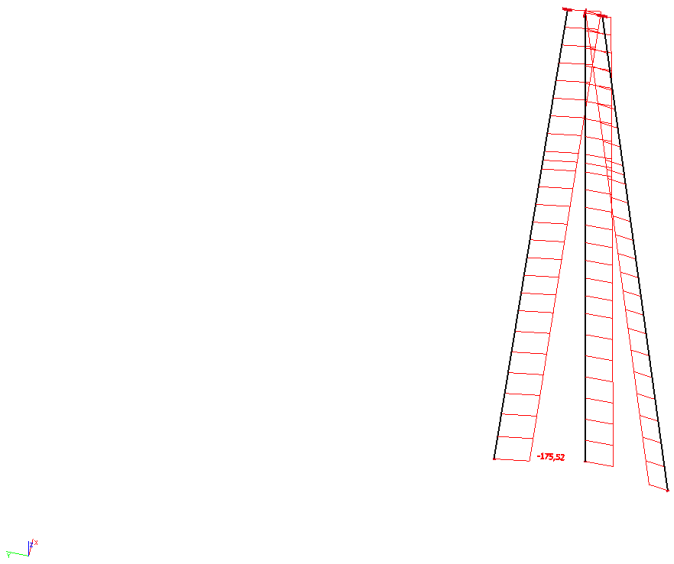

Figure C.12: N, piles at platform, piles under load arm

C.0.5. Vy

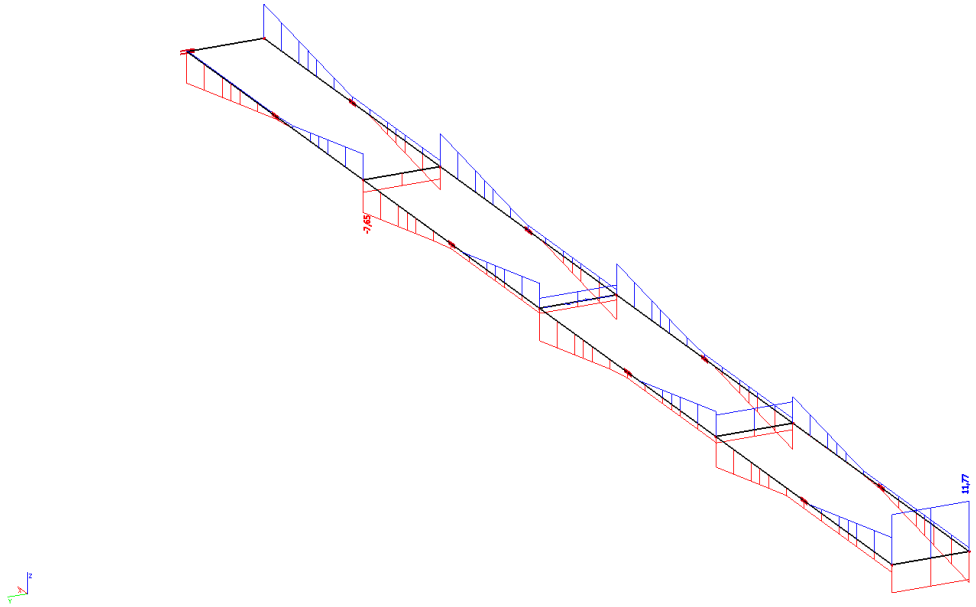

Figure C.13: Vy at access bridge, superstructure

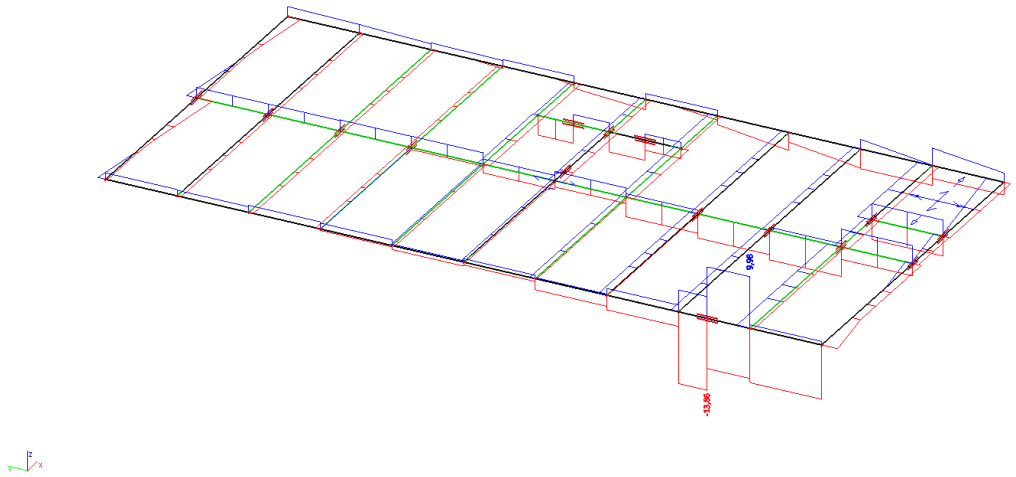

Figure C.14: Vy at platform, superstructure

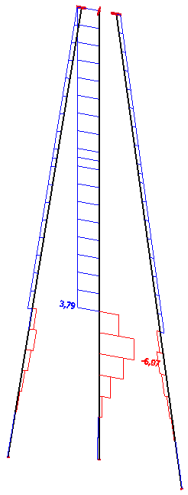

Figure C.15: Vy, piles at platform, piles under load arm

C.0.6. Vz

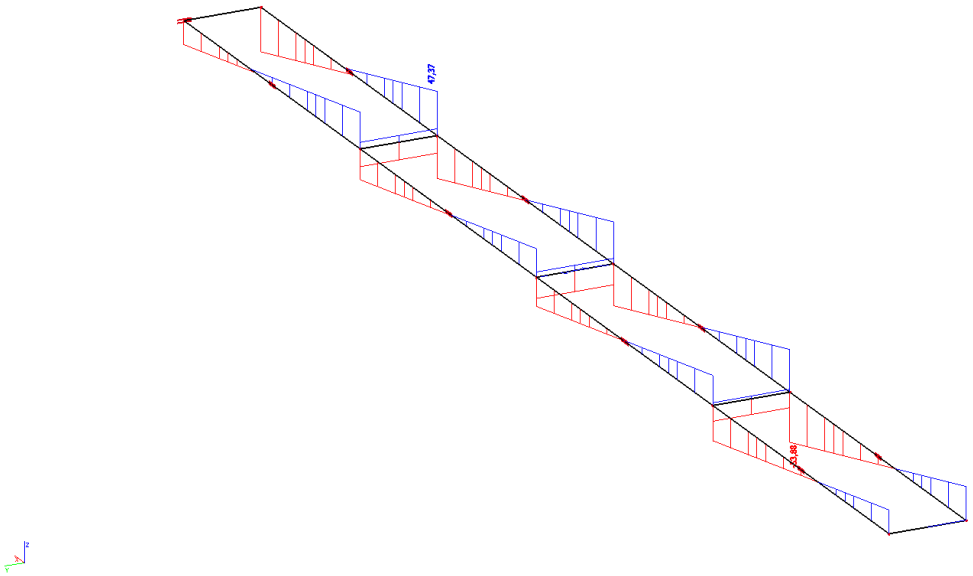

Figure C.16: Vz at access bridge, superstructure

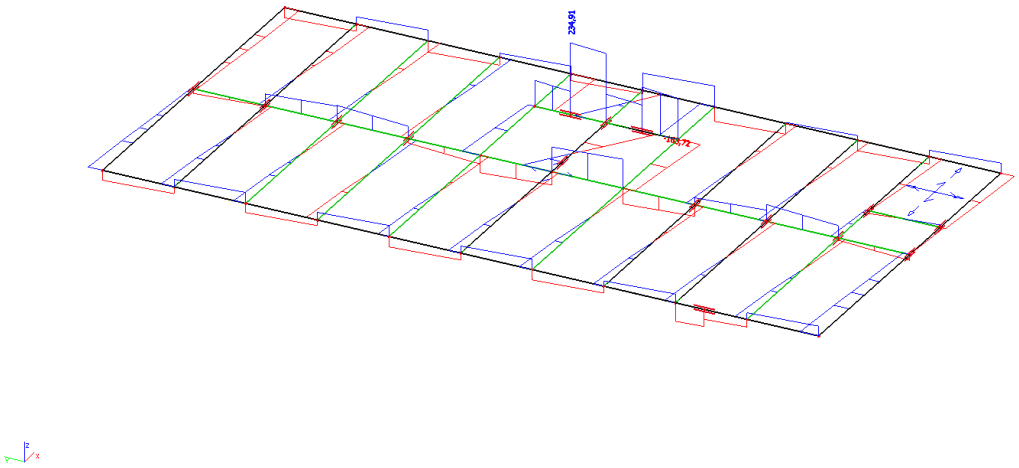

Figure C.17: Vz at platform, superstructure

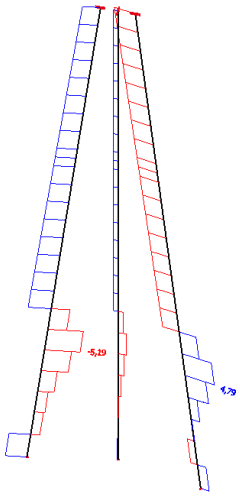

Figure C.18: Vz, piles at platform, piles under load arm

D

Dimensions and properties of structural elements

D.1. Material properties of the structural elements

Beam 1 - access bridge

profile dimensions				laminate - flange			
h	481 [mm]	Ex	31974 [Mpa]	D11	5,0332E-02 [MNm]	d11	893,4763 [MN/m]
b	300 [mm]	Ey	20850 [Mpa]	D22	3,2821E-02 [MNm]	d22	582,617 [MN/m]
tf	26 [mm]	Gxy	7142 [Mpa]	D12	1,0719E-11 [MNm]	d33	185,6871 [MN/m]
tw	14 [mm]			D33	1,0460E-02 [MNm]	d12	190,2832 [MN/m]
A	21607 [mm2]	Vxy	0,33 [-]	D44	3,1333E-04 [MNm]		
		Vyx	0,21 [-]	D55	2,2346E-04 [MNm]		
moment of inertia parameters				laminate - web			
Iy, flange	404300540 [mm4]	Ex	20551 [Mpa]	D11	5,4514E-03 [MNm]	d11	333,7597 [MN/m]
Iy, web	92171475 [mm4]	Ey	24379 [Mpa]	D22	6,4669E-03 [MNm]	d22	395,9315 [MN/m]
Iz, flange	58500000 [mm4]	Gxy	9468 [Mpa]	D12	2,2054E-12 [MNm]	d33	132,5495 [MN/m]
Iz, web	98119 [mm4]			D33	2,1650E-03 [MNm]	d12	135,0244 [MN/m]
Iy	0,0009008 [m4]	Vxy	0,341 [-]	D44	1,0727E-04 [MNm]		
		Vyx	0,405 [-]	D55	1,2150E-04 [MNm]		

crossection properties				SLS crossection properties			
web neglected		web not neglected		web not neglected			
Wy	3361527 [mm3]	Wy	3744704 [mm3]	ΣEI,y	19716104,7 [Nm2]	ΣGA,z	42860476 [N]
Wz	780000 [mm3]	Wz	780654 [mm3]	ΣEI,z	2659500 [Nm2]	ΣGA,y	79161343 [N]
ΣEI,y	2,585E+13 [Nmm2]	ΣEI,y	2,7749E+13 [Nmm2]	Reduced property input for SCIA			
ΣEI,z	3,741E+12 [Nmm2]	ΣEI,z	3,743E+12 [Nmm2]	flange		web	
		Av,z	6371,28106 [mm2]	E,SCIA	22719 [Mpa]	E,SCIA	14602 [Mpa]
		Av,y	15600 [mm2]	G,SCIA	5074 [Mpa]	G,SCIA	6727 [Mpa]
ratio My,Rd/Vz,Rd		ΣGA,z	60322151 [N]	Bending stiffness for lateral torsion			
1,34		ΣGA,y	111412260 [N]	ΣEyIz	2,4418E+12 [Nmm2]		

Stability parameters							
b	150 [mm]	c,my	0,9 [-]	Lateral torsion buckling			
bw	455 [mm]	c,mz	0,9 [-]	C1	1,132 [-]	αf	0,5 [-]
ξ	3 [-]	c,mLT	0,9 [-]	k	1 [-]	λ,LT,f,0	0,5 [-]
q	0,036 [-]	kyy	0,90 [-]	It	3931457,03 [mm4]	Lcr	7500 [mm]
p	0,302 [-]	kyz	0,90 [-]	Iw	6,0579E+12 [mm6]	M,cr	166 [kNm]
f_c,stab,k,f	227 [MPa]	kzy	0,72 [-]	Local flange wrinkling		Local web wrinkling	
f_c,stab,k,v	82 [MPa]	kzz	0,90 [-]	λf,f,LT	2,26 [-]	λf,w,LT	1,36 [-]
ρ,f	0,59 [-]			Φ,f,LT	3,39 [-]	Φ,w,LT	1,58 [-]
ρ,w	0,21 [-]			χ,f,LT	0,17 [-]	χ,w,LT	0,42 [-]
				χ,LT	0,17		

Buckling							
Around strong - axis				Around weak - axis			
L	7,5 [m]	αf	0,50 [-]	L	7,5 [m]	αf	0,75 [-]
K	1 [m]	λf,0	0,50 [-]	K	1 [m]	λf,0	0,50 [-]
		Ncr	4869 [kN]			Ncr	657 [kN]
Local flange wrinkling		Local web wrinkling		Local flange wrinkling		Local web wrinkling	
λf,f	1,00 [-]	λf,w	0,60 [-]	λf,f	2,74 [-]	λf,w	1,64 [-]
Φ,f	1,13 [-]	Φ,w	0,71 [-]	Φ,f	5,08 [-]	Φ,w	2,27 [-]
χ,f	0,61 [-]	χ,w	0,93 [-]	χ,f	0,11 [-]	χ,w	0,26 [-]
Nb,z,f,Rd	1177 [kN]	Nb,z,w,R	647 [kN]	Nb,y,f,Rd	230 [kN]	Nb,y,w,Rd	201 [kN]

Resistance

ηc	0,71 [-]	γM	1,62 [-]

Flange		Web					
fxt,k	384 [MPa]	fxt,k	247 [MPa]	Nc,Rd	3275 [kN]	Nb,z,Rd	647 [kN]
fxc,k	384 [MPa]	fxc,k	247 [MPa]	My,Rd	566 [kNm]	Nb,y,Rd	201 [kN]
fyt,k	250 [MPa]	fyt,k	293 [MPa]	Mz,Rd	131 [kNm]	Nb,Rd	201 [kN]
fyc,k	250 [MPa]	fyc,k	293 [MPa]	Vz,Rd	423 [kN]	Mb,Rd	63 [kNm]
τxy,k,flang	114 [MPa]	τxy,k,web	151 [MPa]	Vy,Rd	782 [kN]		
				ILSS	8,77 [MPa]		

Beam 2 - platform

profile dimensions				laminate - flange			
h	509 [mm]	Ex	31974 [Mpa]	D11	5,03E-02 [MNm]	d11	893,4763 [MN/m]
b	300 [mm]	Ey	20850 [Mpa]	D22	3,28E-02 [MNm]	d22	582,617 [MN/m]
tf	26 [mm]	Gxy	7142 [Mpa]	D12	1,07E-11 [MNm]	d33	185,6871 [MN/m]
tw	14 [mm]			D33	1,05E-02 [MNm]	d12	190,2832 [MN/m]
A	22001 [mm2]	νxy	0,327 [-]	D44	3,13E-04 [MNm]		
		νyx	0,213 [-]	D55	2,23E-04 [MNm]		

moment of inertia parameters		laminate - web					
Iy, flange	455730837 [mm4]	Ex	20551 [Mpa]	D11	5,45E-03 [MNm]	d11	333,7597 [MN/m]
Iy, web	111497998 [mm4]	Ey	24379 [Mpa]	D22	6,47E-03 [MNm]	d22	395,9315 [MN/m]
Iz, flange	58500000 [mm4]	Gxy	9468 [Mpa]	D12	2,21E-12 [MNm]	d33	132,5495 [MN/m]
Iz, web	104547 [mm4]			D33	2,16E-03 [MNm]	d12	135,0244 [MN/m]
Iy	0,001023 [m4]	νxy	0,341 [-]	D44	1,07E-04 [MNm]		
		νyx	0,405 [-]	D55	1,21E-04 [MNm]		

crossection properties				SLS crossection properties			
web neglected		web not neglected		web not neglected			
Wy	3579971 [mm3]	Wy	4017905 [mm3]	ΣEI,y	22335150,3 [Nm2]	ΣGA,z	45507785 [N]
Wz	780000 [mm3]	Wz	780697 [mm3]	ΣEI,z	2659594 [Nm2]	ΣGA,y	79161343 [N]
ΣEI,y	2,914E+13 [Nmm2]	ΣEI,y	3,1435E+13 [Nmm2]	Reduced property input for SCIA			
ΣEI,z	3,741E+12 [Nmm2]	ΣEI,z	3,7431E+12 [Nmm2]	flange		web	
		Av,z	6764,80794 [mm2]	E,SCIA	22719 [Mpa]	E,SCIA	14602 [Mpa]
		Av,y	15600 [mm2]	G,SCIA	5074 [Mpa]	G,SCIA	6727 [Mpa]
ratio My,Rd/Vz,Rd		ΣGA,z	64047994 [N]	Bending stiffness for lateral torsion			
1,34		ΣGA,y	111412260 [N]	ΣEyIz	2,442E+12 [Nmm2]		

Stability parameters							
b	150 [mm]	c,my	0,9 [-]	Lateral torsion buckling			
bw	483 [mm]	c,mz	0,9 [-]	C1	1,132 [-]	αf	0,5 [-]
ξ	3 [-]	c,mLT	0,9 [-]	k	1 [-]	λ,LT,f,0	0,5 [-]
q	0,035 [-]	kyy	0,90 [-]	It	3957167,45 [mm4]	Lcr	7500 [mm]
p	0,301 [-]	kyz	0,90 [-]	Iw	6,8294E+12 [mm6]	M,cr	171 [kNm]
f_c,stab,k,f	225 [MPa]	kzy	0,72 [-]	Local flange wrinkling		Local web wrinkling	
f_c,stab,k,w	72 [MPa]	kzz	0,90 [-]	λf,f,LT	2,30 [-]	λf,w,LT	1,30 [-]
ρ,f	0,59 [-]			Φ,f,LT	3,48 [-]	Φ,w,LT	1,50 [-]
ρ,w	0,19 [-]			χ,f,LT	0,16 [-]	χ,w,LT	0,45 [-]
				χ,LT	0,16		

Buckling							
Around strong - axis				Around weak - axis			
L	5 [m]	αf	0,50 [-]	L	5 [m]	αf	0,75 [-]
K	1 [m]	λf,0	0,50 [-]	K	1 [m]	λf,0	0,50 [-]
		Ncr	12410 [kN]			Ncr	1478 [kN]
Local flange wrinkling		Local web wrinkling		Local flange wrinkling		Local web wrinkling	
λf,f	0,63 [-]	λf,w	0,36 [-]	λf,f	1,83 [-]	λf,w	1,04 [-]
Φ,f	0,73 [-]	Φ,w	0,53 [-]	Φ,f	2,67 [-]	Φ,w	1,24 [-]
χ,f	0,91 [-]	χ,w	1,09 [-]	χ,f	0,22 [-]	χ,w	0,52 [-]
Nb,z,f,Rd	1763 [kN]	Nb,z,w,R	683 [kN]	Nb,y,f,Rd	470 [kN]	Nb,y,w,Rd	364 [kN]

Resistance

ηc	0,71 [-]	γM	1,62 [-]				
Flange		Web		Nc,Rd	3318 [kN]	Nb,z,Rd	683 [kN]
fxt,k	384 [MPa]	fxt,k	247 [MPa]	My,Rd	602 [kNm]	Nb,y,Rd	364 [kN]
fxc,k	384 [MPa]	fxc,k	247 [MPa]	Mz,Rd	131 [kNm]	Nb,Rd	364 [kN]
fyt,k	250 [MPa]	fyt,k	293 [MPa]	Vz,Rd	449 [kN]	Mb,Rd	65 [kNm]
fyc,k	250 [MPa]	fyc,k	293 [MPa]	Vy,Rd	782 [kN]		
τxy,k	114 [MPa]	τxy,k,web	151 [MPa]	ILSS	8,77		

Beam 3 - platform, loading arm

profile dimensions				laminate - flange			
h	509 [mm]	Ex	31974 [Mpa]	D11	5,03E-02 [MNm]	d11	893,4763 [MN/m]
b	300 [mm]	Ey	20850 [Mpa]	D22	3,28E-02 [MNm]	d22	582,617 [MN/m]
tf	26 [mm]	Gxy	7142 [Mpa]	D12	1,07E-11 [MNm]	d33	185,6871 [MN/m]
tw	14 [mm]			D33	1,05E-02 [MNm]	d12	190,2832 [MN/m]
A	22001 [mm2]	Vxy	0,327 [-]	D44	3,13E-04 [MNm]		
		Vyx	0,213 [-]	D55	2,23E-04 [MNm]		
moment of inertia parameters		laminate - web					
Iy, flange	455730837 [mm4]	Ex	20551 [Mpa]	D11	5,45E-03 [MNm]	d11	333,7597 [MN/m]
Iy, web	111497998 [mm4]	Ey	24379 [Mpa]	D22	6,47E-03 [MNm]	d22	395,9315 [MN/m]
Iz, flange	58500000 [mm4]	Gxy	9468 [Mpa]	D12	2,21E-12 [MNm]	d33	132,5495 [MN/m]
Iz, web	104547 [mm4]			D33	2,16E-03 [MNm]	d12	135,0244 [MN/m]
Iy	0,001023 [m4]	Vxy	0,341 [-]	D44	1,07E-04 [MNm]		
		Vyx	0,405 [-]	D55	1,21E-04 [MNm]		

crossection properties				SLS crossection properties			
web neglected		web not neglected		web not neglected			
Wy	3579971 [mm3]	Wy	4017905 [mm3]	ΣEI,y	22335150,3 [Nm2]	ΣGA,z	45507785 [N]
Wz	780000 [mm3]	Wz	780697 [mm3]	ΣEI,z	2659594 [Nm2]	ΣGA,y	79161343 [N]
ΣEI,y	2,914E+13 [Nmm2]	ΣEI,y	3,1435E+13 [Nmm2]	Reduced property input for SCIA			
ΣEI,z	3,741E+12 [Nmm2]	ΣEI,z	3,7431E+12 [Nmm2]	flange		web	
		Av,z	6764,80794 [mm2]	E,SCIA	22718,5228 [Mpa]	E,SCIA	14602 [Mpa]
		Av,y	15600 [mm2]	G,SCIA	5074 [Mpa]	G,SCIA	6727 [Mpa]
ratio My,Rd/Vz,Rd		ΣGA,z	64047994 [N]	Bending stiffness for lateral torsion			
1,34		ΣGA,y	111412260 [N]	ΣEyIz	2,442E+12 [Nmm2]		

Stability parameters							
b	150 [mm]	c,my	0,9 [-]	Lateral torsion buckling			
bw	483 [mm]	c,mz	0,9 [-]	C1	1,132 [-]	αf	0,5 [-]
ξ	3 [-]	c,mLT	0,9 [-]	k	1 [-]	λ,LT,f,0	0,5 [-]
q	0,035 [-]	kyy	0,90 [-]	It	3957167,45 [mm4]	Lcr	2000 [mm]
p	0,301 [-]	kyz	0,90 [-]	Iw	6,8294E+12 [mm6]	M,cr	1712 [kNm]
f_c,stab,k,f	225 [MPa]	kzy	0,72 [-]	Local flange wrinkling		Local web wrinkling	
f_c,stab,k,w	72 [MPa]	kzz	0,90 [-]	λf,f,LT	0,73 [-]	λf,w,LT	0,41 [-]
ρ,f	0,59 [-]			Φ,f,LT	0,81 [-]	Φ,w,LT	0,57 [-]
ρ,w	0,19 [-]			χ,f,LT	0,86 [-]	χ,w,LT	1,04 [-]
				χ,LT	0,86		

Buckling							
Around strong - axis				Around weak - axis			
L	2 [m]	αf	0,50 [-]	L	2 [m]	αf	0,75 [-]
K	1 [m]	λf,0	0,50 [-]	K	1 [m]	λf,0	0,50 [-]
		Ncr	77562 [kN]			Ncr	9236 [kN]
Local flange wrinkling		Local web wrinkling		Local flange wrinkling		Local web wrinkling	
λf,f	0,25 [-]	λf,w	0,14 [-]	λf,f	0,73 [-]	λf,w	0,42 [-]
Φ,f	0,47 [-]	Φ,w	0,42 [-]	Φ,f	0,85 [-]	Φ,w	0,55 [-]
χ,f	1,15 [-]	χ,w	1,22 [-]	χ,f	0,77 [-]	χ,w	1,08 [-]
Nb,z,f,Rd	2244 [kN]	Nb,z,w,R	767 [kN]	Nb,y,f,Rd	1674 [kN]	Nb,y,w,Rd	758 [kN]

Resistance

ηc	0,71 [-]	γM	1,62 [-]

Flange		Web					
fxt,k	384 [MPa]	fxt,k	247 [MPa]	Nc,Rd	3318 [kN]	Nb,z,Rd	767 [kN]
fxc,k	384 [MPa]	fxc,k	247 [MPa]	My,Rd	602 [kNm]	Nb,y,Rd	758 [kN]
fyt,k	250 [MPa]	fyt,k	293 [MPa]	Mz,Rd	131 [kNm]	Nb,Rd	758 [kN]
fyc,k	250 [MPa]	fyc,k	293 [MPa]	Vz,Rd	449 [kN]	Mb,Rd	343 [kNm]
τxy,k	114 [MPa]	τxy,k,web	151 [MPa]	Vy,Rd	782 [kN]		
				ILSS	8,77		

Plank 1 - access bridge

profile dimensions				laminate - flange			
h	36,7 [mm]	Ex	34471 [Mpa]	D11	6,60E-04 [MNm]	d11	220,0002 [MN/m]
b	500 [mm]	Ey	19859 [Mpa]	D22	3,80E-04 [MNm]	d22	126,7424 [MN/m]
tf	6 [mm]	Gxy	6633 [Mpa]	D12	1,23E-13 [MNm]	d33	39,798 [MN/m]
tw	6 [mm]			D33	1,19E-04 [MNm]	d12	40,8586 [MN/m]
A	6594 [mm2]	ν_{xy}	0,322 [-]	D44	7,82E-05 [MNm]		
		ν_{yx}	0,186 [-]	D55	5,02E-05 [MNm]		
moment of inertia parameters		laminate - web					
Iy, flange	717428 [mm4]	Ex	20757 [Mpa]	D11	4,33E-04 [MNm]	d11	144,18 [MN/m]
Iy, web	30263 [mm4]	Ey	24337 [Mpa]	D22	5,07E-04 [MNm]	d22	169,0487 [MN/m]
Iz, flange	62500000 [mm4]	Gxy	9426 [Mpa]	D12	1,73E-13 [MNm]	d33	56,555 [MN/m]
Iz, web	9061753 [mm4]			D33	1,70E-04 [MNm]	d12	57,6156 [MN/m]
# webs	4 [-]	ν_{xy}	0,341 [-]	D44	4,64E-05 [MNm]		
		ν_{yx}	0,400 [-]	D55	5,22E-05 [MNm]		

crossection properties				SLS crossection properties			
web neglected		web not neglected		web not neglected			
Wy	78122 [mm3]	Wy	79769 [mm3]	ΣEI,y	36036 [Nm2]	ΣGA,z	4940018 [N]
Wz	500000 [mm3]	Wz	536247 [mm3]	ΣEI,z	3328900 [Nm2]	ΣGA,y	28277526 [N]
ΣEI,y	4,946E+10 [Nmm2]	ΣEI,y	5,0718E+10 [Nmm2]	Reduced property input for SCIA			
ΣEI,z	4,309E+12 [Nmm2]	ΣEI,z	4,6851E+12 [Nmm2]	flange		web	
		Av,z	737,613078 [mm2]	E,SCIA	24493 [Mpa]	E,SCIA	14749 [Mpa]
		Av,y	6000 [mm2]	G,SCIA	4713 [Mpa]	G,SCIA	6697 [Mpa]
ratio My,Rd/Vz,Rd		ΣGA,z	6952618 [N]	Bending stiffness for lateral torsion			
0,29		ΣGA,y	39798000 [N]	ΣEyIz	2,7029E+12 [Nmm2]		

Stability parameters							
b	83,333333 [mm]	c,my	0,9 [-]	Lateral torsion buckling			
bw	31 [mm]	c,mz	0,9 [-]	C1	1,132 [-]	α_f	0,5 [-]
ξ	0 [-]	c,mLT	0,9 [-]	k	1 [-]	$\lambda_{LT,f,0}$	0,5 [-]
q	0,123 [-]	kyy	0 [-]	It	74212,8392 [mm4]	Lcr	7500 [mm]
p	0,289 [-]	kyz	0 [-]	Iw	2,9518E+10 [mm6]	M,cr	19,04 [kNm]
f_c,stab,k,f	72 [MPa]	kzy	0 [-]	Local flange wrinkling		Local web wrinkling	
f_c,stab,k,w	3287 [MPa]	kzz	0 [-]	$\lambda_{f,f,LT}$	0,55 [-]	$\lambda_{f,w,LT}$	1,32 [-]
ρ_f	0,17 [-]			$\Phi_{f,LT}$	0,66 [-]	$\Phi_{w,LT}$	1,52 [-]
ρ_w	1,00 [-]			$\chi_{f,LT}$	0,98 [-]	$\chi_{w,LT}$	0,44 [-]
				χ_{LT}	0,44		

Buckling							
Around strong - axis				Around weak - axis			
L	1,6 [m]	α_f	0,50 [-]	L	1,6 [m]	α_f	0,75 [-]
K	1 [m]	$\lambda_{f,0}$	0,50 [-]	K	1 [m]	$\lambda_{f,0}$	0,50 [-]
		Ncr	196 [kN]			Ncr	18063 [kN]
Local flange wrinkling		Local web wrinkling		Local flange wrinkling		Local web wrinkling	
$\lambda_{f,f}$	1,56 [-]	$\lambda_{f,w}$	3,73 [-]	$\lambda_{f,f}$	0,16 [-]	$\lambda_{f,w}$	0,39 [-]
$\Phi_{,f}$	1,97 [-]	$\Phi_{,w}$	8,28 [-]	$\Phi_{,f}$	0,39 [-]	$\Phi_{,w}$	0,53 [-]
$\chi_{,f}$	0,31 [-]	$\chi_{,w}$	0,06 [-]	$\chi_{,f}$	1,36 [-]	$\chi_{,w}$	1,11 [-]
$N_{b,z,f,Rd}$	60 [kN]	$N_{b,z,w,R}$	70 [kN]	$N_{b,y,f,Rd}$	282 [kN]	$N_{b,y,w,Rd}$	1330 [kN]

Resistance

η_c	0,71 [-]	γ_M	1,62 [-]

Flange		Web					
$f_{xt,k}$	414 [MPa]	$f_{xt,k}$	249 [MPa]	$N_{c,Rd}$	1105 [kN]	$N_{b,z,Rd}$	60 [kN]
$f_{xc,k}$	414 [MPa]	$f_{xc,k}$	249 [MPa]	$M_{y,Rd}$	14 [kNm]	$N_{b,y,Rd}$	282 [kN]
$f_{yt,k}$	238 [MPa]	$f_{yt,k}$	292 [MPa]	$M_{z,Rd}$	91 [kNm]	$N_{b,Rd}$	60 [kN]
$f_{yc,k}$	238 [MPa]	$f_{yc,k}$	292 [MPa]	$V_{z,Rd}$	49 [kN]	$M_{b,Rd}$	1 [kNm]
$\tau_{xy,k}$	106 [MPa]	$\tau_{xy,k,web}$	151 [MPa]	$V_{y,Rd}$	279 [kN]		
				ILSS	8,77		

Plank 2 - platform

profile dimensions				laminate - flange			
h	79,9 [mm]	Ex	30864 [Mpa]	D11	2,03E-03 [MNm]	d11	300,0713 [MN/m]
b	400 [mm]	Ey	21272 [Mpa]	D22	1,40E-03 [MNm]	d22	206,8135 [MN/m]
tf	9 [mm]	Gxy	7368 [Mpa]	D12	4,58E-13 [MNm]	d33	66,3116 [MN/m]
tw	9 [mm]			D33	4,48E-04 [MNm]	d12	67,9025 [MN/m]
A	9428 [mm2]	ν_{xy}	0,328 [-]	D44	1,05E-04 [MNm]		
		ν_{yx}	0,226 [-]	D55	7,81E-05 [MNm]		
moment of inertia parameters				laminate - web			
Iy, flange	4546904 [mm4]	Ex	20029 [Mpa]	D11	1,42E-03 [MNm]	d11	210,2241 [MN/m]
Iy, web	711118 [mm4]	Ey	24469 [Mpa]	D22	1,73E-03 [MNm]	d22	256,8219 [MN/m]
Iz, flange	48000000 [mm4]	Gxy	9569 [Mpa]	D12	5,92E-13 [MNm]	d33	86,1244 [MN/m]
Iz, web	21300713 [mm4]			D33	5,81E-04 [MNm]	d12	87,7179 [MN/m]
# webs	4 [-]	ν_{xy}	0,342 [-]	D44	6,72E-05 [MNm]		
		ν_{yx}	0,417 [-]	D55	7,77E-05 [MNm]		

crossection properties				SLS crossection properties			
web neglected		web not neglected		web not neglected			
Wy	227664 [mm3]	Wy	245467 [mm3]	ΣEI,y	219665,451 [Nm2]	ΣGA,z	17351595 [N]
Wz	480000 [mm3]	Wz	586504 [mm3]	ΣEI,z	2711534 [Nm2]	ΣGA,y	37692909 [N]
ΣEI,y	2,807E+11 [Nmm2]	ΣEI,y	3,0916E+11 [Nmm2]	Reduced property input for SCIA			
ΣEI,z	2,963E+12 [Nmm2]	ΣEI,z	3,8162E+12 [Nmm2]	flange		web	
		Av,z	2552 [mm2]	E,SCIA	21930 [Mpa]	E,SCIA	14231 [Mpa]
		Av,y	7200 [mm2]	G,SCIA	5235 [Mpa]	G,SCIA	6799 [Mpa]
ratio My,Rd/Vz,Rd		ΣGA,z	24420763 [N]	Bending stiffness for lateral torsion			
0,22		ΣGA,y	53049280 [N]	ΣEyIz	2,5633E+12 [Nmm2]		

Stability parameters							
b	200 [mm]	c,my	0,9 [-]	Lateral torsion buckling			
bw	71 [mm]	c,mz	0,9 [-]	C1	1,132 [-]	αf	0,5 [-]
ξ	0 [-]	c,mLT	0,9 [-]	k	1 [-]	λ,LT,f,0	0,5 [-]
q	0,092 [-]	kyy	0 [-]	It	211625,796 [mm4]	Lcr	7500 [mm]
p	0,273 [-]	kyz	0 [-]	Iw	1,206E+11 [mm6]	M,cr	34,14 [kNm]
f_c,stab,k,f	24 [MPa]	kzy	0 [-]	Local flange wrinkling		Local web wrinkling	
f_c,stab,k,w	1393 [MPa]	kzz	0 [-]	λf,f,LT	0,42 [-]	λf,w,LT	3,16 [-]
ρ,f	0,07 [-]			Φ,f,LT	0,57 [-]	Φ,w,LT	6,01 [-]
ρ,w	3,76 [-]			χ,f,LT	1,04 [-]	χ,w,LT	0,09 [-]
				χ,LT	0,09		

Buckling							
Around strong - axis				Around weak - axis			
L	2 [m]	αf	0,50 [-]	L	2 [m]	αf	0,75 [-]
K	1 [m]	λf,0	0,50 [-]	K	1 [m]	λf,0	0,50 [-]
		Ncr	763 [kN]			Ncr	9416 [kN]
Local flange wrinkling		Local web wrinkling		Local flange wrinkling		Local web wrinkling	
λf,f	0,55 [-]	λf,w	4,15 [-]	λf,f	0,16 [-]	λf,w	1,18 [-]
Φ,f	0,66 [-]	Φ,w	10,02 [-]	Φ,f	0,38 [-]	Φ,w	1,45 [-]
χ,f	0,97 [-]	χ,w	0,05 [-]	χ,f	1,36 [-]	χ,w	0,43 [-]
Nb,z,f,Rd	78 [kN]	Nb,z,w,R	241 [kN]	Nb,y,f,Rd	137 [kN]	Nb,y,w,Rd	2506 [kN]

Resistance

ηc	0,71 [-]	γM	1,62 [-]

Flange		Web					
fxt,k	370 [MPa]	fxt,k	240 [MPa]	Nc,Rd	1228 [kN]	Nb,z,Rd	78 [kN]
fxc,k	370 [MPa]	fxc,k	240 [MPa]	My,Rd	37 [kNm]	Nb,y,Rd	137 [kN]
fyt,k	255 [MPa]	fyt,k	294 [MPa]	Mz,Rd	78 [kNm]	Nb,Rd	78 [kN]
fyc,k	255 [MPa]	fyc,k	294 [MPa]	Vz,Rd	171 [kN]	Mb,Rd	0 [kNm]
τxy,k	118 [MPa]	τxy,k,web	153 [MPa]	Vy,Rd	372 [kN]		
				ILSS	8,77		

Girder 1 - access bridge

profile dimensions				laminate - flange			
h	114 [mm]	Ex	33750 [Mpa]	D11	1,01E-02 [MNm]	d11	540,0242 [MN/m]
b	150 [mm]	Ey	20151 [Mpa]	D22	6,05E-03 [MNm]	d22	322,4227 [MN/m]
tf	15 [mm]	Gxy	6780 [Mpa]	D12	1,96E-12 [MNm]	d33	101,6998 [MN/m]
tw	15 [mm]			D33	1,91E-03 [MNm]	d12	104,3514 [MN/m]
A	5760 [mm2]	Vxy	0,324 [-]	D44	1,91E-04 [MNm]		
		Vyx	0,193 [-]	D55	1,27E-04 [MNm]		
moment of inertia parameters		laminate - web					
Iy, flange	5553752,1 [mm4]	Ex	20223 [Mpa]	D11	6,68E-03 [MNm]	d11	356,0403 [MN/m]
Iy, web	740524 [mm4]	Ey	23754 [Mpa]	D22	7,84E-03 [MNm]	d22	418,2121 [MN/m]
Iz, flange	5727721 [mm4]	Gxy	9720 [Mpa]	D12	2,78E-12 [MNm]	d33	145,7971 [MN/m]
Iz, web	2204094 [mm4]			D33	2,73E-03 [MNm]	d12	148,4487 [MN/m]
y'	100,89698 [mm]	Vxy	0,355 [-]	D44	1,12E-04 [MNm]		
		Vyx	0,417 [-]	D55	1,26E-04 [MNm]		

crossection properties				SLS crossection properties			
web neglected		web not neglected		web not neglected			
Wy	194891 [mm3]	Wy	207885 [mm3]	ΣEI,y	277002 [Nm2]	ΣGA,z	10254282 [N]
Wz	152739,22 [mm3]	Wz	182127 [mm3]	ΣEI,z	306376 [Nm2]	ΣGA,y	21678115 [N]
ΣEI,y	3,749E+11 [Nmm2]	ΣEI,y	3,8985E+11 [Nmm2]	Reduced property input for SCIA			
ΣEI,z	3,866E+11 [Nmm2]	ΣEI,z	4,312E+11 [Nmm2]	flange		web	
		Av,z	1484,79825 [mm2]	E,SCIA	23980 [Mpa]	E,SCIA	14369 [Mpa]
		Av,y	4500 [mm2]	G,SCIA	4817 [Mpa]	G,SCIA	6906 [Mpa]
ratio My,Rd/Vz,Rd		ΣGA,z	14431952 [N]	Bending stiffness for lateral torsion			
0,34		ΣGA,y	30509940 [N]	ΣEyIz	2,8319E+11 [Nmm2]		

Stability parameters							
b	75 [mm]	c,my	0,9 [-]	Lateral torsion buckling			
bw	99 [mm]	c,mz	0,9 [-]	C1	1,132 [-]	αf	0,5 [-]
ξ	1 [-]	c,mLT	0,9 [-]	k	1 [-]	λ,LT,f,0	0,5 [-]
q	0,052 [-]	kyy	0 [-]	It	448859,869 [mm4]	Lcr	7500 [mm]
p	0,305 [-]	kyz	0 [-]	Iw	2,0668E+10 [mm6]	M,cr	14,09 [kNm]
f_c,stab,k,f	361 [MPa]	kzy	0 [-]	Local flange wrinkling		Local web wrinkling	
f_c,stab,k,v	2004 [MPa]	kzz	0 [-]	λf,f,LT	2,31 [-]	λf,w,LT	2,31 [-]
ρ,f	0,89 [-]			Φ,f,LT	3,50 [-]	Φ,w,LT	3,50 [-]
ρ,w	4,95 [-]			χ,f,LT	0,16 [-]	χ,w,LT	0,16 [-]
				χ,LT	0,16		

Buckling							
Around strong - axis				Around weak - axis			
L	2,8 [m]	αf	0,50 [-]	L	2,8 [m]	αf	0,75 [-]
K	1 [m]	λf,0	0,50 [-]	K	1 [m]	λf,0	0,50 [-]
		Ncr	491 [kN]			Ncr	543 [kN]
Local flange wrinkling		Local web wrinkling		Local flange wrinkling		Local web wrinkling	
λf,f	2,06 [-]	λf,w	4,85 [-]	λf,f	1,96 [-]	λf,w	4,61 [-]
Φ,f	3,00 [-]	Φ,w	13,34 [-]	Φ,f	2,96 [-]	Φ,w	12,67 [-]
χ,f	0,19 [-]	χ,w	0,04 [-]	χ,f	0,19 [-]	χ,w	0,04 [-]
Nb,z,f,Rd	160 [kN]	Nb,z,w,R	179 [kN]	Nb,y,f,Rd	176 [kN]	Nb,y,w,Rd	207 [kN]

Resistance

ηc	0,71 [-]	γM	1,62 [-]

Flange		Web					
fxt,k	405 [MPa]	fxt,k	243 [MPa]	Nc,Rd	933 [kN]	Nb,z,Rd	160 [kN]
fxc,k	405 [MPa]	fxc,k	243 [MPa]	My,Rd	35 [kNm]	Nb,y,Rd	176 [kN]
fyt,k	242 [MPa]	fyt,k	285 [MPa]	Mz,Rd	27 [kNm]	Nb,Rd	160 [kN]
fyc,k	242 [MPa]	fyc,k	285 [MPa]	Vz,Rd	101 [kN]	Mb,Rd	5 [kNm]
τxy,k	108 [MPa]	τxy,k,web	156 [MPa]	Vy,Rd	214 [kN]		
				ILSS	8,77		

Girder 2 - not implemented

profile dimensions				laminate - flange			
h	238 [mm]	Ex	33750 [Mpa]	D11	1,01E-02 [MNm]	d11	540,0242 [MN/m]
b	150 [mm]	Ey	20151 [Mpa]	D22	6,05E-03 [MNm]	d22	322,4227 [MN/m]
tf	15 [mm]	Gxy	6780 [Mpa]	D12	1,96E-12 [MNm]	d33	101,6998 [MN/m]
tw	15 [mm]			D33	1,91E-03 [MNm]	d12	104,3514 [MN/m]
A	7625 [mm2]	Vxy	0,324 [-]	D44	1,91E-04 [MNm]		
		Vyx	0,193 [-]	D55	1,27E-04 [MNm]		
moment of inertia parameters		laminate - web					
Iy, flange	28105746 [mm4]	Ex	20223 [Mpa]	D11	6,68E-03 [MNm]	d11	356,0403 [MN/m]
Iy, web	11307541 [mm4]	Ey	23754 [Mpa]	D22	7,84E-03 [MNm]	d22	418,2121 [MN/m]
Iz, flange	7147005 [mm4]	Gxy	9720 [Mpa]	D12	2,78E-12 [MNm]	d33	145,7971 [MN/m]
Iz, web	3144954 [mm4]			D33	2,73E-03 [MNm]	d12	148,4487 [MN/m]
y'	111,07557 [mm]	Vxy	0,355 [-]	D44	1,12E-04 [MNm]		
		Vyx	0,417 [-]	D55	1,26E-04 [MNm]		

crossection properties				SLS crossection properties			
web neglected		web not neglected		web not neglected			
Wy	471647 [mm3]	Wy	566524 [mm3]	ΣEI,y	1510448 [Nm2]	ΣGA,z	23138711 [N]
Wz	190586,8 [mm3]	Wz	232520 [mm3]	ΣEI,z	387965 [Nm2]	ΣGA,y	21678115 [N]
ΣEI,y	1,897E+12 [Nmm2]	ΣEI,y	2,1258E+12 [Nmm2]	Reduced property input for SCIA			
ΣEI,z	4,824E+11 [Nmm2]	ΣEI,z	5,4602E+11 [Nmm2]	flange		web	
		Av,z	3350 [mm2]	E,SCIA	23980 [Mpa]	E,SCIA	14369 [Mpa]
		Av,y	4500 [mm2]	G,SCIA	4817 [Mpa]	G,SCIA	6906 [Mpa]
ratio My,Rd/Vz,Rd		ΣGA,z	32565593 [N]	Bending stiffness for lateral torsion			
0,37		ΣGA,y	30509940 [N]	ΣEyIz	3,6274E+11 [Nmm2]		

Stability parameters							
b	75 [mm]	c,my	0,9 [-]	Lateral torsion buckling			
bw	223 [mm]	c,mz	0,9 [-]	C1	1,132 [-]	αf	0,5 [-]
ξ	3 [-]	c,mLT	0,9 [-]	k	1 [-]	λ,LT,f,0	0,5 [-]
q	0,037 [-]	kyy	0 [-]	It	588782,721 [mm4]	Lcr	7500 [mm]
p	0,302 [-]	kyz	0 [-]	Iw	1,0524E+11 [mm6]	M,cr	18,89 [kNm]
f_c,stab,k,f	303 [MPa]	kzy	0 [-]	Local flange wrinkling		Local web wrinkling	
f_c,stab,k,v	393 [MPa]	kzz	0 [-]	λf,f,LT	3,01 [-]	λf,w,LT	3,43 [-]
ρ,f	0,75 [-]			Φ,f,LT	5,51 [-]	Φ,w,LT	6,95 [-]
ρ,w	0,97 [-]			χ,f,LT	0,10 [-]	χ,w,LT	0,08 [-]
				χ,LT	0,08		

Buckling							
Around strong - axis				Around weak - axis			
L	2 [m]	αf	0,50 [-]	L	2 [m]	αf	0,75 [-]
K	1 [m]	λf,0	0,50 [-]	K	1 [m]	λf,0	0,50 [-]
		Ncr	5245 [kN]			Ncr	1347 [kN]
Local flange wrinkling		Local web wrinkling		Local flange wrinkling		Local web wrinkling	
λf,f	0,66 [-]	λf,w	0,76 [-]	λf,f	1,31 [-]	λf,w	1,49 [-]
Φ,f	0,76 [-]	Φ,w	0,85 [-]	Φ,f	1,66 [-]	Φ,w	1,99 [-]
χ,f	0,88 [-]	χ,w	0,81 [-]	χ,f	0,37 [-]	χ,w	0,30 [-]
Nb,z,f,Rd	746 [kN]	Nb,z,w,R	888 [kN]	Nb,y,f,Rd	378 [kN]	Nb,y,w,Rd	399 [kN]

Resistance

ηc	0,71 [-]	γM	1,62 [-]

Flange		Web					
fxt,k	405 [MPa]	fxt,k	243 [MPa]	Nc,Rd	1132 [kN]	Nb,z,Rd	746 [kN]
fxc,k	405 [MPa]	fxc,k	243 [MPa]	My,Rd	84 [kNm]	Nb,y,Rd	378 [kN]
fyt,k	242 [MPa]	fyt,k	285 [MPa]	Mz,Rd	34 [kNm]	Nb,Rd	378 [kN]
fyc,k	242 [MPa]	fyc,k	285 [MPa]	Vz,Rd	229 [kN]	Mb,Rd	6 [kNm]
τxy,k	108 [MPa]	τxy,k,web	156 [MPa]	Vy,Rd	214 [kN]		
				ILSS	8,77		

Pile 1 - not implemented

Assumptions for the mechanical properties of the piles

vxy = 0,4
Ey = Ex
Lcr =10,4; botom fixed, top fixed in translation but free to rotate
Imperfection factors for a circular profile are equal to those of a square profile

profile dimensions			laminate			moment of inertia parameters			driveability parameters		
d	356	[mm]	Ex	23000	[Mpa]	Iy	206304644	[mm4]	ρ	1927	[m/s]
tf	13	[mm]	Ey	23000	[Mpa]	Iz	206304644	[mm4]	c	3455	[m/s]
r1	165	[mm]	Gxy	8214	[Mpa]	Itorsion	412609288	[mm4]	Z	93	[kg/s]
r2	178	[mm]	Vxy	0,4	[-]	J	819047	[mm4]			
A	14008	[mm2]									

crossection properties						Stability parameters					
Wy	1159015	[mm3]	Av,z	14008	[mm2]	b	343	[mm]	q	1,067	[-]
Wz	1159015	[mm3]	Av,y	14008	[mm2]	ξ	1	[-]	p	1,993	[-]
ΣEI,y	4,745E+12	[Nmm2]	ΣGA,z	115068685	[N]				f_c,stab,k,f	62	[MPa]
ΣEI,z	4,745E+12	[Nmm2]	ΣGA,y	115068685	[N]				ρ,f	0,23	[-]

Buckling

Around x and y axis						Shear influence					
EI	4745007	[Nm2]	zf	1,66	[m]	L	25,5		Ex	2,3E+10	[N/m2]
k	18500000	[N/m3]	e	14,5	[m]	nu	0,4	[-]	Gxz	8,214E+09	[N/m2]
B	0,356	[m]	Lground	11	[m]	b	178	[mm]	Ex/Gxz	2,8	[-]
R	0,9213	[m]	Leff	16,1583503	[m]	a	165	[mm]	A	0,0140084	[m2]
L/R	12	ok; ratio has to be > 4				k	0,58		Iy	0,0002063	[m4]

Local flange wrinkling

αf	0,40	[-]	λf,0	0,50	[-]	λ	96	shear effects not negligible for λ<10

K	L,buck [m]	Ncr [kN]	λf,f	Φ,f	χ,f	Nb,z,Rd [kN]	Model assumption
2	32,3	45	4,41	11,00	0,05	16	free headed
1	16,2	179	2,20	3,27	0,18	60	free in translation but fixed to rotate
0,7071068	11,4	359	1,56	1,93	0,33	111	fixed in translation but free to rotate
0,5	8,1	717	1,10	1,23	0,57	192	fixed

Resistance

ηc	0,63	[-]	γM	1,62	[-]					
fxt,k	276	[Mpa]	Nc	3866	[kN]	Nc,Rd	1507	[kN]	Nb,z,Rd	111 [kN]
fxc,k	276	[Mpa]	My	320	[kNm]	My,Rd	125	[kNm]		
fyt,k	276	[Mpa]	Mz	320	[kNm]	Mz,Rd	125	[kNm]		
fyc,k	276	[Mpa]	Vz	1841	[kN]	Vz,Rd	718	[kN]		
τxy,k	131	[Mpa]	Vy	1841	[kN]	Vy,Rd	718	[kN]		
ILSS	7,80	[MPa]								

Pile 2

Assumptions for the mechanical properties of the piles

vxy = 0,4
Ey = Ex
Lcr =10,72; botom fixed, top fixed in translation but free to rotate
Imperfection factors for a circular profile are equal to those of a square profile

profile dimensions			laminate			moment of inertia parameters			driveability parameters		
d	456	[mm]	Ex	23000	[Mpa]	Iy	565656964	[mm4]	ρ	1927	[m/s]
tf	17	[mm]	Ey	23000	[Mpa]	Iz	565656964	[mm4]	c	3455	[m/s]
r1	211	[mm]	Gxy	8214	[Mpa]	Itorsion	1,131E+09	[mm4]	Z	156	[kg/s]
r2	228	[mm]	vxy	0,4	[-]	J	2346066	[mm4]			
A	23446	[mm2]									

crossection properties						Stability parameters					
Wy	2480952	[mm3]	Av,z	23446	[mm2]	b	439	[mm]	q	1,067	[-]
Wz	2480952	[mm3]	Av,y	23446	[mm2]	ξ	1	[-]	p	1,993	[-]
ΣEI,y	1,301E+13	[Nmm2]	ΣGA,z	192589728	[N]				f_c,stab,k,f	65	[MPa]
ΣEI,z	1,301E+13	[Nmm2]	ΣGA,y	192589728	[N]				ρ,f	0,24	[-]

Buckling

Around x and y axis						Shear influence					
EI	13010110	[Nm2]	zf	2,00589689	[m]	L	18,2	[m]	Ex	2,3E+10	[N/m2]
k	18500000	[N/m3]	e	12,2	[m]	nu	0,4	[-]	Gxz	8,214E+09	[N/m2]
B	0,456	[m]	Lground	6	[m]	b	228	[mm]	Ex/Gxz	2,8	[-]
R	1,1143872	[m]	Leff	14,2058969	[m]	a	211	[mm]	A	0,0234457	[m2]
L/R	5	ok; ratio has to be > 4				k	0,58		Iy	0,0005657	[m4]
Local flange wrinkling											
αf	0,40	[-]	λf,0	0,50	[-]	λ	54	shear effects not negligible for λ<10			

K	L,buck [m]	Ncr [kN]	λf,f	Φ,f	χ,f	Nb,z,Rd [kN]	Model assumption
2	28,4	159	3,09	5,81	0,09	55	free headed
1	14,2	636	1,55	1,91	0,33	197	free in translation but fixed to rotate
0,7071068	10,0	1273	1,09	1,22	0,57	339	fixed in translation but free to rotate
0,5	7,1	2545	0,77	0,85	0,82	489	fixed

Resistance

ηc	0,6315789	[-]	γM	1,62	[-]						
fxt,k	276	[Mpa]	Nc	6471	[kN]	Nc,Rd	2523	[kN]	Nb,z,Rd	339	[kN]
fxc,k	276	[Mpa]	My	685	[kNm]	My,Rd	267	[kNm]	Nb,y,Rd	339	[kN]
fyt,k	276	[Mpa]	Mz	685	[kNm]	Mz,Rd	267	[kNm]			
fyc,k	276	[Mpa]	Vz	3081	[kN]	Vz,Rd	1201	[kN]			
τxy,k	131	[Mpa]	Vy	3081	[kN]	Vy,Rd	1201	[kN]			
ILSS	12	[MPa]									

D.2. Laminates of the structural elements

Laminate name			Beam 1 - flange - v1								
Buildup			[0/-45/90/45/0/45/90/-45/0/45/90/-45/0]s								
Laminate dimensions			ABD matrix						Hygrothermal expansion		
angle [°]	Σti [mm]	%t	893476,3	190283,2	0	0	0	0	αT_x	5,25E-06	[-]
0	14	53,85	190283,2	582617	0	0	0	0	αT_y	1,81E-05	[-]
45	4	15,38	0	0	185687,1	0	0	0	αT_xy	-1,23E-21	[-]
-45	4	15,38	0	0	0	55637818	9563941	209830	β_x	5,62E-02	[-]
90	4	15,38	0	0	0	9563941	29826133	209830	β_y	1,96E-01	[-]
	26		0	0	0	209830	209830	9305027	β_xy	-1,20E-17	[-]

Laminate name			Beam 1 - web - v1								
Buildup			[90/45/0/-45/0/45/90/-45]s								
Laminate dimensions			ABD matrix						Hygrothermal expansion		
angle [°]	Σti [mm]	%t	333759,7	135024,4	0	0	0	0	αT_x	1,37E-05	[-]
0	2	14,29	135024,4	395931,5	0	0	0	0	αT_y	7,84E-06	[-]
45	4	28,57	0	0	132549,5	0	0	0	αT_xy	-1,22E-21	[-]
-45	4	28,57	0	0	0	5302225	1989321	314745,1	β_x	1,48E-01	[-]
90	4	28,57	0	0	0	1989321	7048218	314745,1	β_y	8,44E-02	[-]
	14		0	0	0	314745,1	314745,1	1948899	β_xy	-1,15E-17	[-]

Laminate name			Beam 1 - flange - v1 (identical to flange beam 1)								
Buildup			[0/-45/90/45/0/45/90/-45/0/45/90/-45/0]s								
Laminate dimensions			ABD matrix						Hygrothermal expansion		
angle [°]	Σti [mm]	%t	893476,3	190283,2	0	0	0	0	αT_x	5,25E-06	[-]
0	14	53,85	190283,2	582617	0	0	0	0	αT_y	1,81E-05	[-]
45	4	15,38	0	0	185687,1	0	0	0	αT_xy	-1,23E-21	[-]
-45	4	15,38	0	0	0	55637818	9563941	209830	β_x	5,62E-02	[-]
90	4	15,38	0	0	0	9563941	29826133	209830	β_y	1,96E-01	[-]
	26		0	0	0	209830	209830	9305027	β_xy	-1,20E-17	[-]

Laminate name			Beam 1 - web - v1 (identical to web beam 1)								
Buildup			[90/45/0/-45/0/45/90/-45]s								
Laminate dimensions			ABD matrix						Hygrothermal expansion		
angle [°]	Σti [mm]	%t	333759,7	135024,4	0	0	0	0	αT_x	1,37E-05	[-]
0	2	14,29	135024,4	395931,5	0	0	0	0	αT_y	7,84E-06	[-]
45	4	28,57	0	0	132549,5	0	0	0	αT_xy	-1,22E-21	[-]
-45	4	28,57	0	0	0	5302225	1989321	314745,1	β_x	1,48E-01	[-]
90	4	28,57	0	0	0	1989321	7048218	314745,1	β_y	8,44E-02	[-]
	14		0	0	0	314745,1	314745,1	1948899	β_xy	-1,15E-17	[-]

Laminate name			Plank 1 - flange								
Buildup			[0/-45/90/45/0/45/90/-45/0/45/90/-45/0]s								
Laminate dimensions			ABD matrix						Hygrothermal expansion		
angle [°]	Σti [mm]	%t	220000,2	40858,6	0	0	0	0	αT_x	4,17E-06	[-]
0	3,75	62,50	40858,6	126742,4	0	0	0	0	αT_y	2,06E-05	[-]
45	0,75	12,50	0	0	39798	0	0	0	αT_xy	-1,23E-21	[-]
-45	0,75	12,50	0	0	0	723964,2	108519,9	-546,4	β_x	4,45E-02	[-]
90	0,75	12,50	0	0	0	108519,9	344375,8	-546,4	β_y	2,23E-01	[-]
	6		0	0	0	-546,4	-546,4	105338	β_xy	-1,19E-17	[-]

Laminate name			Plank 1 - web								
Buildup			[90/45/0/-45/0/45/90/-45]s								
Laminate dimensions			ABD matrix						Hygrothermal expansion		
angle [°]	Σti [mm]	%t	144180	57615,6	0	0	0	0	αT_x	1,35E-05	[-]
0	0,9	15,00	57615,6	169048,7	0	0	0	0	αT_y	8,03E-06	[-]
45	1,7	28,33	0	0	56555	0	0	0	αT_xy	-1,39E-21	[-]
-45	1,7	28,33	0	0	0	420860,8	155967,1	24656	β_x	1,46E-01	[-]
90	1,7	28,33	0	0	0	155967,1	552584,9	24656	β_y	8,65E-02	[-]
	6		0	0	0	24656	24656	152785,2	β_xy	-1,31E-17	[-]

Laminate name			Plank 2 - flange								
Buildup			[0/-45/90/45/0/45/90/-45/0/45/90/-45/0]s								
Laminate dimensions			ABD matrix						Hygrothermal expansion		
angle [°]	Σti [mm]	%t	300071,3	67902,5	0	0	0	0	αT_x	5,79E-06	[-]
0	4,5	50,00	67902,5	206813,5	0	0	0	0	αT_y	1,70E-05	[-]
45	1,5	16,67	0	0	66311,6	0	0	0	αT_xy	-1,33E-21	[-]
-45	1,5	16,67	0	0	0	2282793	4021181	-2428,6	β_x	6,21E-02	[-]
90	1,5	16,67	0	0	0	4021181	1251128	-2428,6	β_y	1,85E-01	[-]
	9		0	0	0	-2428,6	-2428,6	391379,1	β_xy	-1,27E-17	[-]

Laminate name			Plank 2 - web								
Buildup			[90/45/0/-45/0/45/90/-45]s								
Laminate dimensions			ABD matrix						Hygrothermal expansion		
angle [°]	Σti [mm]	%t	210224,1	87717,9	0	0	0	0	αT_x	1,43E-05	[-]
0	1,125	12,50	87717,9	256821,9	0	0	0	0	αT_y	7,36E-06	[-]
45	2,625	29,17	0	0	86124,4	0	0	0	αT_xy	-9,76E-22	[-]
-45	2,625	29,17	0	0	0	1377841	533276	84541,8	β_x	1,55E-01	[-]
90	2,625	29,17	0	0	0	533276	1889428	84541,8	β_y	7,93E-02	[-]
	9		0	0	0	84541,8	84541,8	522547,8	β_xy	-1,33E-17	[-]

Laminate name			Girder 1 - flange								
Buildup			[0/-45/90/45/0/45/90/-45/0/45/90/-45/0]s								
Laminate dimensions			ABD matrix						Hygrothermal expansion		
angle [°]	Σti [mm]	%t	540024,2	104351,4	0	0	0	0	αT_x	4,46E-06	[-]
0	9	60,00	104351,4	322422,7	0	0	0	0	αT_y	1,99E-05	[-]
45	2	13,33	0	0	101699,8	0	0	0	αT_xy	-1,18E-21	[-]
-45	2	13,33	0	0	0	10865105	1795267	30114,5	β_x	4,77E-02	[-]
90	2	13,33	0	0	0	1795267	5628421	30114,5	β_y	2,15E-01	[-]
	15		0	0	0	30114,5	30114,5	1745550	β_xy	-1,16E-17	[-]

Laminate name			Girder 1 - web								
Buildup			[90/45/0/-45/0/45/90/-45]s								
Laminate dimensions			ABD matrix						Hygrothermal expansion		
angle [°]	Σti [mm]	%t	356040,3	148448,7	0	0	0	0	αT_x	1,36E-05	[-]
0	2	13,33	148448,7	418212,1	0	0	0	0	αT_y	7,93E-06	[-]
45	4,5	30,00	0	0	145797,1	0	0	0	αT_xy	-1,11E-21	[-]
-45	4,5	30,00	0	0	0	6509123	2521724	412010	β_x	1,47E-01	[-]
90	4	26,67	0	0	0	2521724	8531490	412010	β_y	8,54E-02	[-]
	15		0	0	0	412010	412010	2472006	β_xy	-1,52E-17	[-]

Laminate name			Girder 2 - flange (identical to flange girder 1)								
Buildup			[0/-45/90/45/0/45/90/-45/0/45/90/-45/0]s								
Laminate dimensions			ABD matrix						Hygrothermal expansion		
angle [°]	Σti [mm]	%t	540024,2	104351,4	0	0	0	0	αT_x	4,46E-06	[-]
0	9	60,00	104351,4	322422,7	0	0	0	0	αT_y	1,99E-05	[-]
45	2	13,33	0	0	101699,8	0	0	0	αT_xy	-1,18E-21	[-]
-45	2	13,33	0	0	0	10865105	1795267	30114,5	β_x	4,77E-02	[-]
90	2	13,33	0	0	0	1795267	5628421	30114,5	β_y	2,15E-01	[-]
	15		0	0	0	30114,5	30114,5	1745550	β_xy	-1,16E-17	[-]

Laminate name			Girder 2 - web (identical to web girder 1)								
Buildup			[90/45/0/-45/0/45/90/-45]s								
Laminate dimensions			ABD matrix						Hygrothermal expansion		
angle [°]	Σti [mm]	%t	356040,3	148448,7	0	0	0	0	αT_x	1,36E-05	[-]
0	2	13,33	148448,7	418212,1	0	0	0	0	αT_y	7,93E-06	[-]
45	4,5	30,00	0	0	145797,1	0	0	0	αT_xy	-1,11E-21	[-]
-45	4,5	30,00	0	0	0	6509123	2521724	412010	β_x	1,47E-01	[-]
90	4	26,67	0	0	0	2521724	8531490	412010	β_y	8,54E-02	[-]
	15		0	0	0	412010	412010	2472006	β_xy	-1,52E-17	[-]

D.3. Summary of dimensions of the structural elements: first iteration

Beams

	Beam 1				Beam 2			
	Deformation		Vibrations		Deformation		Vibrations	
	profile dimensions		profile dimensions		profile dimensions		profile dimensions	
h	361,06	[mm]	481,091504	[mm]	492,82	[mm]	509,2	[mm]
b	300	[mm]	300	[mm]	300	[mm]	300	[mm]
tf	26	[mm]	26	[mm]	26	[mm]	26	[mm]
tw	14	[mm]	14	[mm]	14	[mm]	14	[mm]
	laminate - flange		laminate - flange		laminate - flange		laminate - flange	
Ex	22719	[Mpa]	22719	[Mpa]	22719	[Mpa]	22719	[Mpa]
Ey	14814	[Mpa]	14814	[Mpa]	14814	[Mpa]	14814	[Mpa]
Gxy	5074	[Mpa]	5074	[Mpa]	5074	[Mpa]	5074	[Mpa]
vxy	0,33	[-]	0,33	[-]	0,33	[-]	0,33	[-]
	laminate - web		laminate - web		laminate - web		laminate - web	
Ex	14602	[Mpa]	14602	[Mpa]	14602	[Mpa]	14602	[Mpa]
Ey	17322	[Mpa]	17322	[Mpa]	17322	[Mpa]	17322	[Mpa]
Gxy	6727	[Mpa]	6727	[Mpa]	6727	[Mpa]	6727	[Mpa]
vxy	0,34	[-]	0,34	[-]	0,34	[-]	0,34	[-]

Planks

	Plank 1				Plank 2			
	Deformation		Vibrations		Deformation		Vibrations	
	profile dimensions		profile dimensions		profile dimensions		profile dimensions	
h	36,73	[mm]	25,83	[mm]	79,89	[mm]	60,94	[mm]
b	500	[mm]	500	[mm]	400	[mm]	400	[mm]
tf	6	[mm]	6	[mm]	9	[mm]	9	[mm]
tw	6	[mm]	6	[mm]	9	[mm]	9	[mm]
	laminate - flange		laminate - flange		laminate - flange		laminate - flange	
Ex	24493	[Mpa]	24493	[Mpa]	21930	[Mpa]	21930	[Mpa]
Ey	14110	[Mpa]	14110	[Mpa]	15114	[Mpa]	15114	[Mpa]
Gxy	4713	[Mpa]	4713	[Mpa]	5235	[Mpa]	5235	[Mpa]
vxy	0,32	[-]	0,32	[-]	0,34	[-]	0,34	[-]
	laminate - web		laminate - web		laminate - web		laminate - web	
Ex	14749	[Mpa]	14749	[Mpa]	14231	[Mpa]	14231	[Mpa]
Ey	17292	[Mpa]	17292	[Mpa]	17386	[Mpa]	17386	[Mpa]
Gxy	6697	[Mpa]	6697	[Mpa]	6799	[Mpa]	6799	[Mpa]
vxy	0,34	[-]	0,34	[-]	0,34	[-]	0,34	[-]

Girders

	Girder 1				Girder 2			
	Deformation		Vibrations		Deformation		Vibrations	
	profile dimensions		profile dimensions		profile dimensions		profile dimensions	
h	113,99	[mm]	41,47	[mm]	238,36	[mm]	48,71	[mm]
b	150	[mm]	150	[mm]	150	[mm]	150	[mm]
tf	15	[mm]	15	[mm]	15	[mm]	15	[mm]
tw	15	[mm]	15	[mm]	15	[mm]	15	[mm]
	laminate - flange		laminate - flange		laminate - flange		laminate - flange	
Ex	23980	[Mpa]	23980	[Mpa]	23980	[Mpa]	23980	[Mpa]
Ey	14318	[Mpa]	14318	[Mpa]	14318	[Mpa]	14318	[Mpa]
Gxy	4817	[Mpa]	4817	[Mpa]	4817	[Mpa]	4817	[Mpa]
vxy	0,32	[-]	0,32	[-]	0,32	[-]	0,32	[-]
	laminate - web		laminate - web		laminate - web		laminate - web	
Ex	14369	[Mpa]	14369	[Mpa]	14369	[Mpa]	14369	[Mpa]
Ey	16878	[Mpa]	16878	[Mpa]	16878	[Mpa]	16878	[Mpa]
Gxy	6906	[Mpa]	6906	[Mpa]	6906	[Mpa]	6906	[Mpa]
vxy	0,35	[-]	0,35	[-]	0,35	[-]	0,35	[-]

E

SCIA report

1. Table of content

2. General

2.1. Materials

MaterialB

Naam Type	E-mod [MPa] G-mod [MPa]	Poisson - nu	Massa eenheid [kg/m^3]	Log. decrement (niet-uniforme demping enkel)	Specifieke hitte [J/gK]
Beam 1 - flange Algemeen materiaal	2,2719e+04 5,0744e+03	0.326601	2022,0	0.15	6,0000e-01
Beam 1 - web Algemeen materiaal	1,4602e+04 6,7271e+03	0.34103	2022,0	0.15	6,0000e-01
Beam 2 - web Algemeen materiaal	1,4602e+04 6,7271e+03	0.34103	2022,0	0.15	6,0000e-01
Beam 2 - flange Algemeen materiaal	2,2719e+04 5,0744e+03	0.326601	2022,0	0.15	6,0000e-01
Plank 1 - flens Algemeen materiaal	2,4493e+04 4,7129e+03	0.322375	2022,0	0.15	6,0000e-01
Plank 1 - web Algemeen materiaal	1,4749e+04 6,6973e+03	0.340822	2022,0	0.15	6,0000e-01
Plank 2 - flange Algemeen materiaal	2,1930e+04 5,2351e+03	0.341551	2022,0	0.15	6,0000e-01
Plank 2 - web Algemeen materiaal	1,4749e+04 6,6973e+03	0.340822	2022,0	0.15	6,0000e-01
Girder 1 - web Algemeen materiaal	1,4369e+04 6,9062e+03	0.35496	2022,0	0.15	6,0000e-01
Girder 1 - flange Algemeen materiaal	2,3980e+04 4,8174e+03	0.323648	2022,0	0.15	6,0000e-01
Girder 2 - flange Algemeen materiaal	2,3980e+04 4,8174e+03	0.323648	2022,0	0.15	6,0000e-01
Girder 2 - web Algemeen materiaal	1,4369e+04 6,9062e+03	0.35496	2022,0	0.15	6,0000e-01
Pile - Guades Algemeen materiaal	1,4526e+04 5,3603e+03	0.35496	1927,0	0.15	6,0000e-01

2.2. Cross-sections

Beam 1		
Type	Grafische doorsnede	
Vorm type	Dunwandig	
Onderdeelmateriaal	Beam 1 - flange	
	Beam 1 - web	
Bouwwijze	Algemeen	
A [m^2]	1,9460e-02	
A_y [m^2], A_z [m^2]	1,3922e-02	4,2142e-03
A_L [m^2/m], A_D [m^2/m]	2,1340e+00	2,1340e+00
$c_{Y,UCS}$ [mm], $c_{Z,UCS}$ [mm]	150	240
α [deg]	0,00	

I_y [m^4], I_z [m^4]	8,6748e-04	1,1706e-04
i_y [mm], i_z [mm]	211	78
$W_{el.y}$ [m^3], $W_{el.z}$ [m^3]	3,6070e-03	7,8042e-04
$W_{pl.y}$ [m^3], $W_{pl.z}$ [m^3]	4,1931e-03	1,1910e-03
$M_{pl.y.+}$ [Nm], $M_{pl.y.-}$ [Nm]	1,01e+06	1,01e+06
$M_{pl.z.+}$ [Nm], $M_{pl.z.-}$ [Nm]	2,86e+05	2,86e+05
d_y [mm], d_z [mm]	0	0
I_t [m^4], I_w [m^6]	3,4531e-06	6,0452e-06
β_y [mm], β_z [mm]	0	0
Afbeelding	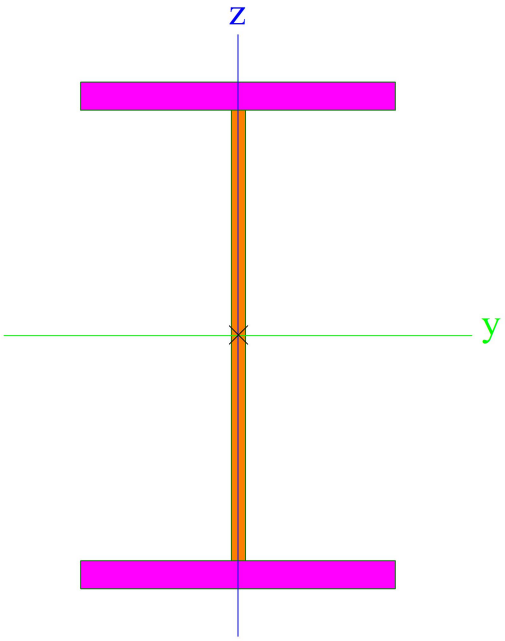	

Beam 2		
Type	1D	
Vorm type	Dunwandig	
Onderdeelmateriaal	Beam 2 - flange	
	Beam 2 - web	
Bouwwijze	Algemeen	
A [m^2]	1,9712e-02	
A_y [m^2], A_z [m^2]	1,3933e-02	4,4564e-03
A_L [m^2/m], A_D [m^2/m]	2,1900e+00	2,1900e+00
$c_{Y.UCS}$ [mm], $c_{Z.UCS}$ [mm]	150	255
α [deg]	0,00	
I_y [m^4], I_z [m^4]	9,8228e-04	1,1707e-04
i_y [mm], i_z [mm]	223	77
$W_{el.y}$ [m^3], $W_{el.z}$ [m^3]	3,8596e-03	7,8045e-04
$W_{pl.y}$ [m^3], $W_{pl.z}$ [m^3]	4,4984e-03	1,1924e-03
$M_{pl.y.+}$ [Nm], $M_{pl.y.-}$ [Nm]	1,08e+06	1,08e+06
$M_{pl.z.+}$ [Nm], $M_{pl.z.-}$ [Nm]	2,86e+05	2,86e+05
d_y [mm], d_z [mm]	0	0
I_t [m^4], I_w [m^6]	3,4679e-06	6,8120e-06
β_y [mm], β_z [mm]	0	0

Afbeelding	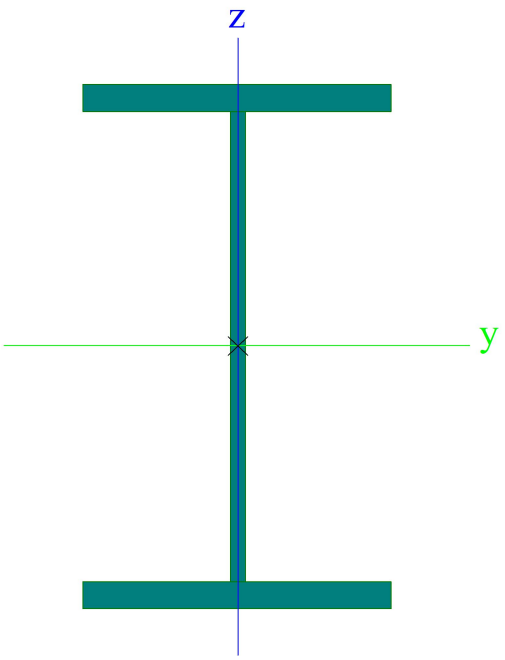		
Plank 1			
Type	1D		
Vorm type	Dunwandig		
Onderdeelmateriaal	Plank 1 - flens		
	Plank 1 - web		
Bouwwijze	Algemeen		
A [m^2]		6,3570e-03	
A_y [m^2], A_z [m^2]		5,2128e-03	5,4402e-04
A_L [m^2/m], A_D [m^2/m]		1,0734e+00	2,1736e+00
$c_{Y.UCS}$ [mm], $c_{Z.UCS}$ [mm]		250	18
α [deg]		0,00	
I_y [m^4], I_z [m^4]		1,4499e-06	1,3713e-04
i_y [mm], i_z [mm]		15	147
$W_{el.y}$ [m^3], $W_{el.z}$ [m^3]		7,9013e-05	5,4851e-04
$W_{pl.y}$ [m^3], $W_{pl.z}$ [m^3]		9,5761e-05	8,4790e-04
$M_{pl.y.+}$ [Nm], $M_{pl.y.-}$ [Nm]		2,30e+04	2,30e+04
$M_{pl.z.+}$ [Nm], $M_{pl.z.-}$ [Nm]		2,03e+05	2,03e+05
d_y [mm], d_z [mm]		0	0
I_t [m^4], I_w [m^6]		4,8838e-06	2,2705e-08
β_y [mm], β_z [mm]		0	0
Afbeelding	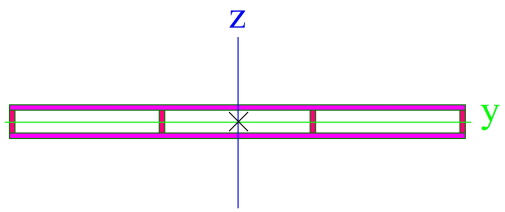		
Plank 2			
Type	1D		
Vorm type	Dunwandig		
Onderdeelmateriaal	Plank 2 - flange		
	Plank 2 - web		
Bouwwijze	Algemeen		
A [m^2]		8,6987e-03	
A_y [m^2], A_z [m^2]		6,6418e-03	1,9478e-03
A_L [m^2/m], A_D [m^2/m]		9,5980e-01	2,0592e+00
$c_{Y.UCS}$ [mm], $c_{Z.UCS}$ [mm]		200	40
α [deg]		0,00	

I_y [m^4], I_z [m^4]	9,5754e-06	1,2798e-04
i_y [mm], i_z [mm]	33	121
$W_{el.y}$ [m^3], $W_{el.z}$ [m^3]	2,3968e-04	6,3992e-04
$W_{pl.y}$ [m^3], $W_{pl.z}$ [m^3]	2,8972e-04	1,0121e-03
$M_{pl.y.+}$ [Nm], $M_{pl.y.-}$ [Nm]	6,95e+04	6,95e+04
$M_{pl.z.+}$ [Nm], $M_{pl.z.-}$ [Nm]	2,43e+05	2,43e+05
d_y [mm], d_z [mm]	0	0
I_t [m^4], I_w [m^6]	2,8032e-05	5,7971e-08
β_y [mm], β_z [mm]	0	0
Afbeelding	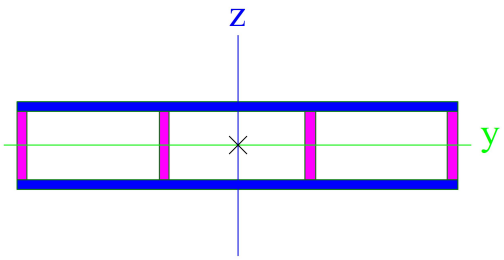	
Girder 1		
Type	1D	
Vorm type	Dunwandig	
Onderdeelmateriaal	Girder 1 - flange	
	Girder 1 - web	
Bouwwijze	Algemeen	
A [m^2]	5,2550e-03	
A_y [m^2], A_z [m^2]	3,9345e-03	9,9465e-04
A_L [m^2/m], A_D [m^2/m]	7,9800e-01	7,9800e-01
$c_{Y.UCS}$ [mm], $c_{Z.UCS}$ [mm]	65	57
α [deg]	0,00	
I_y [m^4], I_z [m^4]	1,1554e-05	1,1397e-05
i_y [mm], i_z [mm]	47	47
$W_{el.y}$ [m^3], $W_{el.z}$ [m^3]	2,0271e-04	1,3457e-04
$W_{pl.y}$ [m^3], $W_{pl.z}$ [m^3]	2,4921e-04	2,4057e-04
$M_{pl.y.+}$ [Nm], $M_{pl.y.-}$ [Nm]	5,98e+04	5,98e+04
$M_{pl.z.+}$ [Nm], $M_{pl.z.-}$ [Nm]	5,77e+04	5,77e+04
d_y [mm], d_z [mm]	-121	0
I_t [m^4], I_w [m^6]	3,7460e-07	2,3918e-08
β_y [mm], β_z [mm]	0	248
Afbeelding	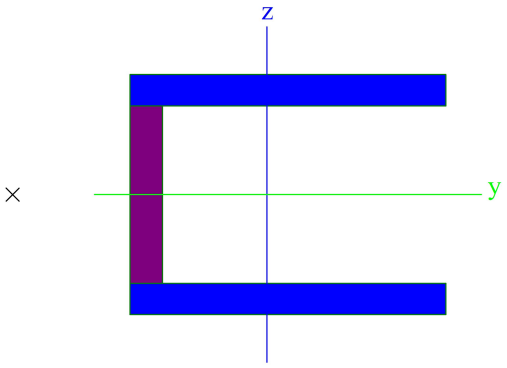	
Girder 2		
Type	1D	
Vorm type	Dunwandig	
Onderdeelmateriaal	Girder 2 - flange	
	Girder 2 - web	
Bouwwijze	Algemeen	
A [m^2]	6,3731e-03	
A_y [m^2], A_z [m^2]	4,0026e-03	2,0183e-03
A_L [m^2/m], A_D [m^2/m]	1,0468e+00	1,0468e+00
$c_{Y.UCS}$ [mm], $c_{Z.UCS}$ [mm]	55	119
α [deg]	0,00	
I_y [m^4], I_z [m^4]	6,3010e-05	1,4499e-05

i_y [mm], i_z [mm]	99	48
$W_{el.y}$ [m^3], $W_{el.z}$ [m^3]	5,2860e-04	1,5288e-04
$W_{pl.y}$ [m^3], $W_{pl.z}$ [m^3]	6,6551e-04	2,9832e-04
$M_{pl.y.+}$ [Nm], $M_{pl.y.-}$ [Nm]	1,60e+05	1,60e+05
$M_{pl.z.+}$ [Nm], $M_{pl.z.-}$ [Nm]	7,16e+04	7,16e+04
d_y [mm], d_z [mm]	-107	0
I_t [m^4], I_w [m^6]	4,5452e-07	1,3373e-07
β_y [mm], β_z [mm]	0	268
Afbeelding	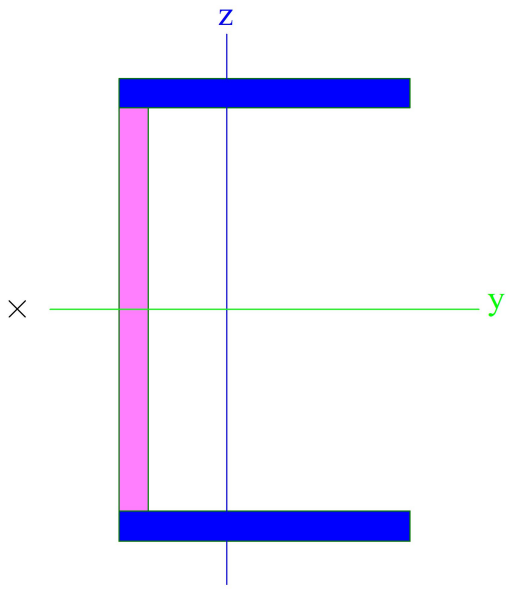	

Pile - 356 mm		
Type	Buis	
Uitgebreid	356; 13	
Vorm type	Dikke wanden	
Onderdeelmateriaal	Pile - Guades	
Bouwwijze	Algemeen	
Kleur		
A [m^2]	1,4008e-02	
A_y [m^2], A_z [m^2]	9,3550e-03	9,3550e-03
A_L [m^2/m], A_D [m^2/m]	1,1184e+00	2,1550e+00
$c_{Y.UCS}$ [mm], $c_{Z.UCS}$ [mm]	178	178
α [deg]	0,00	
I_y [m^4], I_z [m^4]	2,0630e-04	2,0630e-04
i_y [mm], i_z [mm]	121	121
$W_{el.y}$ [m^3], $W_{el.z}$ [m^3]	1,1590e-03	1,1590e-03
$W_{pl.y}$ [m^3], $W_{pl.z}$ [m^3]	1,5302e-03	1,5302e-03
$M_{pl.y.+}$ [Nm], $M_{pl.y.-}$ [Nm]	3,67e+05	3,67e+05
$M_{pl.z.+}$ [Nm], $M_{pl.z.-}$ [Nm]	3,67e+05	3,67e+05
d_y [mm], d_z [mm]	0	0
I_t [m^4], I_w [m^6]	4,0380e-04	1,4586e-20
β_y [mm], β_z [mm]	0	0

Afbeelding	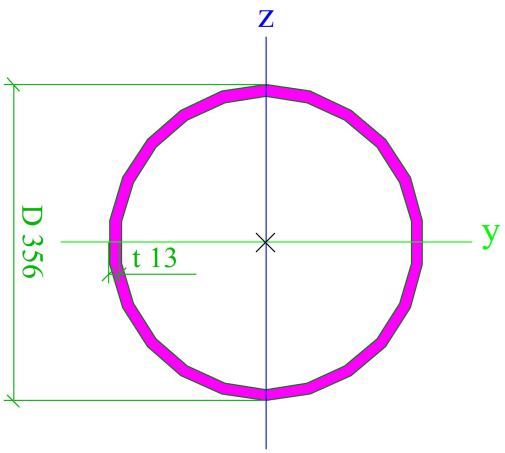	
Pile - 456 mm		
Type	Buis	
Uitgebreid	456; 17	
Vorm type	Dikke wanden	
Onderdeelmateriaal	Pile - Guades	
Bouwwijze	Algemeen	
Kleur		
A [m²]	2,3446e-02	
A_y [m²], A_z [m²]	1,5663e-02	1,5663e-02
A_L [m²/m], A_D [m²/m]	1,4325e+00	2,7582e+00
$c_{Y.UCS}$ [mm], $c_{Z.UCS}$ [mm]	228	228
α [deg]	0,00	
I_y [m⁴], I_z [m⁴]	5,6566e-04	5,6566e-04
i_y [mm], i_z [mm]	155	155
$W_{el.y}$ [m³], $W_{el.z}$ [m³]	2,4810e-03	2,4810e-03
$W_{pl.y}$ [m³], $W_{pl.z}$ [m³]	3,2779e-03	3,2779e-03
$M_{pl.y.+}$ [Nm], $M_{pl.y.-}$ [Nm]	7,86e+05	7,86e+05
$M_{pl.z.+}$ [Nm], $M_{pl.z.-}$ [Nm]	7,86e+05	7,86e+05
d_y [mm], d_z [mm]	0	0
I_t [m⁴], I_w [m⁶]	1,1074e-03	6,2640e-20
β_y [mm], β_z [mm]	0	0
Afbeelding	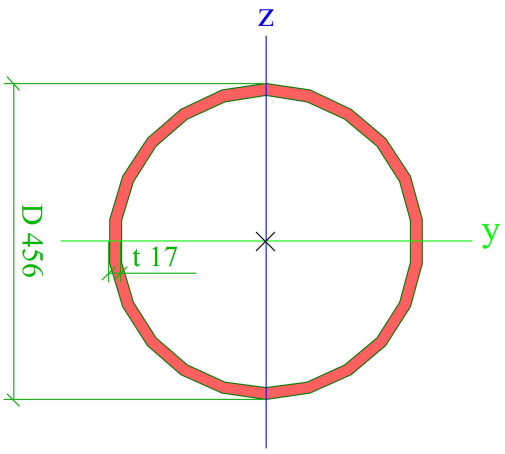	

Verklaring van symbolen	
A	Gebied
A_y	Afschuifoppervlak in hoofd y-richting - Berekend door 2D EEM analyse
A_z	Afschuifoppervlak in hoofd z-richting - Berekend door 2D EEM analyse
A_L	Omtrek per eenheidslengte
A_D	Uithardingsoppervlakte per

Verklaring van symbolen	
	eenheidslengte
$c_{Y.UCS}$	Zwaartepunt coordinaten in Y-richting van het invoer assen systeem
$c_{Z.UCS}$	Zwaartepunt coordinaten in Z-richting van het invoer assen systeem
$I_{Y.LCS}$	Tweede moment van het gebied rond de YLCS as

Verklaring van symbolen	
$I_{Z.LCS}$	Tweede moment van het gebied rond de ZLCS as
$I_{YZ.LCS}$	Product moment van het gebied in het LCS systeem
α	Rotatiehoek van het hoofd assen systeem
I_y	Tweede moment van het gebied rond de hoofd y-as
I_z	Tweede moment van het gebied rond de hoofd z-as
i_y	Traagheidsstraal rond de hoofd y-as
i_z	Traagheidsstraal rond de hoofd z-as
$W_{el.y}$	Elastische doorsnede modulus rond de hoofd y-as
$W_{el.z}$	Elastische doorsnede modulus rond de hoofd z-as
$W_{pl.y}$	Plastische doorsnede modulus rond de hoofd y-as
$W_{pl.z}$	Plastische doorsnede modulus rond de hoofd z-as

Verklaring van symbolen	
$M_{pl.y.+}$	Plastisch moment rond de hoofd y-as voor een positief My moment
$M_{pl.y.-}$	Plastisch moment rond de hoofd y-as voor een negatief My moment
$M_{pl.z.+}$	Plastisch moment rond de hoofd z-as voor een positief Mz moment
$M_{pl.z.-}$	Plastisch moment rond de hoofd z-as voor een negatief Mz moment
d_y	Afschuif middencoordinaat in hoofd y-richting gemeten vanaf het zwaartepunt - Berekend door 2D EEM analyse
d_z	Afschuif middencoordinaat in hoofd z-richting gemeten vanaf het zwaartepunt - Berekend door 2D EEM analyse
I_t	Torsie constante - Berekend door 2D EEM analyse
I_w	Welvings constante - Berekend door 2D EEM analyse
β_y	Mono-symmetrische constante rond de hoofd y-as
β_z	Mono-symmetrische constante rond de hoofd z-as

2.3. Orthotropy

Flens	
Type van orthotropie	Standaard
Dikte van Plaat/Wand [mm]	26
Materiaal	Beam 1 - flens - zonder reductie
D11 [MNm]	5,0332e-02
D22 [MNm]	3,2821e-02
D12 [MNm]	1,0719e-11
D33 [MNm]	1,0460e-02
D44 [MN/m]	3,1333e-04
D55 [MN/m]	2,2346e-04
d11 [MN/m]	8,9348e+02
d22 [MN/m]	5,8262e+02
d12 [MN/m]	1,9028e+02
d33 [MN/m]	1,8569e+02
K xy [MN/m]	1,0000e+00
K yx [MN/m]	1,0000e+00
Lijf	
Type van orthotropie	Standaard
Dikte van Plaat/Wand [mm]	14
Materiaal	Beam 1 - lijf - zonder reductie
D11 [MNm]	5,4514e-03
D22 [MNm]	2,4669e+03
D12 [MNm]	2,2054e-12
D33 [MNm]	2,1650e-03
D44 [MN/m]	1,0727e-04
D55 [MN/m]	1,2150e-04
d11 [MN/m]	3,3376e+02
d22 [MN/m]	3,9593e+02
d12 [MN/m]	1,3502e+02
d33 [MN/m]	1,3255e+02
K xy [MN/m]	1,0000e+00
K yx [MN/m]	1,0000e+00

3. Geometry

3.1. Supports at piles and abutments

Naam Knoop	Systeem UCS	Type Hoek [deg]	X Stijfheid X [MN/m]	Y Stijfheid Y [MN/m]	Z Stijfheid Z [MN/m]	Rx Stijfheid Rx [MNm/rad]	Ry Stijfheid Ry [MNm/rad]	Rz Stijfheid Rz [MNm/rad]
Pile 2 - 5 Pile 2 - bottom - 5	GCS	Standaard	Verend 1,0000e+01	Verend 1,0000e+01	Verend 5,0000e+01	Vrij	Vrij	Vrij
Pile 2 - 2 Pile 2 - bottom - 2	GCS	Standaard	Verend 1,0000e+01	Verend 1,0000e+01	Verend 5,0000e+01	Vrij	Vrij	Vrij
Pile 2 - 8 Pile 2 - bottom - 8	GCS	Standaard	Verend 1,0000e+01	Verend 1,0000e+01	Verend 5,0000e+01	Vrij	Vrij	Vrij
Pile 2 - 3 Pile 2 - bottom - 3	GCS	Standaard	Verend 1,0000e+01	Verend 1,0000e+01	Verend 5,0000e+01	Vrij	Vrij	Vrij
Pile 2 - 9 Pile 2 - bottom - 9	GCS	Standaard	Verend 1,0000e+01	Verend 1,0000e+01	Verend 5,0000e+01	Vrij	Vrij	Vrij
Pile 2 - 4 Pile 2 - bottom - 4	GCS	Standaard	Verend 1,0000e+01	Verend 1,0000e+01	Verend 5,0000e+01	Vrij	Vrij	Vrij
Pile 2 - 10 Pile 2 - bottom - 10	GCS	Standaard	Verend 1,0000e+01	Verend 1,0000e+01	Verend 5,0000e+01	Vrij	Vrij	Vrij
Pile 2 - 11 Pile 2 - bottom - 11	GCS	Standaard	Verend 1,0000e+01	Verend 1,0000e+01	Verend 5,0000e+01	Vrij	Vrij	Vrij
Pile 3 - 2 Pile 3 - bottom - 2	GCS	Standaard	Verend 1,0000e+01	Verend 1,0000e+01	Verend 5,0000e+01	Vrij	Vrij	Vrij
Pile 3 - 1 Pile 3 - bottom - 1	GCS	Standaard	Verend 1,0000e+01	Verend 1,0000e+01	Verend 5,0000e+01	Vrij	Vrij	Vrij
Abutment - 1 Abutment - 1	GCS	Standaard	Vast	Vast	Vast	Vrij	Vrij	Vrij
Pile 1 - 1 Pile 1 - bottom - 1	GCS	Standaard	Verend 1,0000e+01	Verend 1,0000e+01	Verend 5,0000e+01	Vrij	Vrij	Vrij
Pile 1 - 2 Pile 1 - bottom - 2	GCS	Standaard	Verend 1,0000e+01	Verend 1,0000e+01	Verend 5,0000e+01	Vrij	Vrij	Vrij
Pile 1 - 3 Pile 1 - bottom - 3	GCS	Standaard	Verend 1,0000e+01	Verend 1,0000e+01	Verend 5,0000e+01	Vrij	Vrij	Vrij
Pile 1 - 4 Pile 1 - bottom - 4	GCS	Standaard	Verend 1,0000e+01	Verend 1,0000e+01	Verend 5,0000e+01	Vrij	Vrij	Vrij
Pile 1 - 5 Pile 1 - bottom - 5	GCS	Standaard	Verend 1,0000e+01	Verend 1,0000e+01	Verend 5,0000e+01	Vrij	Vrij	Vrij
Pile 1 - 6 Pile 1 - bottom - 6	GCS	Standaard	Verend 1,0000e+01	Verend 1,0000e+01	Verend 5,0000e+01	Vrij	Vrij	Vrij
Abutment - 2 Abutment - 2	GCS	Standaard	Vast	Vast	Vast	Vrij	Vrij	Vrij
Pile 2 - 13 Pile 2 - bottom - 13	GCS	Standaard	Verend 1,0000e+01	Verend 1,0000e+01	Verend 5,0000e+01	Vrij	Vrij	Vrij
Pile 2 - 14 Pile 2 - bottom - 14	GCS	Standaard	Verend 1,0000e+01	Verend 1,0000e+01	Verend 5,0000e+01	Vrij	Vrij	Vrij
Pile 2 - 15 Pile 2 - bottom - 15	GCS	Standaard	Verend 1,0000e+01	Verend 1,0000e+01	Verend 5,0000e+01	Vrij	Vrij	Vrij
Pile 2 - 16 Pile 2 - bottom - 16	GCS	Standaard	Verend 1,0000e+01	Verend 1,0000e+01	Verend 5,0000e+01	Vrij	Vrij	Vrij
Pile 2 - 7 Pile 2 - bottom - 7	GCS	Standaard	Verend 1,0000e+01	Verend 1,0000e+01	Verend 5,0000e+01	Vrij	Vrij	Vrij
Pile 2 - 12 Pile 2 - bottom - 12	GCS	Standaard	Verend 1,0000e+01	Verend 1,0000e+01	Verend 5,0000e+01	Vrij	Vrij	Vrij
Pile 2 - 1 Pile 2 - bottom - 1	GCS	Standaard	Verend 1,0000e+01	Verend 1,0000e+01	Verend 5,0000e+01	Vrij	Vrij	Vrij
Pile 2 - 6 Pile 2 - bottom - 6	GCS	Standaard	Verend 1,0000e+01	Verend 1,0000e+01	Verend 5,0000e+01	Vrij	Vrij	Vrij
Pile 2 - 17 Pile 2 - bottom - 17	GCS	Standaard	Verend 1,0000e+01	Verend 1,0000e+01	Verend 5,0000e+01	Vrij	Vrij	Vrij

4. Loads

4.1. Load cases

Naam	Omschrijving	Actie type	Lastgroep	Richting	Duur	'Master' belastingsgeval
	Spec	Belastingtype				
Eigen gewicht		Permanent	LG1	-Z		
		Eigen gewicht				
Loading arm		Permanent	LG1			
		Standaard				
Variable load		Variabel	LG2		Kort	Geen
	Standaard	Statisch				
Wind longitudinal		Variabel	LG2		Kort	Geen
	Standaard	Statisch				
Wind transversal - direction 2		Variabel	LG2		Kort	Geen
	Standaard	Statisch				
Wind tranversal - direction 1		Variabel	LG2		Kort	Geen
	Standaard	Statisch				
Pipes		Permanent	LG1			
		Standaard				
Sumput		Permanent	LG1			
		Standaard				
Planks		Permanent	LG1			
		Standaard				
Railing		Permanent	LG1			
		Standaard				

4.2. Load combinations

Naam	Omschrijving	Type	Belastingsgevallen	Coëff. [-]
ULS - wind transversal - direction 1		Lineair - UGT	Eigen gewicht	1,20
			Loading arm	1,50
			Variable load	1,50
			Wind tranversal - direction 1	0,90
			Pipes	1,20
			Sumput	1,20
			Planks	1,20
			Railing	1,20
ULS - wind transversal - direction 2		Lineair - UGT	Eigen gewicht	1,20
			Loading arm	1,50
			Variable load	1,50
			Wind transversal - direction 2	0,90
			Pipes	1,20
			Sumput	1,20
			Planks	1,20
			Railing	1,20
ULS - wind longitudinal		Lineair - UGT	Eigen gewicht	1,20
			Loading arm	1,50
			Variable load	1,50
			Wind longitudinal	0,90
			Pipes	1,20
			Sumput	1,20
			Planks	1,20
			Railing	1,20
SLS - wind transversal - direction 1		Lineair - BGT	Eigen gewicht	1,00
			Loading arm	1,00
			Variable load	1,00
			Wind tranversal - direction 1	0,60
			Pipes	1,00
			Sumput	1,00
			Planks	1,00
			Railing	1,00
SLS - wind transversal -		Lineair - BGT	Eigen gewicht	1,00

Naam	Omschrijving	Type	Belastingsgevallen	Coëff. [-]
direction 2				
			Loading arm	1,00
			Variable load	1,00
			Wind transversal - direction 2	0,60
			Pipes	1,00
			Sumput	1,00
			Planks	1,00
			Railing	1,00
SLS - wind longitudinal		Lineair - BGT	Eigen gewicht	1,00
			Loading arm	1,00
			Variable load	1,00
			Wind longitudinal	0,60
			Pipes	1,00
			Sumput	1,00
			Planks	1,00
			Railing	1,00

5. Results

5.1. Internal member forces

Lineaire berekening, Extreem : Globaal, Systeem : Hoofd
Selectie : Alle
Klasse : All ULS

Staaf	css	dx [m]	BG	N [kN]	Vy [kN]	Vz [kN]
Pile 3 - 1	Pile - 456 mm - Buis	0,000	ULS - wind transversal - direction 1/4	**-175,52**	0,01	3,15
Beam 1 - 5	Beam 1 - Grafische doorsnede	0,000	ULS - wind transversal - direction 1/4	**15,93**	-1,12	30,21
Beam 2 - longitudinal - 1	Beam 2 - 1D	1,600	ULS - wind longitudinal/5	-4,10	**-13,86**	-52,65
Beam 1 - abutment	Beam 1 - Grafische doorsnede	0,000	ULS - wind transversal - direction 1/4	0,00	**11,77**	0,40
Beam 2 - 6	Beam 2 - 1D	4,000	ULS - wind transversal - direction 1/4	1,09	0,78	**-163,72**
Beam 3 - reinforcement - 3	Beam 2 - 1D	0,500	ULS - wind transversal - direction 1/4	-13,30	1,61	**234,91**

Lineaire berekening, Extreem : Globaal, Systeem : Hoofd
Selectie : Alle
Klasse : All ULS

Staaf	css	dx [m]	BG	Mx [kNm]	My [kNm]	Mz [kNm]
Beam 2 - longitudinal - 1	Beam 2 - 1D	1,600	ULS - wind transversal - direction 2/6	**-0,30**	8,93	-3,34
Beam 2 - longitudinal - 1	Beam 2 - 1D	1,000	ULS - wind transversal - direction 2/6	**0,22**	21,75	0,27
Beam 3 - reinforcement - 3	Beam 2 - 1D	1,000	ULS - wind transversal - direction 1/4	0,08	**-131,41**	0,41
Beam 3 - reinforcement - 3	Beam 2 - 1D	1,000	ULS - wind transversal - direction 1/4	-0,10	**172,20**	0,39
Pile 2 - 17	Pile - 456 mm - Buis	6,435	ULS - wind transversal - direction 2/6	0,00	-1,27	**-14,53**
Pile 2 - 17	Pile - 456 mm - Buis	19,500	ULS - wind transversal - direction 2/6	0,00	4,25	**34,96**

Lineaire berekening, Extreem : Globaal, Systeem : Hoofd
Selectie : Alle
Klasse : All ULS
Doorsnede : Beam 1 - Grafische doorsnede

Staaf	css	dx [m]	BG	N [kN]	Vy [kN]	Vz [kN]	Mx [kNm]	My [kNm]	Mz [kNm]
Beam 1 - 6	Beam 1 - Grafische doorsnede	0,000	ULS - wind transversal - direction 1/4	**-22,37**	-5,75	45,02	-0,01	-51,40	3,90
Beam 1 - 5	Beam 1 - Grafische doorsnede	0,000	ULS - wind transversal - direction 1/4	**15,93**	-1,12	30,21	-0,01	-41,65	2,79
Beam 1 - 5	Beam 1 - Grafische doorsnede	7,500	ULS - wind transversal - direction 2/6	-6,10	**-7,65**	-32,75	0,00	-45,63	**-11,97**
Beam 1 - abutment	Beam 1 - Grafische doorsnede	0,000	ULS - wind transversal - direction 1/4	0,00	**11,77**	0,40	**0,05**	0,01	-11,69
Beam 1 - 2	Beam 1 - Grafische doorsnede	7,500	ULS - wind transversal - direction 2/6	1,47	0,88	**-53,88**	0,00	-65,54	3,62
Beam 1 - 8	Beam 1 - Grafische doorsnede	0,000	ULS - wind transversal - direction 2/6	6,21	0,68	**47,37**	-0,01	-63,72	-3,24

Staaf	css	dx [m]	BG	N [kN]	Vy [kN]	Vz [kN]	Mx [kNm]	My [kNm]	Mz [kNm]
Beam 1 - 1	Beam 1 - Grafische doorsnede	0,000	ULS - wind transversal - direction 2/6	-4,35	6,35	25,55	**-0,01**	0,02	-7,53
Beam 1 - 8	Beam 1 - Grafische doorsnede	7,500	ULS - wind transversal - direction 1/4	-20,26	8,00	-47,90	0,00	**-66,03**	**12,08**
Beam 1 - 2	Beam 1 - Grafische doorsnede	3,000	ULS - wind transversal - direction 1/4	-15,97	-1,87	0,33	0,01	**55,12**	-2,01

Lineaire berekening, Extreem : Globaal, Systeem : Hoofd
Selectie : Alle
Klasse : All ULS
Doorsnede : Beam 2 - 1D

Staaf	css	dx [m]	BG	N [kN]	Vy [kN]	Vz [kN]	Mx [kNm]	My [kNm]	Mz [kNm]
Beam 3 - reinforcement - 3	Beam 2 - 1D	0,500	ULS - wind transversal - direction 1/4	**-13,30**	1,61	**234,91**	-0,10	56,81	-0,42
Beam 2 - 11	Beam 2 - 1D	0,000	ULS - wind longitudinal/5	**7,24**	-1,64	58,16	-0,01	-54,55	2,70
Beam 2 - longitudinal - 1	Beam 2 - 1D	1,600	ULS - wind longitudinal/5	-4,10	**-13,86**	-52,65	-0,22	7,62	5,37
Beam 2 - longitudinal - 1	Beam 2 - 1D	1,000	ULS - wind transversal - direction 2/6	-2,91	**9,98**	-17,97	**0,22**	21,75	0,27
Beam 2 - 6	Beam 2 - 1D	4,000	ULS - wind transversal - direction 1/4	1,09	0,78	**-163,72**	0,15	-26,51	0,63
Beam 2 - longitudinal - 1	Beam 2 - 1D	1,600	ULS - wind transversal - direction 2/6	4,51	3,15	-50,53	**-0,30**	8,93	-3,34
Beam 3 - reinforcement - 3	Beam 2 - 1D	1,000	ULS - wind transversal - direction 1/4	-9,01	-1,72	93,61	0,08	**-131,41**	0,41
Beam 3 - reinforcement - 3	Beam 2 - 1D	1,000	ULS - wind transversal - direction 1/4	-13,30	1,61	226,88	-0,10	**172,20**	0,39
Beam 2 - longitudinal - 1	Beam 2 - 1D	1,600	ULS - wind transversal - direction 1/4	-7,76	-9,68	-32,16	0,11	6,14	**-3,70**
Beam 2 - longitudinal - 1	Beam 2 - 1D	0,000	ULS - wind transversal - direction 1/4	-10,35	-10,50	23,18	-0,06	5,20	**9,00**

Lineaire berekening, Extreem : Globaal, Systeem : Hoofd
Selectie : Alle
Klasse : All ULS
Doorsnede : Girder 1 - 1D

Staaf	css	dx [m]	BG	N [kN]	Vy [kN]	Vz [kN]	Mx [kNm]	My [kNm]	Mz [kNm]
Girder 1 - support - 1	Girder 1 - 1D	0,000	ULS - wind transversal - direction 2/6	**-37,04**	-1,53	3,11	0,00	-1,57	0,54
Girder 1 - horizontal - 3	Girder 1 - 1D	0,000	ULS - wind transversal - direction 1/4	**0,10**	0,12	0,55	0,01	-0,52	-0,03
Girder 1 - support - 3	Girder 1 - 1D	0,000	ULS - wind longitudinal/5	-28,96	**-2,91**	-5,01	0,00	4,88	1,67
Girder 1 - support - 1	Girder 1 - 1D	0,000	ULS - wind transversal - direction 1/4	-37,01	**5,00**	-16,72	0,00	14,29	**-4,67**
Girder 1 - support - 2	Girder 1 - 1D	1,600	ULS - wind transversal - direction 1/4	-33,73	2,32	**-22,71**	0,00	**-17,16**	1,34
Girder 1 - support - 3	Girder 1 - 1D	0,000	ULS - wind transversal - direction 2/6	-36,27	-0,70	**7,29**	0,00	-4,65	-0,26
Girder 1 - support - 3	Girder 1 - 1D	0,000	ULS - wind transversal - direction 1/4	-35,72	-1,92	-18,88	**0,00**	16,26	0,74
Girder 1 - diagonal - 2	Girder 1 - 1D	0,000	ULS - wind transversal - direction 1/4	-0,39	-0,12	-0,40	**0,01**	0,52	0,03
Girder 1 - support - 2	Girder 1 - 1D	0,000	ULS - wind transversal - direction 1/4	-33,73	2,32	-22,49	0,00	**19,00**	-2,36
Girder 1 - support - 1	Girder 1 - 1D	1,600	ULS - wind transversal - direction 1/4	-37,01	5,00	-16,94	0,00	-12,64	**3,32**

Lineaire berekening, Extreem : Globaal, Systeem : Hoofd
Selectie : Alle

Klasse : All ULS

Lineaire berekening, Extreem : Globaal, Systeem : Hoofd
Selectie : Alle
Klasse : All ULS
Doorsnede : Pile - 456 mm - Buis (456; 17)

Staaf	css	dx [m]	BG	N [kN]	Vy [kN]	Vz [kN]	Mx [kNm]	My [kNm]	Mz [kNm]
Pile 3 - 1	Pile - 456 mm - Buis	0,000	ULS - wind transversal - direction 1/4	**-175,52**	0,01	3,15	0,00	0,00	0,00
Pile 3 - 2	Pile - 456 mm - Buis	19,609	ULS - wind transversal - direction 1/4	**-49,66**	0,55	-2,25	0,00	-20,51	5,29
Pile 2 - 17	Pile - 456 mm - Buis	4,596	ULS - wind transversal - direction 2/6	-139,71	**-6,07**	-0,53	0,00	-0,54	-5,79
Pile 2 - 17	Pile - 456 mm - Buis	6,435	ULS - wind transversal - direction 2/6	-138,98	**3,79**	0,42	0,00	-1,27	-14,53
Pile 1 - 1	Pile - 456 mm - Buis	20,514	ULS - wind transversal - direction 1/4	-94,05	-0,95	**-7,77**	0,06	-23,60	-4,57
Pile 1 - 3	Pile - 456 mm - Buis	8,392	ULS - wind transversal - direction 1/4	-94,44	0,39	**6,73**	0,00	6,47	0,40
Pile 1 - 5	Pile - 456 mm - Buis	6,770	ULS - wind longitudinal/5	-89,86	0,10	-0,04	**0,00**	2,94	-0,44
Pile 1 - 1	Pile - 456 mm - Buis	17,452	ULS - wind transversal - direction 1/4	-95,60	-0,95	-7,26	**0,06**	-0,59	-1,68
Pile 3 - 2	Pile - 456 mm - Buis	19,609	ULS - wind transversal - direction 2/6	-93,99	0,78	-3,45	0,00	**-29,00**	7,39
Pile 3 - 1	Pile - 456 mm - Buis	19,609	ULS - wind transversal - direction 2/6	-126,48	0,75	2,65	0,00	**27,14**	6,71
Pile 2 - 17	Pile - 456 mm - Buis	6,435	ULS - wind transversal - direction 2/6	-139,22	-3,44	-0,26	0,00	-1,27	**-14,53**
Pile 2 - 17	Pile - 456 mm - Buis	19,500	ULS - wind transversal - direction 2/6	-132,03	3,79	0,42	0,00	4,25	**34,96**

5.2. Displacement of nodes

Lineaire berekening, Extreem : Globaal
Selectie : Alle
Klasse : All SLS

Knoop	BG	Ux [mm]	Uy [mm]	Uz [mm]	Fix [mrad]	Fiy [mrad]	Fiz [mrad]
Girder access bridge 10	SLS - wind transversal - direction 1/2	**-15,3**	37,4	-6,1	4,1	10,8	-4,5
Girder access bridge 7	SLS - wind transversal - direction 1/2	**18,7**	31,9	3,2	0,3	3,8	-5,4
Girder access bridge 12	SLS - wind transversal - direction 2/3	-0,4	**-21,2**	-26,3	5,6	13,0	-8,1
Beam 1 - midspan - 6	SLS - wind transversal - direction 1/2	-0,6	**45,1**	-26,3	-1,8	-0,1	-0,9
Girder access bridge 10	SLS - wind transversal - direction 2/3	-10,9	-9,5	**-30,2**	**7,1**	10,2	-3,2
PIle 1 - top - 3	SLS - wind transversal - direction 1/2	0,2	38,7	**6,3**	1,2	-0,6	-0,3
Center loading arm	SLS - wind transversal - direction 1/2	4,7	13,4	-7,3	**-9,0**	-1,4	-1,3
Access bridge - platform connect	SLS - wind transversal - direction 2/3	-0,2	-13,9	-7,6	0,6	**-3,7**	0,7
Girder access bridge 12	SLS - wind transversal - direction 1/2	-3,0	31,4	-4,0	2,7	**13,5**	**-9,3**
Beam 1 - midspan - 1	SLS - wind transversal - direction 1/2	0,0	10,7	-8,3	-0,5	-0,4	**4,2**

5.3. Support reactions

Lineaire berekening, Extreem : Globaal
Selectie : Pile 2 - 5,Pile 2 - 2,Pile 2 - 8,Pile 2 - 3,Pile 2 - 9,Pile 2 - 4,Pile 2 - 10,Pile 2 - 11,Pile 3 - 2, Pile 3 - 1,Pile 1 - 1..Pile 1 - 6,Pile 2 - 13..Pile 2 - 16,Pile 2 - 7,Pile 2 - 12,Pile 2 - 1,Pile 2 - 6,

Klasse : All ULS
Schuine steunpunten

Steunpunt	BG	Rx [kN]	Ry [kN]	Rz [kN]
Pile 2 - 9/Pile 2 - bottom - 9	ULS - wind transversal - direction 1/4	**-5,80**	-0,07	132,94
Pile 2 - 1/Pile 2 - bottom - 1	ULS - wind longitudinal/5	**3,91**	-0,02	88,40
Pile 1 - 5/Pile 1 - bottom - 5	ULS - wind transversal - direction 1/4	0,01	**-28,81**	104,27
Pile 1 - 2/Pile 1 - bottom - 2	ULS - wind transversal - direction 2/6	0,00	**31,15**	113,74
Pile 3 - 2/Pile 3 - bottom - 2	ULS - wind transversal - direction 1/4	1,25	5,25	**59,58**
Pile 3 - 1/Pile 3 - bottom - 1	ULS - wind transversal - direction 1/4	3,73	-14,86	**175,14**

F

List of equations

Indication of location decisive strength resistance capacity
Assume a simply supported beam with a line load q and length l. If the moment distribution is generalized to $M(x) = ax^2 + bx + c$, and boundary conditions related to the supports are defined, the following expressions can be found:

$$V(x) = qx - 0.5ql$$
$$M(x) = 0.5q(lx - x^2)$$

The unity check is for the bending moment and the shear force is:

$$UC = \frac{M(x)}{M_{Rd}} + \frac{V(x)}{V_{Rd}} \leq 0$$

By taking the derivative with respect to the length coordinate along the beam axis (x) and simplifying the ≤ condition to =, an optimum can be found (x'):

$$\frac{dUC}{dx} = \frac{-qx' + 0.5ql}{M_{Rd}} + \frac{q}{V_{Rd}} = 0$$
$$x' = 0.5l + \frac{M_{Rd}}{V_{Rd}}$$

Combining (x') with the expressions found for the bending moment and shear force, expressions for the bending moment and shear force are found which generate the maximum unity check:

$$V(x') = q\frac{M_{Rd}}{V_{Rd}}$$
$$M(x') = -0.5q(0.5l + \frac{M_{Rd}}{V_{Rd}})^2 + 0.5ql(0.5l + \frac{M_{Rd}}{V_{Rd}})$$

It must be noted that once the ratio $\frac{M_{Rd}}{V_{Rd}}$ exceeds certain boundaries the formula is not valid anymore. However, it is useful for a first indication.

In-plane engineering constants For symmetrical laminates, the in-plane engineering can be calculated with the equations from Figure F.1. For non-symmetrical laminates, see (Nettles, 1994). Figure F.2 present the equations which relate the longitudinal- and transversal stiffness to the orthotropic plate engineering constants, based on the Kirchhof theory of thin plates.

D. Summary

The equations for the in-plane engineering constants of a symmetric laminate are:

$$E_x = \frac{A_{11}}{h} + \frac{A_{12}}{h}\left(\frac{A_{26}A_{16}-A_{12}A_{66}}{A_{22}A_{66}-A_{26}^2}\right) + \frac{A_{16}}{h}\left(\frac{-A_{16}}{A_{66}} + \frac{A_{26}A_{12}A_{66}-A_{26}^2A_{16}}{A_{22}A_{66}^2-A_{26}^2A_{66}}\right),$$

$$E_y = \frac{A_{22}}{h} + \frac{A_{12}}{h}\left(\frac{A_{26}A_{16}-A_{12}A_{66}}{A_{11}A_{66}-A_{16}^2}\right) + \frac{A_{26}}{h}\left(\frac{-A_{26}}{A_{66}} + \frac{A_{16}A_{12}A_{66}-A_{16}^2A_{26}}{A_{11}A_{66}^2-A_{16}^2A_{66}}\right),$$

$$G_{xy} = \frac{A_{66}}{h} - \frac{A_{26}^2}{hA_{22}} + \frac{2A_{16}A_{12}A_{22}A_{26}-A_{12}^2A_{26}^2-A_{16}^2A_{22}^2}{h\left(A_{11}A_{22}^2-A_{12}^2A_{22}\right)},$$

$$\nu_{xy} = \frac{\left(A_{12}-\frac{A_{16}A_{26}}{A_{66}}\right)}{\left(A_{22}-\frac{A_{26}^2}{A_{66}}\right)},$$

$$\nu_{yx} = \frac{\left(\frac{A_{16}A_{26}}{A_{66}}-A_{12}\right)}{\left(\frac{A_{16}^2}{A_{66}}-A_{11}\right)}.$$

Figure F.1: In-plane engineering constants (Nettles, 1994)

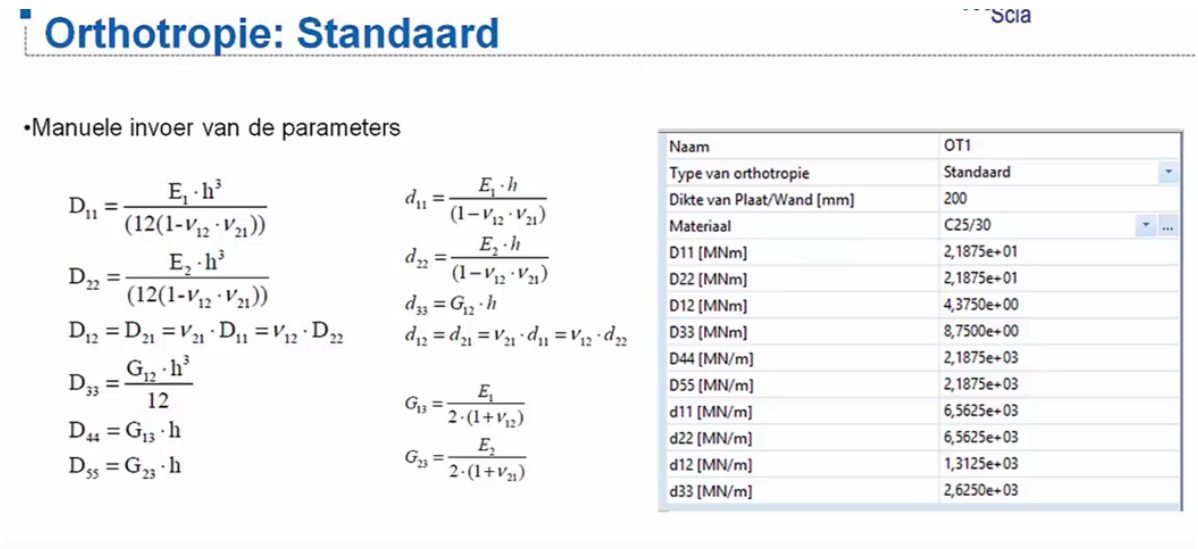

Figure F.2: Orthotropic plate engineering constants (SCIA nv., 2016)

Timoshenko shear coefficient for hollow circular cross section

The Timoshenko shear coefficient k, for a hollow circular cross section is given as (Hutchinson, 2001):

$$\frac{6\left(a^2+b^2\right)^2(1+\nu)^2}{7a^4+34a^2b^2+7b^4+\nu\left(12a^4+48a^2b^2+12b^4\right)+\nu^2\left(4a^4+16a^2b^2+4b^4\right)} \tag{F.1}$$

Where:

a : inner radius in m
b : outer radius in m
ν : Poisson coefficient

G

Life cycle costs

			Unit costs						Costs					
			case 1.1	case 1.2	case 2.1	case 2.2	case 3.1	case 3.2	case 1.1	case 1.2	case 2.1	case 2.2	case 3.1	case 3.2
Material	FRP	[€/kg]	7	7	4	4			72134	72134	41220	41220	0	0
	FRP hollow pile 1	[€/m]	111	111	111	111	111	111	16983	16983	16983	16983	16983	16983
	FRP hollow pile 2	[€/m]	186	186	186	186	186	186	90013,86	90013,86	90013,86	90013,86	90013,86	90013,86
	Beam 1	[€/m]					281	281					17340,32	17340,32
	Beam 2	[€/m]					287	287					22642,88	22642,88
	Plank 1	[€/m]					84	84					7558,311	7558,311
	Plank 2	[€/m]					120	120					15009,38	15009,38
	Girder 1	[€/m]					70	70					3118,236	3118,236
								Subtal FRP	179131	179131	148216	148216	172666	172666
	Concrete	[€/m3]	130	130	130	130	130	130	3251	3251	3251	3251	3251	3251
	Prefab concrete	[€/m3]	173	173	173	173	173	173	2445	2445	2445	2445	2445	2445
	Steel	[€/kg]	1,2	1,2	1,2	1,2	1,2	1,2	29239	29239	29239	29239	29239	29239
	Formwork	[€/m2]	100	100	100	100	100	100	3500	3500	3500	3500	3500	3500
	Concrete piles	[€/m3]	199	199	199	199	199	199	9386	9386	9386	9386	9386	9386
								Subtotal RC	47821	47821	47821	47821	47821	47821
Construction	FRP [% of mat.+const.]		0,63	0,63	0,63	0,63	0,63	0,63	105204	105204	87048	87048	101407	101407
	RC [% of mat.+const.]		0,63	0,63	0,63	0,63	0,63	0,63	28085	28085	28085	28085	28085	28085
								Subtal FRP	284335	284335	235264	235264	274073	274073
								Subtotal RC	75907	75907	75907	75907	75907	75907
Maintenance	FRP jetty	[%/y]	0	0,005	0	0,005	0	0,005	0	1422	0	1176	0	1370
	RC jetty	[%/y]	0,005	0,01	0,005	0,01	0,005	0,01	380	759	380	759	380	759
	Σ NPV FRP	[€]							0	44674	0	36964	0	43062
	Σ NPV RC	[€]							11926	23853	11926	23853	11926	23853
								Total FRP	284335	329009	235264	272228	274073	317135
								Total RC	87833	99759	87833	99759	87833	99759
							ratio [%], r = 2%		224	230	168	173	212	218
							ratio [%], r = 3%		232	232	178	178	220	224
							ratio [%], r = 4%		238	238	183	183	226	229
					ratio [%], r = 2%, [% of mat.+const.] = 70%				191	191	146	146	181	186
					ratio [%], r = 2%, [% of mat.+const.] = 75%				172	172	129	129	162	167

Figure G.1: Calculation of costs with different parameters

H

Life cycle Assessment

Impact category	Equivalent unit [kg]	Abbreviation	Shadow price [€/kg eq.]
Abiotic depletion	Sb	AB	0.16
Global warming (GWP100)	CO2	GWP100	0.05
Ozone layer depletion (ODP)	CFC-11	ODP	30
Human toxicity	1,4-DB	HT	0.09
Fresh water aquatic ecotoxicity	1,4-DP	FWAX	0.03
Marine aquatic ecotoxicity	1,4-DP	MAX	0.0001
Terrestrial ecotoxicity	1,4-DP	TX	0.06
Photochemical oxidation	C2H4	Photo	2
Acidification	SO2	Acid	4
Eutrophication	PO4	Eur	9

Table H.1: Shadow prices per kg equivalent unit for the impact categories

Impact category	AB	GWP100	ODP	HT	FWAX	MAX	TX
Unit	SB	CO2	CFC-11	1,4-DB	1,4-DB	1,4-DB	1,4-DB
FRP, glass in polyester	0.0359	4.4175	0.0000005	7.4115	2.5958	0.0409	405.8957
FRP, glass in vinylester	0.0343	4.6502	0.0000008	8.7093	0.2802	0.0404	535.5476
FRP, glass in epoxy	0.0319	3.4416	0.0000002	5.7257	0.1559	0.0254	283.3707
Concrete C55/67 (CEM I-CEM III)	2.757e-4	9.449e-2	4.504e-9	1.042e-2	2.199e-3	3.627	1.834e-4
Concrete C30/37 (CEM III)	3.306e-4	1.180e-1	5.194e-9	1.193e-2	2.367e-3	3.964	2.170e-4
Reinforcement steel FeB 500	0.0217	1.4873	0.0000001	0.6585	0.6332	590.0001	0.0275
Formwork	0.0829	56.8826	0.0000002	1.1648	0.2431	399.8288	0.0124

Table H.2: Equivalent unit for the impact categories. All equivalents per kg, except formwork in m2

Results of the pile drive analysis

I.1. Pile drive equipment

Pile drive equipment were also modeled in the program; this section briefly describes the mechanical properties of this equipment. The modeled equipment are the hammer (ram), anvil, hammer cushion, and the pile cushion.

Hammer

The hammer is a lightweight hydraulic hammer form manufacturer IHC, type S30. The hammer has a rated impact energy of 60 kNm.

Ram

The ram is made from steel, with a modulus of elasticity of 208 GPa and a mass of 1627 kg. The part is a solid circular part with a diameter of 138 cm.

Anvil

The anvil is made from steel, with a modulus of elasticity of 210 GPa and a mass of 603 kg. The part is a solid circular part with a diameter of 349.7 cm and a length of 0.8 m.

Hammer cushion

The hammer cushion is made from Polypenco, a thermoplastic material. The modulus of elasticity is 3400 MPa. The cushion has a diameter equal to the pile diameter (i.e. 356 mm and 456 mm for pile 1 and pile 2, respectively. The thickness of the hammer cushion is 10 cm. The coefficient of restitution is 0.8.

Pile cushion

The hammer cushion is made from wood, stacked in 3 layers. The modulus of elasticity is 200 MPa. The cushion has a diameter equal to the pile diameter (i.e. 356 mm and 456 mm for pile 1 and pile 2, respectively. The thickness of the hammer cushion is 15 cm. The coefficient of restitution is 0.6.

I.2. Model setup

Model set 0									
#	intended depth [m]	CPT	batter angle	hammer	rated impact energy [kNm]	Bearing capacity [kN]	d_max [m]	Z [MNs/m]	Pile	Adjustment
0.1	13,3	S05	-	Ihc - S30	60	4231	13,3	567	Pile 1	Material is steel
0.2	13,3	S05	-	Ihc - S30	60	1567	8,5	93	Pile 1	
0.3	13,3	S05	-	Ihc - S30	60	3099	10,5	186	Pile 1	E mulitplied by 4
0.4	13,3	S05	-	Ihc - S30	60	2296	9	156	Pile 2	
0.5	13,3	S05	-	Ihc - S120	60	1788	8	156	Pile 2	
0.6	13,3	S05	-	Ihc - S30	60	3828	10	312	Pile 2	E mulitplied by 4
0.7	13,3	S05	-	Ihc - S30	60	5448	12,75	312	Pile 2	ρ multiplied by 4
0.8	13,3	S05	-	Vulcan-20	122	5453	13,3	312	Pile 2	ρ multiplied by 4
0.9	13,3	S05	-	Ihc - S120	60	5448	12,75	312	Pile 2	ρ multiplied by 4
0.10	13,3	S05	-	Vulcan-20	60	1835	8,25	156	Pile 2	

Figure I.1: Model set up 0

Model set 1									
#	intended depth [m]	CPT	batter angle	hammer	rated impact energy [kNm]	Bearing capacity [kN]	d_max [m]	Z [MNs/m]	Pile	Adjustment
1.1	6	S05	-	Ihc - S30	60	1055	6	156	Pile 2	Upper & lower boundary for strength +/- 20%
1.2a	6	S05	-	Ihc - S30	60	575	6	156	Pile 2	Outer friction only
1.2b	6	S05	-	Ihc - S30	60	536	6	156	Pile 2	Inner friction only
1.3	6	S05	-	Ihc - S30	60	905	6	156	Pile 2	Plugged pile

Figure I.2: Model set up 1

Model set 2									
#	intended depth [m]	CPT	batter angle	hammer	rated impact energy [kNm]	Bearing capacity [kN]	d_max [m]	Z [MNs/m]	Pile
2.0	6	S05	-	Ihc - S30	60	1055	6	0,156	Pile 2
2.1	6	S05	1:10	Ihc - S30	60	1056	6	0,156	Pile 2
2.2	6	S05	1:7	Ihc - S30	60	1056	6	0,156	Pile 2
2.3	6	S05	1:4	Ihc - S30	60	1056	6	0,156	Pile 2
2.4	10,5	S04	1:10	Ihc - S30	60	659	10,5	0,093	Pile 1
2.5	10,5	S04	1:7	Ihc - S30	60	654	10,5	0,093	Pile 1
2.6	10,5	S04	1:4	Ihc - S30	60	641	10,5	0,093	Pile 1
2.7	10,5	S04	1:4	Ihc - S30	60	828	10,5	0,156	Pile 2

Figure I.3: Model set up 2

I.3. Results

In this section, the results of model set 2 are presented.

I.3.1. Model 2.0

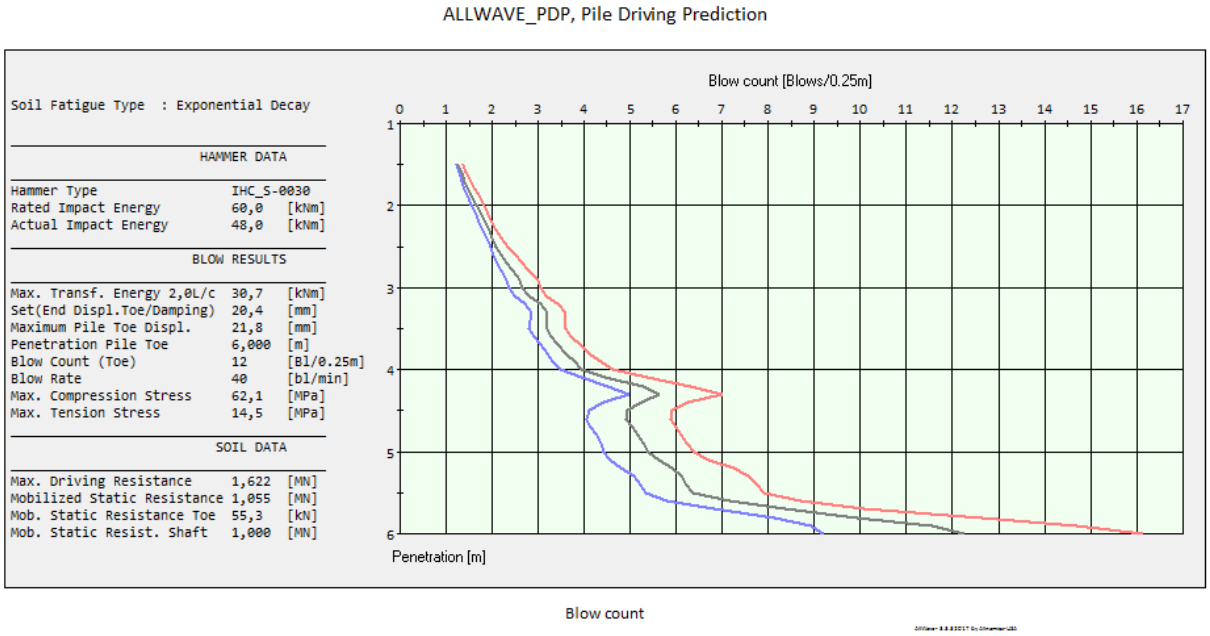

Figure I.4: Blow count for model 2.0

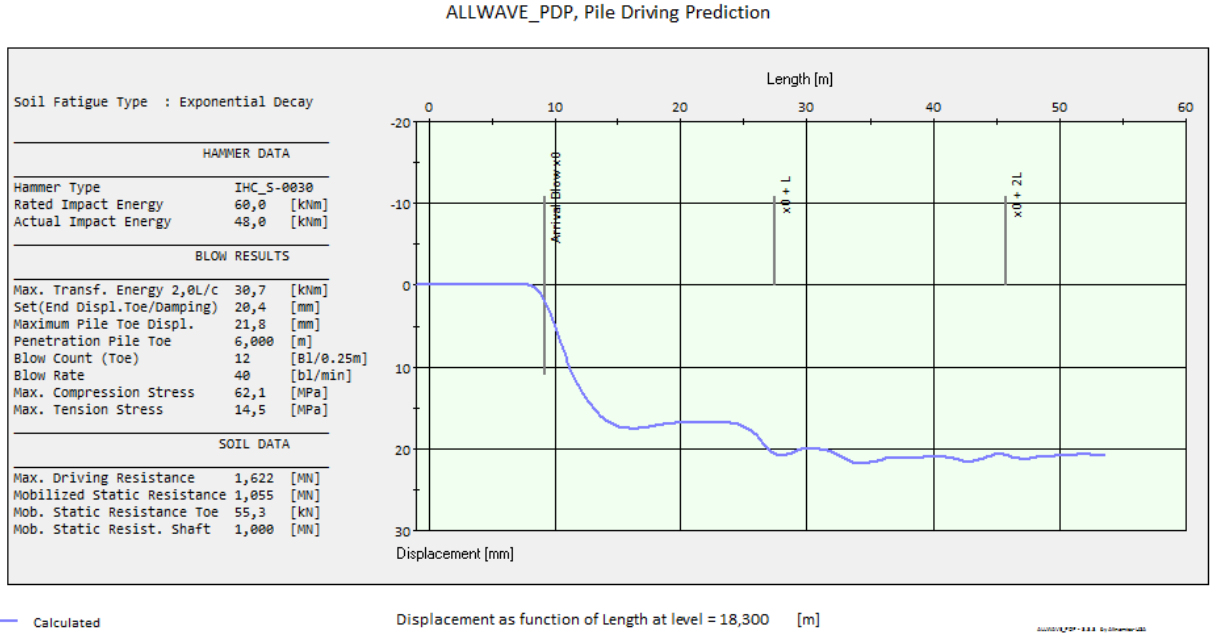

Figure I.5: Pile tip displacement for model 2.0

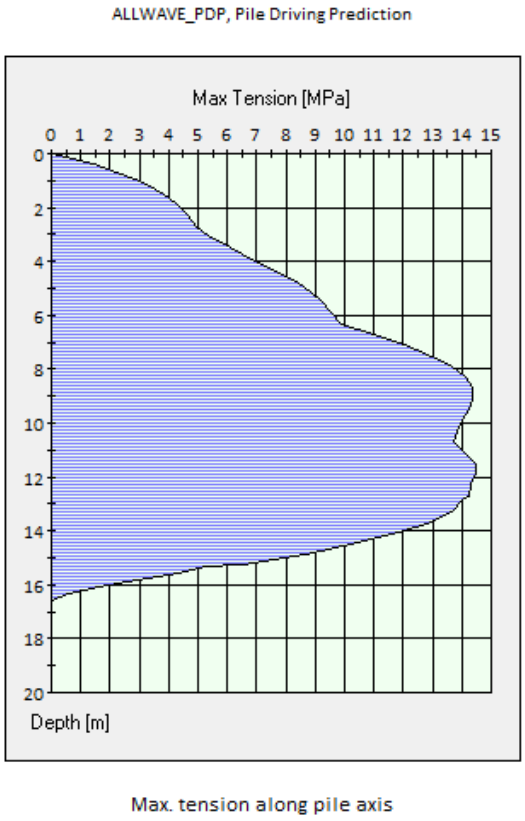

Figure I.6: Maximum tension stress during driving in model 2.0

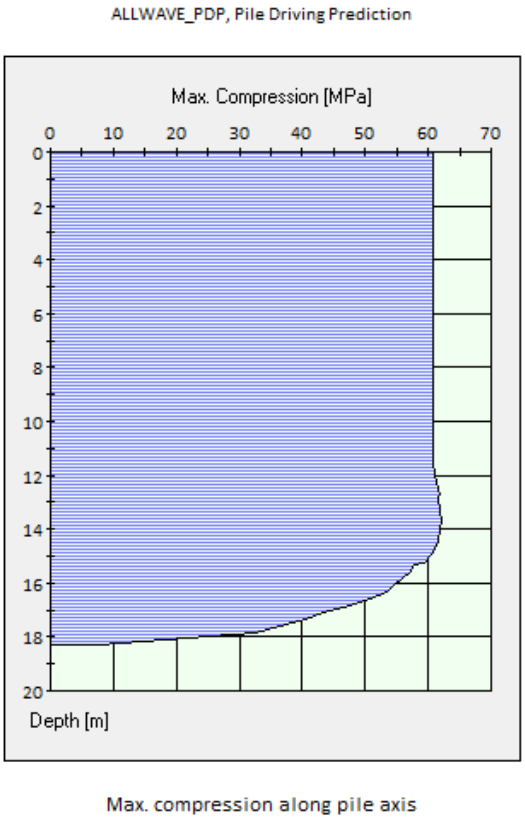

Figure I.7: Maximum compression stress during driving in model 2.0

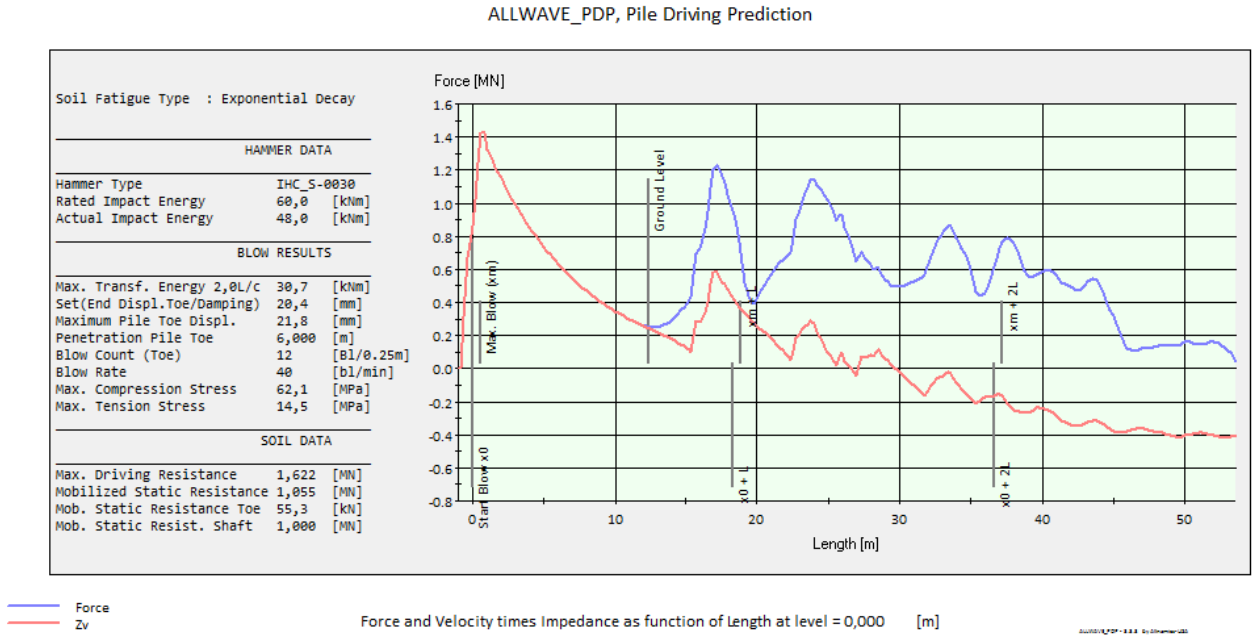

Figure I.8: Force versus impedance times velocity of model 2.0

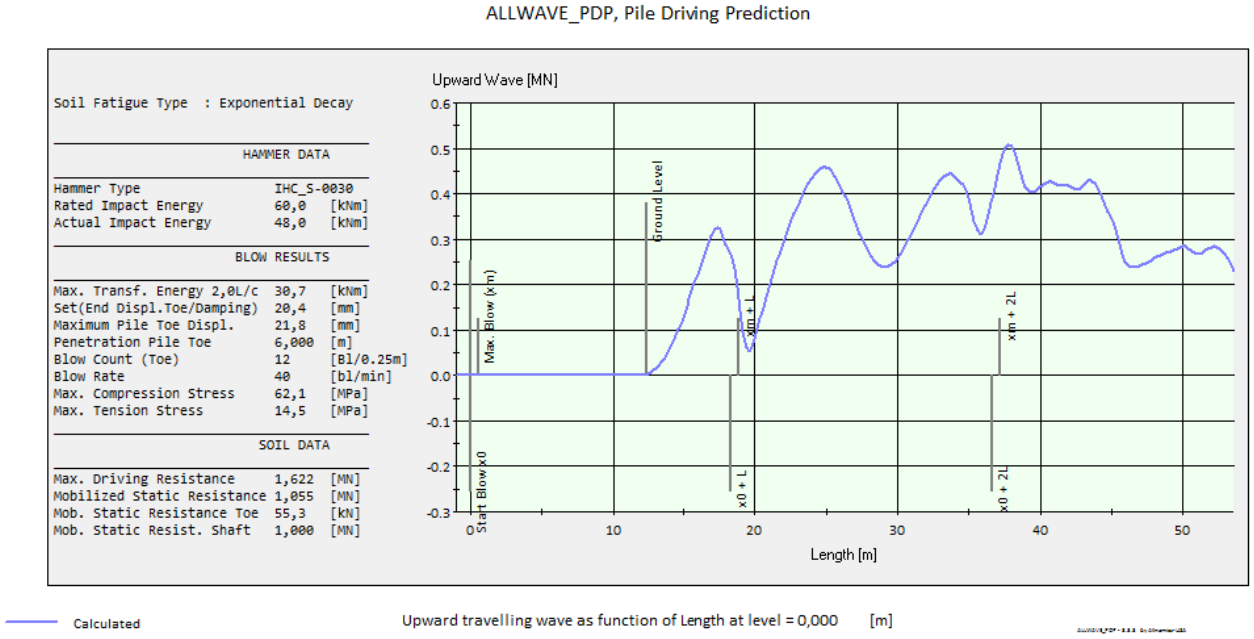

Figure I.9: Upward force at pile head of model 2.0

I.3.2. Model 2.1

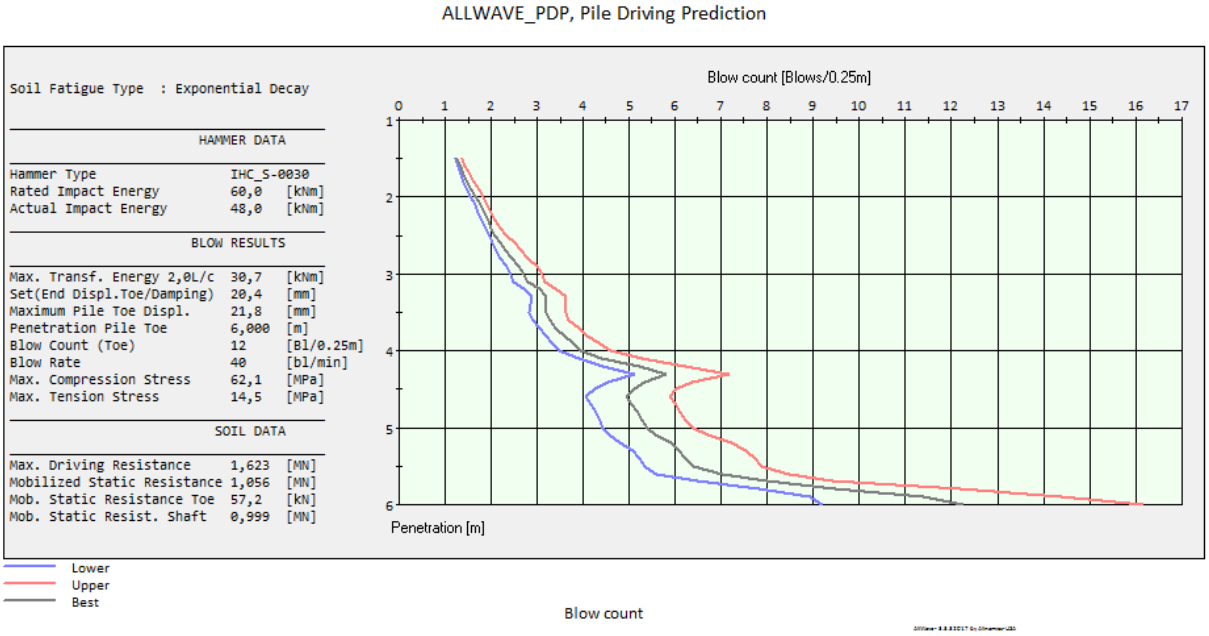

Figure I.10: Blow count for model 2.1

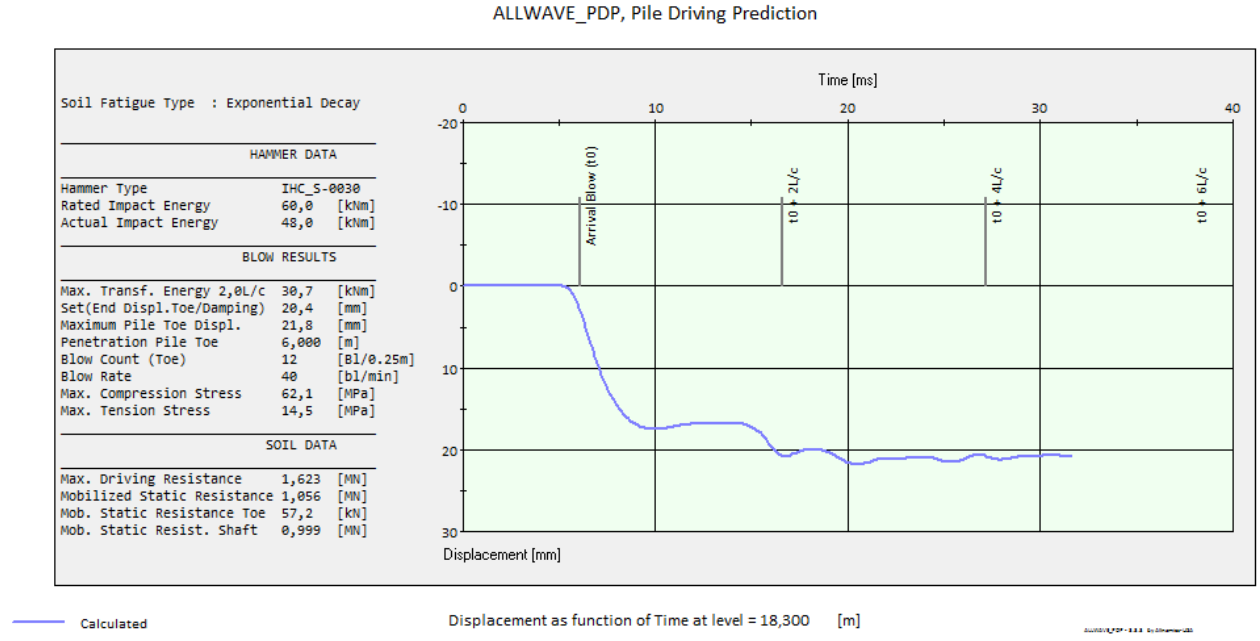

Figure I.11: Pile tip displacement for model 2.1

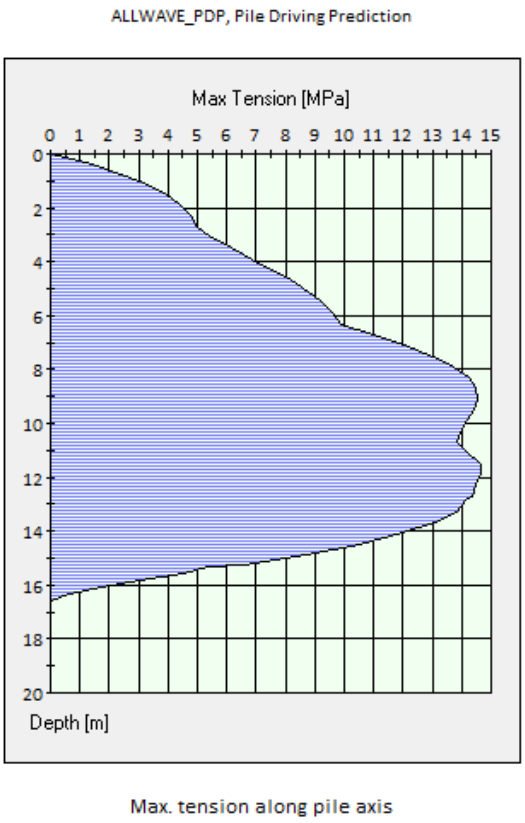

Max. tension along pile axis

Figure I.12: Maximum tension stress during driving in model 2.1

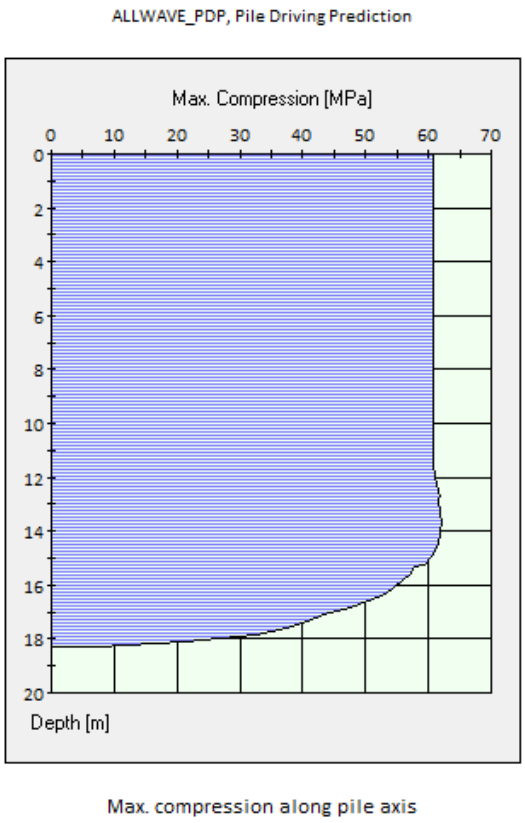

Max. compression along pile axis

Figure I.13: Maximum compression stress during driving in model 2.1

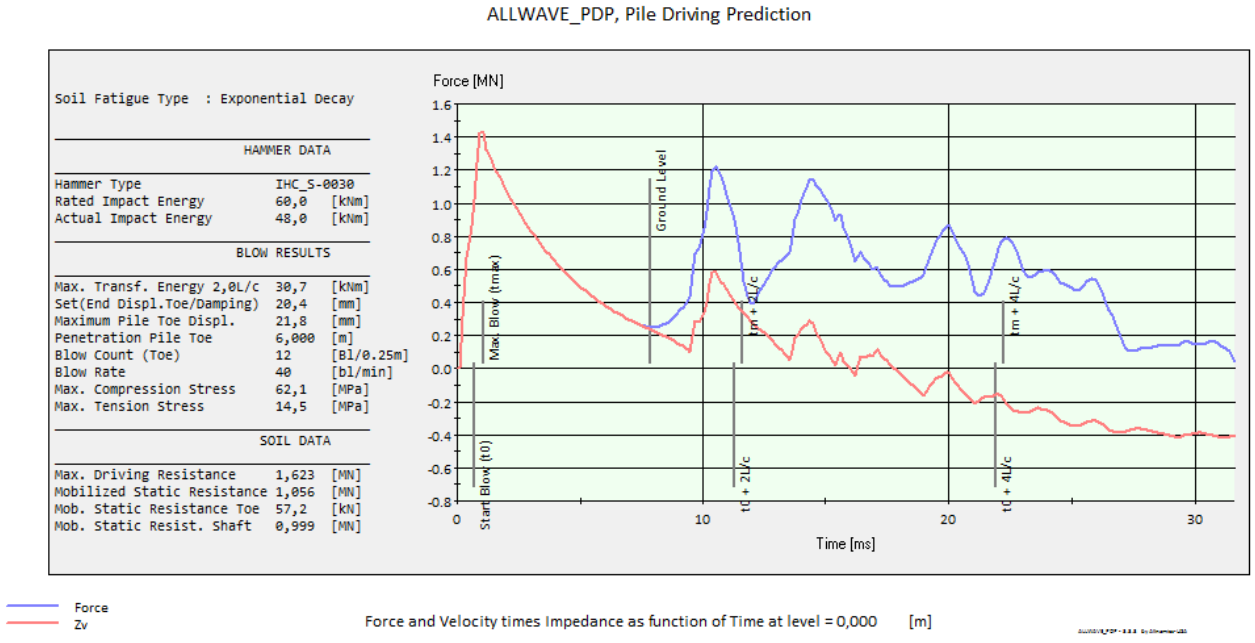

Figure I.14: Force versus impedance times velocity of model 2.1

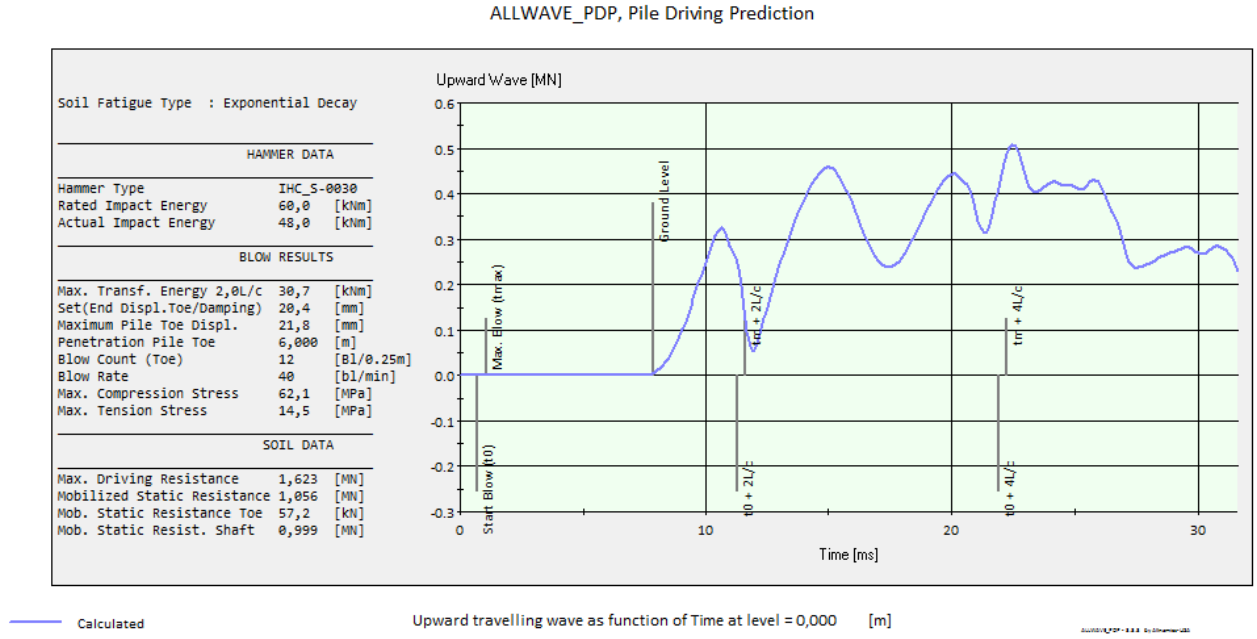

Figure I.15: Upward force at pile head of model 2.1

I.3.3. Model 2.3

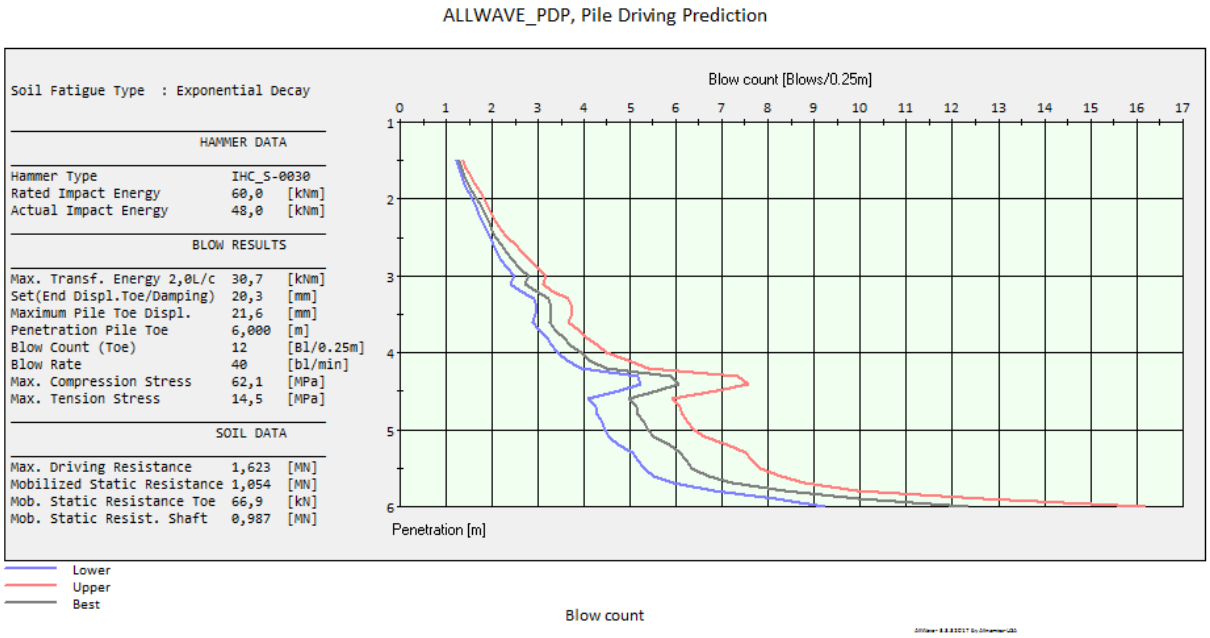

Figure I.16: Blow count for model 2.3

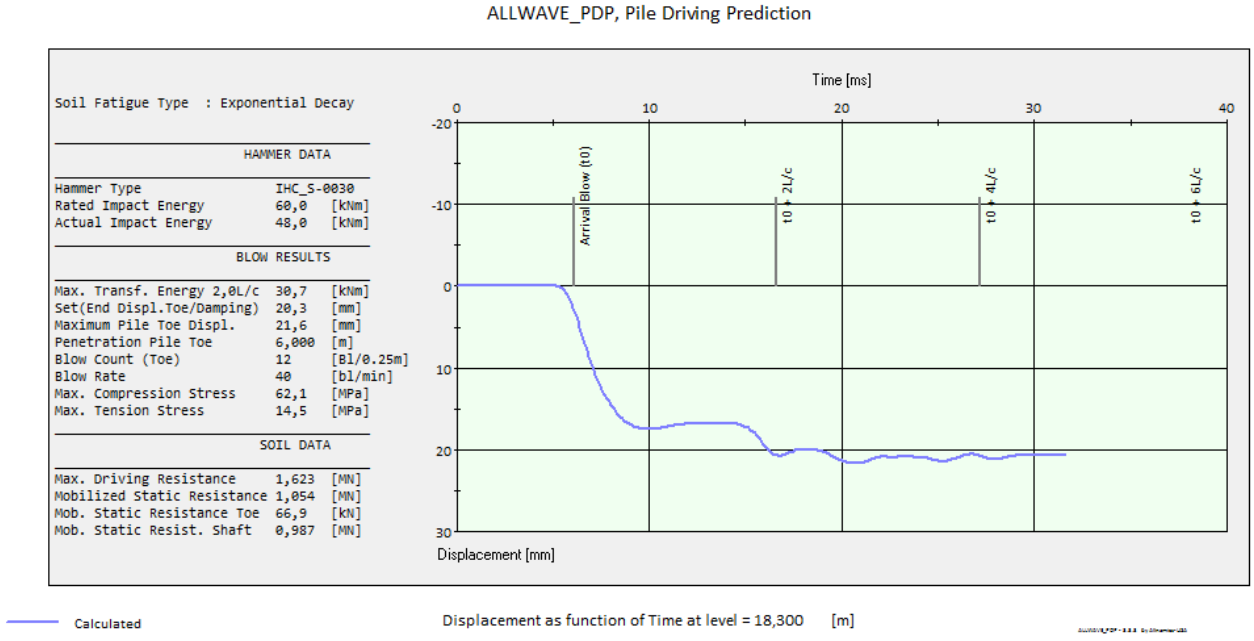

Figure I.17: Pile tip displacement for model 2.3

I.3.4. Model 2.7

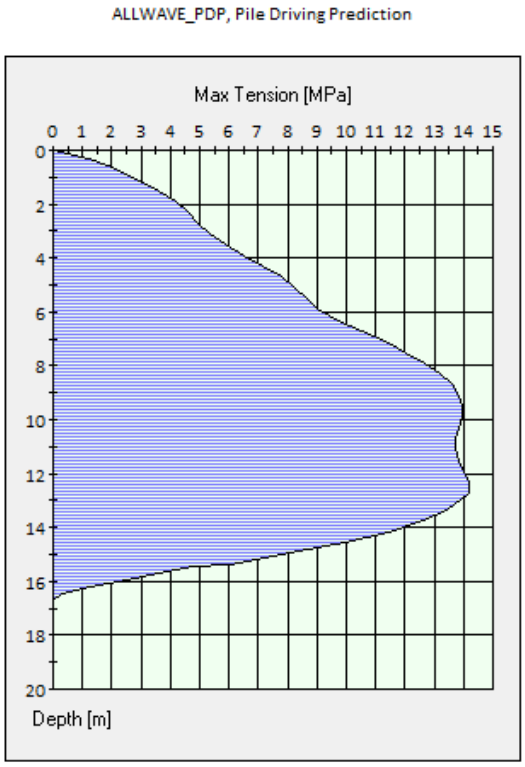

Figure I.18: Maximum tension stress during driving in model 2.3

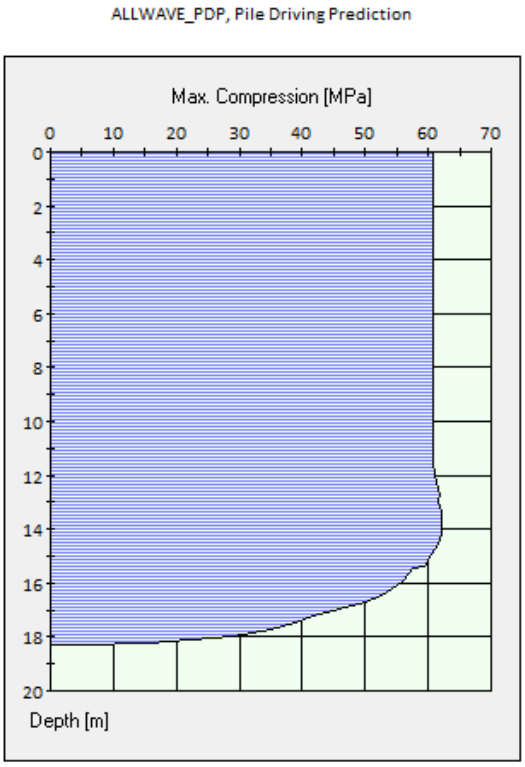

Figure I.19: Maximum compression stress during driving in model 2.3

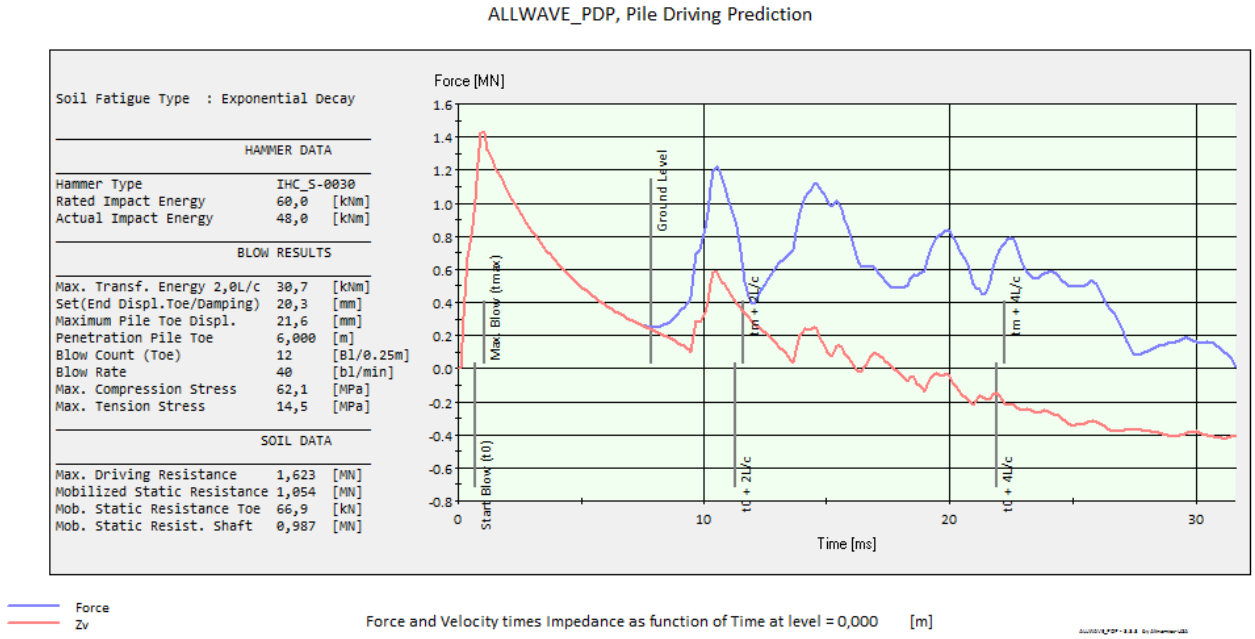

Figure I.20: Force versus impedance times velocity of model 2.3

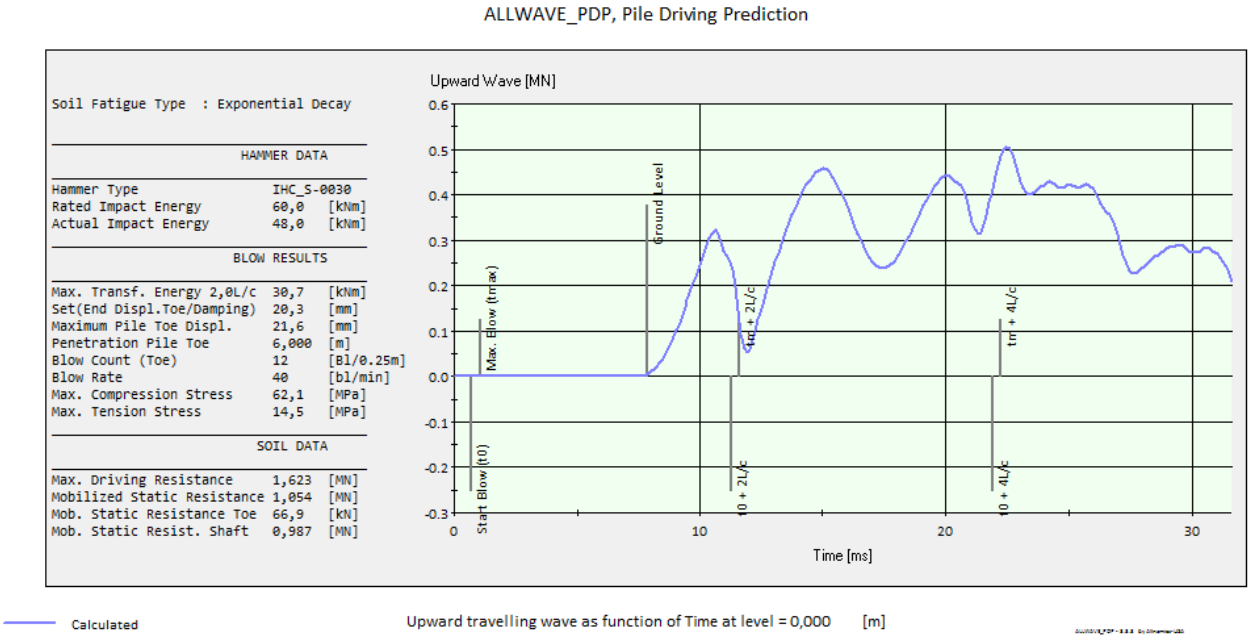

Figure I.21: Upward force at pile head of model 2.3

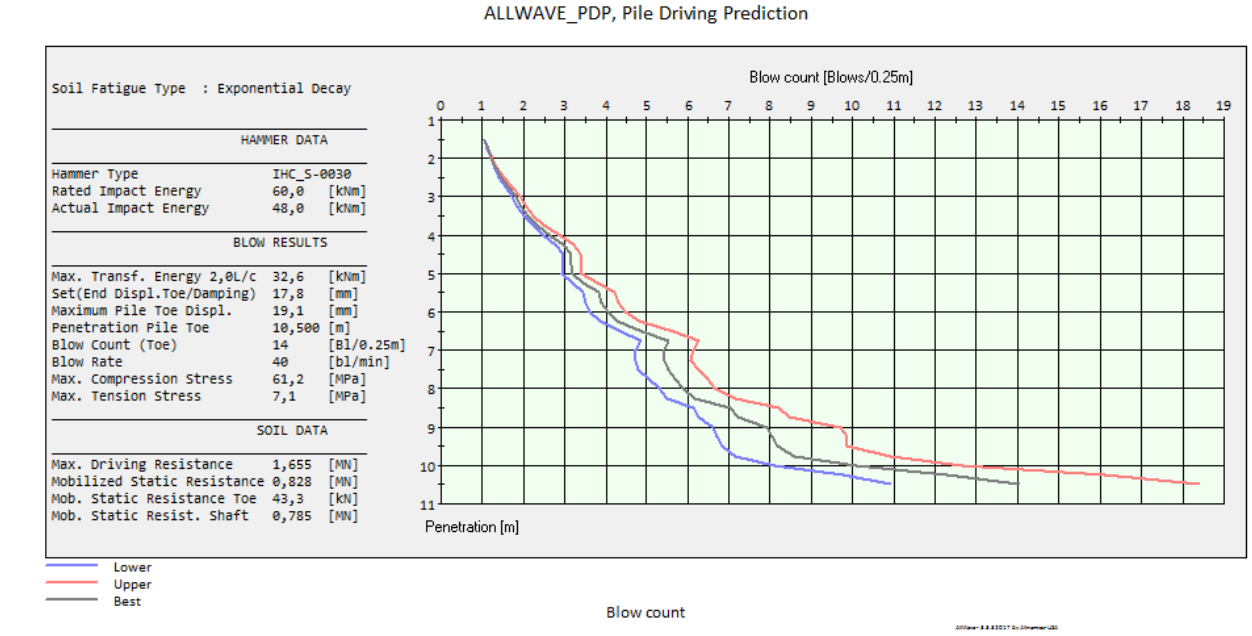

Figure I.22: Blow count for model 2.7

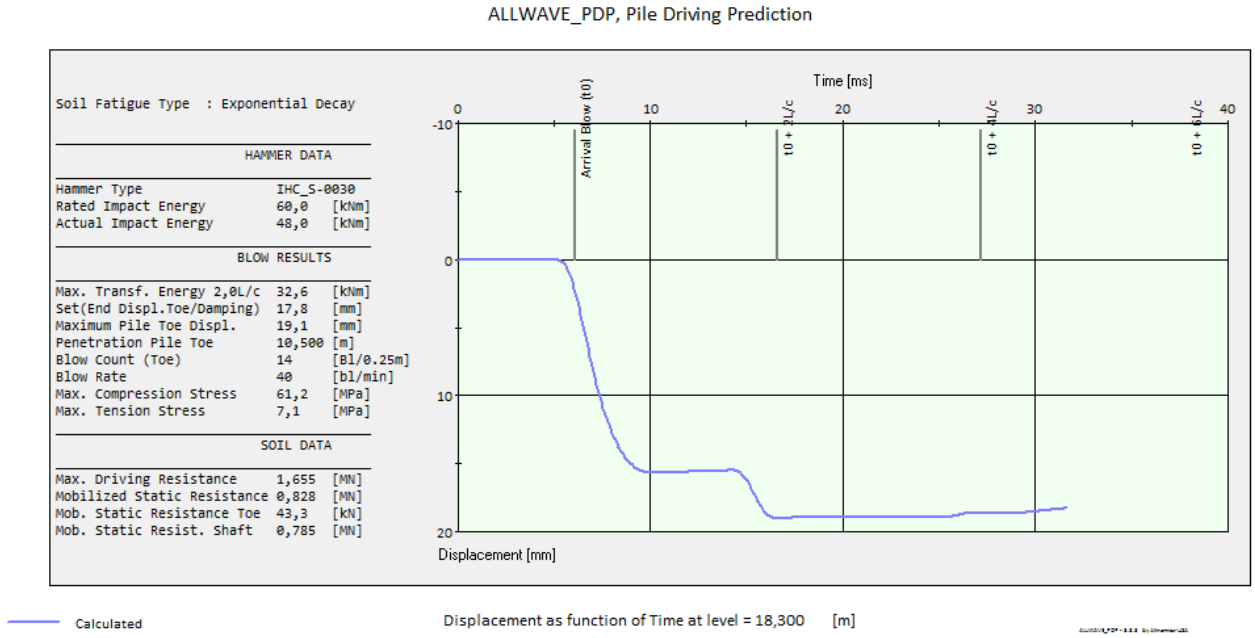

Figure I.23: Pile tip displacement for model 2.7

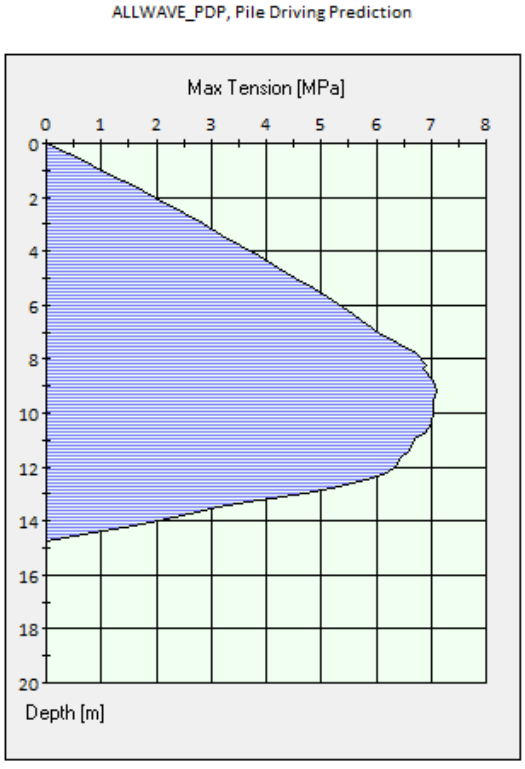

Figure I.24: Maximum tension stress during driving in model 2.7

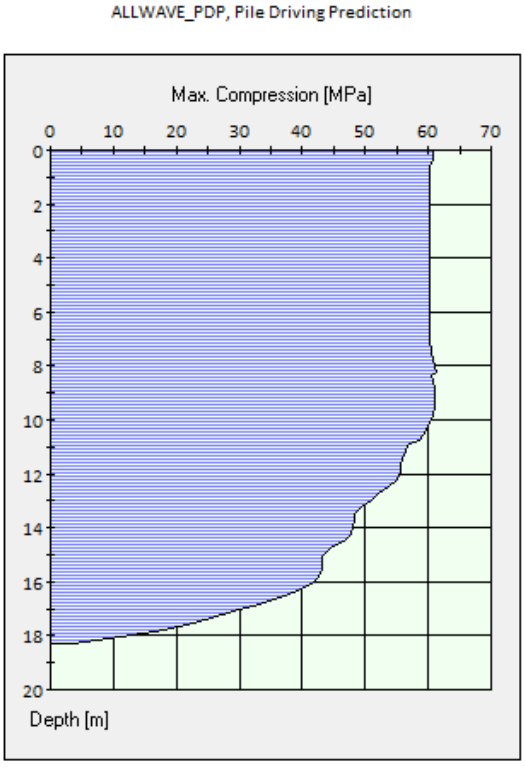

Figure I.25: Maximum compression stress during driving in model 2.7

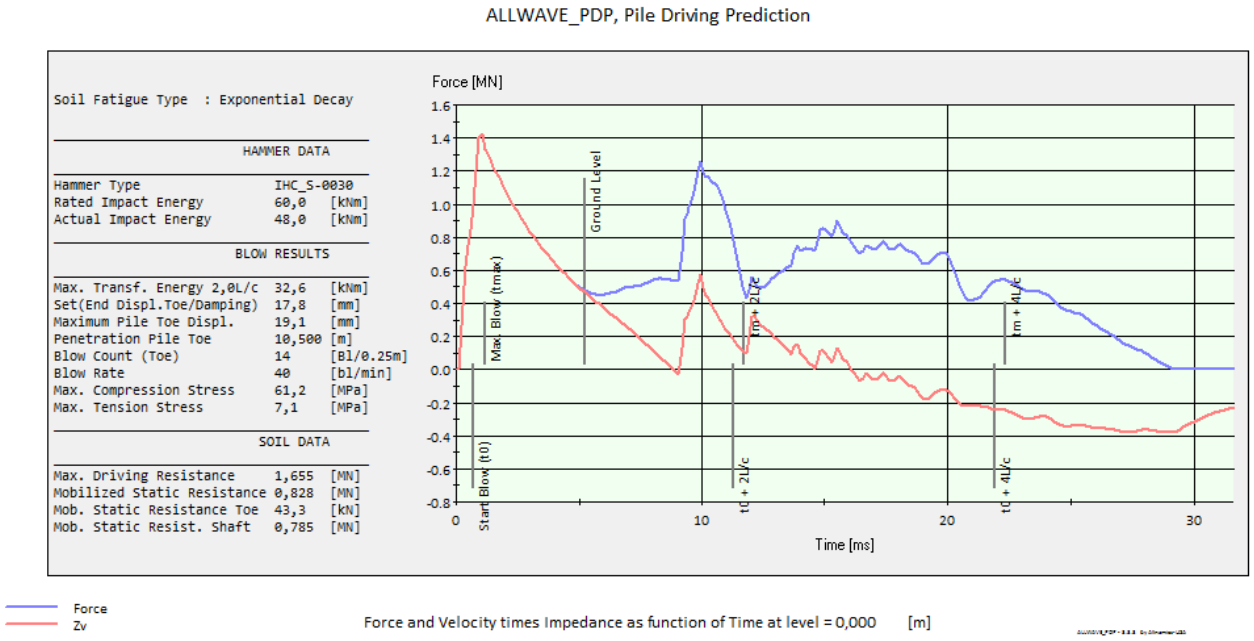

Figure I.26: Force versus impedance times velocity of model 2.7

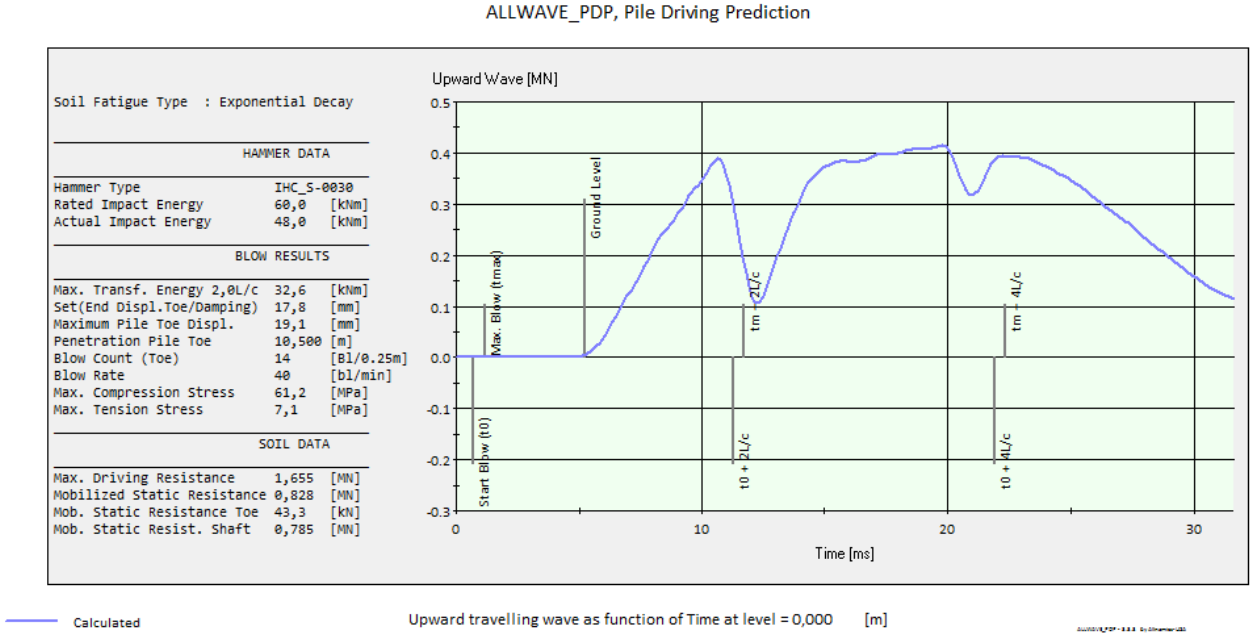

Figure I.27: Upward force at pile head of model 2.7